

Anviloy Wire – H13 Cladding Development

THESIS

Presented in Partial Fulfillment of the Requirements for the Degree Master of Science in
the Graduate School of The Ohio State University

By

Jerry L. Kovacich, B.S.W.E.

Graduate Program in Welding Engineering

The Ohio State University

2020

Master's Examination Committee :

Professor Dennis Harwig, Advisor

Professor Boyd Panton

Copyright by
Jerry L. Kovacich
2020

Abstract

High pressure die casting is used to quickly and repeatably manufacture high volumes of aluminum parts with good surface finish. Thermal fatigue cracking (heat checking) from thousands of thermal cycles, local soldering of aluminum part features to the surface, and buildup of lubricant residue leads to damage of die surfaces. Manual repair of hot work tool steel (HWTS) dies using arc welding is burdensome, involving high preheats and post weld heat treatment (PWHT) to restore HWTS properties. Improved automated repair procedures and materials are necessary to reduce die casting costs. This effort focused on developing automated arc welding repair procedures, characterizing clad deposit microstructure, evaluating tempering effects in the H13 heat affected zone (HAZ), and cladding shot block dies for in-plant trials using an experimental Anviloy (W-27.5Ni-12.5Fe) alloy wire on H13 HWTS dies.

Mechanized hot wire gas tungsten arc welding (HW-GTAW) procedures were developed to produce low dilution single and double layer deposits. The minimum weld dilution with HW-GTAW required to produce sound clads was 18%. HW-GTAW trials showed that consistent, sound Anviloy wire clads could be deposited onto H13 using arc welding. Robotic gas metal arc welding pulse (GMAW-P) procedures were developed for conformal cladding the shot block. The robotic GMAW-P system provided better accessibility to accommodate shot block features. Both a DC+ and DC- advanced waveform were evaluated, but only the DC- waveform resulted in stable and sound deposition of Anviloy wire consumable. The die block's complex shape mandated the use of sub-optimal torch angles when cladding in the 2G position. Work angle oscillation was used to improve bead shape in these adverse torch positions. A weld stop procedure was developed to improve conformal cladding complex shapes. The developed two layer cladding procedure minimized number of weld passes and amount of deposited material

needed to create a 10mm clad layer repair. These trials verified GMAW-P could be used to conformally clad H13 using Anviloy wire. Single layer GMAW conformal cladding procedures will require PWHT since the deposits are too thick for temperbeading.

HW-GTAW heat input and preheat effect on H13 HAZ size was related to HAZ tempering effects on double layer deposits. H13 HAZ lengths were measured using metallography and verified with hardness mapping. Reduced preheat at 25kJ/in heat input were found to produce preferred HAZ conditions for tempering H13. Hardness maps comparing double layer non-temperbead to temperbead double layer clad deposits revealed reduction of hardness indents over 600HV from 15% to only 1%, respectively. These results indicate feasibility for implementing temperbead weld repairs of HWTS dies using the GTAW process.

Since no prior literature was published on the W-27.5Ni-12.5Fe weld clad microstructure, characterization was used to understand effects of cladding procedure on fusion and HAZ microstructures. Metallography, scanning electron microscopy (SEM), energy dispersive X-ray spectroscopy (EDS), and Thermocalc simulation software were used to identify potential phases present. Undiluted fusion zone microstructure was composed of gamma Ni-Fe FCC matrix phase and secondary alpha tungsten BCC phase. Upon dilution with H13, a third phase was observed in SEM and EDS analysis. Thermocalc simulations indicated this phase could potentially be an intermetallic Mu phase or M_6C carbide. An additional cladding procedure was developed using a butter layer of 308L between the Anviloy wire and H13 to help investigate the deposit phases. The Anviloy-308L butter clads were subjected to H13 normalization and double temper heat treatment. Attempts to identify the unknown phase with EDS were inconclusive. Metallography using selective alkaline sodium picrate etchant indicated that the unknown phase was likely M_6C .

Acknowledgements

This research would not have been possible if not for the guidance of my advisor, Dr. Dennis Harwig, who provided invaluable expertise every step of the way.

Thank you to Dr. Boyd Panton for providing important characterization insight throughout the project, and for serving as a member of my examination committee.

Thank you to Dr. Boian Alexandrov for helping mold me into the engineer I am today as my undergraduate research advisor.

I would also like to thank the entirety of Ohio State's Welding Engineering community: the supporting staff, students, and professors alike never failed to provide training, advice, helpful critiques, and a place to call home throughout my career at Ohio State.

Finally, I would like to thank my mother, father, grandparents, and friends for their unwavering encouragement, support, and love as I pursue my dreams.

Vita

November 14, 1995.....Born – Youngstown, OH U.S.A.

2014.....B.S. Welding Engineering

The Ohio State University

Columbus, OH

2015-Present.....Graduate Research Associate

The Ohio State University

Columbus, OH

Field of Study

Welding Engineering

Table of Contents

ABSTRACT	iii
Acknowledgements.....	v
Vita.....	vi
List of Figures	viii-xi
List of Tables	xii
Chapter 1 : Introduction.....	1
Chapter 2 : Background.....	3
Chapter 3: Objectives	25
Chapter 4 : Results and Discussion.....	27
4.1 Anviloy Wire HW-GTAW Cladding Procedure Development for H13.....	27
4.2 Anviloy Wire Robotic GMAW-P Conformal Cladding Die Development.....	32
4.3 Feasibility of H13 Temperbead Repair using Anviloy HW-GTAW Cladding Procedures.....	40
4.4 Microstructure Characterization of Anviloy Deposits on H13 Die Steel	45
Chapter 5 : Conclusions	62
Works Cited.....	64
Appendix A : Anviloy Wire HW-GTAW Cladding Procedure Development for H13.....	66
Appendix B: Anviloy Wire Robotic GMAW-P Conformal Cladding Die Development.....	93
Appendix C: Feasibility of H13 Temperbead Repair using Anviloy HW-GTAW Cladding Procedures.....	124
Appendix D: Microstructure Characterization of Anviloy and Anviloy-308L Clad Deposits on H13 Die Steel.....	143

List of Figures

Figure 1: HPDC Schematic	5
Figure 2: Mushet Steel Compositions from Early 1900's (7)	7
Figure 3 : Fe-Fe ₃ C Phase Diagram.....	8
Figure 4: H13 Isothermal Transformation Diagram.....	9
Figure 5 : Martensite Crystal Lattice.....	10
Figure 8 : 9Cr1Mo Continuous Cooling Transformation Diagram.....	13
Figure 9 : 3.25Cr1Mo.2V Continuous Cooling Transformation Diagram.....	13
Formula 1: Nobutaka et. al's Carbon Equivalency Formula.....	14
Figure 10 : Precipitate Stability in Steels.....	15
Figure 11 : Softening VS. Exposure Temp for Several HWTS.....	16
Figure 12 : Kindbom Theory.....	19
Figure 13 : Formula for Heat Checking Resistance.....	20
Figure 14 : Intermetallic Formation on H13 in a Soldering Simulation.....	21
Figure 15 : Rehbinder Effect.....	22
Figure 16: CW-GTAW Welds Made Without Wire Straightener (Top) Vs. Early Development HW-GTAW Welds Made with Wire Straightener (Bottom)	28
Figure 17 : Anviloy Wire-H13 HW-GTAW Clads with (top) and without (bottom) Unmelted Wire Defects Indicated by Arrow	29
Figure 18 : HW-GTAW Low Dilution Trial Clads and Parameters.....	31
Figure 19 : 1G GMAW Synchrofeed Welds Showing Lack of Fusion and Parameters.....	32
Figure 20 : Clads and Parameters Using the DC- Wave 1.2mm SuS waveform at 270A.....	34
Figure 21 : Weld and Parameters Using the DC- Wave 1.2mm SuS waveform at 260A Using Oscillation	35
Figure 22 : Multi-pass 1G Robotic GMAW Clad Procedure.....	36
Figure 23 : GMAW Torch Oscillation Resulting in Sound 2G Clad	37
Figure 24 : 2G Position Clads Employing Torch Angle Oscillations.....	38
Figure 25 : Robotic GMAW Conformal Cladding Procedure.....	39

Figure 26 : Robotic GMAW Weld Stop Metallographic Sample.....	40
Figure 27 : 300C and 25C Preheat HAZ Sizes Made with HW-GTAW.....	41
Figure 28 : Anviloy Wire-H13 HW-GTAW HAZ Sizes Vs. Heat Input with Bracketed Temperbead Region	42
Figure 29 : Non-temperbead Clad Hardness Map.....	46
Figure 30 : Temperbead Optimized Clad Hardness Map.....	43
Figure 31 : Temperbead and Non-Temperbead Hardness Distribution Histogram	44
Figure 32 : Metallographic Section of Anviloy Wire Arc Casted Button Showing Undiluted Two Phase Microstructure	46
Figure 33 : HW-GTAW Build Up Final Pass Showing Macroseggregation, SEM Image	47
Figure 34 : Thermocalc Property Diagram of Undiluted Anviloy Wire Showing 2 Phase Equilibrium Microstructure	48
Figure 35 : EDS Phase Mapping of Undiluted Anviloy Wire.....	49
Figure 36 : EDS Data for Undiluted Tungsten Rich Phase.....	49
Figure 37 : EDS Data for Undiluted Matrix Phase.....	50
Figure 38 : Diluted Anviloy Wire H13 Microstructure Showing 3 Phases, SEM Image	51
Figure 39 : Thermocalc Property Diagram of Anviloy Wire with 10% H13 Dilution Showing 4 Phase Predicted Equilibrium Microstructure	52
Figure 40 Thermocalc Property Diagram of Anviloy Wire with 40% H13 Dilution Showing 3 Phase Predicted Equilibrium Microstructure	53
Figure 41 : EDS Map of Diluted Anviloy Wire – H13 Microstructure.....	54
Figure 42 : Diluted Tungsten Rich Phase EDS Data.....	54
Figure 43 : Diluted Matrix Phase EDS Data.....	55
Figure 44 : Unidentified Third Phase EDS Data.....	55
Figure 45 : Anviloy Wire-H13 Diluted Region Elemental Heat Map Gathered by EDS	57
Figure 46 : Heat Treated Anviloy Wire –H13 Clad (left) and Diluted Region of Anviloy Wire Buildup on H13 (right) Showing Same 3 Phase Microstructure as Seen in SEM/EDS	58
Figure 47 : Hardness indent at Fusion Boundary (left) and Hardness Indent at Plate Midpoint ..	59

Figure 48 : 70% Anviloy wire + 30% * (70% 308L + 30% H13) Thermocalc Property Diagram Showing 4 Phase Predicted Equilibrium Microstructure	60
Figure 49 : The Anviloy Wire-308L-H13 Overlay Etched with Alkaline Sodium Picrate.....	61
Figure A1 : Gas Tungsten Arc Welding.....	65
Figure A2 : Uninterrupted Bridging Metal Transfer in Rear Feed Cold Wire.....	66
Figure A3 : Hot Wire Gas Tungsten Arc Welding.....	67
Figure A4: Recurring and Continuous Melting Bridge HW-GTAW Transfer Modes.....	68
Figure A5 : GTAW Welds From OSU Capstone	70
Figure A6 : Miller Jetline 9800 Mechanized Welding System.....	73
Figure A7 : Anviloy Wire Cast.....	76
Figure A8 : Anviloy Wire Helix.....	77
Figure A9 : Two Axis Wire Straightener.....	78
Figure A10 : Clads Made with Two Axis Wire Straightener.....	78
Figure A11 : Insufficient Hotwire Power to Ensure Bridging Metal Transfer Resulting in Unmelted Wire Inclusion (arrow) in Anviloy Wire Clad Deposit Trial 19.	82
Figure A12 Uniform Anviloy Clad Deposits Made using Deposit Trial 20	83
Figure A13 : Low Dilution Constant Deposit Area Bead on Plate Tests conducted at three different currents (140, 160 and 180 amps) at constant travel speed, wire feed speed, arc voltage and hot wire conditions of 4 volts and 0.75 inch stickout.	85
Figure B1 : GMAW Process.....	94
Figure B2: GTAW Process.....	94
Figure B3: Robotic GTAW Welding Torch.....	95
Figure B5: Advanced Pulse Waveform and High Speed Weld Imaging of Process.....	97
Figure B6: FCA Die Block Used for Anviloy Cladding In-plant Trials.....	99
Figure B7: OTC GMAW Robot.....	101
Figure B8 : OTC Robot Controller and OTC Welding Power Supply	102
Figure B9 : Miller Proheat 35 Induction Heating Unit	103
Figure B10 : Induction pre-heating set up.....	104
Figure B11: Synchrofeed Welds and Parameters.....	105
Figure B12: High Current DC- Pulse Clads	107
Figure B13: Oscillation Adjusted Flat (1G) Clad and Parameters.....	108

Figure B14 : Multi-Pass Anviloy Wire Clad on H13.....	109
Figure B15 : Torch Angle for Horizontal Clads.....	111
Figure B16 : Initial Horizontal (2G) Clads	112
Figure B17 : Horizontal (2G) Oscillation Procedure.....	113
Figure B18 : Horizontal (2G) Clads with Refined Oscillation.....	114
Figure B19 : NADCA Standard FCA Die Block.....	115
Figure B20 : Conformal Cladding Procedure	116
Figure B16 : Single Weld Stop.....	118
Figure C1: Damage on a HPDC Die Surface.....	122
Figure C2: Temperbead Welding (6)	125
Figure C3: Jetline 9800 Mechanized Welding System.....	130
Figure C5: 300C vs. 25C Preheat HAZ Sizes.....	133
Figure C6 : Hardness Map of 300C Preheated Sample.....	135
Figure C7: 5IPM Sample Travel Speed Test HAZ Measurements.....	136
Figure C8: HAZ Sizes Vs. Heat Input.....	136
Figure C9: 3 Pass Non-Temperbead Procedure Hardness Map.....	138
Figure C10: 5 Pass Temperbead Procedure Hardness Map.....	139
Figure C11: Temperbead Vs. Non-Temperbead Hardness Distribution.....	140
Figure D1 : Softening VS. Exposure Temp for Different Steels	146
Figure D2 : Easterling Precipitate Dissolution in Steels.....	147
Figure D3 : Cr-Fe-Ni Isotherms at (a) 1300C (b) 1200C (c) 1100C and (d) 1000C by Miettinen	151
Figure D4 W-Cr Phase Diagram.....	152
Figure D5 : Miller Jetline 9800 Mechanized Welding System.....	154
Figure D6 : Anviloy Wire Button Microstructure at Low Magnification.....	157
Figure D7 : Anviloy Wire Button at High Magnification.....	158
Figure D8: Anviloy Wire Property Diagram.....	159
Figure D9: Secondary Electron Image of 6 Pass Anviloy Wire Build.....	161
Figure D10: EDS Map of Undiluted Anviloy Wire.....	163
Figure D11 : Tungsten Rich Phase EDS Data.....	164

Figure D12 : Matrix Phase EDS Data.....	164
Figure D13: Anviloy Wire H13 Single Pass Overlay Diluted Structure.....	166
Figure D14: Fusion Boundary Microstructure in H13-Anviloy Wire Clads.....	167
Figure D15: EDS Map of Anviloy-H13 Fusion Boundary Microstructure	168
Figure D16 : EDS Data and Composition of Phase for Alpha BCC Tungsten Phase	169
Figure D17 : EDS Data and Composition of Phase for Matrix Phase.....	170
Figure D18: EDS Data and Composition of Phase for Tungsten Intermediate Phase.....	170
Figure D19 : Property Diagram for 10% Dilution.....	172
Figure D20: Property Diagram for 40% Dilution.....	174
Figure D21 : EDS Phase Map and Elemental Heat Map Including Carbon.....	176
Figure D22 : Normalize & Double Tempered Anviloy Wire – H13 Clad Macro.....	177
Figure D23 : Normalized & Double Tempered Anviloy Wire – H13 Clad Fusion Boundary...	178
Figure D24 : Anviloy 6 Pass Build Fusion Boundary Etched with Alkaline Sodium Picrate..	179
Figure D25 : Normalized & Double Tempered Anviloy Wire – H13 Clad Fusion Zone.....	180
Figure D26 : H13-Anviloy Wire N+2T Hardness Indent 10mm Away From Fusion Boundary.	182
Figure D27: H13-Anviloy Wire N+2T Hardness Indent Near Fusion Boundary.....	182
Figure D28 : H13-308L-Anviloy Wire N+2T Fusion Boundaries.....	184
Figure D29 : Property Diagram for .7*Anviloy Wire + .3(.7*308L+.3*H13)	185

List of Tables

Table 1 : H13 Tool Steels and Compositions.....	11
Table 2 : H11 Tool Steel Grades and Compositions.....	11
Table 3 : Mu and M ₆ C Carbide Composition at 900C for 10% Dilution Predicted by Thermocalc	56
Table 4 : Mu and M ₆ C Carbide Composition at 700C for 40% Dilution Predicted by Thermocalc	56
Table 19 : 1G GMAW Synchrofeed Welds Showing Lack of Fusion Parameters	32
Table 20 : Welds Parameters for the DC- Wave 1.2mm SuS waveform at 270A	34
Table 21 : Parameters for DC- Wave 1.2mm SuS waveform Weld at 260A Using Oscillation..	35
Table A1: Chemical Compositions of Alloys (wt.%)	72
Table A12 : Uniform Anviloy Clad Deposits Made using Deposit Trial 20 Parameters	83
Table C1: Chemical Compositions of Alloys (wt.%)	128
Table C2 : Heat Input Trial Parameters	131
Table C3 : Preheat Trial Parameters	131
Table C4 : Temperbead Trial Parameters	131
Table C5: 300C vs. 25C Preheat HAZ Size Measurements.....	133
Table D1 : Orvar Supreme, Anviloy Wire, and 308L Compositions.....	153
Table D2 : Composition of Phases Predicted by Thermocalc at 1465C.....	165
Table D3 : Thermocalc Predicted Composition of Mu and M ₆ C Phases for 10% Dilution at 900C.....	172
Table D4 : Thermocalc Predicted Composition of Mu and M ₆ C Phases for 40% Dilution at 700C..	174

Introduction

High pressure die casting (HPDC) of aluminum alloys is commonly used to mass produce precision parts in the automotive industry (1). The process involves the injection of superheated molten aluminum at thousands of tons of force into a metal die, most often made of hot work tool steel (HWTS). Thermal fatigue cracking (heat checking) from thousands of cycles, soldering of casted metal to die surfaces, and carbonaceous buildup of die lubricants used to cool down die blocks between casting cycles (2) leads to die surface failure. Automotive companies repair die casting dies using manual arc welding methods and need automated methods and better materials to extend die life and performance.

The most commonly used HWTS in die casting applications are the chromium bearing hot work tool steels, particularly H13 (1). H13 is selected based on its advantageous relative cost, toughness, high temperature strength, and resistance to in-service softening and damage. H13's resilience comes from a composition and heat treatment designed to form a stable tempered martensitic microstructure consisting of vanadium and molybdenum carbides (3). H13 has high hardenability to ensure transformed microstructures in thick sections needed to make large die casting dies. This hardenability is advantageous for production of thick dies, but complicates repair procedures as it makes untempered martensite formation inevitable.

Repair technology for HWTS dies centers around fusion welding processes. Different forms of wire or powder fed laser and electron beam methods have been studied, but by far the most common repair methods utilize arc welding, particularly gas tungsten arc welding (GTAW) (2). Manual GTAW is preferred due to the widely available, highly trained work force as well as a ready supply of consumables. Though GTAW is widely used for die repair, post weld heat treatment (PWHT) is required to temper martensite formed during repair. PWHT of HWTS die

block is an expensive and time consuming endeavor involving multiple thermal treatments to achieve desired properties. Welding procedures also require the use of high preheats, which may exceed 300C to mitigate hydrogen cracking concerns.

Though matching consumables are available for HWTS die repair, lower carbon consumables are often used to eliminate PWHT and reduce required preheat. Though they make repair procedures simpler, these consumables have significantly lower life than matching consumables (2). In the most demanding HPDC applications, refractory alloy inserts are used due to their increased life (4). Refractory metal consumables such as Anviloy 1150 have historically been used, but these materials are only available in rod form which makes automated repair and cladding impossible. A new experimental W-27.5Ni-12.5Fe (Anviloy wire) consumable with improved wire drawability has been developed for automated die repair, cladding, and wire arc additive manufacturing applications. This effort focused on developing automated arc welding repair procedures, characterizing clad deposit microstructure, evaluating tempering effects in the H13 heat affected zone (HAZ), and cladding shot block dies for in-plant trials using this experimental Anviloy wire on H13 die material. The Hot Wire Gas Tungsten Arc Welding (HW-GTAW) was primarily used to evaluate clad procedure effects on deposit microstructures and H13 heat affected zone tempering. Robotic Gas Metal Arc Welding Pulse (GMAW-P) procedures were developed to clad production shot block dies, which had complex features. Cladded shot blocks made with these procedures will be used in plant trials, and the resulting performance evaluation is an area for future work.

BACKGROUND

Metal Casting in Antiquity

Casting is one of the oldest forms of metal production, with discovered artifacts dating back thousands of years. The origin and date of the oldest castings in the world is a somewhat contentious topic, but most historians agree that by 3200BC, ancient Mesopotamians had mastered the art of copper casting (1). A casted copper frog from this time period is considered by many to be the oldest known example of a casting. These early castings were produced using sand or clay mold molds, since the discovery of these natural refractory materials and their use at pottery and other items long predates the use of metal.

Metallurgical progress continued into the Bronze Age, as primitive casters began adding tin to copper to produce bronze. However, the next breakthrough would not occur until roughly the 8th century BC when Chinese civilization began producing cast iron with primitive bloomeries, and perhaps even primitive blast furnaces by the 4th century AD (2). Cast pig iron was produced in Europe starting around 1500AD, but commercialization of ductile cast iron did not begin until 18th century AD, when a Frenchman named René Antoine Ferchault de Réaumur described the first method for producing a ductile iron (1). By 1800, cast iron was a widely available commercial product in the West. Ironically, the development of cast iron was essential for development of new permanent die materials to cast other metals, and the history of die casting begins with the use of cast iron as a die material.

History of Die Casting

Prior to the mid 1800's, sand and clay molds were most commonly used in metal casting due to their abundance and low cost. However, they lacked robustness and could not be re-used to create large volumes of parts. It wasn't until 1838 that die casting first took shape, with the Brooklyn-Soss die casting company filing the first die casting patent (3). This patent differed from previous casting methods since it used a permanent iron die to cast tin-lead alloys for buttons for printing typewriters (3). The robustness of these dies and the repeatability of the process allowed the Brooklyn-Soss die casting machine to gain widespread use in other industries by the late 19th century. Metal molds for die casting also result in higher cooling rates from molten temperatures, resulting in a fine grain structure which improves strength (4).

The next advancement in casting technology came with the introduction of zinc, aluminum, and magnesium casting alloys in the early 20th century. By the mid 1930's, many of the low melting point casting alloys used today were already available (3). By the mid-twentieth century, machinery advancements enabled high pressure injection of molten metal into dies. High pressure die casting (HPDC) resulted in cast parts that had superior surface finish and less defects than ever before (3). High pressure die casting has since remained the preeminent method for producing large quantities of low melting point metals with minimal defects and good surface finish.

High Pressure Die Casting

High pressure die casting (HPDC) today is a high throughput process that quickly creates precision components out of low melting point materials. The process involves melting of a low

temperature metal, commonly aluminum, magnesium, or zinc, and forcing it into a die cavity at high pressure.

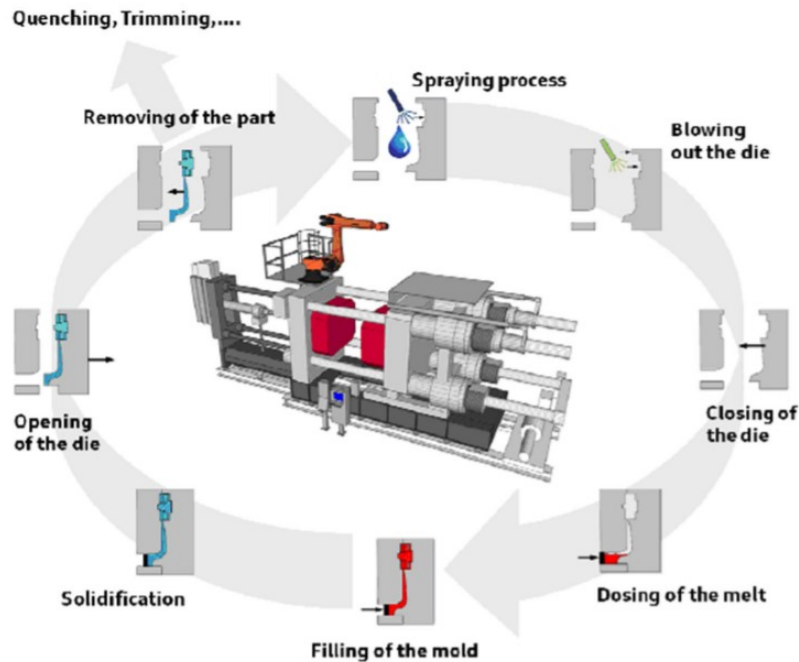


Figure 1: HPDC Schematic (4)

Aluminum is, per ton, the most commonly high pressure die casted metal (5). Melts are forced into die cavities at temperatures often 100C higher than the alloy liquidus using thousands of tons of force. Die casted parts that are hundreds of pounds can be produced in a single shot in cycle times as little as three minutes. The high pressure injection of molten metal results in castings that possess excellent surface finish and dimensional repeatability. Metal dies used in high pressure die casting usually have water cooling lines running through them to help actively cool the casted parts and dies to further improve cycle time. These attributes make die casting the preferred method for producing a wide variety of automotive parts, especially powertrain components that require extremely high precision. Modern light-weighting initiatives designed to reduce auto emissions are also making zinc, magnesium, and aluminum more attractive as

automotive and aerospace materials, increasing the relevance for die casting and even expanding its role to large structural components in some cases.

Dies are machined from multiple thick section of hot work tool steel. Die casting die manufacturing is expensive and dies need a long life to maximize productivity and minimize part costs. Die maintenance and replacement is a major source of down time for casting operators, highlighting the need for more resistant die materials. Die casting machine down time has a negative effect to die casters' profitability. Robust die materials are essential for increasing profits.

High Pressure Die Casting Die Materials

Since the inception of die casting, ferrous alloys have by far been the most commonly used die materials (6). Although cast iron and other variations were used for decades, tool steels enabled casters to get more parts made per die before their failure. The creation of the first tool steels, referred to as high speed steels due to their wide use in high speed machining operations, is most commonly accredited to England's Robert Mushet (7). Mushet was one of the first metallurgists to discover how some alloying elements increased steel's hardenability. In the 1860's, it was understood that quenching ferrous alloys resulted in an increase in hardness, but Mushet discovered that some alloying elements resulted in hardened steel independent of cooling rate, tungsten (W) in Mushet's case (7). Commercial Mushet steel compositions from the early 1900's are shown below.

C.	W.	Cr.	Mn.	Mo.
1.67	7.60	3.70	.48	.00
2.20	5.90	.60	1.35	.00
1.20	8.05	2.10	.35	.00
1.40	.00	3.50	1.60	4.50

Figure 2: Mushet Steel Compositions from Early 1900's (7)

High speed steels did not gain wider acceptance until the importance of thermal cycle on steel microstructure was developed by McKenna whose work developed better steel properties through high temperature treatment and quenching (7). After the discoveries of Mushet's air hardening steel compositions and McKenna's heat treatments, many patents were filed for improved steels. At the turn of the 20th century and the decade following, the importance of vanadium (V) and molybdenum (Mo) were realized, resulting in cheaper, tougher, and more resilient steels. Subsequent advancements in composition and processing eventually resulted in the high temperature die materials used today.

Phases and Phase Transformations in Steels

Tool steels remain the backbone of the casting industry, and their widespread use in other applications has enabled numerous advancements since adoption for casting dies in the late 19th century. Steels are iron based alloys that contain carbon in concentrations under approximately 2 wt.%. Over 3,500 steel grades exist, all of which have compositions tailored to achieve certain properties. Steel is an extremely versatile material family with a huge range of properties possible due a range of strengthening mechanisms. In particular allotropic (solid state) phase transformations that occur during cooling after solidification to room temperature can be used to achieve a range of microstructure and properties. Steel alloys are comprised primarily of 3

phases: ferrite, austenite, and carbides. The Iron-Iron Carbide phase diagram is shown below to illustrate the equilibrium microstructure in Fe-C alloys.

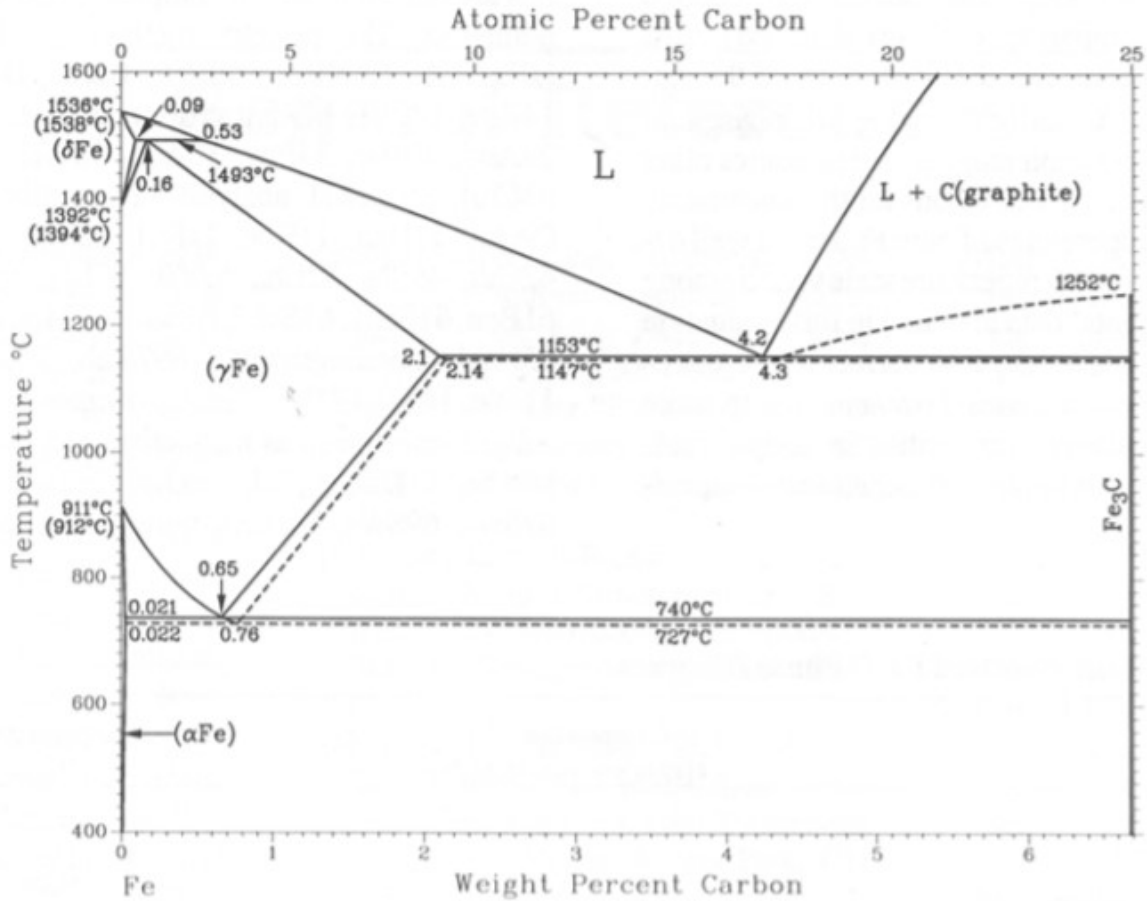


Figure 3 : Fe-Fe₃C Phase Diagram (8)

Ferrite is present just before the melting temperature is reached and at temperatures below the eutectoid temperature (727°C) in low carbon and ferritic low alloy steels. Between the two ferrite phase fields, FCC austenite is stable, and it is this allotropic phase transformation from austenite back to ferrite that enables such diversity in steel microstructures. Below the eutectoid temperature, microstructure combinations of ferrite and cementite (carbides) are possible depending on composition and cooling rate. Different morphologies of ferrite plus metal

(MxCy) carbides present even more avenues for property refinement for steels. This is illustrated in isothermal transformation diagrams such as those shown below for an H13 steel.

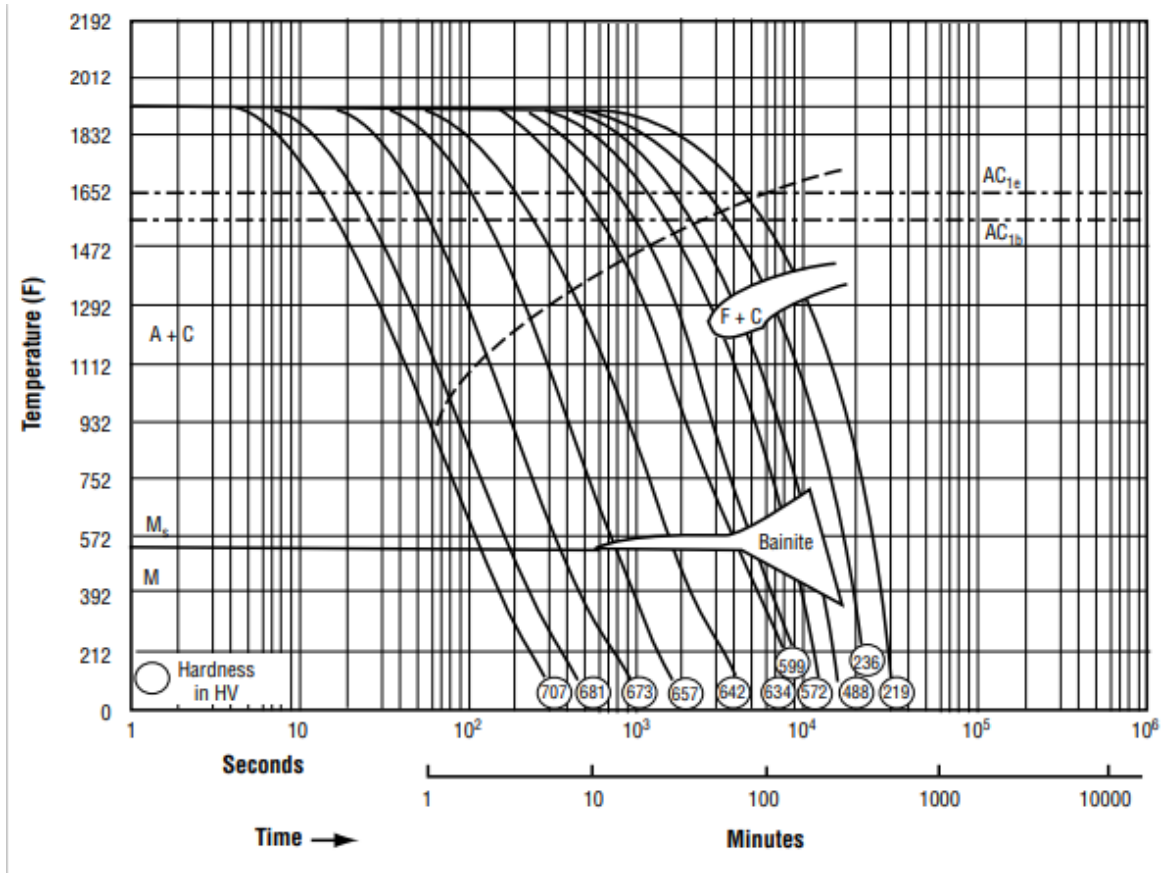


Figure 4: H13 Continuous Cooling Transformation Diagram (9)

If austenite is cooled quickly before diffusion can take place to form ferrite, a microstructural constituent known as martensite is formed. Low carbon solubility in the ferrite phase vs. austenite prevents ferrite of the same composition as austenite from forming during cooling, instead forcing the microstructure into a metastable Body Centered Tetragonal (BCT) arrangement, known as martensite (10). BCT martensite is essentially an intermediary between FCC austenite and BCC ferrite crystal structures. This is illustrated in the Figure 5.

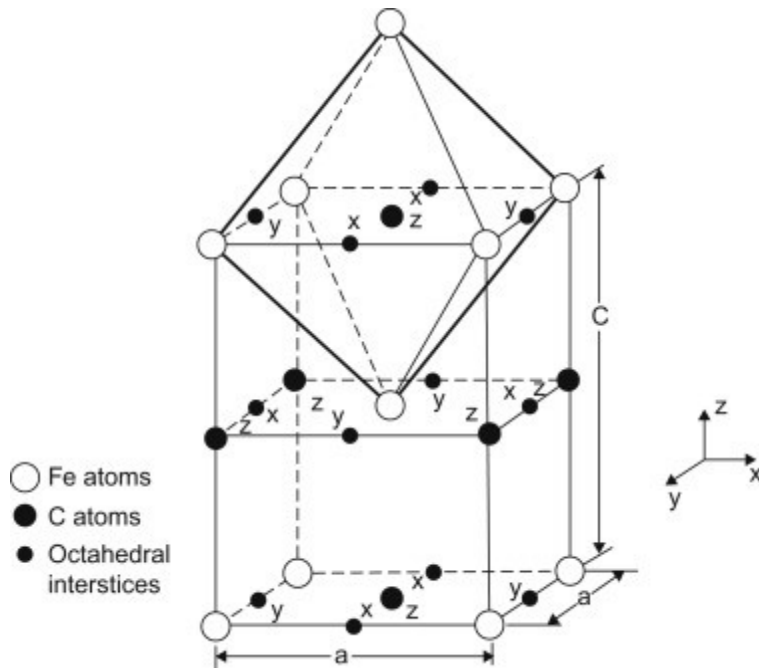


Figure 5 : Martensite Crystal Lattice (10)

Martensite formation involves a diffusionless, displacive transformation from FCC austenite into what is essentially a BCC structure supersaturated with carbon. Upon heating to elevated temperatures below the eutectoid temperature, this structure begins to rearrange into a network of ferrite and carbides. This structure is known as tempered martensite. Tempered martensite is renowned for its combination of high strength and toughness and is relied on in numerous applications. Hot work tool steels are designed to form martensite over a wide range of cooling rates, which is then tempered to form high temperature stable carbides. Hot work tool steel compositions are formulated to enable thick blocks to have through-thickness tempered martensitic microstructure.

Hot Work Tool Steel Metallurgy

Hot work tool steels, given the H designation by AISI, are divided into three main groups depending on the main alloying element present. These groups are chromium hot work tool steels

(types H10 - H19), tungsten hot work tool steels (types H21 - H26) , and molybdenum hot work tool steels (types H42 and H43) (6). In die casting applications involving light metals, by far the most common choice are chromium-type hot work tool steels due to their lower cost. In particular, H11 and H13 are widely used grades which possess excellent combinations of high temperature strength and toughness, and resistance to softening, heat checking, and liquid metal corrosion (8). H11 and H13 differ mainly in their vanadium content, with H13 possessing around 1 wt.% vanadium whereas H11 steel possesses around .6 wt.% vanadium (8). Higher amounts of vanadium give H13 increased softening and wear resistance vs. H11, but the lower amounts of vanadium in H11 result in increased toughness relative to H13. Some H13 and H11 tool steel grades are shown below.

ASTM A681	C		Mn		P	S	Si		Cr		V		Mo	
H13	0.32	0.45	0.2	0.6	0.03	0.03	0.8	1.25	4.75	5.5	0.8	1.2	1.1	1.75
DIN ISO 4957	C		Mn		P	S	Si		Cr		V		Mo	
1.2344 /X40CrMoV5-1	0.35	0.42	0.25	0.5	0.03	0.02	0.8	1.2	4.8	5.5	0.85	1.15	1.1	1.5
JIS G4404	C		Mn		P	S	Si		Cr		V		Mo	
SKD61	0.35	0.42	0.25	0.5	0.03	0.02	0.8	1.2	4.8	5.5	0.8	1.15	1.0	1.5

Table 1 : H13 Tool Steels and Compositions (11)

ASTM A681	C		Mn		P	S	Si		Cr		V		W	Mo	
H11/T20811	0.35	0.45	0.20	0.60	0.03	0.03	0.80	1.25	4.75	5.50	0.30	0.60	...	1.10	1.60
DIN ISO 4957	C		Mn		P	S	Si		Cr		V		W	Mo	
1.2343/X37CrMoV5-1	0.28	0.35	0.10	0.40	0.80	1.20	2.70	3.20	0.40	0.70	...	1.10	1.50
JIS G4404	C		Mn		P	S	Si		Cr		V		W	Mo	
SKD6	0.32	0.42	...	0.50	0.03	0.03	0.80	1.20	4.50	5.50	0.30	0.50	...	1.00	1.50
BS 4659	C		Mn		P	S	Si		Cr		V		W	Mo	
BH11	0.32	0.40	...	0.40	0.35	0.35	0.85	1.15	4.75	5.25	0.30	0.50	...	1.25	1.75

Table 2 : H11 Tool Steel Grades and Compositions (11)

It should be noted that different regions have industrial preferences for hot work tool steel selection for high pressure die casting applications. Whereas H13 is the most common grade used for dies in the western hemisphere and particularly the U.S.A, H11 is used more frequently in Europe.

Role of Alloying Elements in Tool Steels

Chromium is one of the most important alloying elements for ferrous alloys, a fact that's true for hot work tool steels as well. Although additions of chromium are normally associated with improved oxidative corrosion resistance, oxidation is generally not a major concern for die casting dies made of hot work tool steels. Corrosion in high pressure die casting applications does not normally involve oxidation induced failures, but rather liquid metal corrosion (2). The alloying additions of chromium in common hot work tool steels such as H13 of around 5 wt.% are insufficient to prevent this type of damage. Instead, chromium is added to hot work tool steels to ensure adequate hardness over a wide range of cooling rates.

Chromium is often termed a ferrite stabilizing element, but it has a profoundly important effect on the hardenability of steels by retarding the formation of pearlite. Chromium bearing steels form martensite at slower cooling rates vs. steels without chromium. This is illustrated by comparing continuous cooling transformation diagrams of 3.25Cr1Mo.2V and 9Cr1Mo steels.

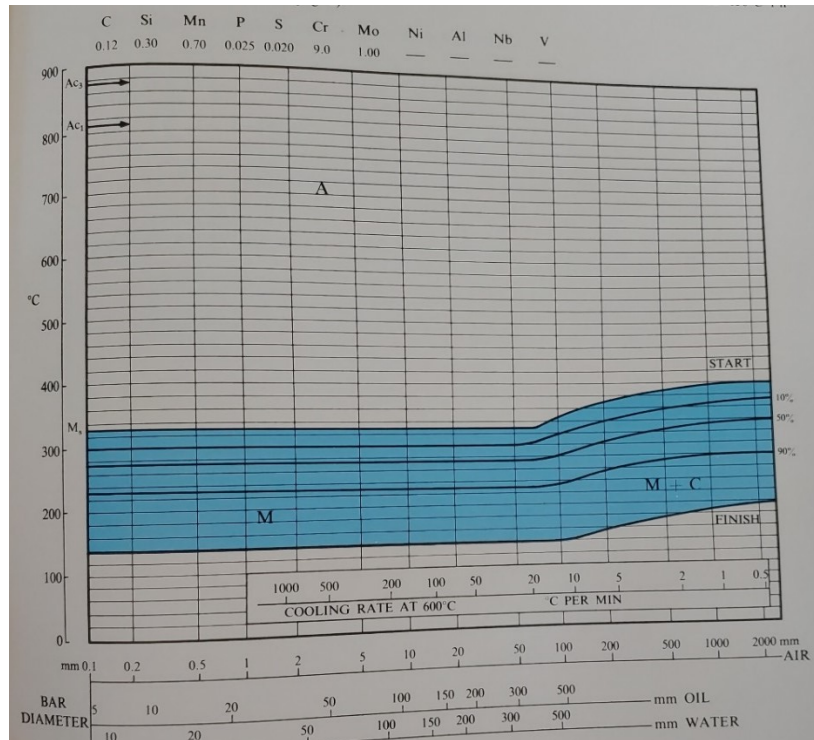


Figure 8 : 9Cr1Mo Continuous Cooling Transformation Diagram (12)

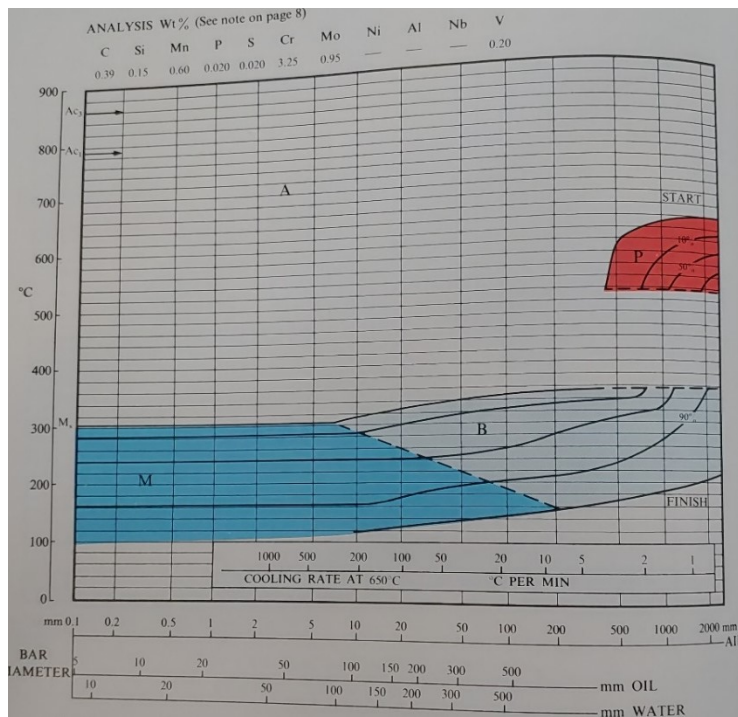


Figure 9 : 3.25Cr1Mo.2V Continuous Cooling Transformation Diagram (12)

As seen in figure 8 and 9, although the 3.125Cr1Mo.2V composition listed has a significantly higher composition of the hardenability increasing element carbon, the grade 91 sample forms martensite over slower cooling rates. Chromium's role on hardenability is fundamentally important to die steels since these materials are often formed in blocks up to 4 feet thick (2). The cooling rate in large thick pieces depends on the location in thickness, with external surfaces experiencing significantly higher cooling rates than the center. Slow cooling rates can result in inferior microstructures such as bainite, pearlite, or ferrite that lack the sought-after properties of tempered martensite formed in hardenable steels. The relative effect of alloying elements on hardenability has been quantified by numerous formulas which seek to quantify the relative action of certain alloying elements. These formulas are commonly used in arc welding to predict hydrogen cracking susceptibility. One such formula that encompasses a wider range of carbon contents and interaction effects was developed by Nobutaka et. al (33). This carbon equivalency (CE_N) equation is shown below in Formula 1:

$$CE_N = C + A(C) * \left(\frac{Si}{24} + \frac{Mn}{6} + \frac{Cu}{15} + \frac{Ni}{20} + \frac{Cr + Mo + Nb + V}{5} + 5B \right)$$

$$A(C) = .75 + .25 \tanh[20(C - .12)]$$

Formula 1: Nobutaka et. al's Carbon Equivalency Formula (32)

By adding Chromium and Molybdenum, martensite forms upon cooling at slower cooling rates. Chromium is also a carbide forming element, although it does not contribute to high temperature resilience to the same extent of other alloy carbides.

Vanadium is an alloying element added to steels to form stable carbides in order to improve hot hardness (12). Vanadium carbides are stable up to very high temperatures, but if

nitrogen is present in sufficient quantities, vanadium nitrides / carbonitrides can form which are stable at even higher temperatures, as shown in the figure below.

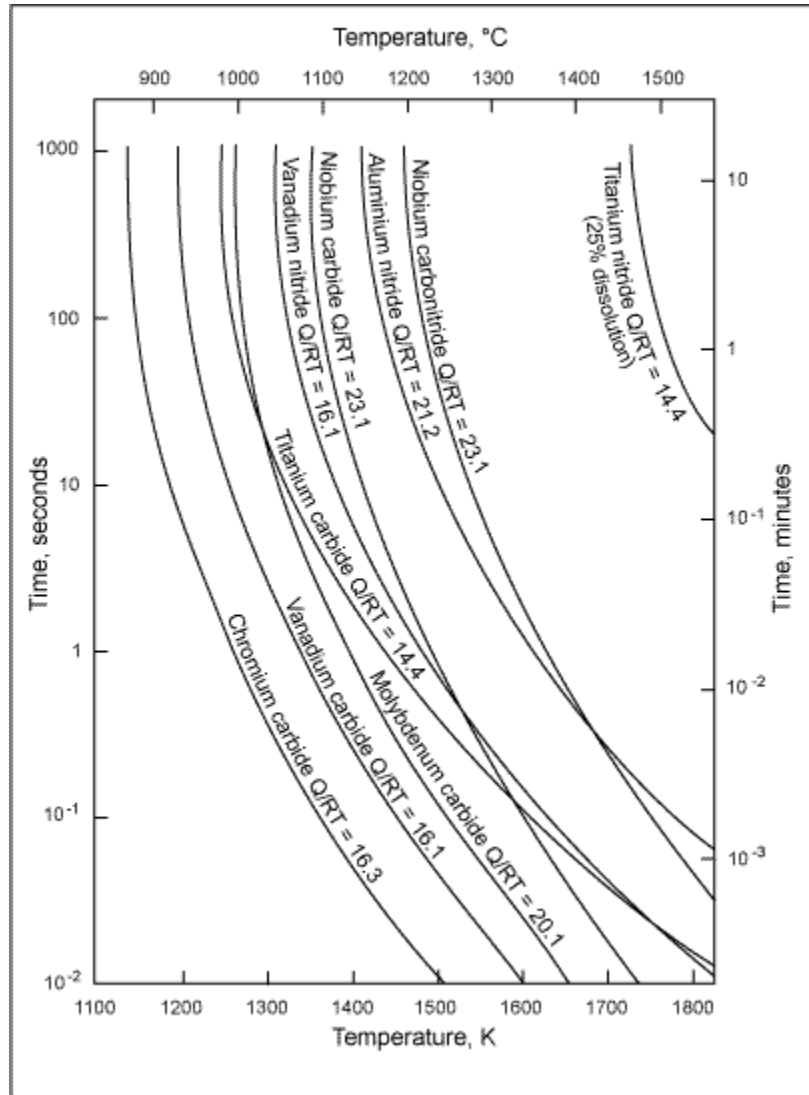


Figure 10 : Precipitate Stability in Steels (13)

The high temperature stability of vanadium precipitates in steels contributes to its widespread use in a wide range of alloys, not just hot work tool steels. Investigators have previously found that nitrogen additions to nominal H13 compositions can lead to improved service lives due to the presence of Vanadium carbonitrides, but this is not yet common practice

(15). Previous researchers have found that, in the composition range common for hot work tool steels, vanadium additions can provide increased hardness and wear resistance without sacrificing toughness dramatically (13). Since vanadium forms at high temperatures, it also acts as an effective grain size refiner (16).

Other important carbide forming elements in hot work tool steels are Molybdenum and Tungsten, which provide a large contribution to hot hardness and strength. Both molybdenum and Tungsten form similar types of carbides, but Molybdenum is more commonly used in hot work tool steels due to its lower cost. Steels containing elevated Molybdenum levels have been shown to perform well in high pressure die casting applications, the primary reason being their resistance to softening, Figure 11 during exposure to elevated temperatures (17).

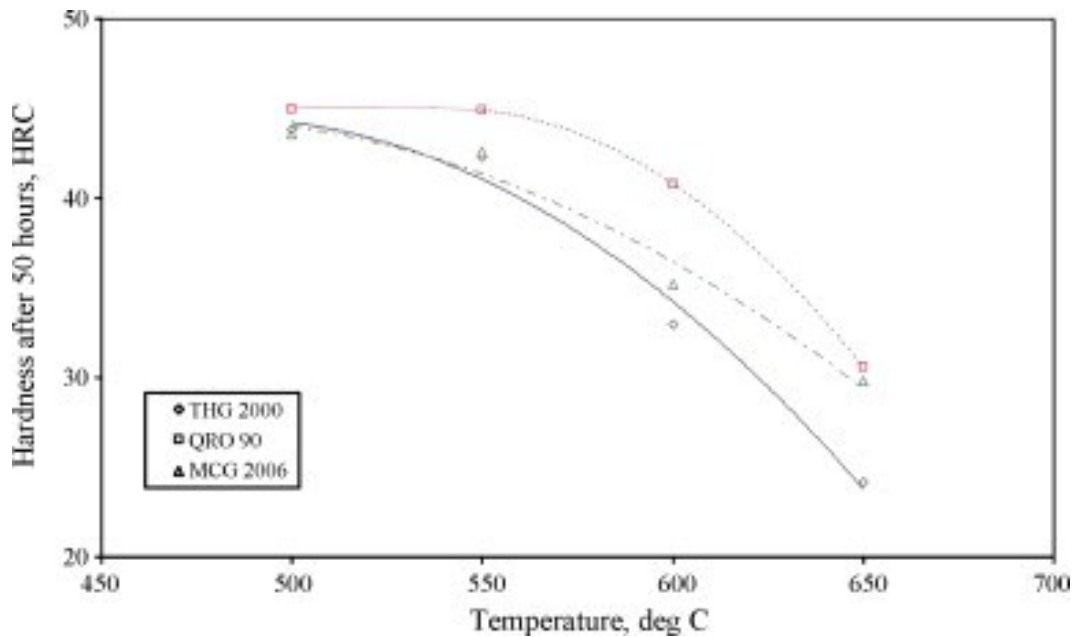


Figure 11 : Softening VS. Exposure Temp for Several HWTS (17)

Alloying additions are intended to increase high temperature strength through secondary carbide precipitation. The largest contribution to elevated temperature strength comes from primary Mo₆C carbide and primary VC carbides in hot work tool steels such as H13 and H11 (18).

Molybdenum and Vanadium carbide additions give hot work tool steels advantageous properties such as good hot hardness and resistance to softening vs. other carbides. This helps limit microstructural aging during service and retards softening of the dies. Unfortunately, even new grades of hot work tool steels begin to form heat checking cracks in as little as 500 cycles, with soldering and washout damage occurring shortly thereafter (2). Hot work tool steels age at temperatures used for die casting, Figure 11. In service softening lowers the hot yield strength of hot work tool steel dies, which eventually leads to plastic surface damage and cracking and need for repair.

Refractory Materials In Die Casting

In particularly demanding applications, casting operators sometimes choose to use refractory alloy die inserts over tool steels based on insufficient life of die steels. Both molybdenum and tungsten alloys have been used in the past, but tungsten alloys are generally preferred over molybdenum because of their superior resistance to liquid metal corrosion and oxidation and increased strength (10). Refractory dies are more resilient than tool steels not just due to liquid metal corrosion resistance, but also a host of other advantageous properties as well. Both molybdenum and tungsten possess extremely high thermal conductivity vs. tool steels, which enables more efficient cooling of die surfaces and reduced cycle times. Both materials also have significantly higher heat capacity and significantly lower thermal expansion vs. tool steels. These refractory material properties prevent large thermal stresses from developing at die

surfaces, an aspect that furthers their resistance to cracking resulting from thermal fluctuations during casting, which is perhaps the most important criteria for die life.

High cost is the main factor limiting implementation of refractory die casting dies. Since they are often an order of magnitude more expensive than die steels, wholly tungsten or molybdenum alloy dies are cost-prohibitive. This limits refractory alloy applications to the most demanding applications and are selectively used as bolt-on inserts for small regions of die. Tungsten based Anviloy inserts have been preferred in the most challenging die regions since the 1970's (18).

Claddings/overlays are often used in corrosion applications to limit expensive material usage to working surfaces only, but tungsten and molybdenum both form intermetallics with iron, complicating cladding of steel dies with refractories. Tungsten and molybdenum also possess poor wire drawability, making it difficult to automate a potential process using these pure metals. New advances in Anviloy alloy formulation (W-27.5Ni-12.5Fe alloy) and drawing technology have enabled wire production with this alloy. This new alloy possesses increased ductility that enables wire drawing, but also helps reduce intermetallic formation compared to pure tungsten when clad onto H13. These enhanced characteristics are achieved through greater nickel and iron alloying additions.

Failure Mechanisms in HPDC

Due to the extreme environment in HPDC, die lives are much shorter than predicted fatigue lives if mechanical forces alone are considered. Failures in aluminum high pressure die casting operations generally involve one or more phenomena including: thermal fatigue cracking or heat checking of the die, soldering of molten melt to the die face, or carbonaceous buildup

from lubricating compounds used between cycles. Exact failure mechanism depends on factors such as die material, injected material, die stress state, and die temperature, which is dependent on process parameters and die geometry.

Thermal Fatigue Cracking : Heat Checking

Thermal fatigue cracking of dies is the main concern for parts that experience high thermal stresses. Runners and pins are subjected to high thermally-induced stresses during initial contact with molten aluminum. Thermal fatigue cracking also occurs on edge surfaces of dies such as corners or geometric features. This type of cracking is also known in the die casting industry as heat checking, and the mechanism behind it can be explained by the Kindbom Theory (6).

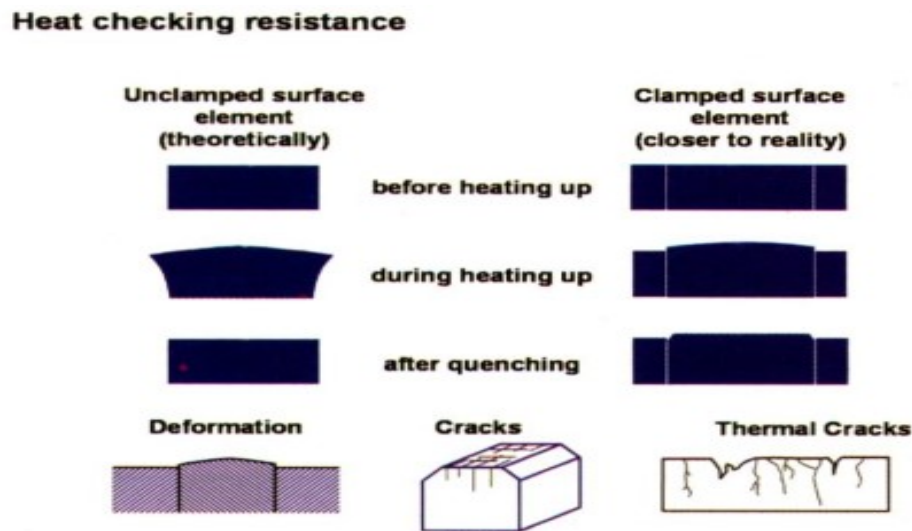


Figure 12 : Kindbom Theory (6)

The Kindbom theory states that surface elements in casting are subject to restraint from cooler surrounding material. During the hot phase of die casting, surface elements are subject to very high compressive forces that often lead to compressive plastic strain. The heated surface is

constrained by surrounding material that is cooler and therefore stronger, ultimately leading to compressive plastic strain accumulation at the die surface. When the surface that has been plastically deformed to smaller dimensions cools down, such as during part ejection and in between cycles, tensile stresses then develop. These tensile stresses are then able to open and propagate cracks. Formulae for resistance to heat checking have been developed according to their general material properties. One of these formulas is shown below in Figure 13.

$$D = Rp_{0.2} * \lambda / (\alpha * E * cp * \rho)$$

Where: D=heat checking resistance, $Rp_{0.2}$ =hot yield strength, λ =thermal conductivity, α = thermal expansion coefficient, E=Young's Modulus, cp = heat capacity, ρ = density

Figure 13 : Formula for Heat Checking Resistance (14)

The higher the value of D, the more resistant a material is to heat checking. High hot yield strength and thermal conductivity are beneficial to the resistance of heat checking, whereas high CTE and modulus play an adverse role. High thermal conductivity reduces the temperature gradient and resulting thermal stresses experienced by the constrained surface elements. Low thermal expansion is beneficial due to the decreased deformation upon heating. Examples of internal restraint can be differences in thermal expansion between adjacent phases in materials themselves, or simply temperature gradients within materials (13). After crack initiation, thermal fatigue cracks will enter a regime of controlled crack growth dictated by material fracture toughness and induced stress, eventually leading to gross uncontrolled failure.

Liquid Metal Damage : Soldering and Washout

Corrosive damage occurs by two main mechanisms in aluminum die casting: soldering and washout damage. For common tool steels used in aluminum die casting, most of the alloying elements are somewhat soluble in molten aluminum, leading to the formation of brittle intermetallics that can act as stress concentrators or crack initiation sites during service (20). An example of soldering buildup on H13 is shown below in Figure 14.

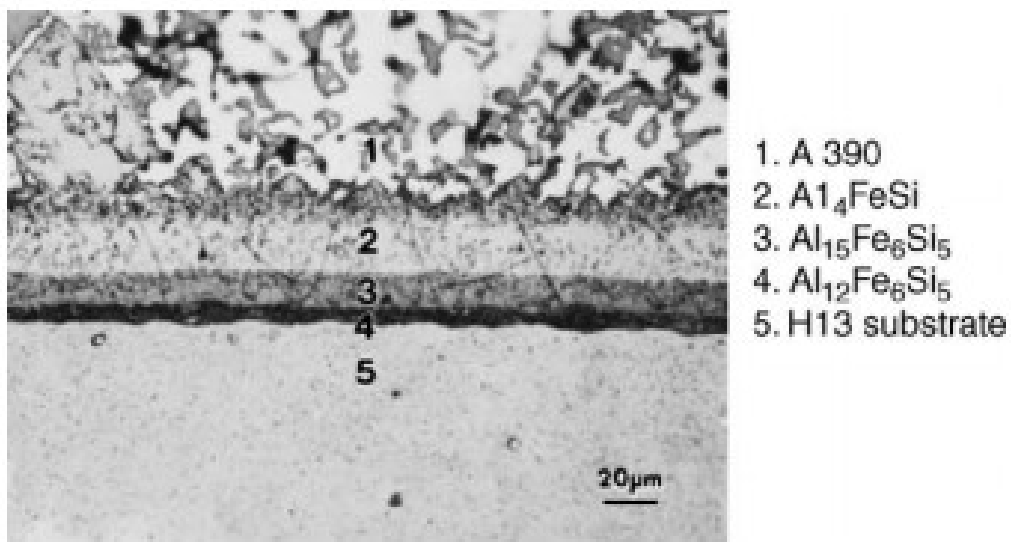


Figure 14 : Intermetallic Formation on H13 in a Soldering Simulation (20)

Soldering of aluminum onto surfaces requires some level of chemical interaction between molten aluminum and the die material. This chemical interaction can also cause liquid impingement into previously propagated cracks at the surface, potentially exacerbating washout damage (20). Although erosion and formation of metallurgical bonds between die cast parts and molds is colloquially referred to as “soldering” in the die casting industry, it should be noted that the temperatures associated with die casting of aluminum make the phenomenon more akin to brazing than soldering.

In some material combinations, such as copper based alloy dies for aluminum die casting, another form of chemical attack occurs where die surfaces are slowly dissolved away by the aluminum melt. This dissolution of the die surface, where the liquid metal essentially acts as a solvent that gradually removes material, is different from soldering because it involves weight loss without the formation of intermetallics. It also differs from mechanical washout because it is not associated with physical wear resulting from high flow. Rather, chemical dissolution occurs strictly because of chemical solvation of the die material in the molten melt (20). The higher the solubility of the die material in the molten melt, the higher the susceptibility to this form of damage. For steel and refractory dies in aluminum die casting, this is generally not a major concern (9).

Erosive wear can occur in die casting when the high temperature melt is injected at high speeds into the die. Mechanical erosion of the die is related to several factors, including the presence of solid particles in the melt leading to mechanical wear of the die, the formation and collapse of bubbles in the molten melt due to pressure fluctuations (cavitation) during injection, or adhesive wear caused by excess sticking of the part to the die surface leading to wear during ejection (2).

Another possible contributor to the short lives of die casting materials is the Rehbinder effect. This phenomena involves reactive wetting of a liquid onto a solid. A schematic of the Rehbinder effect can be seen in Figure 15.

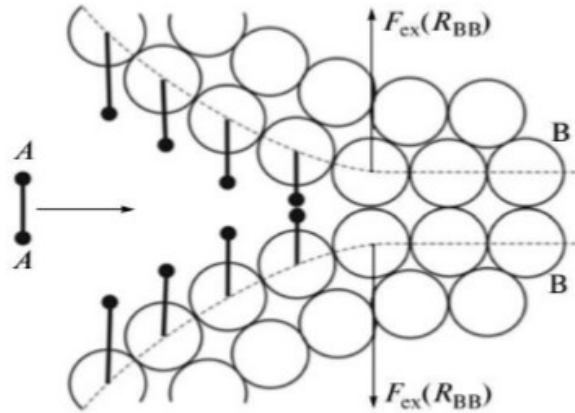


Figure 15 : Rehbinder Effect (22)

Wetting of molten aluminum onto steel occurs as a result of reactive wetting. Adsorption of a reactive liquid to the surface of a solid reduces the surface energy related to crack opening and propagation. This occurs when liquid-solid atom attraction is greater than solid-solid atom attraction, as is the case with thermodynamically favorable intermetallic formation reactions seen in die casting. The result of reduction in solid-solid atom attraction is a dramatic reduction in the fracture strength of the solid in the reactive liquid, leading to easier crack opening and propagation.

Die repair Methodologies

Repair of damaged dies usually involves removal of cracked or soldered die material by abrasive grinding, burring or machining followed by repair welding deposition. This material deposition can be carried out via a number of processes such as powder or wire fed laser or electron beam systems or arc welding processes (5, 24-32). Laser and electron beam processes are generally automated, but arc welding processes can also be carried out by manual welders (24, 27-30). The most common method for die repair are the manual arc welding processes, particularly the gas tungsten arc welding (GTAW) process (5, 24). GTAW is regularly employed

due to a combination of factors including robust consumable market, relatively cheap machine costs, and a highly developed work force. GTAW provides more precise control over heat input and material deposition than other arc welding processes, which is a valuable attribute when considering the high complexity of many die casting dies.

Unfortunately, the heat from all fusion based repair processes causes detrimental effects on die microstructures in unmelted heat affected zone regions adjacent to repairs (5, 25). Heat input from repair methods results in dissolution of carbides into austenite and transformation to untempered martensite upon cooling. This elicits a need for heat treatment after repair (5, 6, 25). Since die casting dies regularly reach thousands of pounds in size, heat treatment is often a time consuming and costly endeavor, especially when multiple tempering cycles are often needed to achieve an acceptable microstructure (6, 19).

Chapter 3: Objectives

This effort focused on developing automated arc welding repair procedures, characterizing clad deposit microstructures, evaluating tempering effects in H13 heat affected zones (HAZ), and developing cladding parameters for future in-plant trials using new Anviloy alloy wire on H13 die material. The Hot Wire Gas Tungsten Arc Welding (HW-GTAW) was primarily used to evaluate clad procedure effects on deposit microstructures and H13 heat affected zone tempering. Robotic Gas Metal Arc Welding Pulse (GMAW-P) procedures were developed to clad production shot block dies, which had complex features. The cladded shot blocks will be used in plant trials and the resulting performance are an area for future work. The research objectives were divided into four related studies as follows:

1. Anviloy Wire HW-GTAW Cladding Procedure Development for H13
 - a. Develop HW-GTAW procedures for Anviloy wire cladding of H13 in flat (1G) position using bead on plate tests.
 - b. Determine minimum heat input / dilution for acceptable Anviloy wire-H13 clad deposits with HW-GTAW process.
2. Anviloy Wire Robotic GMAW-P Conformal Cladding Die Development
 - a. Evaluate commercial OTC GMAW-P waveforms for Anviloy wire metal transfer and H13 cladding by making flat (1G) bead on plate clads using a robotic GMAW-P system.
 - b. Develop 6-axis robotic Anviloy cladding procedures for conformal cladding the shot block face (1G - flat position) and shoulder profile (2G - horizontal position) while shot block die is positioned flat.

- c. Develop robotic conformal cladding procedure and provide cladded shot-block dies for ongoing in-plant trials, which will evaluate Anviloy cladding performance on a high volume drive train component casting.
3. Feasibility of H13 Temperbead Repair using Anviloy HW-GTAW Cladding Procedures
- a. Determine effect of weld preheat on H13 HAZ size distribution using metallography to measure HAZ lengths
 - b. Determine preferred heat input range for temperbead repair of H13 using Anviloy wire by measuring HAZ lengths with metallograph
 - c. Quantify effectiveness of H13 temperbead repair procedure vs. normal procedures using microhardness mapping
4. Microstructure Characterization of Anviloy Cladding Deposits on-H13 Die Steel
- a. Metallographically characterize arc melted Anviloy wire microstructures of undiluted cast samples
 - b. Characterize Anviloy wire – H13 clad fusion zones with metallography, SEM, and EDS of clad deposits
 - c. Compare Characterization results to Thermocalc™ simulations
 - d. Characterize heat treated Anviloy and Anviloy - 308L butter clads on H13 using metallography

Each of these studies are reported as separate papers in Appendix A, B, C and D respectively. A summary of the key results and discussion is provided in Chapter 4.

Chapter 4 : Results and Discussion

4.1 Anviloy Wire HW-GTAW Cladding Procedure Development for H13

The detailed paper for this research study can be found in Appendix A. All HW-GTAW welds were made using a Jetline 9800 mechanized welding system with a Dynasty 500 power supply and Jetline 200Amp AC hot wire power supply. All Anviloy deposits on H13 were made using pure argon shielding gas. Clad deposits were inspected visually and metallographically sectioned to determine clad quality. On initial trials to establish preferred hot wire setup conditions, wire cast and helix inconsistency led to bead uniformity issues. These issues were rectified by using two in-line single axis miller wire straighteners mounted 90 degrees relative to each other's roll forming directions. Preliminary bead plate weld with and without the wire straightener are shown Figure 16. A range of additional experiments were conducted to develop preferred hot wire conditions that yielded smooth, uniform deposits that were sound.

One issue that was discovered was Anviloy wire inclusions, Figure 17. Several factors were found to influence incomplete melting of Anviloy wire filler material. Insufficient welding heat input can promote unmelted wire inclusions by providing insufficient heat to melt the consumable. Insufficient hot wire heating due to interruptions in the hot wire electrical circuit, such as breakdown of bridging metal transfer, can also cause unmelted wire inclusions. These disruptions to hot wire heating are exacerbated by large hot wire stickouts or irregular wire cast and helix that cause the wire to make contact outside of the weld pool. Another variable influencing unmelted wire defects was weave dwell time in multi pass clad procedures. This issue was eliminated with the wire straightener and preferred hot wire parameters.



Figure 16: CW-GTAW Welds Made Without Wire Straightener (Top) Vs. Early Development HW-GTAW Welds Made with Wire Straightener (Bottom)

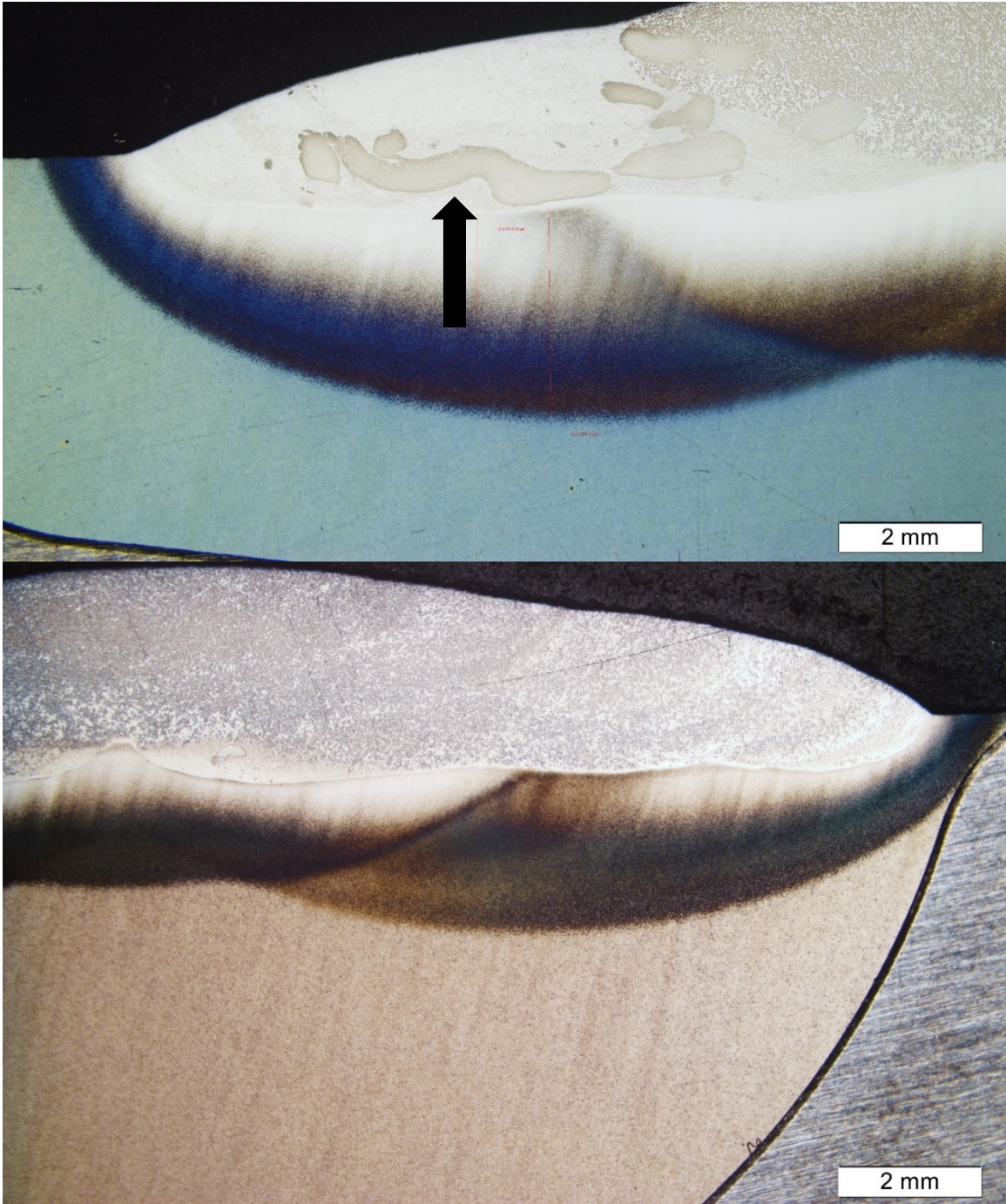


Figure 17 : Anviloy Wire-H13 HW-GTAW Clads with (top) and without (bottom) Unmelted Wire Defects Indicated by Arrow

Preferred hot wire setup conditions were determined to be $\frac{3}{4}$ -inch stickout, 4V hot wire, 80-ipm wire feed speed, 3-ipm travel speed, and 11.5 volts GTAW. The latter provided a long arc length that was approximately $\frac{3}{16}$ to $\frac{1}{4}$ -inch and made it easier to control the hot wire feed. These conditions produced continuous bridging metal transfer where the wire fully melted before entering the weld pool. Using these constant deposit area conditions, the effects of current on base metal dilution was investigated. Three welds at 140, 160, and 180Amp currents are shown with their parameters in Figure 18.

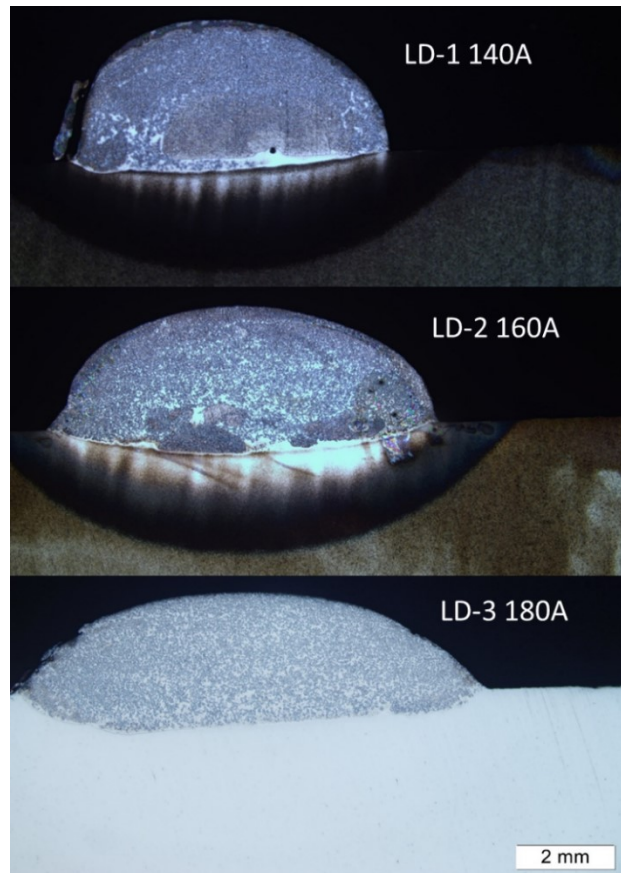


Figure 18 : Low Dilution Trial Welds

Weld	Arc Current (A)	Arc Voltage (V)	Travel Speed (in./min.)	HW-Stickout (in.)	Wire Feed Speed	Hotwire Voltage (V)
LD-1	140	11.5	3	0.75	80	4
LD-2	160	11.5	3	0.75	80	4
LD-3	180	11.5	3	0.75	80	4

Table 18 : Low Dilution Trial Weld Parameters

Welds using 140 and 160Amps at the listed weld parameters resulted in welds with high toe angles and porosity. Adequate base metal fusion and good toe angles were achieved using 180Amp current, which resulted in welds with dilutions of 18%. Using these conditions as a starting point, a range of single and double layer deposits were made to evaluate HAZ tempering in section 4.3

4.2 Anviloy Wire-H13 Robotic GMAW conformal Cladding Parameter Development

Robotic GMAW was selected to conformally clad the trial shot block because of its improved accessibility compared to robotic HW-GTAW systems. Preprogrammed pulse waveforms for Anviloy wire did not exist, so commercial waveform for other materials were evaluated. The robotic GMAW-P bead on plate tests used an OTC robot with a Welbee 500 power supply. Initial tests used the OTC Synchrofeed Ferrite 1.2mm waveform which was reported to require higher energy to help melt the Anviloy Wire. A series of flat bead on plate welds were made over a varied travel speed range to this waveform's feasibility for Anviloy GMAW-P cladding of H13. The Synchrofeed Ferrite 1.2mm waveform was limited to a 250A

maximum current and was found to have insufficient heat to produce smooth and uniform Anviloy beads, Figure 19.



Figure 19 : 1G GMAW Synchrofeed Welds Showing Lack of Fusion

	Weld 21	Weld 22	weld 23	weld 24
OTC waveform type	MIG_4 DC Sfeed 1.2 ferrite	MIG_4 DC Sfeed 1.2 ferrite	MIG_4 DC Sfeed 1.2 ferrite	MIG_4 DC Sfeed 1.2 ferrite
CTWD (inches)	.75"	.75"	.75"	.75"
Welding Current (Amps)	250	250	250	250
Welding travel speed (IPM)	12	23	16	9

Table 19 : 1G GMAW Synchrofeed Welds Showing Lack of Fusion Parameters

These bead on plate tests showed poor quality deposits at each tested travel speed. Welds had irregular bead height, width, and surface appearance due to unstable melting and fusion. All welds had insufficient fusion at weld toes, indicating a higher power waveform was necessary to achieve good fusion of Anviloy Wire to H13.

The next waveform evaluated was the DC- Pulse 1.2mm SuS waveform and over high power levels with weld currents up to 270 amps. Weld beads produced at 250amps using the DC- Pulse 1.2mm SuS waveform had better quality upon visual examination than those produced with the Synchrofeed Ferrite 1.2mm waveform at 250A. Welds made at 270A using the DC- Pulse waveform resulted in significantly lower bead height variation than those made with Synchrofeed at 250A. Also, beads produced at 270A show much better fusion to the base material and were made without lack of fusion defects. These welds are shown in Figure 20.

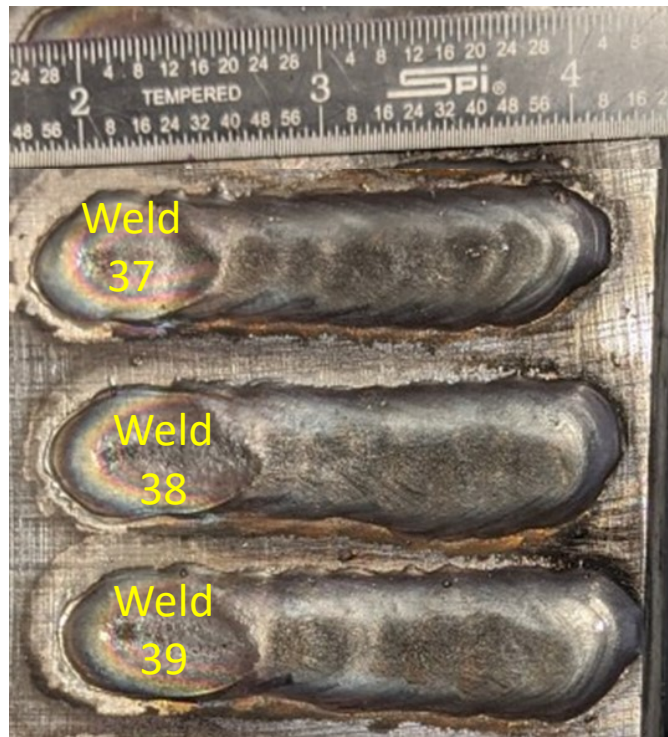


Figure 20 : Welds Using the DC- Wave 1.2mm SuS waveform at 270A

Weld #	37	38	39
OTC waveform type	DC- Pulse 1.2 Ferrite	DC- Pulse 1.2 Ferrite	DC- Pulse 1.2 Ferrite
CTWD (inches)	.75"	.75"	.75"
Welding Current (Amps)	270	270*	270
Welding travel speed (IPM)	45	50	50

Table 20 : Welds Parameters for the DC- Wave 1.2mm SuS waveform at 270A

Though these welds resulted in superior fusion, width irregularities are still evident. Trim settings were varied in the asterisked weld 38, but waveform trim alterations had little effect on bead quality. A welding weave oscillation was employed to help improve bead shape consistency. Using oscillation, the preferred bead on plate parameters and test deposits are shown in Figure 21.



Figure 21 : Weld Using the DC- Wave 1.2mm SuS waveform at 260A Using Oscillation

OTC waveform type	DC- Pulse 1.2 Ferrite	Oscillation Type	Linear
CTWD (inches)	.75"	Oscillation Amplitude (mm)	8
Welding Current (Amps)	260	Oscillation Frequency (Hz)	1
Welding travel speed (IPM)	40	Oscillation Dwell Time (sec.)	0

Table 21 : Parameters for DC- Wave 1.2mm SuS waveform Weld at 260A Using Oscillation

The weld in Figure 21 had uniform bead width. These parameters were then used to verify multi-pass tie ins were possible using the DC- Wave 1.2mm SuS waveform at 260A. That sample is shown in Figure 22.



Figure 22 : Multi-pass 1G Robotic GMAW Clad Procedure

The 5 weld passes shown in Figure 22 verified preferred GMAW-P procedure for making multi-pass clads. This 5 pass layer resulted in low bead height and width variation as well as excellent tie-in to adjacent passes.

Horizontal (2G) parameter development was needed to clad the vertical section of the shot block. This shot block section was complicated by torch accessibility issues which mandated sub-optimal torch work angles. Sub-optimal work angle resulted in poor bead appearance due to “humping” and extreme height irregularity. A torch angle oscillation was then employed to improve horizontal position welding. The torch work angle oscillation is pictured in Figure 23.

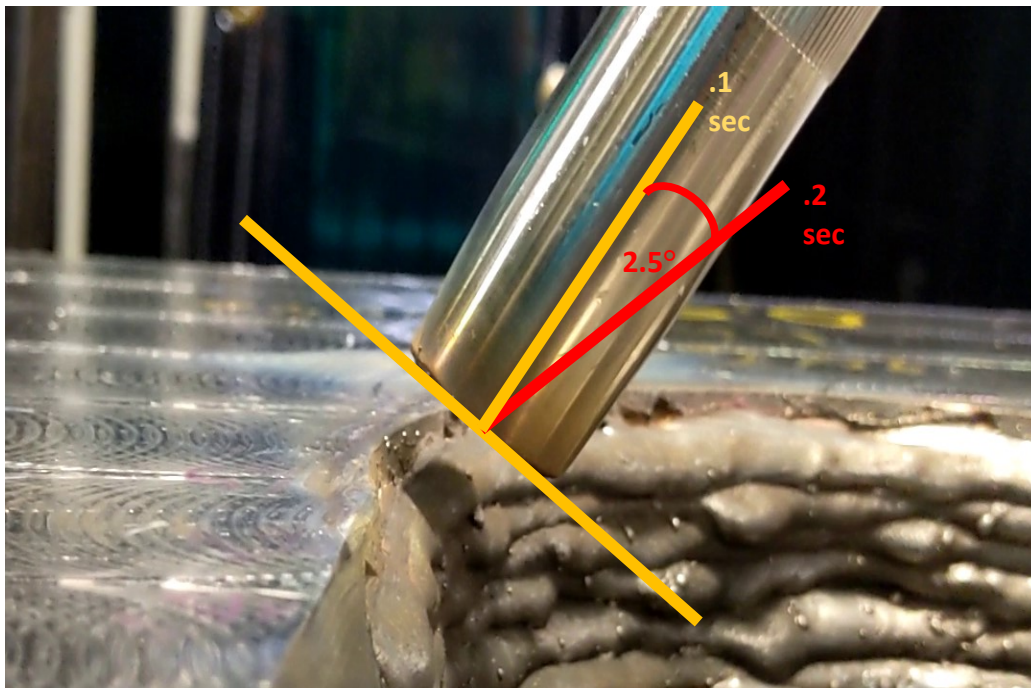


Figure 23 : GMAW Torch Oscillation Resulting in Sound 2G Clad

The torch work angle oscillation used here involved two separate motions with differing dwell times and no other weave oscillation. The first component of the oscillation shown in orange

involved a dwell time at the standard torch angle for .1 seconds. The second component of this oscillation shown in red involved a 2.5 degree shift in torch angle and a .2 second dwell at this angle. This oscillation was sufficient to improve horizontal position bead quality, which is shown in Figure 24.



Figure 24 : 2G Position Clads Employing Torch Angle Oscillations

Torch angle oscillations resulted in highly regular 2G deposits with good tie in to subsequent beads and base material.

The complicated shape of the trial die block mandated thoughtful procedure development. Several variables were under consideration when making this procedure, including: minimization of deposited material and number of weld passes; avoidance of weld passes with multiple positions, i.e. avoiding cladding the flat portion and the sidewall; and minimizing the amount of weld starts/stops on the die block. The resulting procedure is shown in Figure 25. It should be noted that this Figure illustrates one of two layers needed to clad the shot block.

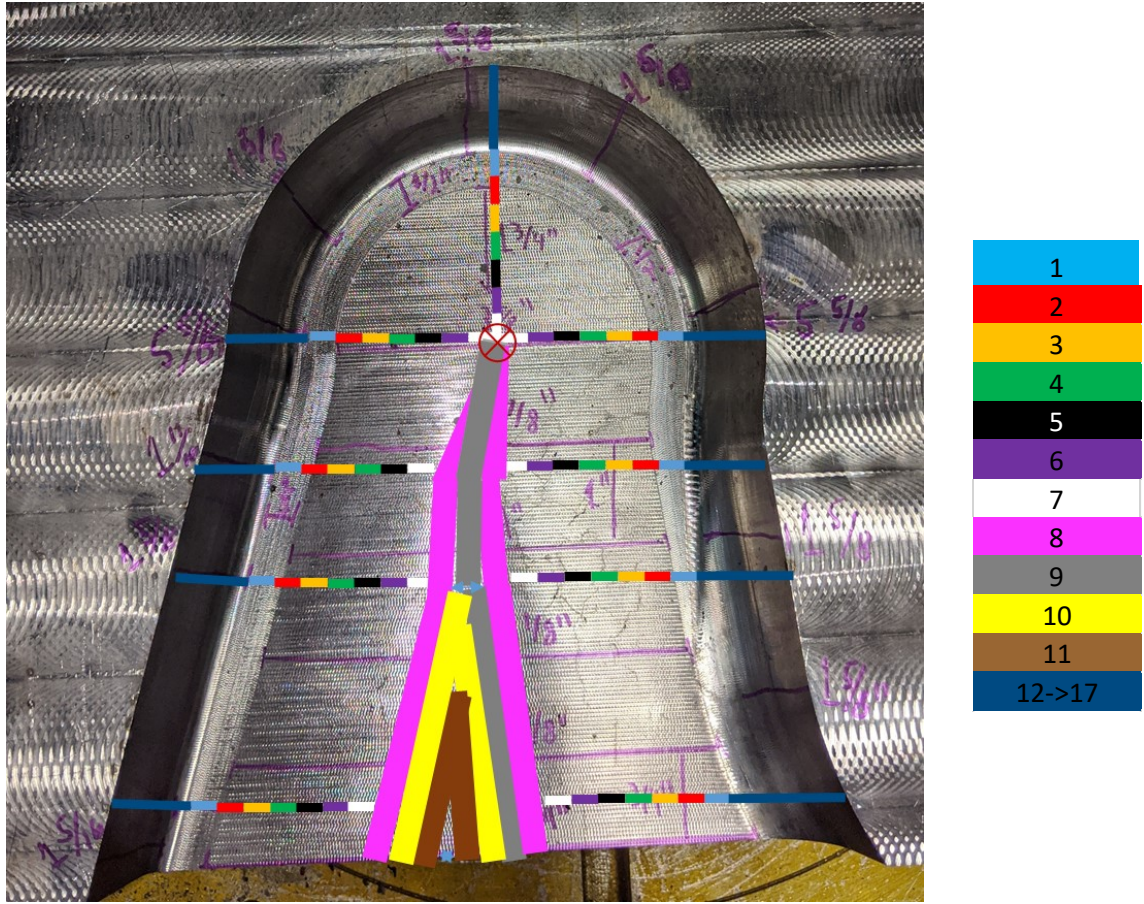


Figure 25 : Robotic GMAW Conformal Cladding Procedure

Weld passes 1-11 are used to clad the flat feature in the 1G position by traveling along the outer circumference of the feature. Clad passes 12-17 clad the vertical wall of the shot block in the 2G position. A single weld stop was incorporated pass 9 to complete the layer and ensure sound bead tie-ins, indicated by the red x-in-circle in Figure 25. After passing visual examination, welds stop tests were sectioned to determine the fusion quality and microstructure. A sectioned weld stop is shown in Figure 26 which shows good fusion profile.

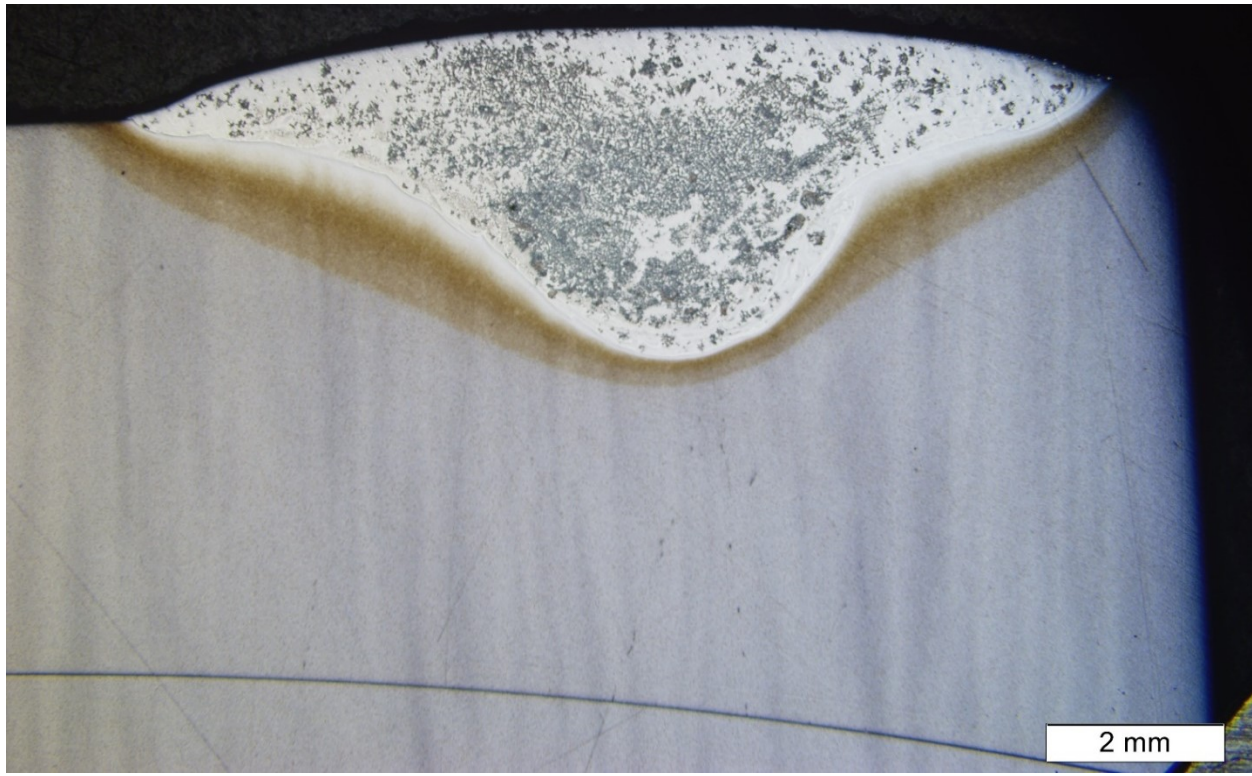


Figure 26 : Robotic GMAW Weld Stop Metallographic Sample

The weld stop showed excellent wetting of base material, low tow angle, and good penetration into the base material. No evidence of cracking, porosity, or lack of fusion was observed in this sample. This sample also showed the desired 2 phase microstructure, indicating dilution is appropriate for clad surfaces. Due to the lack of observable defects, weld stops were considered acceptable for use in the cladding procedure. These GMAW-P cladding procedures were used to clad production shot block dies that will be evaluated in the future using in-plant trials.

4.3 Feasibility of H13 Temperbead Repair using Anviloy HW-GTAW Cladding Procedures

Anviloy HW-GTAW cladding procedure were used to evaluate H13 temperbead repair feasibility. Here, the H13 HAZ from layer one is tempered by the Anviloy clad layer two minimizing the need for post weld heat treatment and/or reducing the risk for repair cold

cracking. A series of double layer clad tests were produced using different weld preheat and heat input. The goal was to change the HAZ size for what is called the high temperature (HT) - HAZ that transforms to martensite, and the low temperature (LT)-HAZ that is used to temper the former in layer two. A metallography method employing a 10% Nital etchant was used to etch the low temperature HAZs while leaving untempered martensite unetched. The trial showing HAZ sizes for 25C and 300C preheats is shown in Figure 27 employing identical weld parameters except for varied heat input.

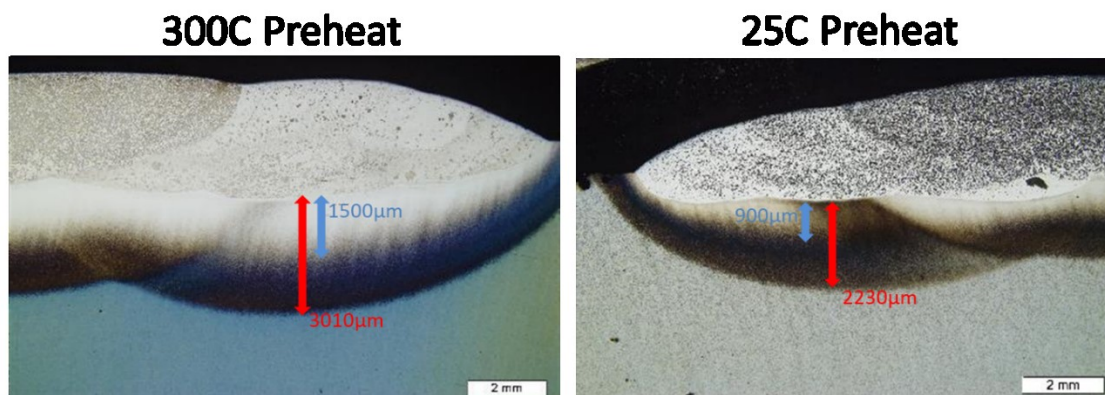


Figure 27 : 300C and 25C Preheat HAZ Sizes Made with HW-GTAW

The 300C preheat resulted in a larger total HAZ size. Interestingly, the ratio of low temperature HAZ (LT-HAZ) size to high temperature HAZ (HT-HAZ) size was larger for the 25C preheat. This indicated reduced preheat is likely to help create advantageous HAZ size distributions for temperbead. The metallography approach used here was validated with a microhardness map showing accuracy was within the resolution of the hardness maps.

Heat input trials involved identical weld parameters except for a travel speed varied from 4-11-ipm at 100C preheat. This produced welds with heat input ranges 12.7-47kJ/in. Resulting

HAZ sizes were measured with the same metallography approach shown in the preheat trials. The resulting HAZ size data was gathered and compiled into the graph shown in Figure 28.

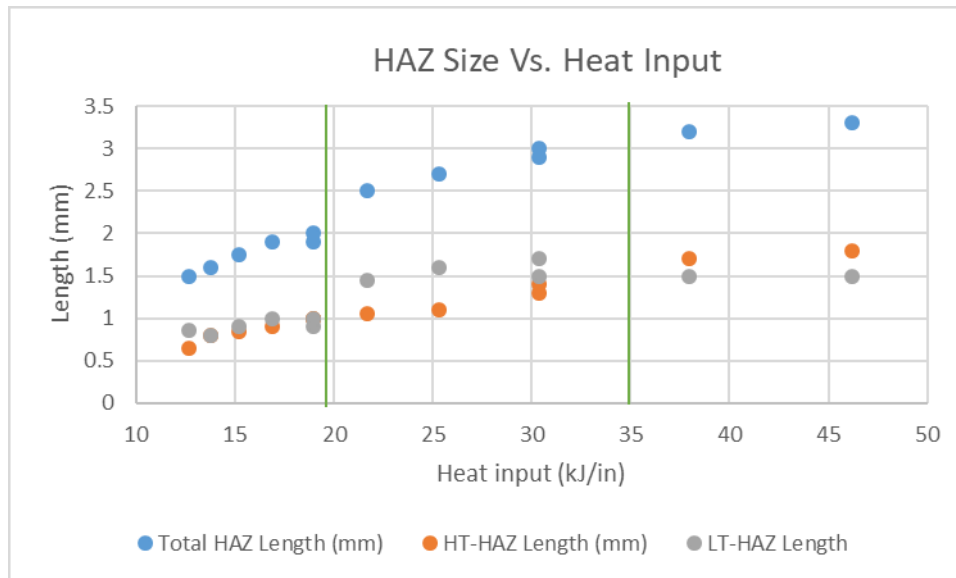


Figure 28 : Anviloy Wire-H13 HW-GTAW HAZ Sizes Vs. Heat Input with Bracketed Temperbead Region

Heat inputs above 35kJ/In were shown to promote larger HT-HAZs than LT-HAZs, which renders temperbead welding impossible. Interestingly, the low end of the heat input range produced negligibly larger LT-HAZs than HT-HAZs. For a temperbead procedure to have resistance to process variation, the LT-HAZ size should be maximized relative to the HT-HAZ. This was shown to occur at heat inputs from 19-35kJ/in., with ratio maximixed around 25kJ/in. These findings indicate minimization of weld heat input may not be the best strategy to achieve temperbead welding, and that heat input should be maintained around 25kJ/in for temperbead of H13 with these Anviloy deposit sizes.

Two multi-pass clads were made to illustrate the effectiveness of the developed temperbead procedure. The non-temperbead procedure used welding parameters that optimized

deposition rate and bead appearance but not HAZ size distribution. That weld is shown below in Figure 29

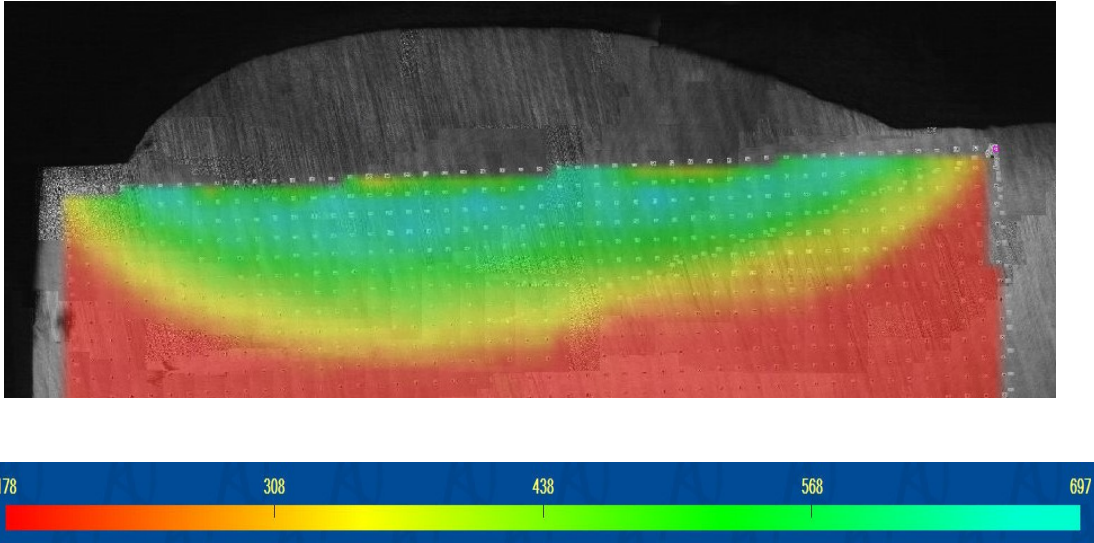


Figure 29 : Non-temperbead HW-GTAW Clad Hardness Map

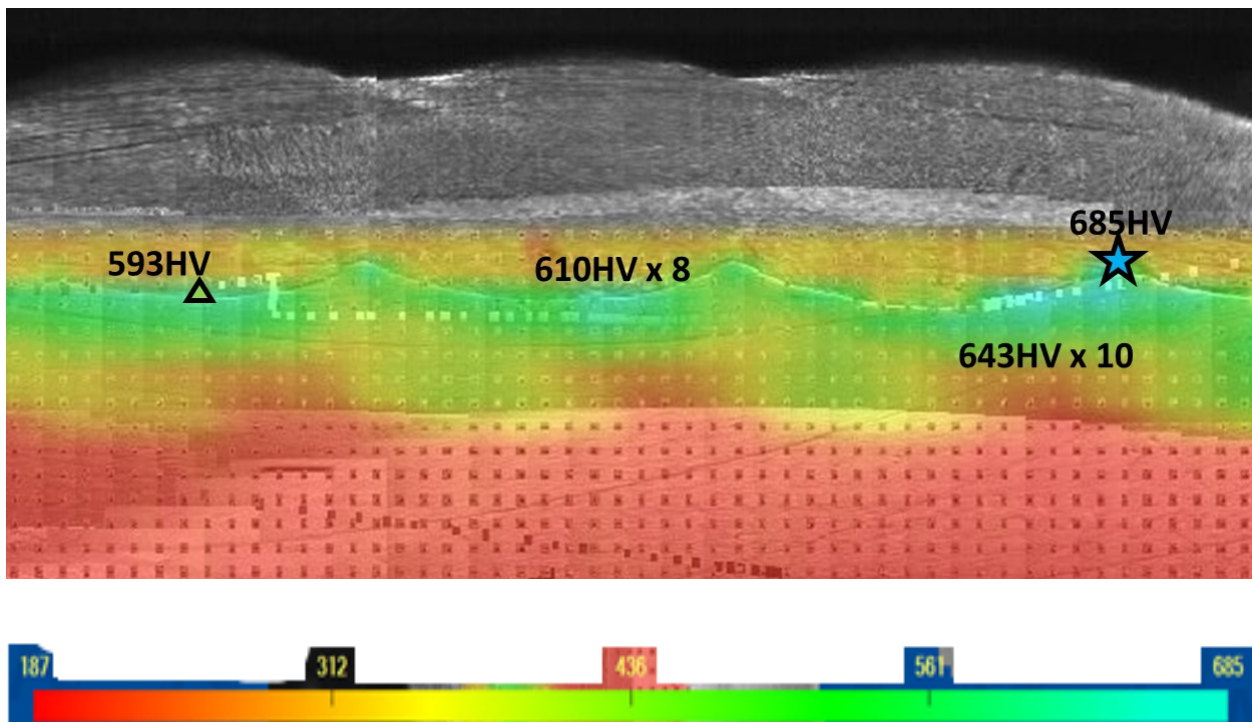


Figure 30 : Temperbead Optimized HW-GTAW Clad Hardness Map

A continuous high hardness band with hardness over 650HV was observed in the non-temperbead sample. This hardness morphology is detrimental for service life due to the risk of brittle crack propagation through the low toughness untempered martensite in this region. Figure 30 shows the hardness map for the temperbead optimized procedure using heat inputs between 22.5 and 25kJ/in. and 100C preheat.

The double layer temperbead optimized weld procedure produced a significantly more tempered HAZ versus a single bead as-welded HAZ. Aside from 18 measured hardness indents over 600HV, the majority of the temperbead HAZ had hardness under 600HV, and had a hardness range near the max target hardness for his H13 grade. Hardness map data was gathered to produce a histogram showing the prevalence of high hardness points vs. tempered regions shown in Figure 31.

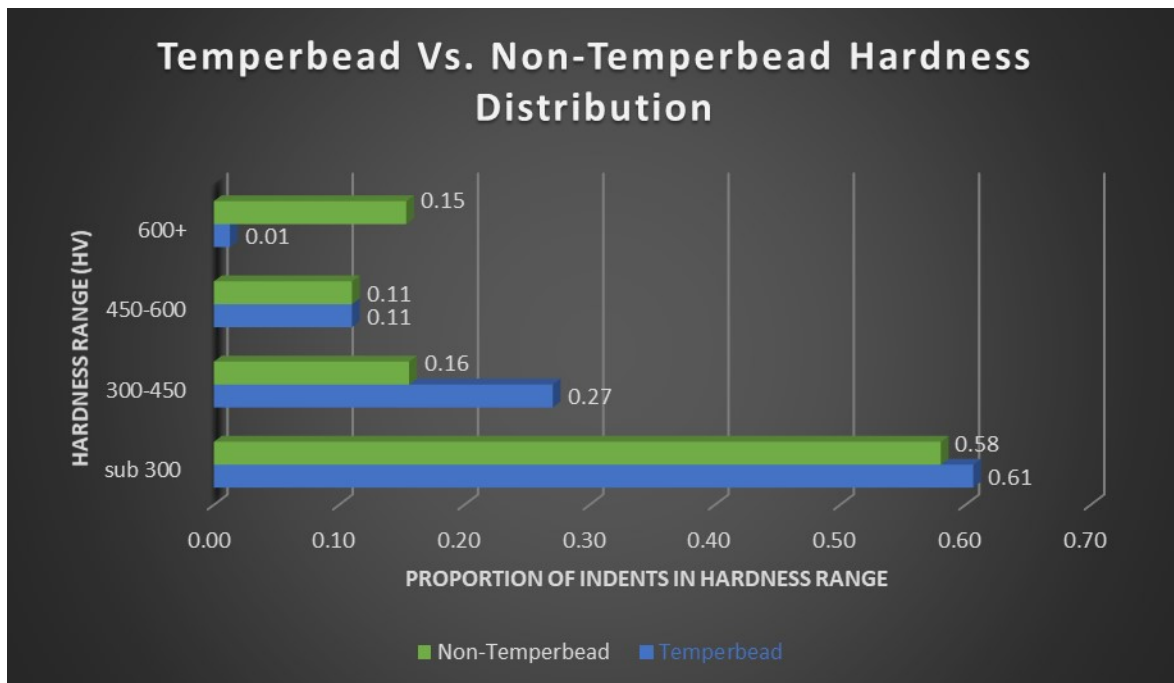


Figure 31 : Temperbead and Non-Temperbead Hardness Distribution Histogram

The temperbead procedure resulted in a mostly tempered HAZ with only 1% hardness indents above 600HV. This is a drastic improvement compared to the single layer deposit (non-temperbead) sample, which had 15% hardness indents over 600HV. The temperbead clad also resulted in significantly more indents in the lower hardness range of 300-450HV, which is likely beneficial for toughness of clad repairs. Results shown here indicate the feasibility of using temperbead repair procedures for Anviloy wire – H13 cladding.

Chapter 4.4 : Microstructure Characterization of Anviloy Cladding Deposits on H13 Steels

Since no there was no prior characterization work on Anviloy wire welding deposits and H13 repair, an effort was undertaken to identify phases present in both pure and diluted Anviloy deposits using metallography, SEM, EDS, and Thermocalc simulation software. Undiluted microstructure was studied using arc-casted Anviloy wire “buttons”. The button microstructure was compared to a 6 pass buildup. Figure 32 shows a metallographic section of the casted “button.”



Figure 32 : Metallographic Section of Anviloy Wire Arc Casted Button Showing Undiluted Two Phase Microstructure

The Anviloy cast button microstructure had distinct two phase microstructure that consisted of a matrix phase and secondary cellular and cellular dendritic phase. This microstructure was also observed in the 6 pass HW-GTAW build-up shown via SEM in Figure 33.

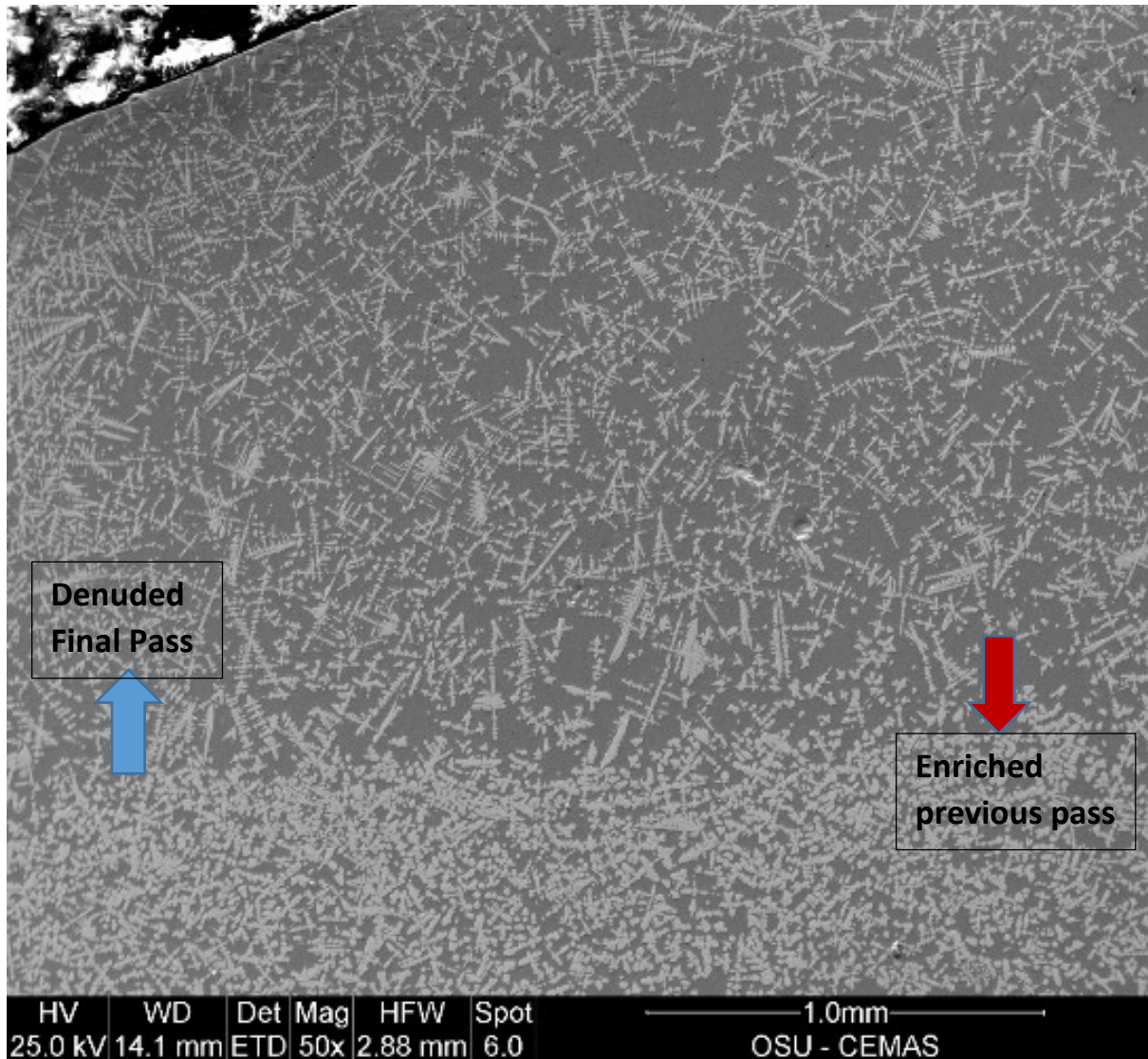


Figure 33 : HW-GTAW Build Up Final Pass Showing Macrosegregation, SEM Image

The same two phase structure was observed, with the secondary dendritic phase appearing a brighter color which indicates a higher content of high atomic number element(s). Also evident in this image is macrosegregation of the secondary phase, evidenced by its higher content at the bottom of Figure 33. Thermocalc was used to help identify phases present using single composition equilibrium phase vs. temperature diagrams (property diagrams) in Thermocalc.

Undiluted Anviloy wire was simulated, with the resulting property diagram shown below in Figure 34.

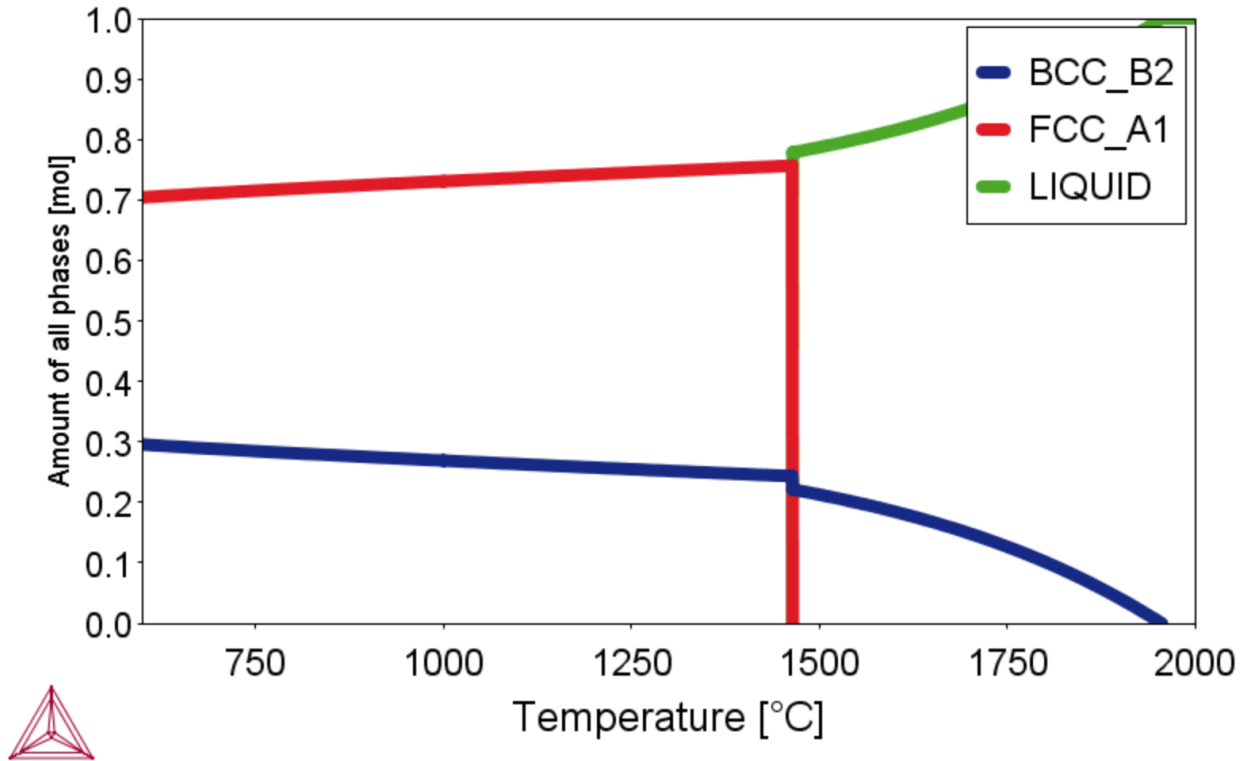


Figure 34 : Thermocalc Property Diagram of Undiluted Anviloy Wire Showing 2 Phase Equilibrium Microstructure

Thermocalc confirmed the presence of a two phase microstructure in undiluted Anviloy wire. The two phases predicted were primary alpha BCC tungsten and gamma FCC Ni/Fe phase. EDS mapping was also used to identify phases present, with TEAMS EDS software producing the data shown in Figures 35-37.

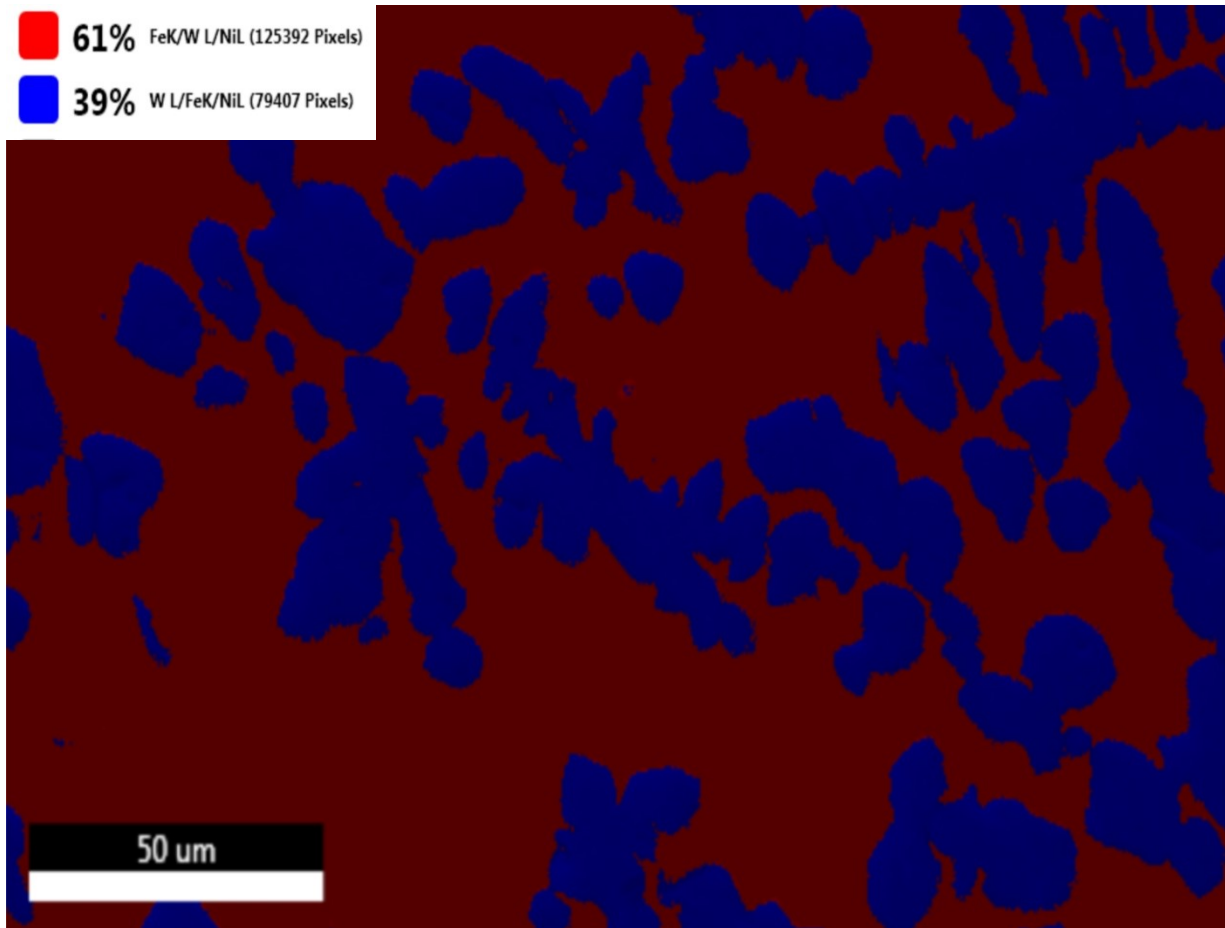


Figure 35 : EDS Phase Mapping of Undiluted Anviloy Wire

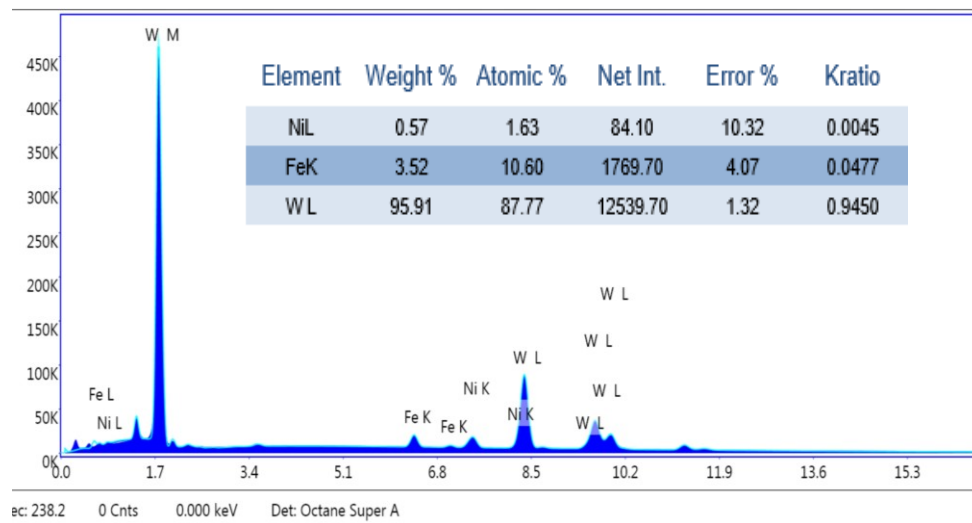


Figure 36 : EDS Data for Undiluted Tungsten Rich Phase

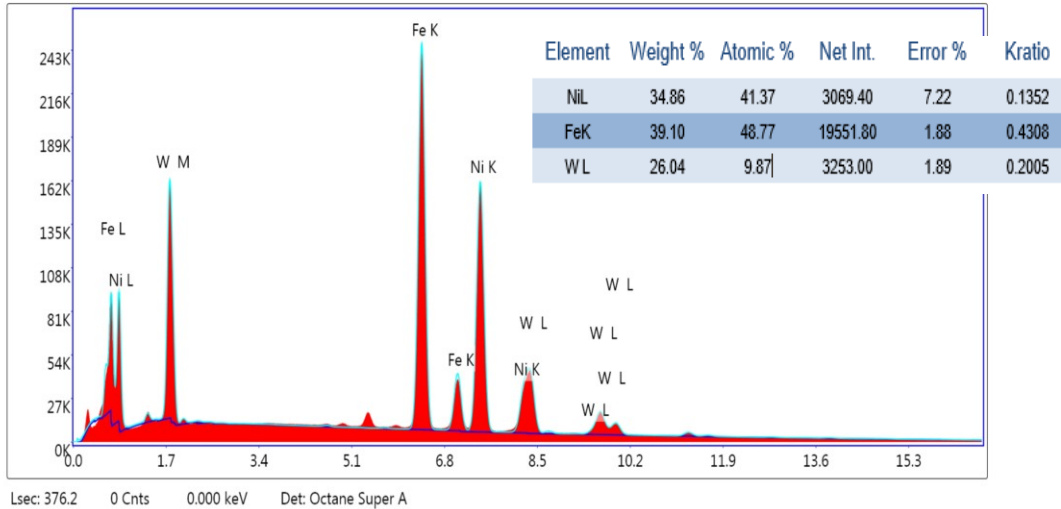


Figure 37 : EDS Data for Undiluted Matrix Phase

TEAMs EDS software identified two phases present in the undiluted Anviloy wire microstructure. EDS composition data supports the ThermoCalc finding of a BCC tungsten rich phase and a Ni/Fe FCC matrix phase. The high quantity of tungsten in the tungsten rich phase is likely the reason for the macrosegregation observed due to its high density and sinking effect in the molten weld pool.

Diluted Anviloy Wire-H13 microstructures differed from undiluted microstructures with the inclusion of a third phase. This is shown in an SEM image captured in Figure 38.

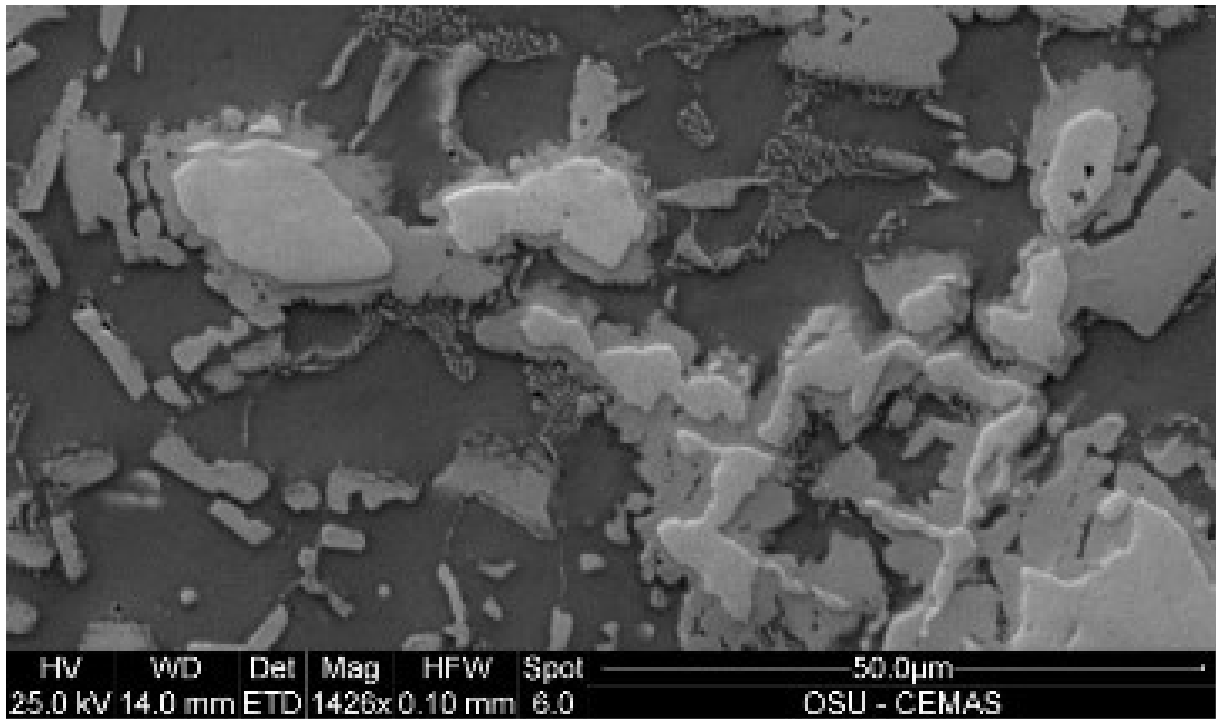


Figure 38 : Diluted Anviloy Wire H13 Microstructure Showing 3 Phases, SEM Image

The third phase appears to form around the tungsten rich phase as well as in a lamellar eutectic structure shown in Figure 38. The unidentified phase appears to have intermediate tungsten content due to contrast with the BCC and FCC phases. Figures 39 and 40 shows Thermocalc property diagrams for 10% and 40% dilutions of H13 into Anviloy wire.

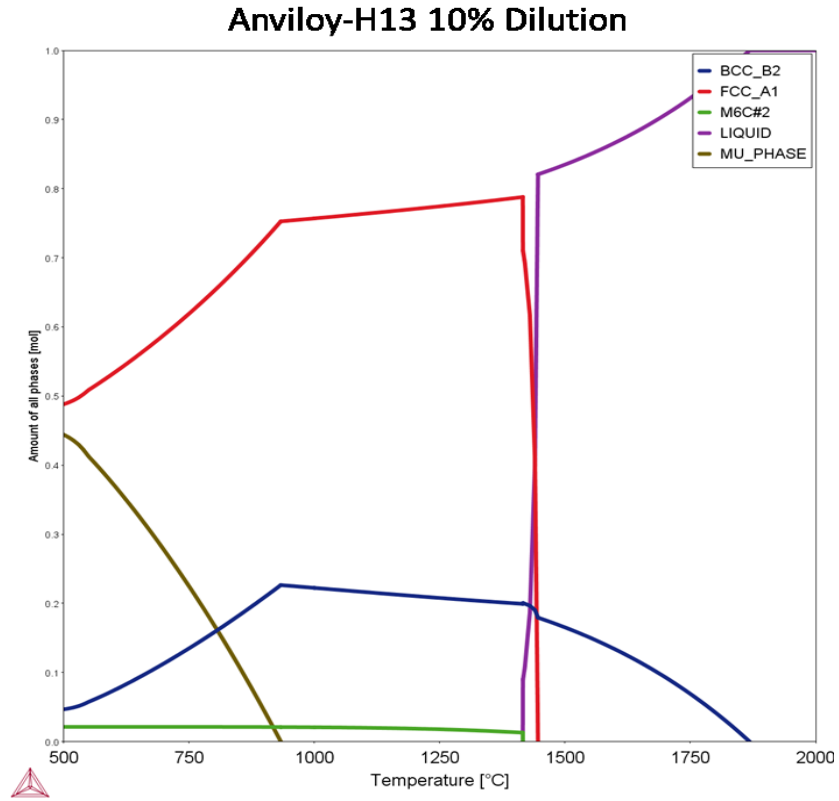


Figure 39 : Thermocalc Property Diagram of Anviloy Wire with 10% H13 Dilution Showing 4 Phase Predicted Equilibrium Microstructure

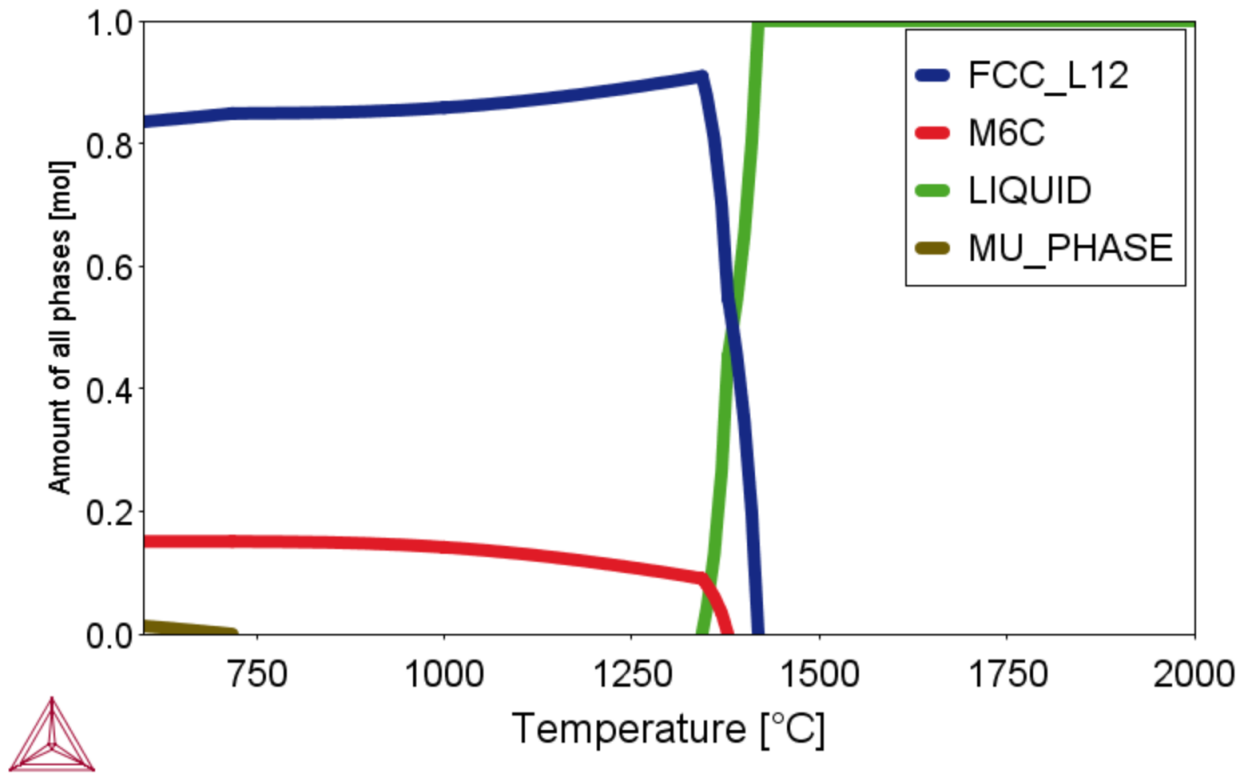


Figure 40 : Thermocalc Property Diagram of Anviloy Wire with 40% H13 Dilution Showing 3 Phase Predicted Equilibrium Microstructure

Thermocalc predicts BCC and FCC as well as Mu phase and M₆C carbide phase at 10% dilution, whereas 40% dilution is too high to form the tungsten BCC phase. In order to determine the identity of the unknown third phase, EDS scans were gathered in the region from Figure 38 shown in Figures 41-44.

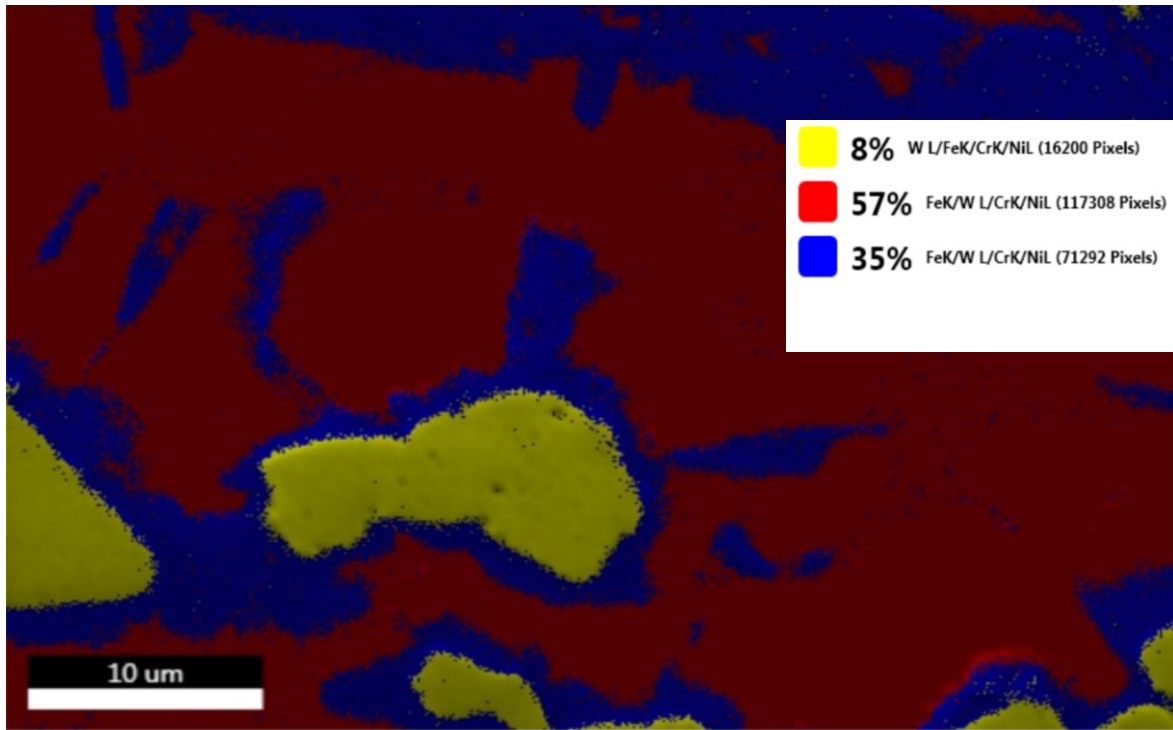


Figure 41 : EDS Map of Diluted Anviloy Wire – H13 Microstructure

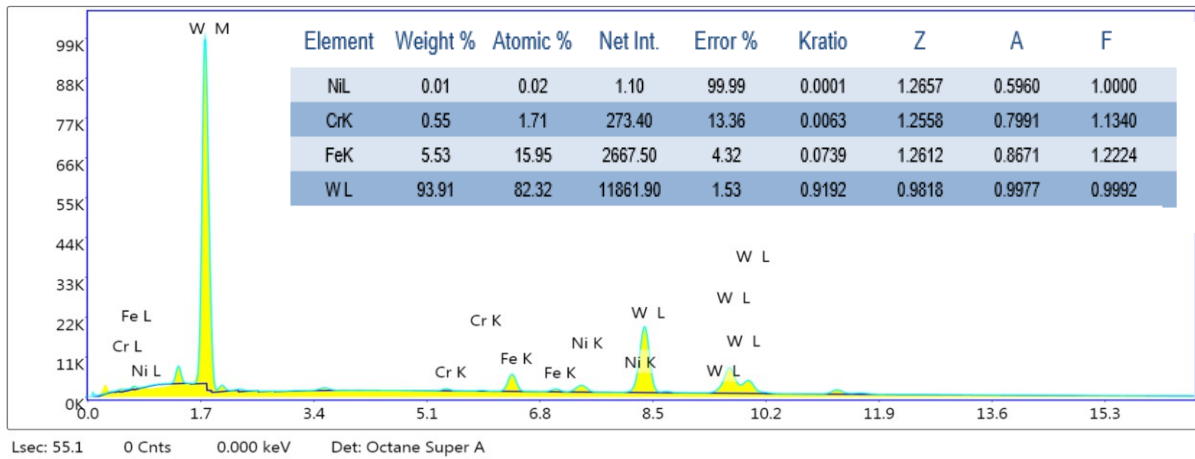


Figure 42 : Diluted Tungsten Rich Phase EDS Data

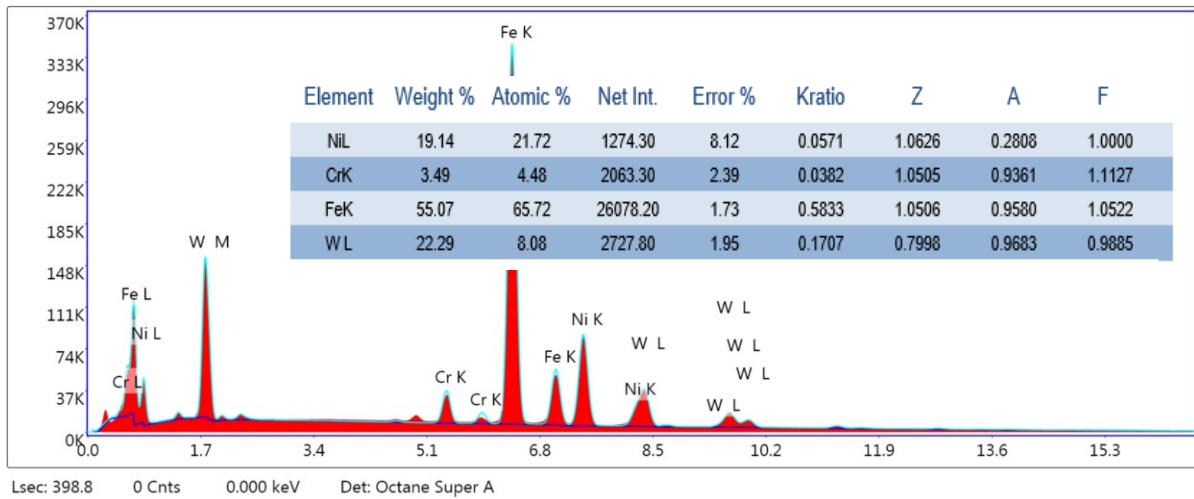


Figure 43 : Diluted Matrix Phase EDS Data

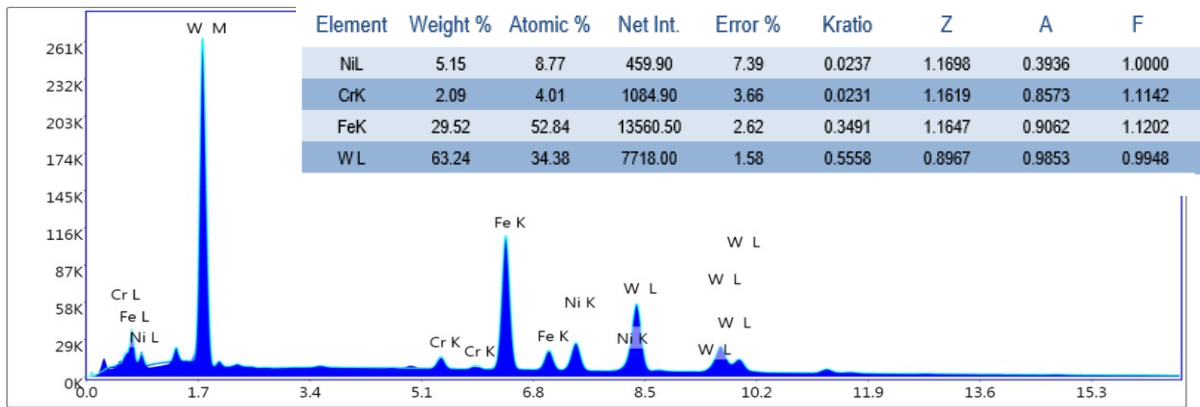


Figure 44 : Unidentified Third Phase EDS Data

EDS data from the diluted region indicates the primary alpha BCC tungsten phase (yellow) and matrix phase (red) are likely the same phases. The intermediate tungsten content of the unidentified phase was also confirmed. However, EDS data does not match well with predicted Thermocalc composition data for Mu and M_6C phases as shown in Table 1 and 2.

Mole Percent W in Mu	Mole Percent Ni in Mu	Mole Percent Fe in Mu
27.5	50.9	21.6
Mole Percent W in M ₆ C	Mole Percent Ni in M ₆ C	Mole Percent Fe in M ₆ C
44.6	12.2	40.2

Table 3 : Mu and M₆C Carbide Composition at 900C for 10% Dilution Predicted by Thermocalc

Mole Percent W in Mu	Mole Percent Ni in Mu	Mole Percent Fe in Mu
41.2	4.4	47.7
Mole Percent W in M ₆ C	Mole Percent Ni in M ₆ C	Mole Percent Fe in M ₆ C
40.8	6.1	35.4

Table 4 : Mu and M₆C Carbide Composition at 700C for 40% Dilution Predicted by Thermocalc

EDS data for the unidentified phase does not match particularly well with Mu or M₆C carbide compositions predicted by Thermocalc. These scans did not include carbon due to the unreliability of its detection in bulk samples with EDS. Although carbon would be present if the unidentified phase was M₆C, the ratio of metallic elements would still remain the same. To help determine if carbon was present in higher quantities in any of the phases, EDS scans including carbon were used to make the elemental heat map shown in Figure 45.

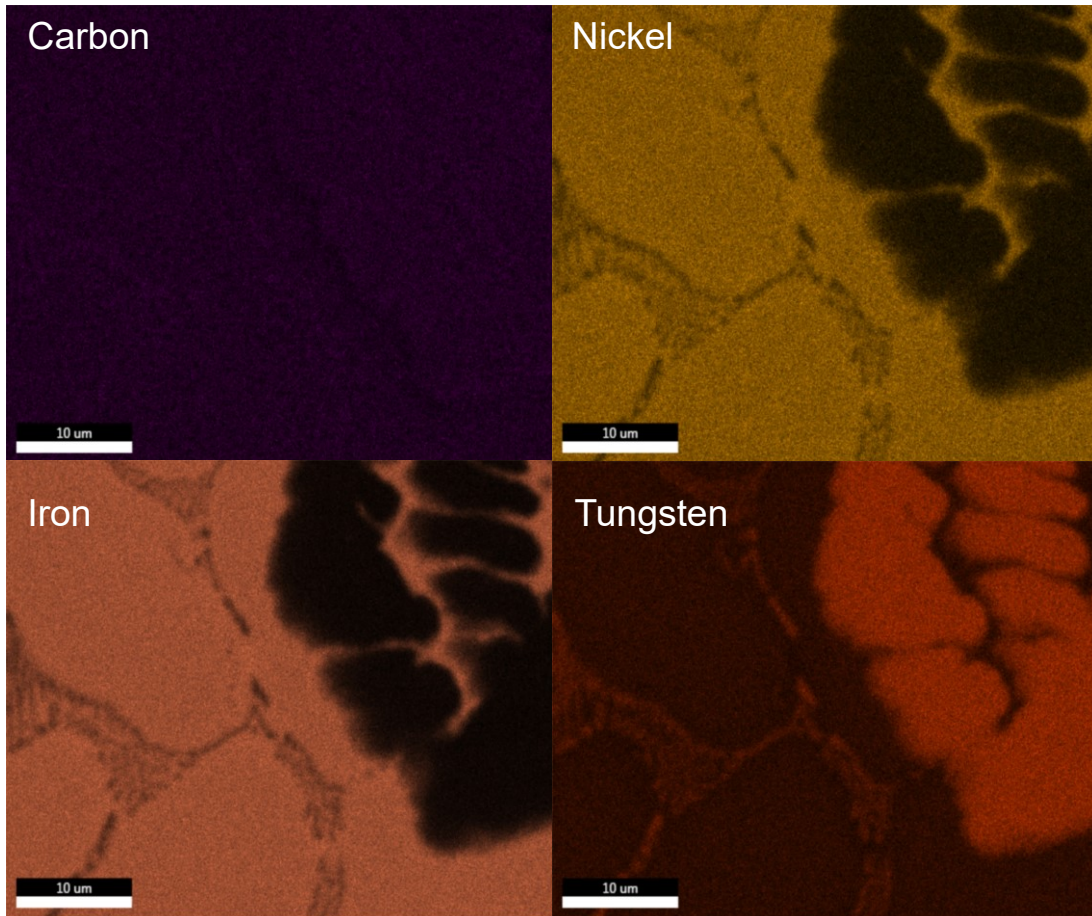


Figure 45 : Anviloy Wire-H13 Diluted Region Elemental Heat Map Gathered by EDS

Although carbon detection is unreliable in bulk samples using EDS, the large compositional difference of carbon in the M_6C carbide phase vs. others is still likely to produce contrast.

Although contrast cannot be seen in Figure 45, M_6C carbide phase cannot be ruled out due to the inability of EDS to reliably detect carbon.

The use of heat treatment to facilitate carbon diffusion from H13 into Anviloy wire deposits was used to help identify the unknown phase using an alkaline sodium picrate etchant that selectively attacks tungsten rich M_6C carbide. The structures revealed by this etchant bear strong similarity to those seen in the Anviloy wire buildup where the diluted microstructure was

observed. Comparisons of these two samples are shown in Figure 46, which were both etched using the alkaline sodium picrate solution.

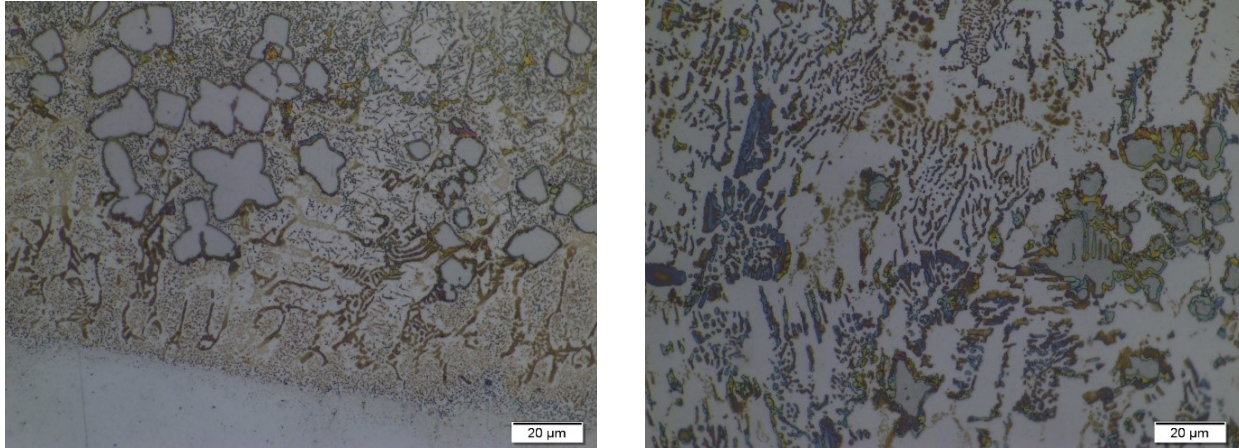


Figure 46 : Heat Treated Anviloy Wire –H13 Clad (left) and Diluted Region of Anviloy Wire Buildup on H13 (right) Showing Same 3 Phase Microstructure as Seen in SEM/EDS

The alkaline sodium picrate etch did not attack the alpha bcc tungsten phase or matrix phase. This etchant did attack the eutectic structure as well as matrix phase grain boundaries in both samples. This indicates the unidentified phase seen in SEM is also present in the heat treated samples and revealed with the alkaline sodium picrate etch. It was hypothesized that carbon diffusion from H13 into the heat treated Anviloy wire clad deposit was the cause of M_6C carbide formation. Carbon diffusion leads to softening in H13, which was observed near the fusion boundary but not at the plate midpoint of heat treated samples. Microhardness indents are shown in Figure 47 in these two locations.

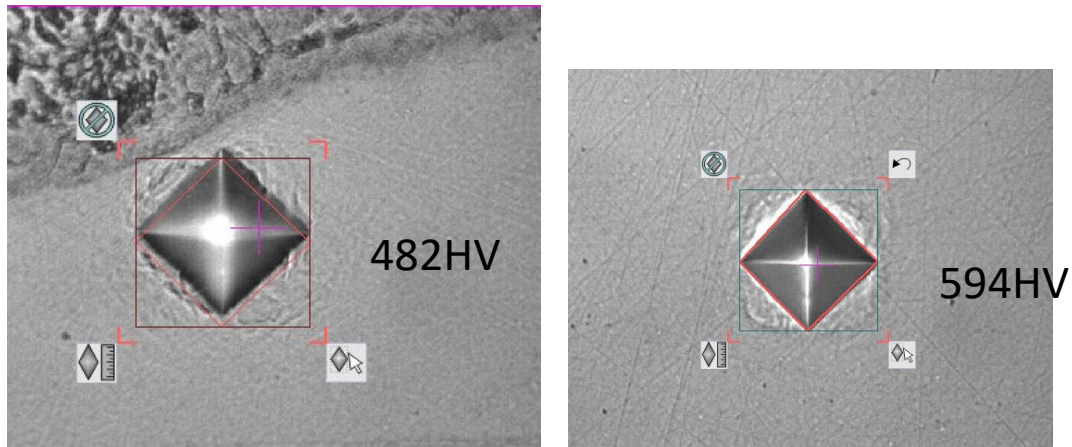


Figure 47 : Hardness indent at Fusion Boundary (left) and Hardness Indent at Plate Midpoint (right)

Softening from 594HV to 482HV was observed, indicating sizeable carbon diffusion into the Anviloy wire deposit. To determine if carbon diffusion / dilution into the Anviloy wire deposit was the cause of the M_6C carbide phase formation, a 308L “butter” layer plus an Anviloy wire clad layers sample was created to see if alkaline sodium picrate would reveal the presence of the unknown phase in these deposits. 308L was selected due to its low carbon content and austenitic microstructure. Thermocalc simulations for 70% Anviloy wire + 30% * (70% 308L + 30% H13) were run, with the property diagram for this composition shown in Figure 48.

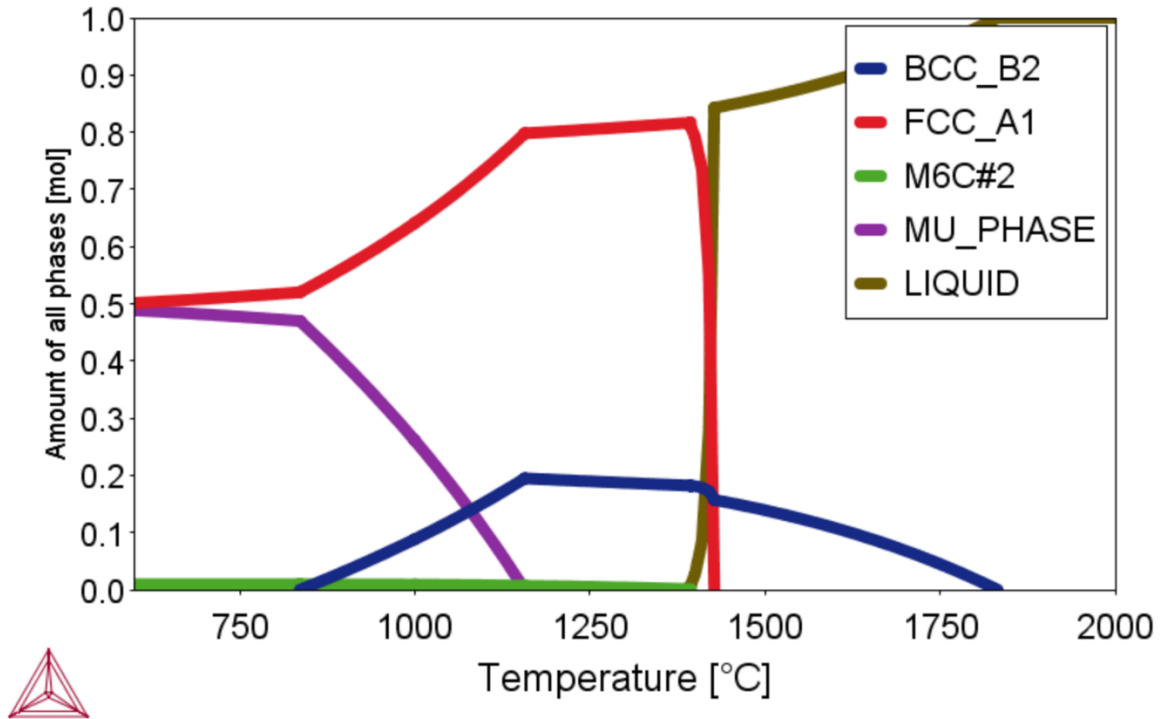


Figure 48 : 70% Anviloy wire + 30% * (70% 308L + 30% H13) Thermocalc Property Diagram
 Showing 4 Phase Predicted Equilibrium Microstructure

Mu phase and M_6C carbide are predicted in this sample as well, though the phase fraction of M_6C is much smaller for this composition. Since Mu phase is predicted in similar fractions in both property diagrams, it would be revealed in the Anviloy Wire-308L-H13 clad if in fact the alkaline sodium picrate etched it. The Anviloy Wire-308L-H13 overlay was etched with alkaline sodium picrate, and is shown in Figure 49.

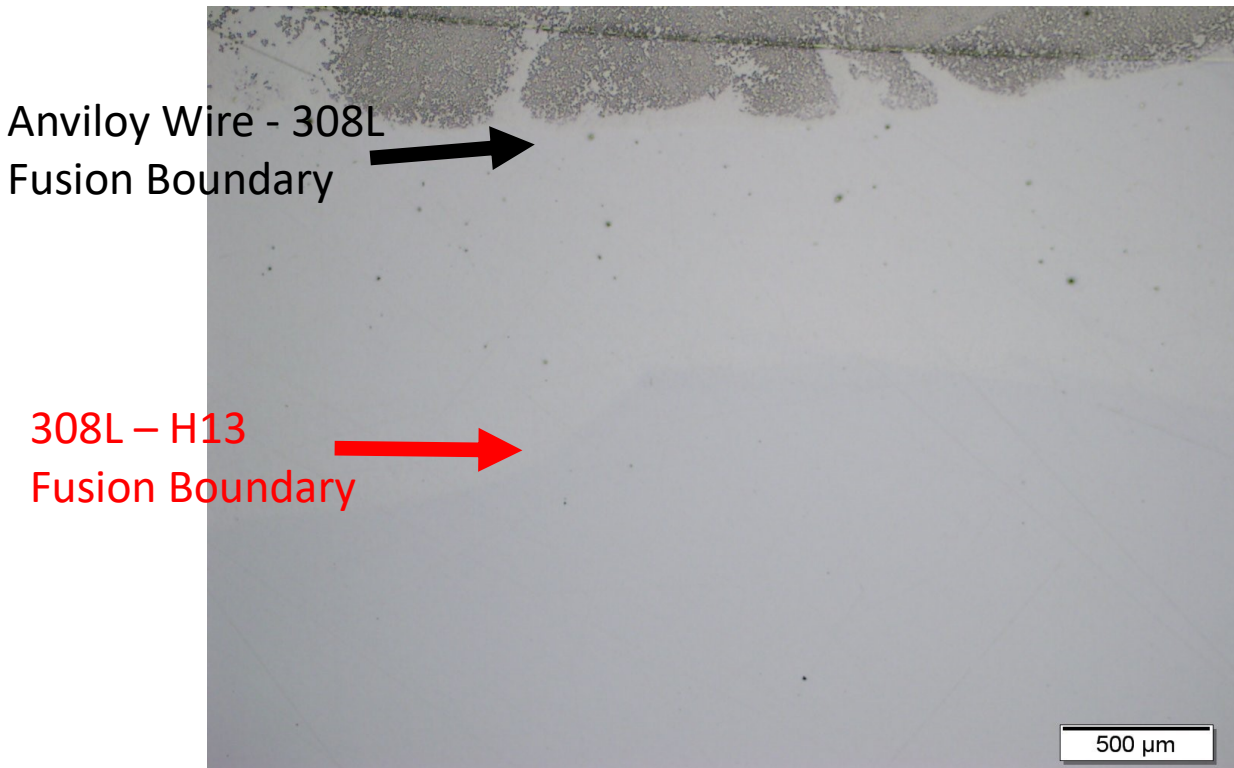


Figure 49 : The Anviloy Wire-308L-H13 Overlay Etched with Alkaline Sodium Picrate

The lack of etching in this sample indicates that M_6C carbide is the likely phase, since μ phase if present would be etched by the alkaline sodium picrate. This indicates that M_6C carbide phase was the third phase encountered in diluted clads, but this must be validated with further crystallography in the future.

Chapter 5 : Conclusions

The conclusions of each study are summarized below:

Anviloy Wire-H13 HW-GTAW Cladding Procedure Development

- Preferred HW-GTAW setup conditions were determined for steady-state bridging metal transfer with Anviloy wire.
- Anviloy wire cast and helix was important for bridging metal transfer position control and bead uniformity. A two-axis wire straightener was found to straighten the wire sufficient to produce uniform clad deposits.
- Hot wire voltage of 4V was sufficient to achieve bridging metal transfer at 3/4" electrical stickout with wire feed speeds from 60 to 80IPM.
- Metallographically sound HW-GTAW clad deposits were produced with dilutions as low as 18% compared to CW-GTAW where the minimum was 30% dilution. Lower dilutions are feasible with preheat and torch oscillation.

Anviloy Robotic GMAW-P Conformal Cladding Die Development

- Visually and metallographically sound Anviloy wire cladding of H13 was feasible using commercial GMAW pulse waveforms that were developed for other materials. The preferred waveform was DC- Wave SuS 1.2mm.
- Weld oscillation helped improve bead consistency for Anviloy deposits in both the flat and horizontal position. A torch work angle oscillation was necessary to deposit a vertical clad using horizontal beads on the shot block sidewall.

Feasibility of H13 Temperbead Repair using Anviloy Wire HW-GTAW Cladding Procedures

- Anviloy HW-GTAW procedures can be used to temperbead weld H13 tool steel.
- Low preheat repair temperatures showed a more effective temperbead effect on the H13 HAZ.
- The hardness range of as-welded (non-temperbead) double layer overlays was 200HV-700HV where there was a continuous band above 600HV along fusion boundary.
- The hardness range of double layer temperbead samples was 200HV-590HV with just small isolated regions of higher hardness.
- The preferred temperbead procedure was validated with hardness mapping which resulted in only 1% of hardness indents above 600HV / 53HRC.

Microstructure Characterization of Anviloy Wire and Anviloy-308L HW-GTAW Cladding

Deposits on H13 Die Steel

- Undiluted Anviloy cast button microstructure consisted of tungsten alpha BCC phase dendrites and a matrix (Ni/Fe) gamma FCC phase
- Anviloy wire clad deposit microstructure consisted of primary tungsten alpha BCC phase, (Ni/Fe) gamma FCC phase, and a third phase that is potentially TCP intermetallic Mu phase or M_6C carbide phase
- Heat treated samples and hardness indents indicate carbon diffusion from H13 into Anviloy clad deposit during heat treatment which forms a phase etched with alkaline sodium picrate, most likely M_6C carbide
- Alkaline sodium picrate etching strongly suggests M_6C carbide formation vs. Mu phase formation in Anviloy clad deposits on H13, but further crystallography is required to verify identity of third phase

Works Cited

1. Turkeli, Altan, "History of Metal Casting" MSE-432 Foundry Technology Lecture.
2. Wagner, Donald B. "Early iron in China, Korea, and Japan" Korean excavations of iron armour: Political and technological implications for protohistoric East Asia, organised by Dr. Gina Barnes at the Annual Meeting of the Association for Asian Studies, Los Angeles, 25-28 March 1993.
3. "History of Die Casting: How Die Casting Evolved." *Die Casting Blog*, 20 July 2020, diecasting.com/blog/2016/02/29/a-brief-history-of-die-casting/.
4. Bonollo, F., Gramegna, N. & Timelli, G. "High-Pressure Die-Casting: Contradictions and Challenges." *JOM* 67, 901–908 (2015).
5. Jhavar, S., et al. "Causes of Failure and Repairing Options for Dies and Molds: A Review." *Engineering Failure Analysis*, vol. 34, Elsevier BV, Dec. 2013, pp. 519–535. Crossref, doi:10.1016/j.engfailanal.2013.09.006.
6. Sjöström, Johnny. Chromium Martensitic Hot-Work Tool Steels : Damage, Performance and Microstructure. 2004, <http://urn.kb.se/resolve?urn=urn:nbn:se:kau:diva-2553>.
7. Gill, James Presley, "High speed steel - its history, development, manufacture, metallography, and constitution, including an extended bibliography" (1922). Masters Theses. 5036.
8. Okamoto, H. "The C-Fe (Carbon-Iron) System" *Journal of Phase Equilibria* Vol. 13 No.5, 1992. Pp 543-565.
9. ThyssenKrupp Specialty Steels .Throtherm 2344 Data Sheet, 2020.
10. Krauss, G. "Physical Metallurgy of Steels." *Automotive Steels*, 2017, pp. 95–111., doi:10.1016/b978-0-08-100638-2.00004-3.
11. Klobčar, D., et al. "Thermal Fatigue of Materials for Die-Casting Tooling." *Materials Science and Engineering: A*, vol. 472, no. 1–2, Elsevier BV, Jan. 2008, pp. 198–207. Crossref, doi:10.1016/j.msea.2007.03.025.
12. "H13 Tool Steel: 1.2344: X40CrMoV5-1: SKD61 Hot Work Steel." *Otai Special Steel*, 10 Mar. 2020, www.astmsteel.com/product/h13-tool-steel-x40crmov5-1-skd61-hot-work-steel/.
13. ASM High Speed Steels "High-Speed Steels." *Tool Steels*, CRC Press, 2016, 229–252. Crossref, doi:10.1201/9781315181516-12.
14. Zhang, Zhuyao, and R. A. Farrar. *An Atlas of Continuous Cooling Transformation (CCT) Diagrams Applicable to Low Carbon Low Alloy Weld Metals*. Institute of Materials, 1995.
15. Strid, J., & Easterling, K. E. (1985). On the chemistry and stability of complex carbides and nitrides in microalloyed steels. *Acta Metallurgica*, 33(11), 2057–2074. [https://doi.org/10.1016/0001-6160\(85\)90129-4](https://doi.org/10.1016/0001-6160(85)90129-4) N Bearing HWTS
16. HEIKKILÄ, IRMA. "The Positive Effect of Nitrogen Alloying of Tool Steels ..." *Digital Comprehensive Summaries of Uppsala Dissertations from the Faculty of Science and Technology* , 2013, uu.diva-portal.org/smash/get/diva2:617657/FULLTEXT01.pdf.
17. Schwam, D., Wallce, J., Birceanu, S. "DIE MATERIALS FOR CRITICAL APPLICATIONS AND INCREASED
18. PRODUCTION RATES" Case Western Reserve University. 2002.
19. Rudiger Ehrhardt, R., Klaus-Dieter, F., Gehricke, B., Beckstegge, J., Schruff, I.

- “Improving the heat checking characteristics of H13 by Modification of the Chemical Composition.” *Die Casting Engineer* 47(6). 2003. Pp 30-37.
20. Tentardini, E. K., Kunrath, A. O., Aguzzoli, C., Castro, M., Moore, J. J., & Baumvol, I. J. R. (2008). Soldering mechanisms in materials and coatings for aluminum die casting. *Surface and Coatings Technology*, 202(16), 3764–3771.
<https://doi.org/10.1016/j.surfcoat.2008.01.019>
 21. Joshi, V., Srivastava, A., & Shivpuri, R. (2004). Intermetallic formation and its relation to interface mass loss and tribology in die casting dies. *Wear*, 256(11–12), 1232–1235.
<https://doi.org/10.1016/j.wear.2003.08.001>
 22. Malkin, A. I. (2012). Regularities and mechanisms of the Rehbinder’s effect. *Colloid Journal*, 74(2), 223–238. <https://doi.org/10.1134/s1061933x12020068>
 23. Thompson, Steve. *Handbook of Mold, Tool and Die Repair Welding*. William Andrew Inc., 1999.
 24. Grum J, Slabe JM. A comparison of tool-repair methods using CO2 laser surfacing and arc surfacing. *Appl Surf Sci* 2003;208–209:424–31.
 25. Pleterski M, Tuek J, Kosek L, Muhi M, Muhi T. Laser repair welding of molds with various pulse shapes. *METABK* 2010;49–1:41–4.
 26. Pleterski M, Tuek J, Muhi T, Kosek L. Laser cladding of cold-work tool steel by pulse shaping. *J Mater Sci Technol* 2011;27–8:707–13.
 27. Kosnik A, Tuek J, Kosec L, Muhi T. The manufacturing of a two-layered injection mould by welding. *METABK* 2011;50–4:231–4.
 28. Borrego LP, Pires JTB, Costa JM, Ferreira JM. Mould steels repaired by laser welding. *Eng Fail Anal* 2009;16:596–607.
 29. Capello E, Colombo D, Previtali B. Repairing of sintered tools using laser cladding by wire. *J Mater Process Technol* 2005;164–165:990–1000.
 30. Zou JX, Grosdidier T, Zhang KM, Dong C. Cross-sectional analysis of the graded microstructure in an AISI D2-steel treated with low energy high-current pulsed electron beam. *Appl Surf Sci*, *Appl Surf Sci* 2009;255:4758–64.
 31. Lee JC, Kang HJ, Chu WS, Ahn SH. Repair of damaged mold surface by cold-spray method. *Ann CIRP* 2007;56–1:577–80.
 32. YURIOKA, Nobutaka. Review of *Physical Metallurgy of Steel Weldability*, *ISIJ International*, vol. 41, no. 6, 2001, pp. 566–570.

Appendix A : Anviloy HW-GTAW Cladding Procedure Development for H13

Abstract:

Aluminum die casting is commonly used to produce lightweight metal parts for the automotive industry due to its high productivity. Although hot work tool steels (HWTS) such as H13 have been commonly used for die casting dies for decades, new advances in refractory metal wire consumables are opening avenues for advanced repair, conformal cladding, and wire arc additive. A new Anviloy W-27.5Ni-12.5Fe wire consumable was previously deposited without defects using the cold wire feed gas tungsten arc welding (CW-GTAW) process, but these deposits had high base metal dilutions to accommodate the higher energy melting requirements of refractory metal alloys (1). In this study, a mechanized hot wire GTAW (HW-GTAW) system was used to investigate the applicability of this process for low dilution cladding of H13 dies. In this study, preferred HW-GTAW parameters such as hot wire stickout, hot wire voltage, and weave dwell were obtained for clad deposits that were 6mm thick. Preferred hot wire voltage for adequate melting without developing weld spatter was 4V. The preferred HW wire contact trip to puddle electrical stickout was $\frac{3}{4}$ " to promote adequate wire preheating as well as feeding consistency and accuracy. The minimum base metal dilution achievable for sound deposits was approximately 18% for HW-GTAW vs. 30% for GTAW. HW-GTAW was proven a capable process for producing low dilution, sound welds between the new Anviloy wire and H13.

Objectives :

- Develop HW-GTAW procedures for cladding Anviloy alloy (W-27.5Ni-12.5Fe) on H13 tool steel in flat (1G) position.

- Determine minimum heat input / dilution for acceptable Anviloy Wire-H13 clad deposits with HW-GTAW process.
- Develop both single layer and double layer procedures to characterize clad quality and ability to temper H13 heat affected zones (Appendix C)

Background

GTAW and HW-GTAW

Gas tungsten arc welding (GTAW) is one of the most widely used arc welding processes. GTAW heat is generated using a non-consumable tungsten electrode, which forms an arc with the workpiece via thermionic emission of electrons, Figure 1. Thermionic emission of electrons from the tungsten electrode allows for a stable arc to form in inert gas that is typically argon, helium or mixture thereof. The arc provides the heat for melting and fusion of metals and typically operates in either the electrode negative (EN) or alternating current (AC) polarity. The electrode positive (EP) polarity is avoided or the electrode will typically melt and fail. In the EN polarity, the tungsten is the cathode and is a thermionic emitter of electrons. The EN tungsten arc operates at lower voltages as only a small voltage is required to thermionically emit electrons. The EN arc heat balance is often cited to be 30% at the cathode and 70% at the anode. The GTAW arc current must be sufficient to melt a weld pool in the base material and consumables that are fed into the weld pool side. Rod filler materials are fed manually while wire filler materials are continuously fed in mechanized applications. For the latter, a bridging metal transfer is preferred that streams the molten filler metal into to pool through a surface tension bridge (Figure A2). This process is widely used on a range of ferrous and non-ferrous materials, and is known for its high quality, spatter free welds.

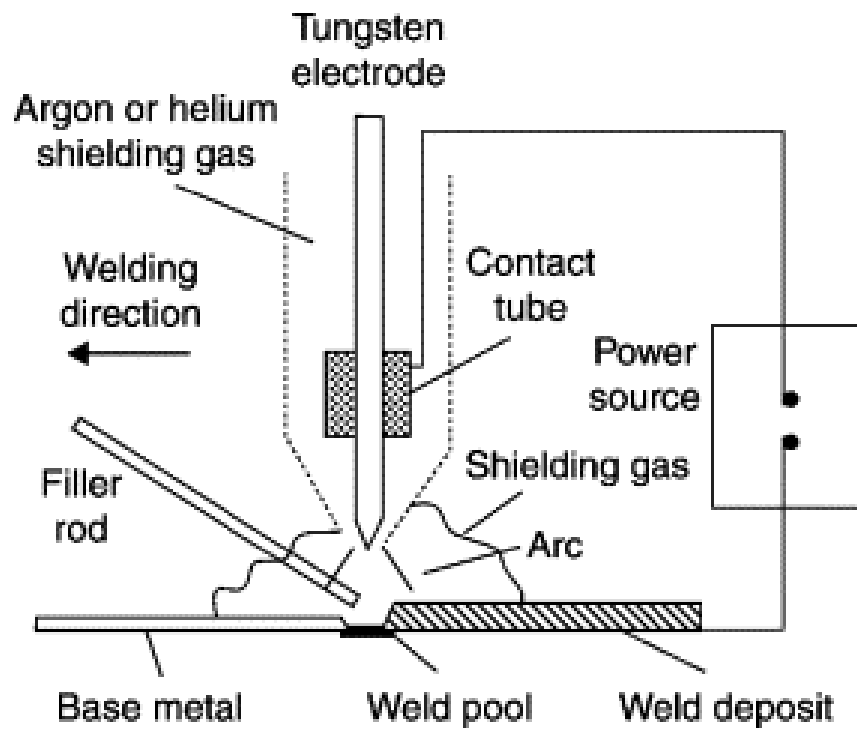


Figure A1 : Gas Tungsten Arc Welding (2)

The consumable is usually fed “cold” into conventional GTAW weld pools using bridging metal transfer (4). Here the heat from the arc and puddle melt the wire as it feeds into pool, and this melting is observed visually in Figure A2.



Figure A2 : Uninterrupted Bridging Metal Transfer in Rear Feed Cold Wire GTAW (5)

The molten wire mixes with the molten weld pool forming a uniform heterogeneous weld deposit. If the feed is too slow, the wire may form droplets that are deposit at a non-uniform frequency that results in nonuniform deposits. If the feed is too fast, the wire may enter the pool as a solid and could be solidified before fully melting as a solid wire inclusion. Uninterrupted bridging transfer ensures wire melting and pool mixing and improves bead shape uniformity (10). The latter is related to bridging wire feed position as the wire momentum can change the shape of the weld deposit if the wire feed position changes.

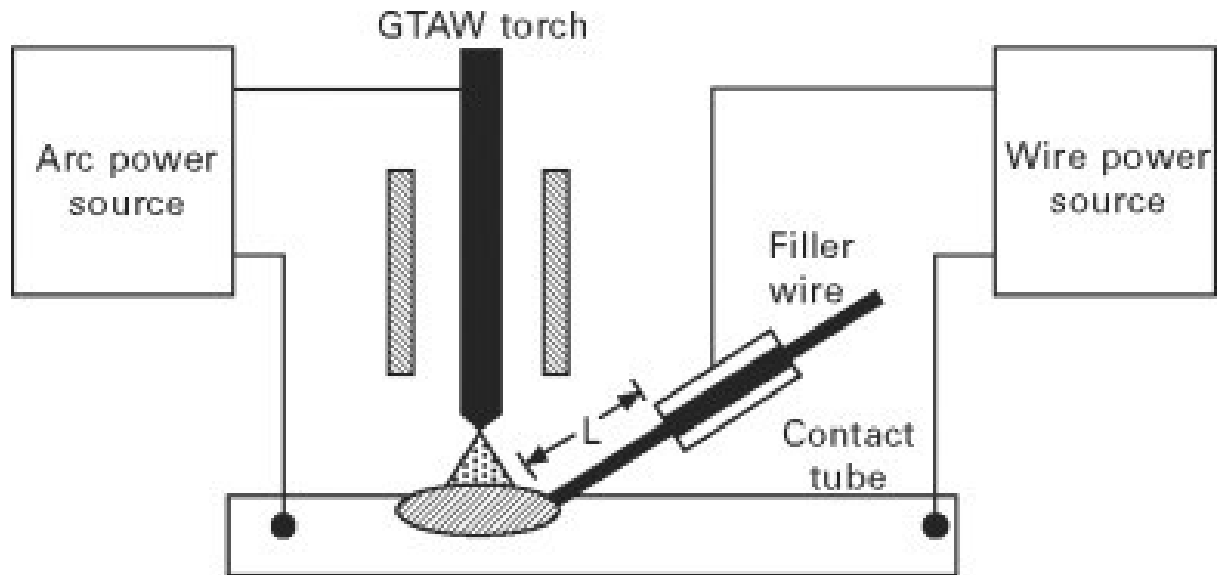


Figure A3 : Hot Wire Gas Tungsten Arc Welding (8)

To improve wire feed melting rate, a second hot wire (HW) power supply can be used to electrically preheat the wire extension between a conductive contact tip and the weld pool. This process is shown in Figure A3 and was developed in Manz and Saenger in 1964 to increase deposition rate compared to cold wire GTAW (6, 7). In hot wire GTAW (HW-GTAW), the hot wire power supply passes a low voltage current that resistively preheats the wire without forming an arc. Joule (I^2R) heating of the wire occurs when electrical current flow is established so a continuous wire bridge is needed between the wire contact tip and weld pool. Because contact of the wire to the workpiece is essential, wire feed instabilities can result in wire heating interruption and defects such as unmelted wire inclusions or lack of fusion. Hot wire process metal transfer mode is generally defined as one of two forms of bridging transfer as shown in Figure 4 and defined below (11):

- Continuous bridging transfer where the molten filler continuously streams into the weld pool promoting uniform repeatable bead profiles, and

- Recurring bridge transfer where the molten wire feed is interrupted as the hot wire current melting rate is greater than the wire feed speed. This mode is usually accompanied by a snapping noise as the wire breaks and shorts with the weld pool to re-establish current flow.

Transfer mode in HW-GTAW was found to be influenced by hot wire power, wire feed speed, wire feed angle, weld current, and wire feed direction (11). Both of these modes can produce sound uniform weld deposits.

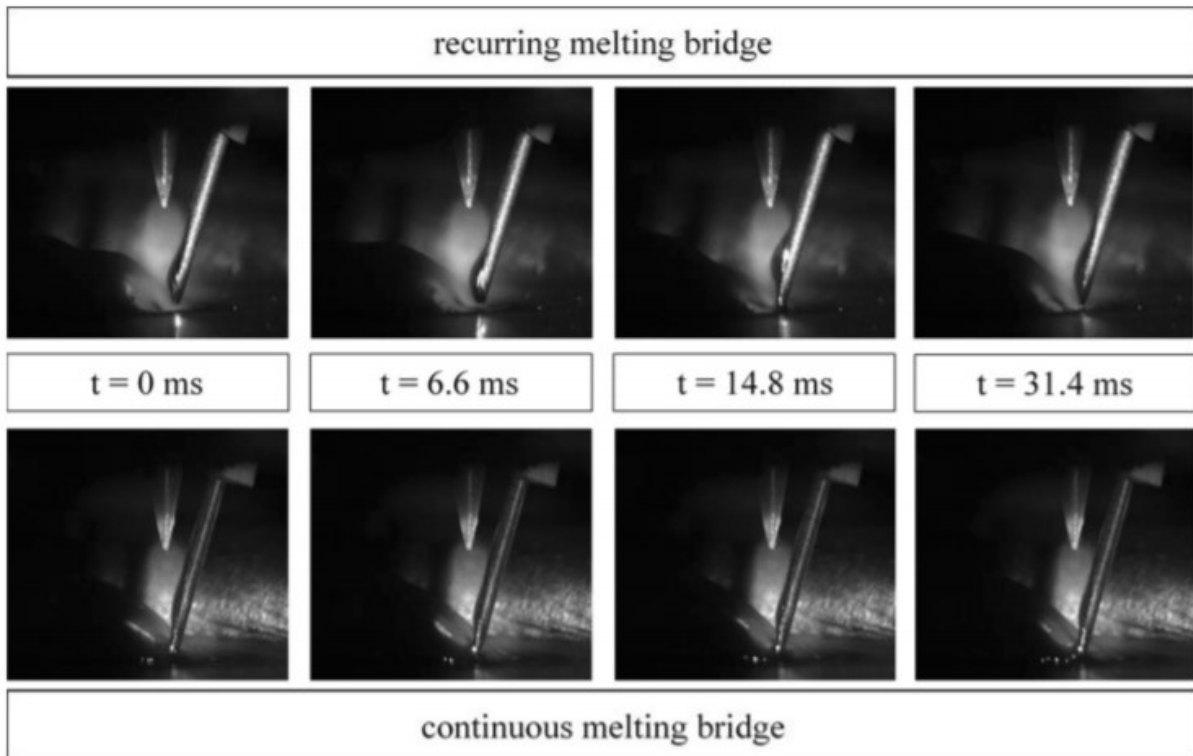


Figure A4: Recurring and Continuous Melting Bridge HW-GTAW Transfer Modes (11)

Hot wire feed is preferred for GTA cladding applications to improve deposition rates, often 2-3X cold wire feed, and minimize dilution of the clad deposit for surface engineering performance.

Hot wire is also preferred on applications that deposit consumables which have higher melting

energy requirements compared their base material, which was the case for cladding Anviloy wire on H13. HW-GTAW parameters can be developed to minimize base metal dilution on cladding applications so the required corrosion or hardfacing clad composition is met with the minimal number of layers and cost (12-14). By definition, dilution is mixing of the cladding wire with the based material. The cladding procedures needs to account for dilution by either using an over-matched “rich” cladding wire, or using multiple clad layers to reduce dilution effects and meet composition requirements. HW-GTAW can provide both higher deposition rate and lower dilution compared to cold wire GTAW (15-20). The preheating of the consumable wire in HW-GTAW also enables lower heat inputs to the base material which may reduce residual stress and distortion compared to cold wire GTAW (8-13).

Anviloy GTAW

Manual GTAW can be used with rod materials that are difficult to draw into continuous wire, which is the case for Anviloy 1150 (90W- 4Ni – 2Fe-4Mo) (3). GTAW has been used for decades to deposit this refractory alloy on die materials with good results. For this reason, and the relative simplicity of the process, GTAW was chosen as the initial process to evaluate a new Anviloy alloy (W-27.5Ni-12.5Fe) wire. Welding conditions and preferred welding parameters needed to be developed to establish mechanized die cladding feasibility. The first attempt at welding this material was conducted by undergraduate capstone researchers at The Ohio State University (OSU) using cold wire (CW) GTAW (3). They conducted a series of bead on plate weld deposit tests on H13 hot work tool steel base materials. Early in their trials, the researchers encountered wire feed cast and helix inconsistencies. The wire was very stiff and the feed was hard to control due to inconsistent cast and helix, which promoted irregular weld bead as shown in Figure A5 (2).



Figure A5 : GTAW Welds From OSU Capstone Group (3)

Sound welds were successfully created without porosity, cracking, or lack of fusion. However, the initial bead on plate weld tests had irregular weld edges. The irregular serpentine shaped deposits were due to changing wire cast and bridging feed position into the weld pool. These mechanized welds were applied as stringer beads, with no oscillation or weaving. The CW-GTAW weld deposits were sectioned for metallographic bead shape analysis. Base metal dilution was measured by divided the base metal fusion area by the whole bead “nugget” (cross section) area. The base metal dilution ranged from 30% to 60%. High base metal dilutions were necessary to achieve good CW-GTAW Anviloy fusion on H13 due to the higher melting energy characteristics of Anviloy versus steel (2). The findings from this preliminary study showed promise for cladding with Anviloy wire but also presented a set of challenges that needed to be mitigated to develop high quality multi-pass die cladding procedures. As a result of this study, Astaras made a series of wire drawing improvements to improve Anviloy wire quality (uniform cast and helix), and supplied heats in both 0.035 and 0.045 diameter for this project.

In this project, these new heats of Anviloy wire were used to develop HW-GTAW procedures and ultimately robotic gas metal arc welding (GMAW) procedures for cladding a production shot-block die for in-plant trials. Both of these mechanized processes provide improved consumable heating and deposition rates. This Appendix describes the results of HW-GTAW bead on plate and cladding tests. GMAW procedures development can be referenced in Appendix B. For Anviloy die cladding, there was an objective to deposit thin clad layers with minimal dilution to maximize Anviloy clad composition and minimize the number of layers for achieving heat checking resistance. There was also an objective to temper the H13 HAZ so both single and double layer clad procedures were evaluated as a minimum where the latter evaluated temperbead relationships that are reported in Appendix C.

Experimental Procedure

The purpose of this project task was to develop preferred HW-GTAW cladding procedures with Anviloy W-27.5Ni-12.5Fe alloy wire on H13 tool steel. Both single and double layer procedures were developed that could be used to clad die structures. The double layer procedures had an additional goal to temper H13 heat affected zone and minimize the need for post weld heat treatment.

Materials

The base material used for this study was an Uddeholm Orvar Supreme HWTS, the chemical composition of which is presented in Table 1.

wt.%	Fe	Cr	Mo	V	C	Si	Mn	W	Ni
Orvar Supreme	Bal.	5.1	1.5	0.9	0.39	0.9	0.4		
Anviloy Wire	12.5							Bal.	27.5

Table A1: Chemical Compositions of Alloys (wt.%)

The H13 base material plates was in the soft-anneal condition, with a starting microstructure consisting of ferrite and coarse alloy carbides, with a hardness around 180HV. The material is supplied in this condition for ease of machining. Base plate thickness for these tests was 3/4". All plates were cleaned to remove oxide scale using abrasive grinding wheels and then wiped clean with ethanol to remove any residue. The welding new Anviloy filler wire used for this study was developed by Astaras, Table A1. This Anviloy W-27.5Ni-12.5Fe wire is an experimental alloy for die casting applications. Its microstructure consists of alpha BCC tungsten phase in a Ni-Fe FCC matrix. The metallurgical characterization of Anviloy deposits is provided in Appendix D.

HW-GTAW Welding

Anviloy-H13 hot wire GTAW parameters were developed for single and double-layer cladding builds. The cladding procedures were intended for either cladding new dies or repairing die components that have heat checking damage. For the latter, the heat checked (cracked) surface area would be removed before rebuilding using Anviloy cladding. A range of HW-GTAW bead on plate welds, and multipass clad layer builds were made with varied parameters to identify preferred HW-GTAW parameter ranges. The preferred weld parameters were initially chosen based on visual appearance of welds. Bead on plate clad deposits were visually examined for toe angle profile, deposit height, and bead length uniformity as well as for weld defects such as cracking, lack of fusion, and porosity.

All hot wire GTAW tests were performed using a Jetline 9800 mechanized system, Miller Dynasty 500 power supply, and Jetline 200 Amp AC hot wire power supply. Initial tests were made with .035” diameter Anviloy wire and pure argon was used for the shielding gas. Wire feed angle used in this study was 45 degrees. Wire was fed into the leading edge of the weld pool in a front feed set up.

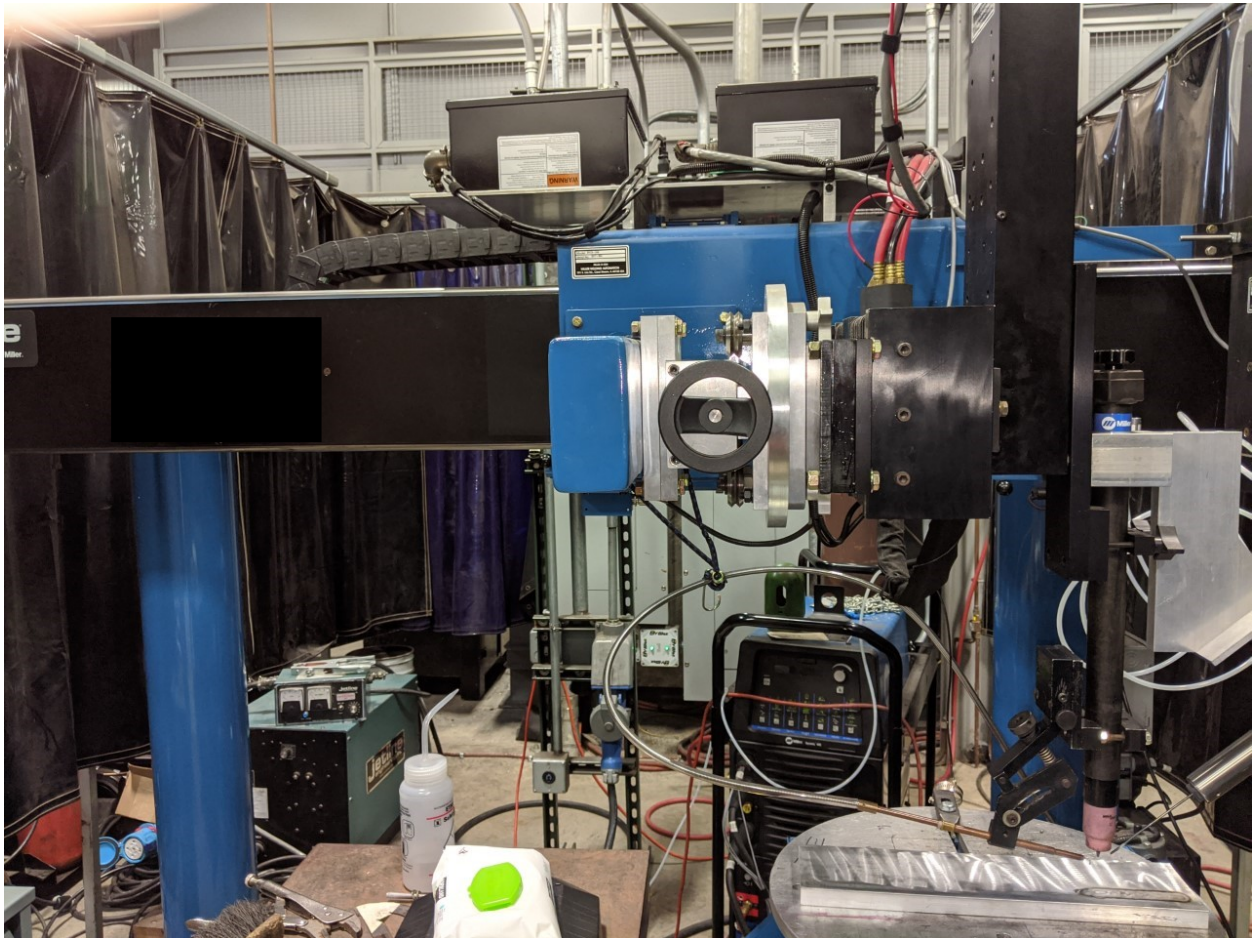


Figure A6 : Miller Jetline 9800 Mechanized Welding System

Clad Deposit Quality Assesment

Clad quality was based foremost on visual examination of the deposit’s surface and secondarily on microstructural features seen on metallographic clad deposit cross sections that

passed visual assessment. Clad bead uniformity was qualitatively measured using a straight edge ruler. Deposit height variations along weld length were measured using a Mitutoyo dial caliper. Clad deposit toe profile (or angle) was qualitatively analyzed using visual examination for most deposits, but was analyzed using metallographic procedures for preferred tests that were cross-sectioned for metallographic examination.

All metallographic samples were prepared by polishing with 240, 400, 600, and 800 grit SiC abrasive followed by 9, 6, and 3 micron colloidal diamond abrasive. Samples were submersion etched using a 10% Nital (10% Aqueous Nitric Acid in Ethanol) solution for 30-45 seconds. All metallographic images were taken with an Olympus GX-51 microscope using DP2-BSW software. Base metal dilution (BMD) calculations were made using imageJ software and gathered images of metallographically prepared samples. To determine BMD, the total area of the clad deposit fusion zone was divided by the area of the fusion in the base material.

$$BMD = (Total\ Area\ of\ Clad\ Fusion\ Zone)/(Area\ of\ Fusion\ in\ Base\ Material)$$

The resulting BMD value represents base metal dilution of the clad deposit.

Results and Discussion

Wire Cast and Helix

The bead irregularities seen by prior researchers (3) were results of excessive wire cast and helix. This would make the ability to build multi-pass claddings difficult. Therefore, one of the first priorities of his study was to improve the wire cast and helix so bridging transfer position could be precisely controlled during HW-GTAW cladding. As noted above, excessive wire cast and helix was the main cause for nonuniform Anviloy deposits in the prior research. Per AWS filler specifications, there is an acceptable level of “cast” and “helix” in all spooled

consumables, and there are methods to measure these wire characteristics. Irregular cast and helix is not acceptable for precision welding. This study worked with the Anviloy wire supplier who improved the wire cast and helix. In addition, a 2-axis wire straightener was integrated into the Jetline wire feed system. This straightener was added to change and “set” the cast and helix for better precision feed. Consistent and small cast and helix lead variations accommodate precise bridging wire transfer position into the weld pool and precision multi-pass cladding.

Wire cast and helix is measured by cutting a section of wire long enough to form a single loop and measuring the loop diameter, as shown with Anviloy wire in Figure A7.

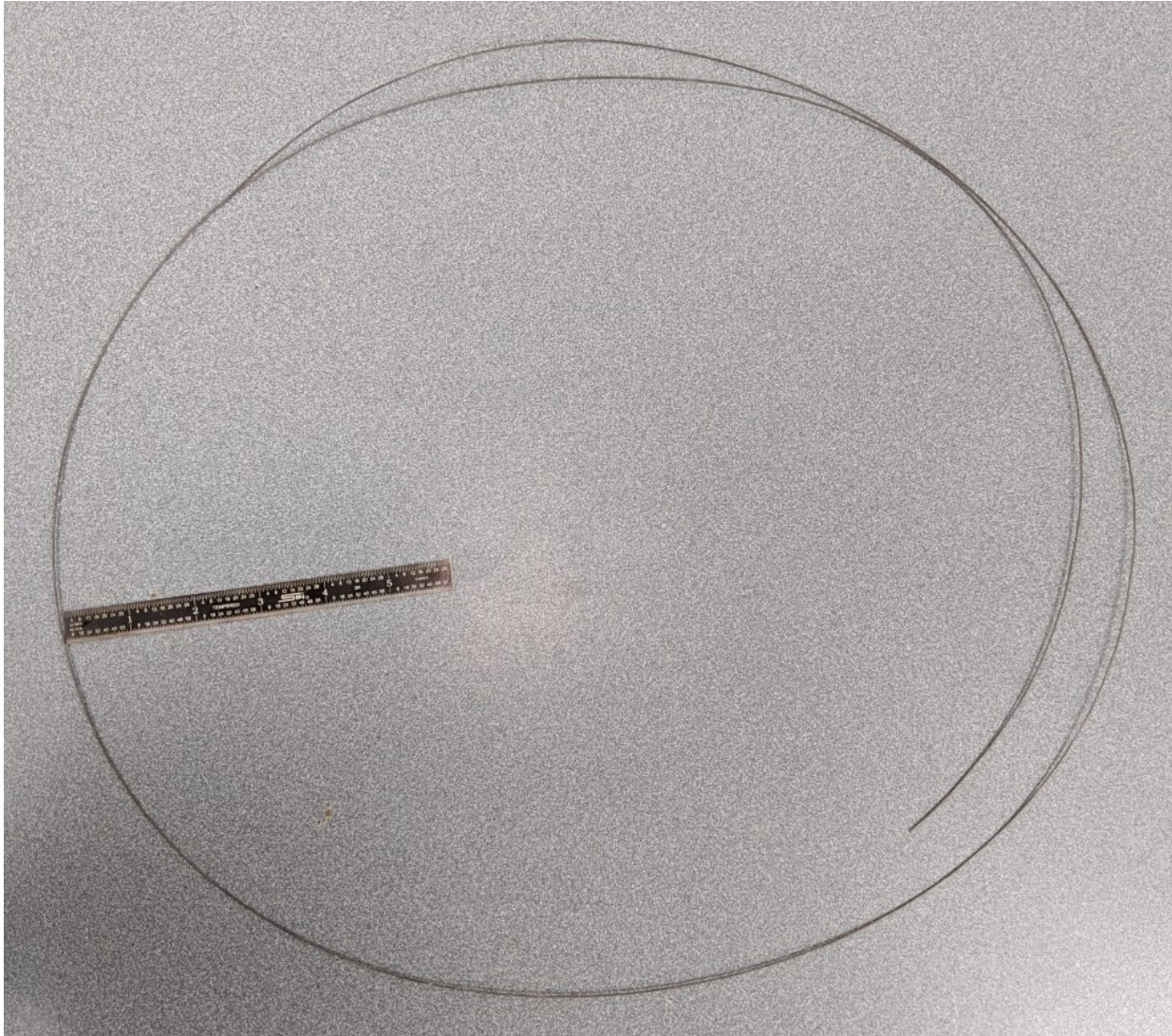


Figure A7 : Anviloy Wire Cast

The cast of the Anviloy wire was measured to be 14 inches. This value indicates a significant curvature in the wire that could potentially lead to feeding inconsistencies. Helix is quantified using the same loop section, but instead of the loop diameter, the height variation is measured from a flat surface. It should be noted that Anviloy wire's high density of 14.5g/cm^3 likely contribute to a lessening of the measured helix value due to gravity. Nevertheless, the Anviloy wire's helix was measured and shown in Figure A8.



Figure A8 : Anviloy Wire Helix

It should also be noted that the wire cast and helix was inconsistent at different locations in the wire spool. Acceptable ranges for these cast and helix are quantified in numerous AWS standards for different material types, but Anviloy wire standards have not been developed so the project worked with the supplier to improve the wire quality. It should be noted that, since the Anviloy Wire consumable used in these studies was a prototype / development heat, more variation should be expected versus an established consumable supplier who will resolve quality issue and improve product performance over time. Since cast and helix for Anviloy wire was found to vary when making bead on plate HW-GTAW deposits, a two axis wire straightening system was integrated into the Jetline feed system to straighten the wire, Figure 9. The two axis wire straightener was positioned between the spool and the wire feeder. The wire straightener system consisting of two conjoined single axis Miller wire straighteners mounted 90 degrees relative to each straightener's roll forming direction.

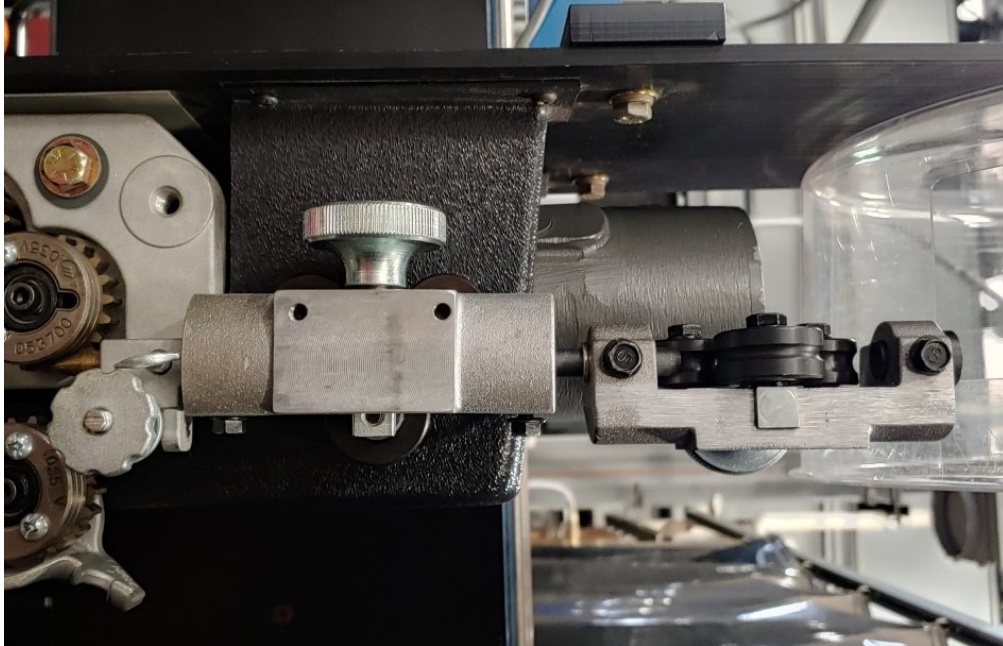


Figure A9 : Two Axis Wire Straightener

After the wire straightener was added to the mechanized welding system, additional bead on plate tests were created to evaluate whether or wire cast and helix uniformity was the cause of the serpentine shaped welds. Those welds are shown using a range of parameters in Figure A10.



Figure A10 : Welds Made with Two Axis Wire Straightener

Even though HW-GTAW parameters were not fully developed to provide ideal deposit shape, the wire straighteners provided uniform wire feed position and better bead uniformity. Due to

the increased repeatability enabled by the wire straightener, all subsequent welds were made using the two axis wire straightener. Bead quality was further improved in subsequent HW-GTAW trials.

HW-GTAW Setup Conditions and Parameter Development

Hot wire GTAW welding conditions were developed to produce smooth Anviloy clad deposits. The hot wire electrical stickout, voltage, current and feed position were varied using a series of trial and error tests, Table A2 to establish preferred hot wire setup conditions. Some of the tests produced unacceptable deposits where the main defects were bead irregularity, excess spatter, high toe angle, and unmelted wire inclusions, Figure 11. Several factors can influence incomplete melting of the filler material in HW-GTAW. Insufficient weld heat input can cause unmelted wire inclusions by failing to provide enough heat to melt the consumable. Disruptions of hot wire heating due to an interruption in the electrical circuit, such as by breakdown of bridging metal transfer caused by improper wire feed position, are another potential cause of unmelted wire inclusions. This is exacerbated by large hot wire stickouts or irregular wire cast and helix, which can cause wire to make contact outside of the weld pool. Another potential cause is insufficient weave dwell to achieve full melting and tie in for multi pass clad procedures

With alternating current hot wire power supplies, the voltage is set and current draw is a results of the electrical stickout (distance between contact tip to pool) and the wire resistance. Joule (I^2R) heating is used to preheat the wire ideally to the melting point as it enters the weld pool and enables good bridging transfer. The hot wire power supply used was a Miller Jetline 200 Amp hot wire power supply. This unit sets the voltage which was manually trimmed during tests on the power supply. Excessive voltage promoted interrupted bridging transfer and arcing between preheated wire and base plate. Interrupted bridging transfer was not stable with the

Anviloy wire so it was necessary to determine the preferred voltage and stickout to achieve preheating and bridging metal transfer without arcing. Weld oscillation was added to further improve bead shape as the Anviloy weld pool was very viscous and need to be distributed over the base material.

Weld Number	Arc Current (A)	Arc Voltage (V)	Travel Speed (in./min.)	HW-Stickout (in.)	Wire Feed Speed	Hotwire Voltage (V)	Osc. Width (in.)	Osc. Dwell (sec.)	Comments
13	200-280	11.5	3	1"	70	4	.25"	0.2	Good toe angle and longitudinal straightness, uniform bead appearance
14	200-280	11.5	3	1"	70	4	.25"	0.2	Good toe angle and longitudinal straightness, uniform bead appearance
15	200-280	11.5	3	1"	70	6	.25"	0.2	Good toe angle and longitudinal straightness, some bead height irregularity, excessive spatter
16	200-280	11.5	3	1"	70	6	.25"	0.2	Good toe angle and longitudinal straightness, some bead height irregularity, excessive spatter
17	220	11.5	3	1.5"	60	4	0	0	Longitudinal irregularity, bead height irregularity, marginally increased toe angle
18	220	11.5	3	.75"	60	4	0	0	Good longitudinal straightness and bead height regularity, marginally increased toe angle
19	240	11.5	3	.75"	80	3	.25"	0	Excellent longitudinal bead straightness and bead regularity, good toe angle. Unmelted wire upon sectioning
20	240	11.5	3	.75"	80	3	.25"	0.2	Excellent longitudinal bead straightness and bead regularity, good toe angle. Good appearance upon sectioning

Table A2 : Clad Development Parameters

All tests were performed at 3 inch/min travel speed which is a normal level for mechanized GTAW procedures. Based on these setup tests, it was determined that the preferred electrical stickout was 0.75-inch which provided good position control for hot wire deposition. The preferred voltage was approximately 11.5 volts (based on readings from the Analog dial indicator) and provided a long (3/16- to ¼-inch) arc length. A long arc was preferred to help spread the Anviloy deposit and minimize risk of hot wire contact with the electrode. The preferred oscillation was from 0.25-inch width with 0.25 second dwells. These preferred setup conditions were then further refined to evaluate both single and double layer clad characteristics. An example of a clad build using weld 20 parameters is shown in Figure 12. This clad build shows uniform fusion between all deposits and had a smooth uniform surface appearance.

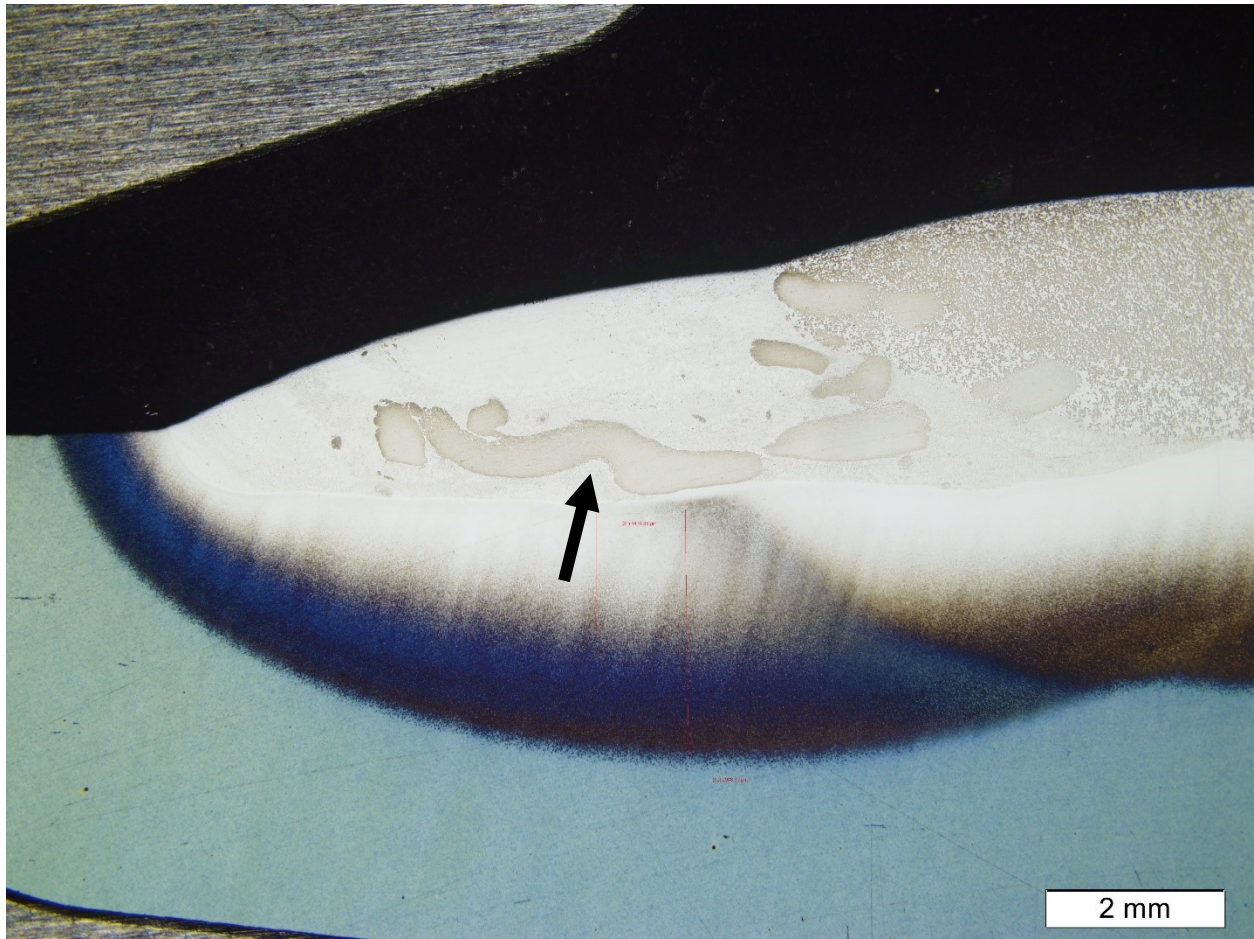


Figure A11 : Insufficient Hotwire Power to Ensure Bridging Metal Transfer Resulting in Unmelted Wire Inclusion (arrow) in Anviloy Wire Clad Deposit Trial 19.

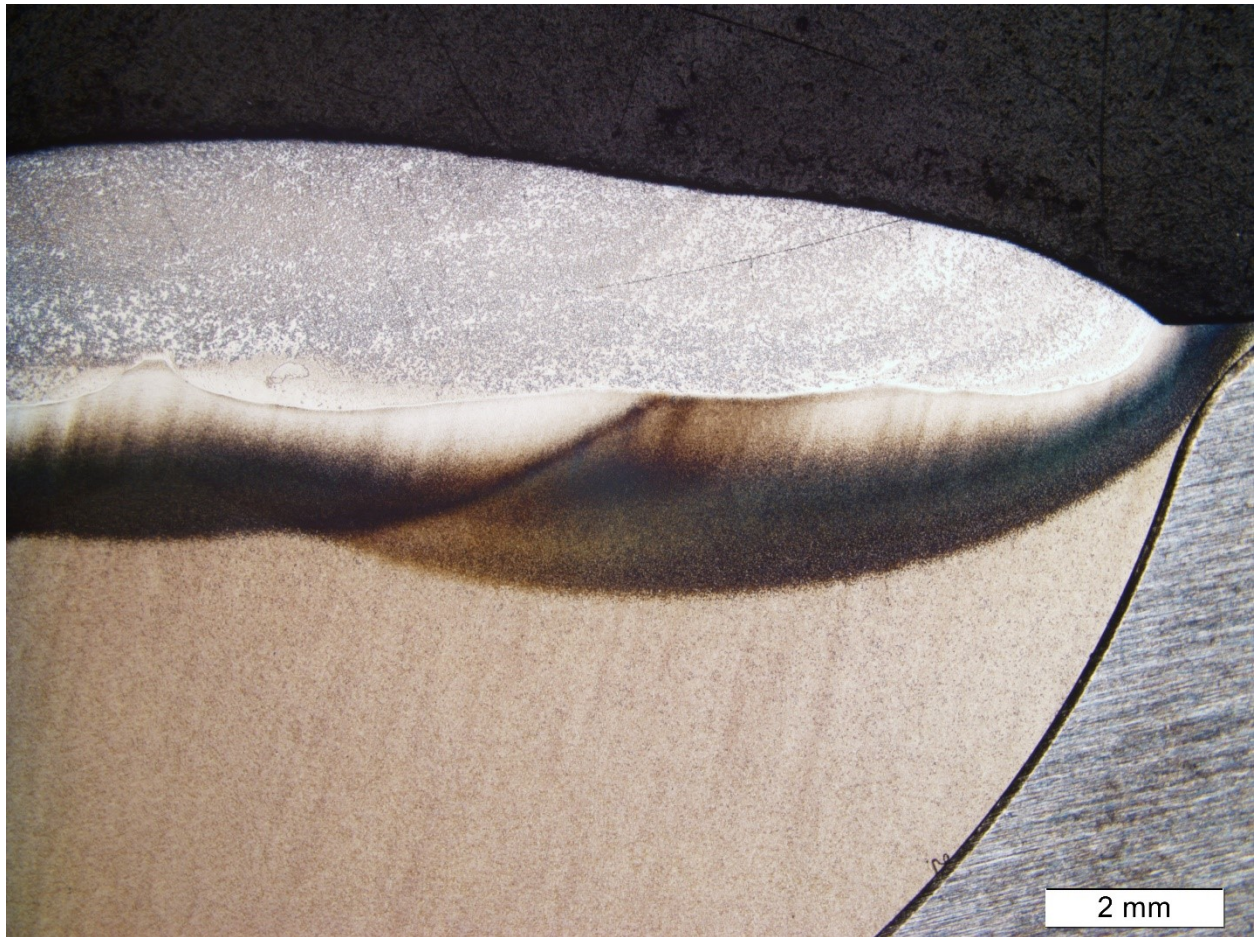


Figure A12: Uniform Anviloy Clad Deposits Made using Deposit Trial 20 Parameters

HW-GTAW Parameter Effects on Base Metal Dilution

Since a benefit of hot wire gas tungsten arc welding is reduced dilution, a series of bead on plate tests were undertaken to determine the minimum dilution possible while achieving adequate fusion using Anviloy wire. These constant deposit area stringer bead tests (no oscillation) involved welding with fixed set-up conditions and constant arc length, wire feed speed and travel speed. GTAW current was varied to change the heat input and dilution, Table 3. A bead shape map comparing the welds is shown in Figure A13 for tests LD-1, LD-2 and LD-3.

Weld	Arc Current (A)	Arc Voltage (V)	Travel Speed (in./min.)	HW-Stickout (in.)	Wire Feed Speed	Hotwire Voltage (V)
LD-1	140	11.5	3	0.75	80	4
LD-2	160	11.5	3	0.75	80	4
LD-3	180	11.5	3	0.75	80	4

Table A3 : Low Dilution Trial Parameters

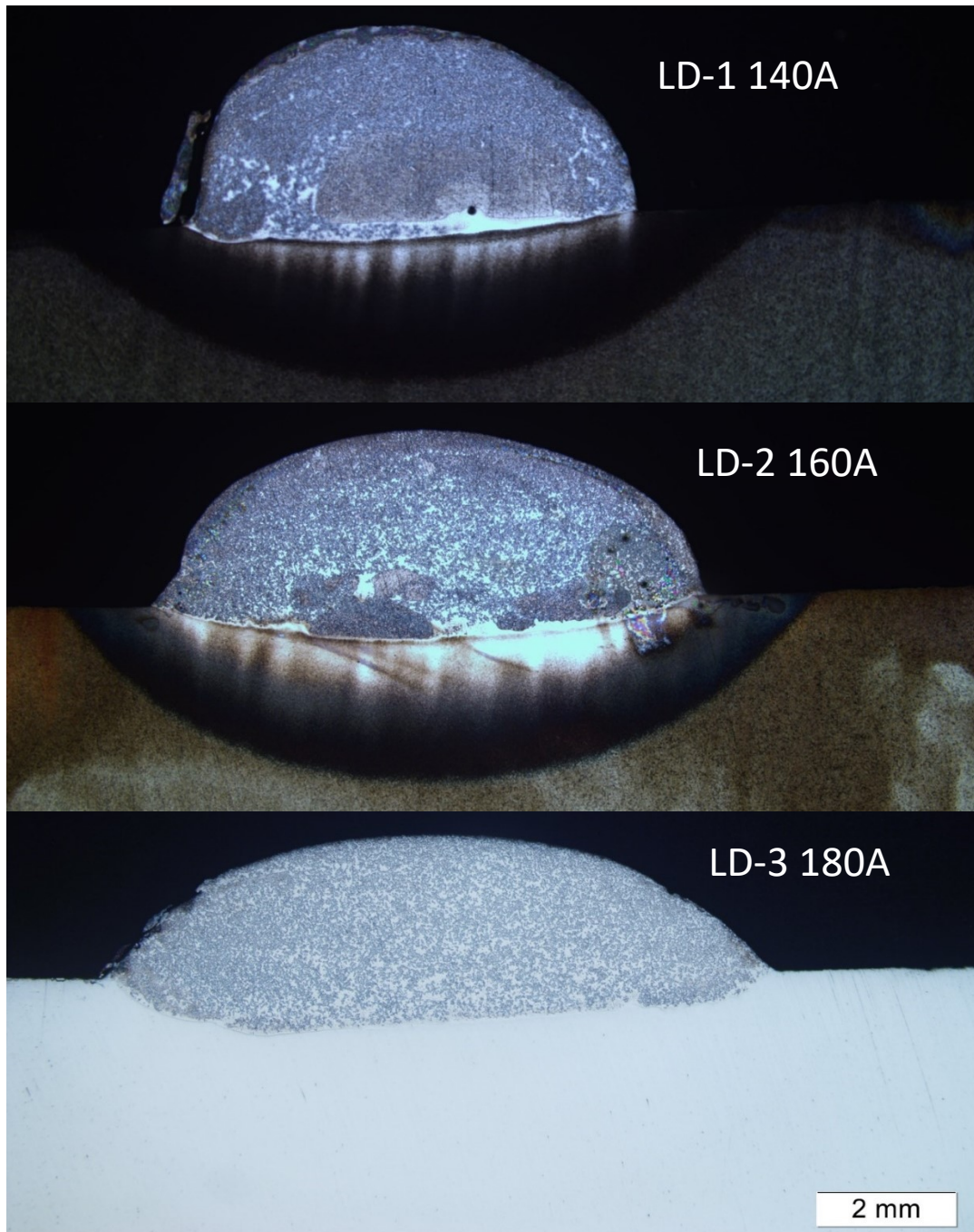


Figure A13 : Low Dilution Constant Deposit Area Bead on Plate Tests conducted at three different currents (140, 160 and 180 amps) at constant travel speed, wire feed speed, arc voltage and hot wire conditions of 4 volts and 0.75 inch stickout.

As current increased, bead width and dilution increased while deposit height decreased. In addition, the deposit toe angle decreased as current and heat input increased. The weld produced using a 140A current resulted in a base metal dilution (BMD) of only 7% when measured using the imageJ method. Although this is a very low dilution value, the weld had a gas pore defect towards the bottom of the fusion boundary. The origin of pores in Anviloy deposits is an area for future work but higher current tended to minimize small pores from the deposit. In addition to the gas pore, a very high weld toe angle can be observed which indicates poor wetting of the base material by Anviloy wire. Due to the presence of a gas pore and adverse toe angle, current was raised to 160 Amps for test LD-2. The 160Amp weld shown in the above figure resulted in a dilution of 12%. Although this is also a low dilution value compared to previous efforts, this weld suffered from small pores seen in the 140 Amp sample. Although toe angle was somewhat improved vs. the 140A sample, three small gas pores can be seen on the right flank of the deposit. These pores indicate insufficient heat input was applied to out-gas pores, or the porosity source (moisture on filler and base materials) needs to be eliminated to make low dilution Anviloy deposits. The next attempt at achieving sound welds with minimal dilution employed a 180Amp current for test LD-3. The 180Amp weld resulted in a base metal dilution of around 18% when calculated with the imageJ method. Although higher than the 140Amp and 160Amp trials, this clad had no porosity defects with an acceptable toe angle. Overall, the HW-GTAW was successful in reducing heat input and dilution compared to CW-GTAW and produced smooth Anviloy bead on plate deposits with good fusion. Future studies may be able to improve the bead shape using LD-1 and LD-2 parameters by oscillating the torch and by using preheat which can drive moisture off surfaces. The preferred setup conditions and

baseline parameters developed in this task were used to develop multipass clad deposits and evaluate HAZ tempering relationships in Appendix C.

Conclusions

- Preferred HW-GTAW setup conditions were determined to get precision bridging metal transfer with Anviloy wire.
- Anviloy wire cast and helix was important for bridging metal transfer position control and bead uniformity. A two-axis wire straightener was found to straighten the wire sufficient to produce uniform clad deposits.
- Hot wire voltage of 4V was sufficient to achieve bridging metal transfer at $\frac{3}{4}$ " electrical stickout with wire feed speeds from 60 to 80IPM.
- Sound HW-GTAW clad deposits were produced with dilutions as low as 18% compared to CW-GTAW where the minimum was 30% dilution. Lower dilutions are feasible with preheat and torch oscillation.

Works Cited

1. Johnson, L., Kenney, C., Tyrell, R. “Automated Die Repair Using Anviloy Wire.” Ohio State University Welding Engineering Capstone Program. 2017.
2. Lancaster, J.F. “IOPscience.” *Physics in Technology*, IOP Publishing, 20 Nov. 2002, iopscience.iop.org/article/10.1088/0305-4624/15/2/I05.
3. Endemann, A., & Hoehn, T. (2018). “New materials in mould making are required to meet the new challenges in die casting.” Paper presented at the *73rd World Foundry Congress "Creative Foundry", WFC 2018 - Proceedings*, 489-490.
4. Yudodibroto, B. Y. B., et al. “Influence of Filler Wire Addition on Weld Pool Oscillation during Gas Tungsten Arc Welding.” *Science and Technology of Welding and Joining*, vol. 9, no. 2, Informa UK Limited, Apr. 2004, pp. 163–168. Crossref, doi:10.1179/136217104225012274.
5. “Soldagem TIG Com Sistema De Alimentação Tangencial (b Hsf).” *LABSOLDA*, 2020, labsolda.ufsc.br/videos/videos-tecnicos/video/soldagem-tig-com-sistema-de-alimentacao-tangencial-b-hsf.
6. Saenger JF (1968) High deposition gas tungsten arc welding. *WeldJ* 47(5):386–393
7. Manz AF, Saenger JF, Freeman ND, Stanchus FT (1969) ‘Method for depositing metal with a tig arc’, US3483354A.
8. Tejedor, T. Álvarez, et al. “Maintenance and Repair of Gas Turbine Components.” *Modern Gas Turbine Systems*, Woodhead Publishing, 27 Mar. 2014, www.sciencedirect.com/science/article/pii/B9781845697280500136?via=ihub
9. Longlong, Guo, et al. “Formation Quality Optimization and Corrosion Performance of Inconel 625 Weld Overlay Using Hot Wire Pulsed TIG.” *Rare Metal Materials and Engineering*, vol. 45, no. 9, Elsevier BV, Sept. 2016, pp. 2219–2226. Crossref, doi:10.1016/s1875-5372(17)30006-1. Influence of filler wire addition on weld pool oscillation during gas tungsten arc welding
10. Ungethüm, T., et al. “Analysis of Metal Transfer and Weld Geometry in Hot-Wire GTAW with Indirect Resistive Heating.” *Welding in the World*, vol. 64, no. 12, Springer Science and Business Media LLC, Sept. 2020, pp. 2109–2117. Crossref, doi:10.1007/s40194-020-00986-0.
11. Silva IG. Study of the influence of the parameters of corrosion-resistant overlay welding by the hot-wire TIG process on dilution [master’s dissertation]. Curitiba: Paraná Federal University of Technology; 2007.
12. Fratari RQ, Schvartzman MMAM, Scotti A. Optimization of the parameters of weaving for buttering on sheets of carbon steel by the TIG process with AWS ER309L wire. *Soldagem e Inspeção*, São Paulo. 2010;15(3):209–217
13. Dupont JN, Marder AR. Dilution in single pass arc welds. *Metall Mater Trans B*. 1996;27B(3):481–489. Doi:10.1007/BF02914913.

14. Henon BK. Advances in automatic hot wire GTAW (TIG) welding [Internet page]. Pacoima: Arc Machines; 2015
15. Lucas W. TIG and plasma welding: process techniques, recommended practices and applications. Cambridge:Abington Publishing; 1990
16. Shinozaki K, Yamamoto M, Nagamitsu Y, et al. Melting phenomenon during ultra-high-speed GTA welding method using pulse-heated hot-wire. Q J Jpn Weld Soc. 2009;27(2):22s–26s. Doi:10.2207/qjws.27.22s
17. Lv SX, Tian XB, Wang HT, et al. Arc heating hot wire assisted arc welding technique for low resistance welding wire. Sci Technol Weld Joining. 2007;12(5):431–435. Doi:10.1179/174329307X213828
18. Lv SX, Xu ZW, Wang HT, et al. Investigation on TIG cladding of copper alloy on steel plate. Sci Technol Weld Joining. 2008;13(1):10–16.

Appendix B : Anviloy Robotic GMAW Conformal Cladding

Parameter Die Development

Abstract:

Robotic welding, wire arc additive manufacturing, and conformal cladding are attractive pursuits in die casting due to their potential for reducing die manufacturing and repair costs. A new W-27.5Ni-12.5Fe (Anviloy Wire) refractory alloy was evaluated that shows promise for automated die cladding. Anviloy is a high performance die casting die material that offers better heat checking resistance than hot work tools steel (1). Historically, Anviloy is used selectively for solid die inserts based on its premium cost, or for isolated manual arc welding repairs using rod. In this study, gas metal arc welding (GMAW) parameters were developed to conformal cladding an H13 tool steel shot block using the new W-26.5Ni-13.5Fe wire in an effort to improve shot block repair and die life performance. GMAW cladding parameters were developed for flat (1G) and horizontal (2G) welding positions using an OTC robotic GMAW - pulse (P) system. Good Anviloy electrode metal transfer was achieved by selecting the preferred OTC GMAW-P waveform. Two waveforms were evaluated. The first waveform (Synchrofeed Ferrite 1.2mm) used electrode positive (EP) pulsing and was found to have insufficient power to achieve adequate Anviloy wire melting and H13 steel base metal fusion. The second waveform (DC-Wave SuS 1.2mm) used electrode negative (EN) pulsing which is known to provide more electrode heating versus EP pulsing. The EN waveform was found to provide good metal transfer and fusion with Anviloy which as higher melting point, heat capacity and thermal conductivity compared to steels. Using the EN waveform, a range of parameters were developed to identify the wire feed speed and travel speed combination that provided sufficient power and

heat input for good fusion. The die block's complex shape mandated sub-optimal torch work angle when welding horizontal (2G) sections. Special weld oscillation pattern was employed with adverse torch angles to accommodate the die 2G die profile clad deposition. The die blocks complicated shape also mandated the development of high quality weld stop welding procedure to ensure conformal clad quality. The quality of the weld stops was validated with visual inspection and metallographic sectioning. These trials showed the feasibility of Anviloy GMAW-P conformal cladding of H13 die casting dies. Ongoing efforts are in-place to evaluate the performance of Anviloy clad shot blocks on a high volume drive train component die casting.

Objectives:

- Evaluate commercial OTC GMAW-P waveforms for Anviloy wire metal transfer and H13 cladding by making flat (1G) bead on plate welds using a robotic GMAW-P system.
- Develop 6-axis robotic Anviloy cladding procedures for conformal cladding the shot block face (1G - flat position) and shoulder profile (2G - horizontal position) while shot block die is positioned flat.
- Develop robotic conformal cladding procedure and provide cladded shot-block dies for ongoing in-plant trials, which will evaluate Anviloy cladding performance on a high volume drive train component casting.

Background

Die repair, cladding, and additive manufacturing is carried using a range of automated welding processes. Laser wire, laser powder and electron beam wire deposition as well as methods based on traditional arc welding are commonly used processes (1). In terms of depositing or repairing large sections of dies, arc welding processes provide high deposition rates and lower system costs compared to laser and electron beam processes (2). Previous researchers have proven similar results, with hot work tool steel deposition rates reaching upwards of 3.6kg/hr with gas metal arc welding (GMAW) (3). The most common arc welding processes used for die repair and die additive manufacturing are gas metal arc welding (GMAW) and gas tungsten arc welding (GTAW). The preferred process is based on the die cladding feature requirements. For near net shape large scale features, GMAW is preferred over GTAW since it provides higher deposition rates and is simpler to automate. GMAW is omni-directional since the consumable electrode is fed through the center of the torch (Figure B1) versus GTAW where

the electrode is fed into the side of the torch using additional apparatus (Figures B2 and B3). An omni-directional torch improves the robotic build volume and access to complicated features that are found on die casting dies. GTAW is preferred on high integrity applications that demand precision arc starting and stopping and can be welded directionally using the side wire feed. Both GTAW and GMAW were evaluated for Anviloy cladding on H13 tool steel.

Heat generation in arc welding occurs by forming an arc between the torch electrode and the workpiece. In GMAW, the arc is formed using a consumable electrode which is fed through a torch (Figure B1). The metal is transferred by either short circuit, globular, spray or pulse spray transfer. Most of these metal transfer modes operate in the direct current electrode positive (DC-EP) polarity. Here the workpiece is the cathode and the consumable electrode is the anode. The majority of the heat generated is at the non-thermionic cathode, which must boil to emit electrons and ensure good base metal fusion. For GMAW, the metal transfer mode changes as a function of electrode type and diameter, current, electrical stickout and arc length. For continuous arcs that do not short, the metal transfer changes from globular to drop spray at a current known as the spray transition current. Globular drop transfer is more susceptible to spatter as gravity is used to detach the drops and drop transfer frequency is irregular. Above the spray transition current, the drops are propelled across the arc at a steady frequency which minimizes susceptibility to spatter. Modern power supplies can pulse the current about the spray transition current to provide spatter-free pulse metal transfer at average currents that are below the spray transition current. Here, a synergic algorithm is programmed in the power supply which automatically changes the waveform background and peak pulse parameters as a function of wire feed. In this study, two pre-programmed pulse waveforms that were developed for other

materials were screened and “trimmed” to develop pulse parameters for Anviloy wire consumables.

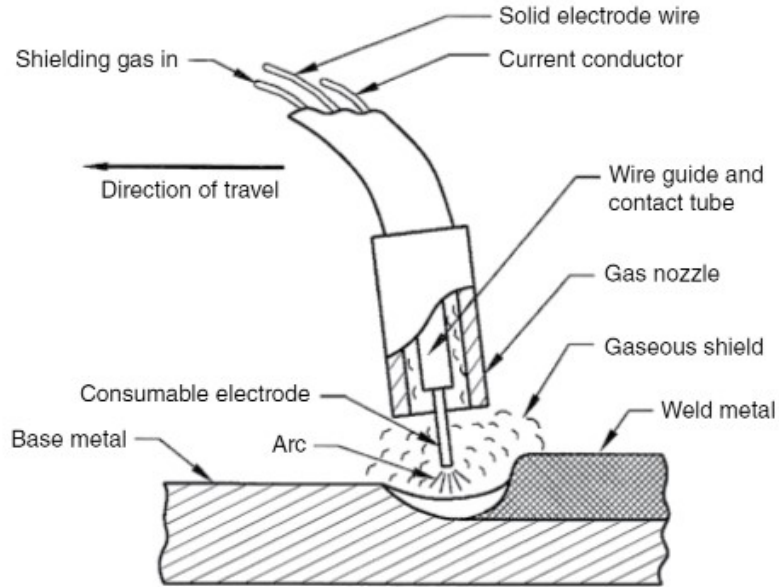


Figure B1 : GMAW Process (3)

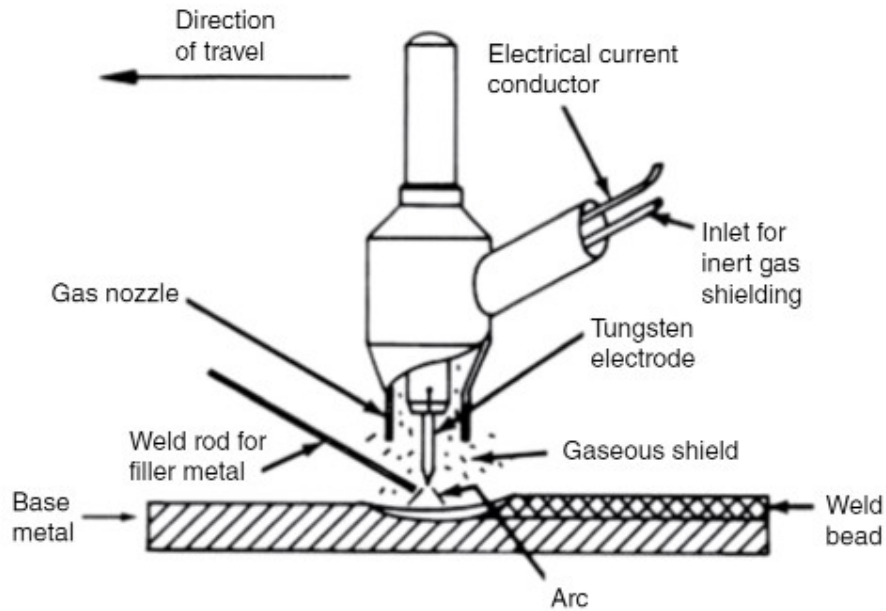


Figure B2: GTAW Process (3)

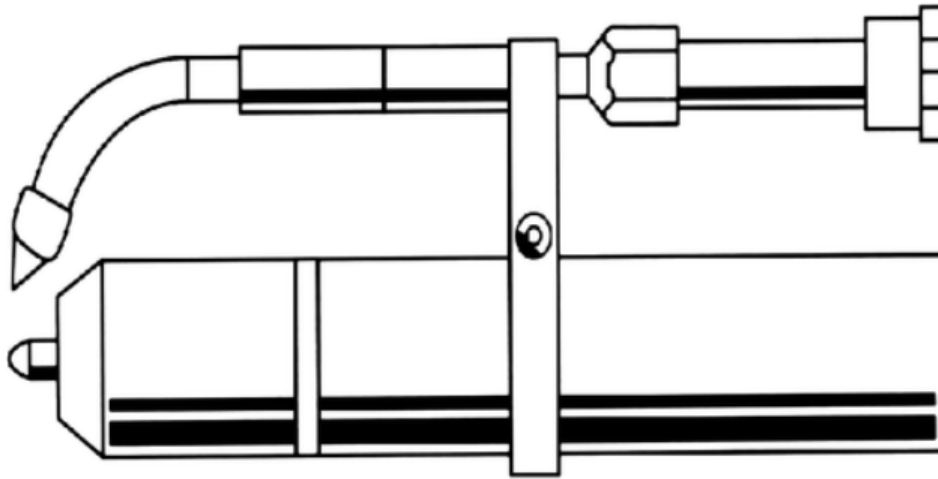


Figure B3: Robotic GTAW Welding Torch (3)

Heat generation in GTAW is by an electric arc between a non-consumable tungsten electrode and the workpiece. GTAW arc can operate in EP, EN or alternating current. When in the EN polarity, the tungsten is the cathode and is a thermionic emitter of electrons. The EN tungsten arc operates at lower voltages as only a couple volts are required to thermionically emit electrons. The EN GTAW heat balance is often cited to be 30% at the cathode and 70% at the anode. The GTAW arc current must be sufficient to create weld pool in the base material and provide enough radiant heat to melt the consumable as it is fed into the pool side. In general, side feeding an electrode into the weld pool is inefficient and results in significantly lower deposition rates compared to consumable electrode process like GMAW. For GTAW, the consumable is usually fed cold into the pool. Hot wire (HW) power supplies can be used to preheat the wire and improve deposition rates. Hot wire feed requires a second power supply that passes a low voltage current that preheats the wire, often to the melting point before entering the weld pool. Hot wire feed is preferred for consumables that have higher melting points and

energy requirements compared their base materials, which was the case for cladding Anviloy on H13. A range of experiments were performed to evaluate HW-GTAW of Anviloy clad on H13 (Appendix A). This process was appropriate for studying clad and HAZ microstructures and evaluating temperbead effects on multi-layer clad deposits. However, HW-GTAW apparatus was too bulky and difficult to program to fully clad the shot-block that was chosen for in-plant trials in this project. Therefore, Robotic GMAW-P was chosen to conformally clad die blocks using Anviloy wire since the process is omni-directional and pulse waveforms can be developed to ensure Anviloy melting. GMAW is usually considered a higher heat input process than GTAW since it deposits larger beads, but new advanced pulse waveforms enable higher deposition at relatively lower heat inputs and base metal dilution. The latter was important for Anviloy cladding where excessive dilution needs to be avoided or it will lower the heat checking resistance of the clad layer. In general, low dilution cladding procedures are advantageous for die casting applications.

With the GMAW-P process, most waveforms use electrode positive (EP) pulsing (6). The heat balance with GMAW is opposite of GTAW. The majority of the heat is developed at the cathode which is a field emitter and must boil to emit electrons. As a result, maximum penetration and base dilution occur in the EP polarity. The majority GMAW applications and GMAW-P waveforms are setup to operate in the EP mode. The EN polarity can be used with the GMAW process under special circumstances as metal transfer can be hard to control since the melting rate will often double. If metal transfer can be controlled, the EN polarity is preferred for cladding since it will increase deposition rate and decrease base metal dilution. Some advanced GMAW pulse power supplies have EN or variable polarity pulse waveforms that use EN heating to improve consumable electrode deposition rate. Though they can enable much

greater operational efficiency, development of advanced pulsed waveforms for GMAW is a difficult and time consuming endeavor.

Advanced waveform development generally involving the use of high speed weld videos to determine optimal current and wire feed pulsation and ramp parameters such as those shown in Figure B5 (6). For this study, there was not sufficient project resources to develop a special waveform algorithm for Anviloy wire. Instead, waveforms that were developed for other materials were tested for their metal transfer suitability with Anviloy. The power supplies also offer power “trim” with each waveform so by adjusting the trim, waveforms that were developed for other materials should work on Anviloy.

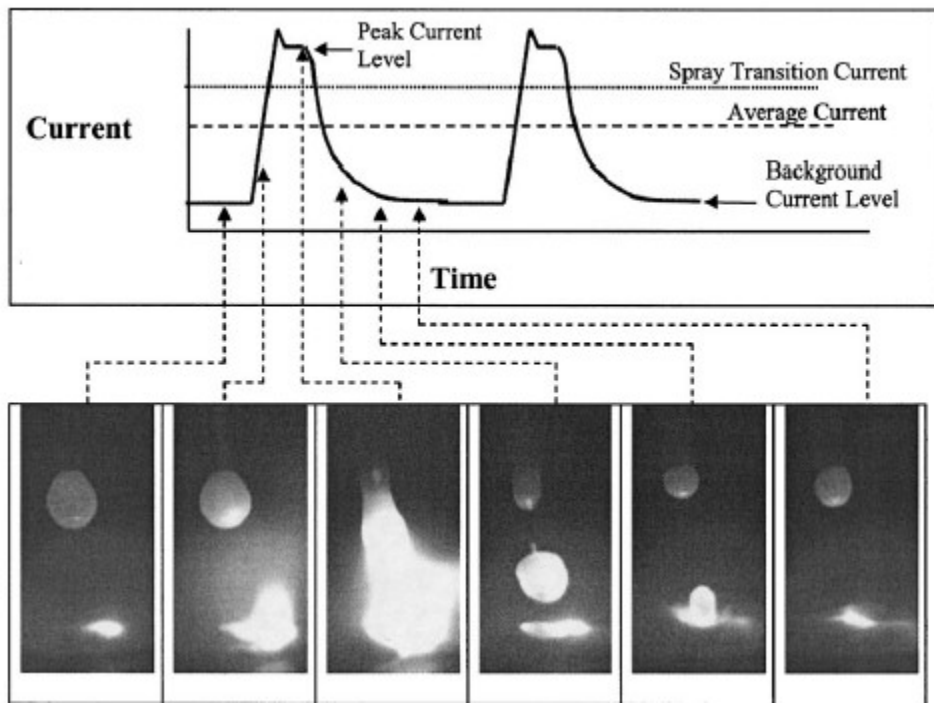


Figure B5: Advanced Pulse Waveform and High Speed Weld Imaging of Process

Typically, individual weld suppliers keep GMAW-P waveforms proprietary, but all generally include some form of background and peak current as well as pulse and background period, in

addition some method to adjust the shape of the waveform via arc trimming (6). Advanced pulse waveforms are generally used with a secondary servo driven wire feed mechanism in addition to standard drive rolls common to all welding wire feed systems (6). Servo motors enable high speed wire start/stops timed in concert with the waveform that are necessary for precise wire feeding of advanced pulse GMAW.

Since these advanced waveforms are specially designed for more standardized materials like carbon steels, stainless steels, and aluminum alloys, they must be analyzed for applicability for welding Anviloy wire. Advanced pulse welding waveforms use algorithms that change all the pulse parameters, usually current as a function of wire feed speeds. Welding current is the main factor determining melting rate of the wire during GMAW. For pulsing, the relationship between current waveform and wire feed speed is somewhat unique to each power supply manufacturer where each supplier offers a range of pre-programmed GMAW-P waveforms for different electrodes. This greatly simplifies parameter development for the established materials, but gives less freedom for waveform parameter design for new materials. Because the algorithms correlate current to wire feed, either wire feed or current mode can be selected in the control pendant. To accommodate new materials, the weld power supplies provide waveform trim to help make minor adjustments to the waveform and provide less or more power. This project evaluated two GMAW-P waveforms that were reported to have higher melting characteristics as a function of wire feed speed for the Anviloy wire. The waveforms were trimmed to produce the best Anviloy wire metal transfer within the trim range.

Experimental Procedure

In this part of the project, Anviloy GMAW-P procedures were developed for cladding H13 die materials. The preferred procedures were then used to clad production shot blocks for in-plant

trials using different procedures to accommodate shot block section features and characteristics.

The base material used for bead on plate parameter development was an Uddeholm Orvar

Supreme HWTS, the chemical composition of which is presented in Table B1.

Table B1: Chemical Compositions of Alloys (wt.%)

wt.%	Fe	Cr	Mo	V	C	Si	Mn	W	Ni
Orvar Supreme	Bal.	5.1	1.5	0.9	0.39	0.9	0.4		
Anviloy Wire	12.5							Bal.	27.5

The heat treat condition of the welded plates was in the soft-anneal condition, with a starting microstructure consisting of ferrite and coarse alloy carbides, with a hardness around 180HV.

Material is supplied in this condition for ease of machining. Base plate thickness for bead on plate tests was $\frac{3}{4}$ ". All plates were cleaned of oxide using abrasive grinding wheels and then cleans with ethanol to remove any residue. These plates were used to evaluate GMAW-P waveforms for Anviloy wire using bead on plate tests.

Horizontal (2G) welding trials were carried out using a trial shot block provided by FCA. This shot block is shown in Figure B6 consisting of a bell-shaped relief on a rectangular prism.

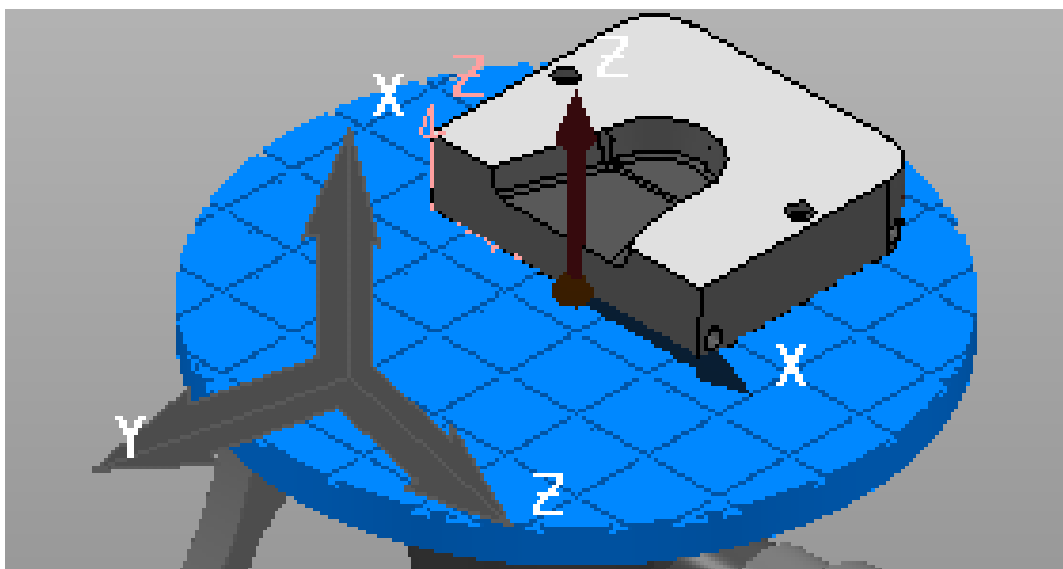


Figure B6: FCA Die Block Used for Anviloy Cladding In-plant Trials

The welding filler material used for this study was Anviloy welding wire alloy in development by Astaras, with the composition also shown in Table 1. This new W-26.5Ni-13.5Fe based material is an experimental alloy for die casting applications. Its microstructure consists of BCC tungsten phase in a Ni-Fe FCC matrix and is described in further detail in Appendix D.

GMAW Welding Procedure Development

Anviloy wire GMAW-P 1G parameters were developed by making numerous single pass bead on plate welds at varying parameters on a $\frac{3}{4}$ " plate. Two waveforms were evaluated. The first waveform (Synchrofeed Ferrite 1.2mm) used electrode positive (EP) pulsing and was found to have insufficient power to achieve adequate Anviloy wire melting and H13 steel base metal fusion. The second waveform (DC- Wave SuS 1.2mm) used electrode negative (EN) pulsing which is known to provide more electrode heating versus EP pulsing. The EN waveform was found to provide good metal transfer and fusion with Anviloy which as higher melting point, heat capacity and thermal conductivity compared to steels. Using the EN waveform, a range of

parameters were developed to identify the wire feed speed and travel speed combination that provided sufficient power and heat input for good fusion. Parameters were altered until welds with a satisfactory bead appearance were achieved. All trial 1G position welds were made without preheat. Parameters tested included voltage, current, wire feed speed, and travel speed. No oscillation was used in 1G trials.

Anviloy Wire-H13 GMAW 2G parameters were developed in a similar manner, but this time only by varying oscillation parameters and using the preferred waveform, DC- Wave SuS 1.2mm. Using the ideal parameters gathered from 1G testing, different oscillations width, speed, and dwell times were tested in order to achieve acceptable sidewall fusion and bead appearance. All horizontal welds were produced with a 200C preheat using trial shot blocks.

Weld quality was analyzed qualitatively by noting the weld height / width regularity, toe angle, and presence of welding defects such as lack of fusion or porosity. Welds with satisfactory visual appearance were then sectioned metallographically to check for sub surface defects. All GMAW tests were performed using an OTC FD-V8 robot system controlled by an OTC FD11 controller.

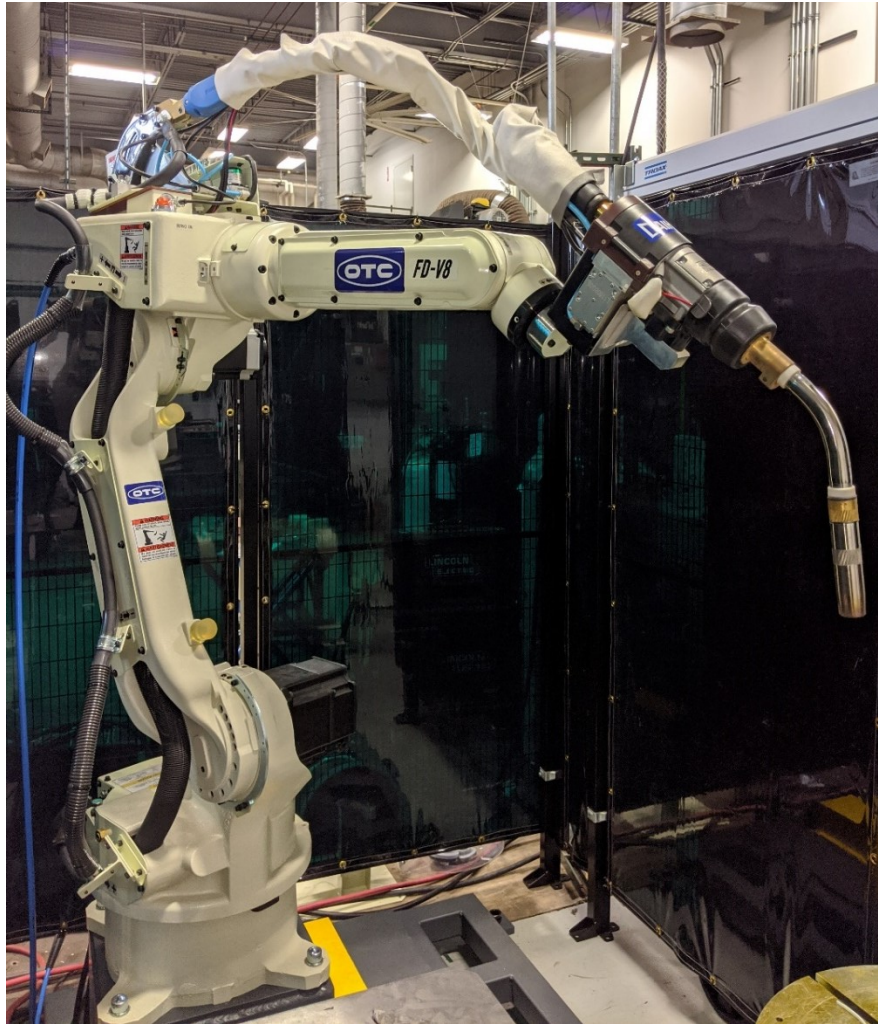


Figure B7: OTC GMAW Robot

The welding power supply was an OTC Wellbee P500L power supply. All welds were made using a .045" Anviloy filler wire with pure argon shielding gas.



Figure B8 : OTC Robot Controller and OTC Welding Power Supply

Weld Quality Assessment

Weld quality was assessed primarily on presence of visible welding defects and discontinuities and secondarily on microstructure seen during metallography on samples that passed initial visual assessment. Weld toe angle was qualitatively analyzed visually. Metallography was performed primarily to check for sub surface porosity or lack of fusion defects.

Preheat

Preheat is recommended for H13 die materials to minimize risk of hydrogen cracking since this material has a high hardenability and high hardness microstructure after welding. The recommended preheat was 300C. The large size and complicated geometry of the shot block mandated careful application of preheat. Through thickness preheat is important to avoid the formation of thermal stresses. The large thermal mass of this shot block meant flame preheating of the entire through thickness of this block was unfeasible, and harder to manage when using robotic welding equipment. To avoid difficulties associated with flame preheating, a Miller Proheat 35 induction heating system was employed to preheat the die block.



Figure B9 : Miller Proheat 35 Induction Heating Unit

The programmed heating rate was 200C/hr. Two contact thermocouples in different locations were used to verify temperature and prevent fluctuation throughout the die. To avoid overheating at dimensional discontinuities, induction heating was applied through the bottom of the shot block, which was positioned flat. Start and stop temperature was tested between each pass using a contact Type K thermocouple to ensure preheat was within +/-10C from 200C. Set up used for induction heating is shown in Figure 9.

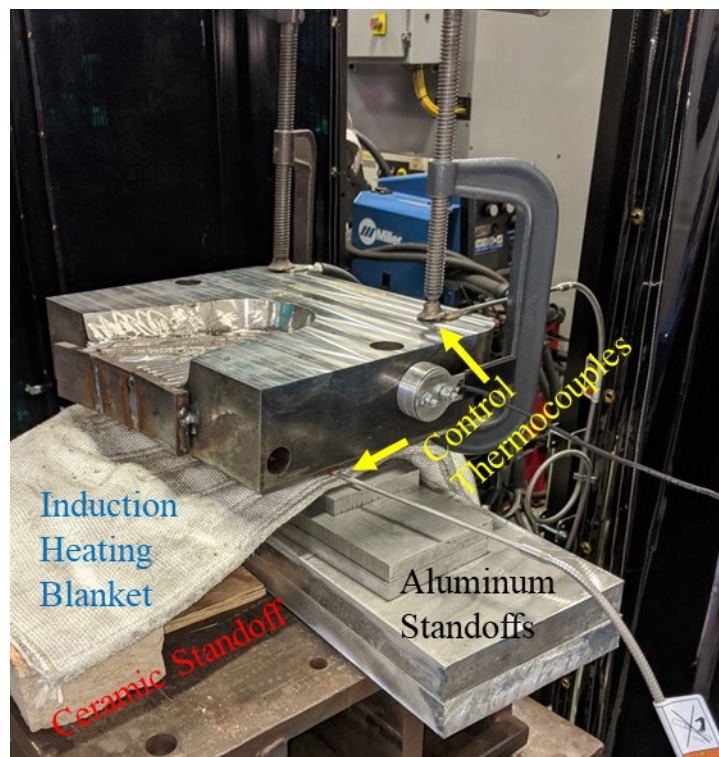


Figure B10 : Induction pre-heating set up

Metallography

All metallographic samples were prepared by polishing with 240, 400, 600, and 800 grit SiC abrasive followed by 9, 6, and 3 micron colloidal diamond abrasive. Samples were submersion etched using a 10% Nital (10% Aqueous Nitric Acid in Ethanol) solution for 30-45

seconds. All metallographic images were taken with an Olympus GX-51 microscope using DP2-BSW software.

Results

1G Parameter Development

As noted above, commercial GMAW-P waveforms do not exist for Anviloy wire. A series of feasibility tests were performed to evaluate Anviloy wire using pre-installed commercial waveforms that are standard on the OTC Wellbee 500 power supply. The power supply used for these trials is equipped with advanced GMAW pulsed waveforms named Synchrofeed™ that enable high deposition at low heat input. The waveform selected to begin trials was the 1.2mm Ferrite Synchrofeed waveform that had a maximum current of 250 Amps. The bead on plate trials used the max current of 250A with Anviloy wire. Welds were produced using varied travel speed of 9, 12, 16, and 23 IPM to test weld quality. Table B11 shows the weld parameters used, and the image shows the resulting welds those parameters produced.



Figure B11 : Synchrofeed Welds

	Weld 21	Weld 22	weld 23	weld 24
OTC waveform type	MIG_4 DC Sfeed 1.2 ferrite	MIG_4 DC Sfeed 1.2 ferrite	MIG_4 DC Sfeed 1.2 ferrite	MIG_4 DC Sfeed 1.2 ferrite
CTWD (inches)	.75"	.75"	.75"	.75"
Welding Current (Amps)	250	250	250	250
Welding travel speed (IPM)	12	23	16	9

Table B11 : Synchrofeed Weld Parameters

The Anviloy bead on plate tests using 1.2 mm Ferrite Synchrofeed waveform at 250A produced poor quality deposits at each tested travel speed. These welds had irregular bead height, width, and surface appearance. Of all these welds, the 16 IPM travel speed had the best appearance but still had a bead height irregularity of over 0.5mm. Bead height irregularity makes prediction of deposit thickness difficult, as well as complicating the deposition of subsequent weld passes on top of these welds. The welds produced here were limited to 250A max current. At this waveform current, the bead also had poor fusion into the base material, resulting in lack of fusion defects along the weld toes. Insufficient fusion at weld toes is likely to result in defects detrimental to performance and clad longevity. It was concluded that higher power waveform is necessary to achieve high quality clad weld deposits. At constant deposit size, higher power will allow higher travel speeds and melting efficiency which will improve base metal wetting and

mitigate lack of fusion defects that were seen in these bead on plate tests with the 1.2 mm Ferrite Synchrofeed waveform.

Since 250A is the maximum possible current for the Synchrofeed waveforms chosen, a DC EN pulse waveform with a 500A max current was selected as the next option to weld Anviloy Wire. This waveform offered high power. Using a DC EN Waveform (DC- Wave 1.2mm SuS) designed for 1.2mm wire, several welds were made to test the deposit soundness at higher currents. Those welds and their parameters are shown in Table B12.

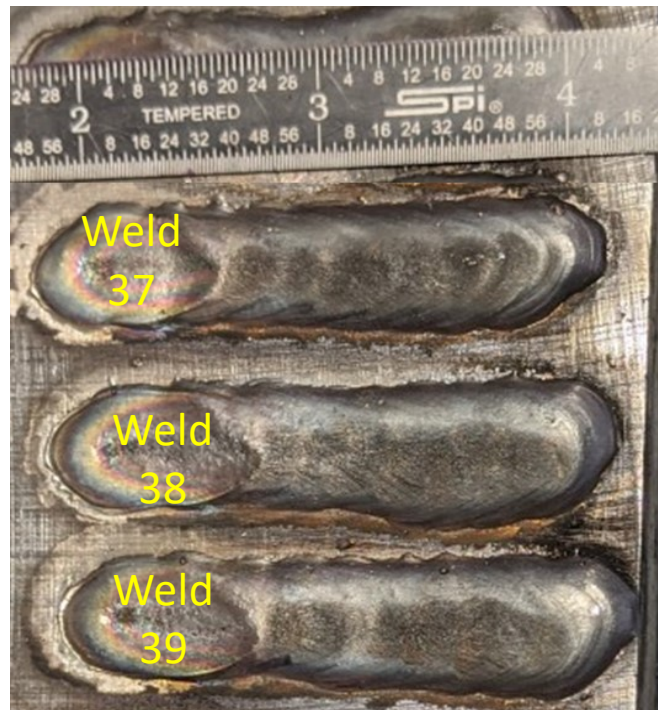


Figure B12 : High Current DC- Pulse Welds

Weld #	37	38	39
OTC waveform type	DC- Pulse 1.2 Ferrite	DC- Pulse 1.2 Ferrite	DC- Pulse 1.2 Ferrite
CTWD (inches)	.75"	.75"	.75"
Welding Current (Amps)	270	270*	270
Welding travel speed (IPM)	45	50	50

Table B12 : High Current DC- Pulse Weld Parameters

Weld beads produced at 250A currents using the DC- Pulse 1.2mm Ferrite waveform had better quality upon visual examination than those produced with the Synchrofeed waveform at 250A. Welds made at 270A using the DC- Pulse waveform resulted in significantly lower bead height variation than those made with Synchrofeed at 250A. Also, beads produced at 270A show much better fusion to the base material and were made without lack of fusion defects. However, bead width inconsistencies can still be seen along the longitudinal direction of the weld, with beads gradually increasing in size along the weld length. Bead width inconsistencies make high fidelity tie-in with previous weld passes difficult. Since bead width must be known to ensure a sound cladding procedure has been developed, further developments were undertaken to ensure bead width consistency along the weld length. It should be noted that weld 38 employed a significantly altered arc trim value programmed into the controller, but this had relatively little effect in terms of altering the bead quality / shape compared to weld 39, which used identical parameters except for no arc trim alteration.

Torch weaving / oscillation is known to help improve bead shape consistency as well as bead tie in / fusion to base material. For these reasons, oscillation was employed to help give Anviloy wire deposits a more regular shape. A simple linear type oscillation was employed using a DC- Pulse waveform to produce the weld shown in Figure B13. Parameters are also listed in the adjacent table B13.



Figure B13 : Oscillation Adjusted Flat (1G) Weld

OTC waveform type	DC- Pulse 1.2 Ferrite	Oscillation Type	Linear
CTWD (inches)	.75"	Oscillation Amplitude (mm)	8
Welding Current (Amps)	260	Oscillation Frequency (Hz)	1
Welding travel speed (IPM)	40	Oscillation Dwell Time (sec.)	0

Table B13 : Oscillation Adjusted Flat (1G) Weld Parameters

The resultant weld produced using the listed oscillation parameters proved to be high quality, lacking any visually discernible weld defects or bead irregularities. This weld possessed

extremely low bead height variation, as well as negligible width variation along the longitudinal direction. Also, these weld parameters resulted in a fully fused weld with good fusion along the weld toe. No lack of fusion was observed in this weld. Due to the high quality of resulting welds, these parameters were used as the basis for all subsequent cladding efforts.

Although the parameters gathered in previous efforts resulted in high quality single pass deposits, little was known about their feasibility for making multi-pass clad layers. Since good tie-in and fusion between different weld beads is essential for quality cladding, it was necessary to test the quality of weld tie-ins by making a multi-pass layer that was representative of a hoit block curved feature. Since conformal cladding involves complex weld profiles, the choice was made to make multi pass, interconnecting welds in the shape of arches / crescents to better prepare for welding the circular section of the die block used in this study. The resulting 5 pass weld sequence is shown in Figure B14.



Figure B14 : Multi-Pass Anviloy Wire Clad on H13

The 5 weld passes shown in Figure B12 show consistent bead shape in each weld bead and good fusion between the beads. The welding parameters used in this trial resulted in low weld bead height and width variations as well as excellent tie-in to adjacent passes. Based on this trial, the parameters were acceptable for multi-pass cladding the shot block face in the 1G / flat position.

2G Parameter Development

To clad the shot block sidewall, cladding parameters needed developed for the horizontal (2G) position. Normally, a 2-axis positioner would be used to tilt and rotate the part to clad the sidewall. Since the shot block was positioned flat, an alternative approach is to stack horizontal fillet welds along the wall and vertically clad the sidewall (Figure B13). Also, the shot block had a horse shoe sidewall profile that made the use of ideal torch work angles more difficult while cladding each region of the die surface. Due to the shape of the die block, a much higher torch work angle was required versus the ideal angle for horizontal welding. The torch angle used in the sidewall section is shown in Figure B13.



Figure B15 : Torch Angle for Horizontal Welds

Without oscillation, the Anviloy parameters developed for the flat position were found to cause excess penetration in the horizontal position. Ideal torch angle in horizontal position results in penetration further into the base material sidewall vs. the previous weld. Ideal perpendicular torch angle allows for the previous passes to be used as a ledge/platform while the base material is penetrated. However, the high torch work angle resulted in excess melting of previous passes, which ultimately leads to the “humping” and extreme bead height irregularity due to gravity’s influence on the molten weld pool. Welds using the high torch angle are shown in Figure B16.



Figure B16 : Initial Horizontal (2G) Welds

Because of the poor appearance of these welds using previous developed oscillation parameters, a new torch weaving strategy was developed to improve the bead appearance and integrity. The new weaving strategy involved varying the torch work angle in the oscillation and by adjusting weave dwell parameters. This oscillation is illustrated using the same still as before, with torch angle in Figure B17 representing the programmed work angle and graphics illustrating the torch work angle adjustment and dwell times from the oscillation.

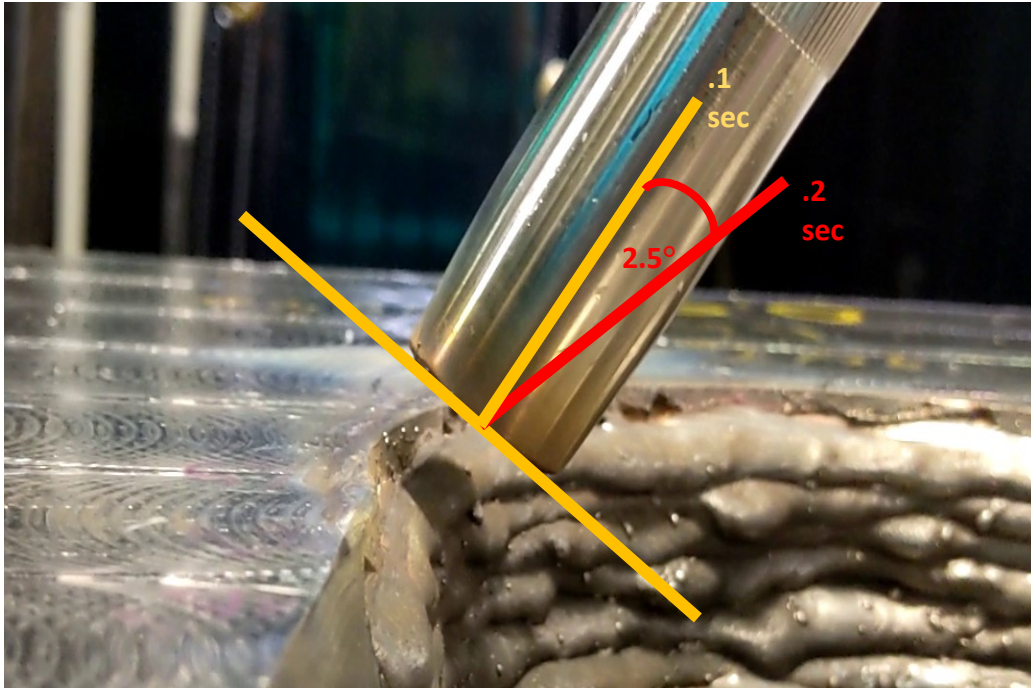


Figure B17 : Horizontal (2G) Oscillation Procedure

The torch work angle oscillation used here involved two separate motions with differing dwell times. The first component of the oscillation shown in green involved a dwell time at the standard torch angle for .1 seconds. The second component of this oscillation shown in red involved a 2.5 degree shift in torch angle and a .2 second dwell at this angle. This seemingly minor change in torch angle weaving enabled much better bead regularity. Figure B18 shows the resulting welds after using the newly developed horizontal (2G) torch angle oscillation.

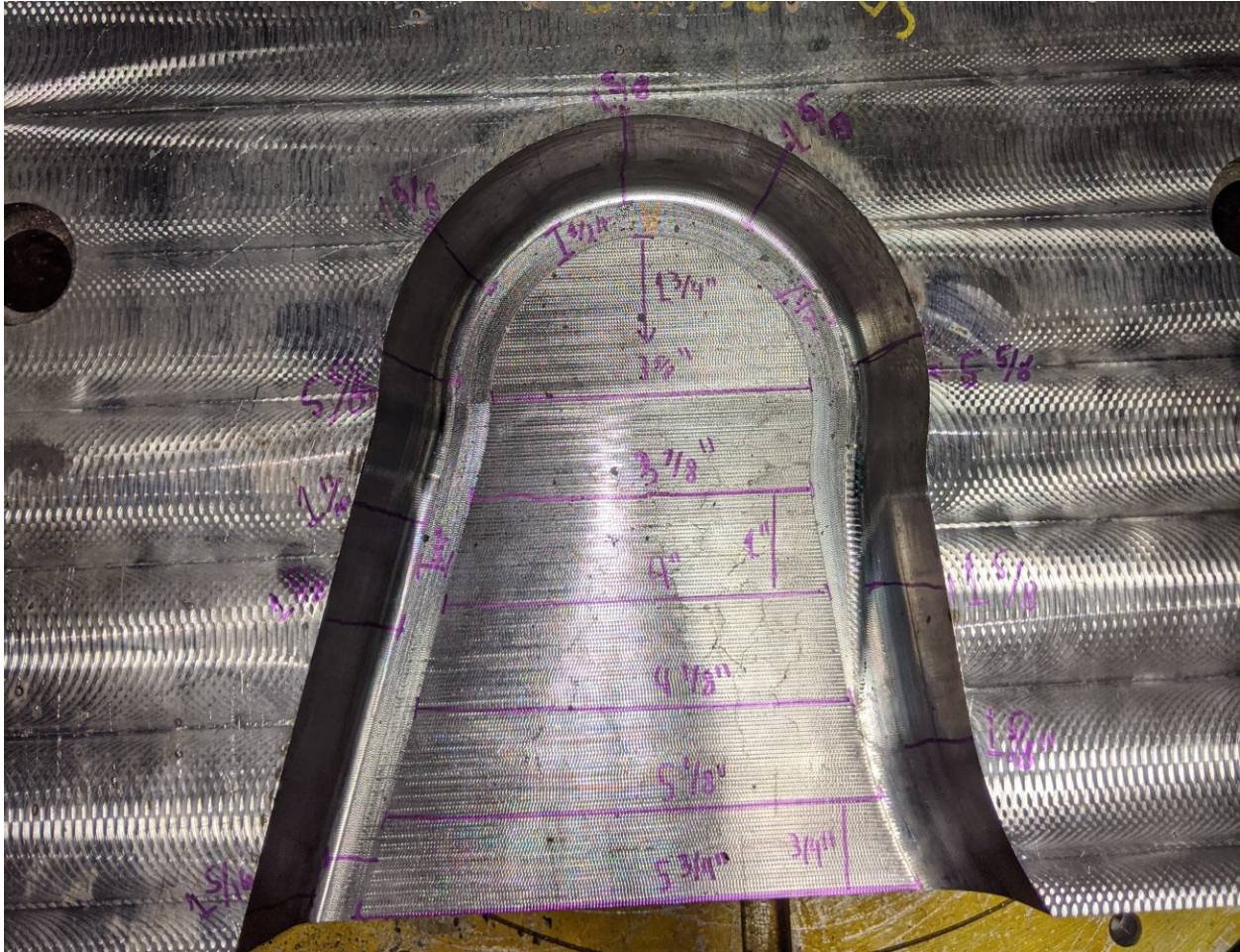


Figure B18 : Horizontal (2G) Welds with Refined Oscillation

The welds pictured in Figure B18 showed no defects as well as significantly improved bead tie in and uniform bead shape versus those created without torch angle oscillation. Torch work angle oscillation was required to clad the vertical sidewalls of the block with horizontal weld beads and sub-optimal torch angles.

Conformal Cladding Build Planning

The complicated shape of the die block used in this study mandated thoughtful development of the welding procedure. Figure B19 shows the shot block geometry in the as-machined condition. The shot block will require a 10mm thick layer requiring two passes on both the flat surface and the vertical sidewalls to for service. As noted in Appendix C, a double layer procedure is preferred for tempering the H13 HAZ. This shot block geometry involved careful robotic path planning to clad the face and sidewall with different procedures.



beads, or the overlapping constant width beads while welding from the exit towards the radius. The final weld need to wedge beads in to complete the flat layer. The final overlaps require the use of grinding to remove excess overlap material. Several variables were under consideration when making this procedure, including: minimization of deposited material and number of weld passes; avoidance of weld passes with multiple positions, i.e. avoiding cladding the flat portion and the sidewall; and minimizing the amount of weld starts/stops on the die block. With these considerations in mind, the following weld procedure was superimposed on the previous image with color coded passes.

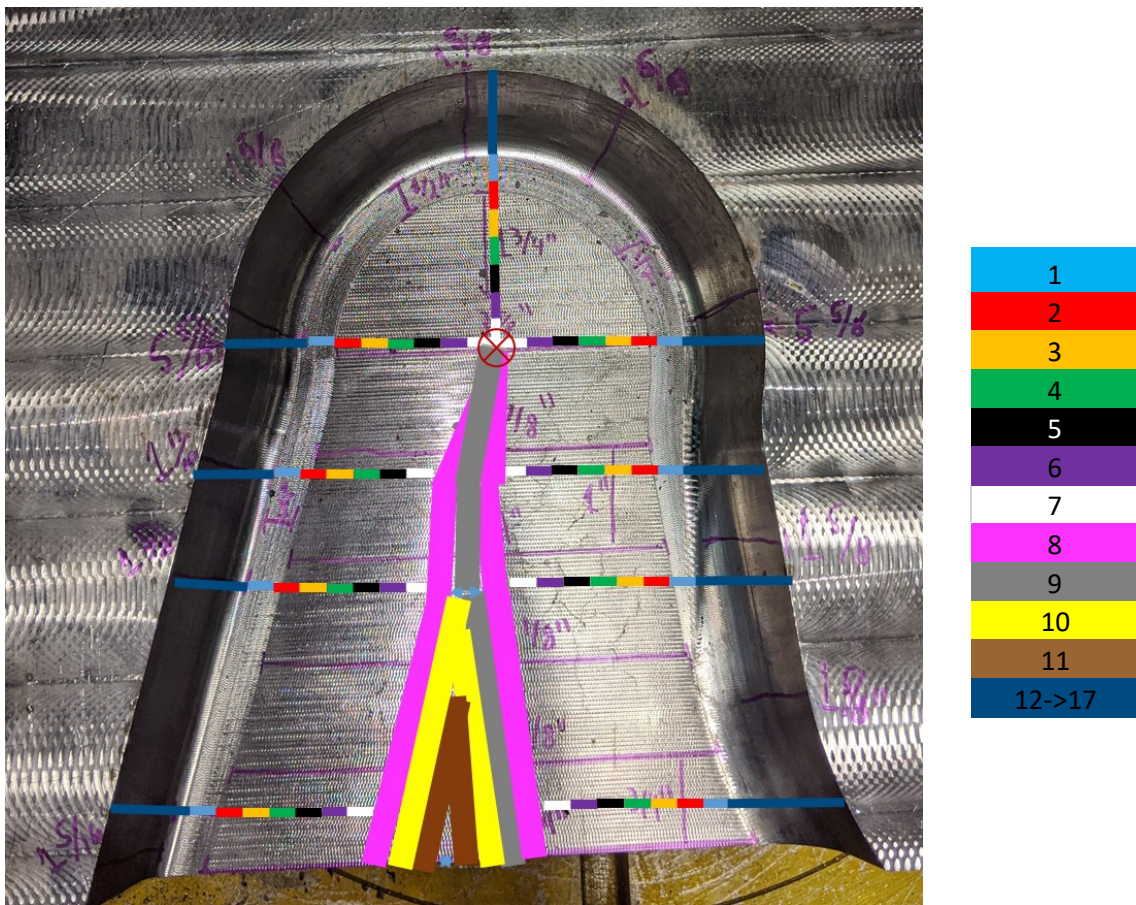


Figure B20 : Conformal Cladding Procedure

The first pass (light blue) followed the outer profile of the horseshoe face perimeter. It began at the exterior edge on the right flank and continues circumferentially around the feature, ending at the bottom left of the feature. Subsequent passes follow a circumferential path which gradually decreases in width as more weld passes are added until the circular section is nearly completely clad on the 7th pass (white). One weld stop is listed in the procedure at the center of the circular section, indicated by the red x-in-circle mark at the top of the 9th (dark gray) pass. The procedure includes grinding down the area under the x-in-circle mark back down to the original die block surface height to accommodate the weld stop in this location. The 9th and 11th passes also include two regions of varied oscillation, where the welding oscillation was adjusted to widen beads .4” for the 9th pass and .2” for the 11th pass, with locations indicated by the blue arrows. Then, the sidewall sections are clad using the horizontal welding parameters. Six passes were required to clad the sidewalls (weld passes 12-17). It should be noted that this Figure B18 represents only 1 layer of a 2 layer procedure of the same design.

Because this procedure includes a weld stop on the die block, it was important to ensure weld quality in that location. Weld starts and stops are generally considered the most likely positions for welding defects, which is especially true for GMAW. Because of this risk regarding stop defects in the clad, a single weld stop sample was prepared to evaluate the bead shape and fusion characteristics of this regions. The stop area was found acceptable for inclusion into the welding procedure. The sectioned weld stop is shown in Figure B21.

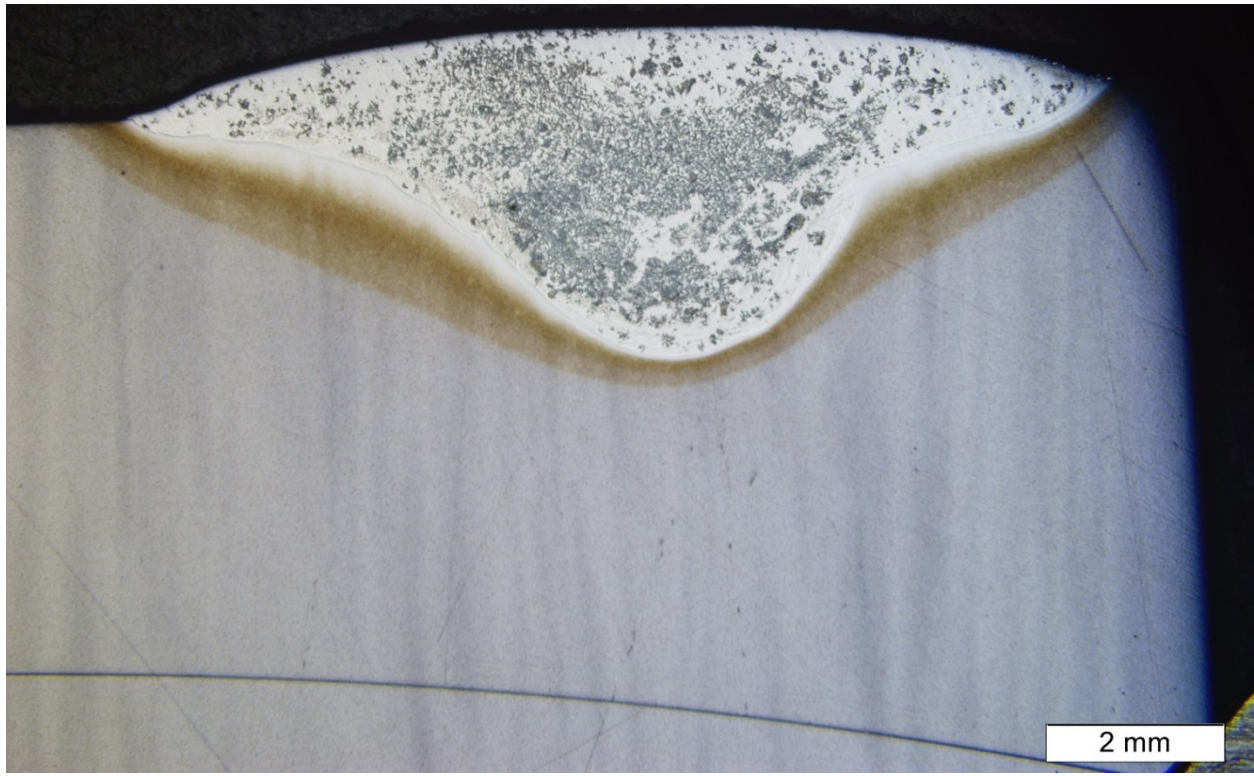


Figure B21 : Single Weld Stop

The weld stop showed excellent wetting of base material, low tow angle, and good penetration into the base material. No evidence of cracking, porosity, or lack of fusion was observed in this sample. Due to the lack of observable defects, weld stops were considered acceptable for use in the cladding procedure. The microstructure also consists of the same two phase microstructure detected in previous welds.

Conclusions

- Sound Anviloy Wire – H13 cladding was feasible using commercial GMAW pulse waveforms that were developed for other materials. The preferred waveform was DC-Wave SuS 1.2mm.
- Weld oscillation helped improve bead consistency for Anviloy deposits in both the flat (1G) and horizontal (2G) positions. A torch work angle oscillation was necessary to deposit a vertical clad using horizontal beads on the shot block sidewall.

Works Cited

1. S. Jhavar, C.P. Paul, N.K. Jain, "Causes of failure and repairing options for dies and molds: A review" *Engineering Failure Analysis*, Volume 34, 2013, Pages 519-535, ISSN 1350-6307
2. Y. Ali, P. Henckell, J. Hildebrand, J. Reimann, J.P. Bergmann, S. Barnikol-Oettler, "Wire arc additive manufacturing of hot work tool steel with CMT process." *Journal of Materials Processing Technology*, Volume 269, 2019, Pages 109-116, ISSN 0924-0136
3. Phillips, David H. *Welding Engineering: an Introduction*. John Wiley & Sons Inc., 2016.
4. T. Opderbecke & S. Guiheux (2009) TOPTIG: robotic TIG welding with integrated wire feeder, *Welding International*, 23:7, 523-529, DOI: [10.1080/09507110802543146](https://doi.org/10.1080/09507110802543146)
5. "Structural Welding Manual." MDOT, Michigan, 2017.
6. Joseph, D. Farson, D. Harwig & R. Richardson (2005) Influence of GMAW-P current waveforms on heat input and weld bead shape, *Science and Technology of Welding and Joining*, 10:3, 311-318, DOI: [10.1179/174329305X40624](https://doi.org/10.1179/174329305X40624)
7. C.G. Pickin, S.W. Williams, M. Lunt, "Characterisation of the cold metal transfer (CMT) process and its application for low dilution cladding." *Journal of Materials Processing Technology*, Volume 211, Issue 3, 2011, Pages 496-502, ISSN 0924-0136

Appendix C : Feasibility of H13 Temperbead Repair using Anviloy

HW-GTAW Cladding Procedures

Abstract

Repair of die casting dies represents a significant portion of cost for die casting operators. Improvement of repair procedures and the development of more robust die repair consumables represents a valuable opportunity for reducing process costs. In this study, H13 tool steel was clad using a new W-Ni-Fe (Anviloy) wire with a mechanized hot wire gas tungsten arc welding (HW-GTAW) process. A range of welding parameters and sequences were analyzed to better understand how cladding procedures affect H13 Heat Affected Zone (HAZ) hardness and hardness distributions. Double layer procedures were investigated in an attempt to obviate Post-Weld Heat Treatment (PWHT) in emergency repairs with temperbead welding techniques. Temperbead welding has historically been employed in a wide variety of structural steel repair applications to improve HAZ and weld metal properties without PWHT, but literature on Temperbead welding of hot work tool steels was lacking. Cladded samples were characterized using microhardness mapping to understand the effects of heat input and weld preheat on H13 HAZ hardness distributions. Hardness mapping revealed as-welded single pass overlays had a hardness range from approximately 200-700HV, with a continuous high hardness band along the weld fusion boundary. Preferred Temperbead welding parameters using two-layers resulted in H13 HAZ hardness mainly from 200HV-590HV, with isolated regions with hardness above 600HV. Optimized temperbead parameters resulted in 1% of measured hardness indents over 600HV vs. 15% for non-optimized procedures. These trials support feasibility of temperbead

welding procedures on hot work tool steels, and hardness distributions can be improved on these materials by employing temperbead welding techniques.

Introduction

Repair welding procedures are an integral component of high pressure die casting (HPDC) operations because of the extreme environment. When molten metal is injected at high pressure into a die cavity, die surfaces are damaged very early in their life cycles, sometimes forming cracks in as little as 1% of expected die life (1). Over time, the modes of die damage may include thermal fatigue cracking, soldering/washout damage, and carbonaceous buildup (1-4).



Figure C1: Damage on a HPDC Die Surface

Accumulation of damage on dies directly impacts the surface finish of casted parts. In powertrain components commonly cast using HPDC, this can quickly result in rejected castings if damage is not repaired.

Many processes have been used to repair HPDC dies, including wire fed laser, powder blown laser, wire fed electron beam, and traditional arc welding (2). Arc welding is the dominant method for die repair. Arc welding equipment is lower cost and can be applied manually which is preferred in high mix die repair conditions. Laser and electron beam processes are applied though automated motion systems, have higher costs, and take longer to program and setup for repair. These processes may be preferred for unique conditions where precision and / or properties offset the costs. Arc welding can be applied manually or through automated systems like robots. The latter is preferred for larger repairs where properties are more critical, and for building dies using additive manufacturing. Of the arc welding methods, gas tungsten arc welding (GTAW/TIG) is a preferred process for making small die feature repair. Gas metal arc welding (GMAW) is preferred for repairing larger surfaces and features since it offers higher deposition rates and bead sizes. Although repair of HWTS dies is an essential aspect of HPDC, they generally result in adverse effects on die microstructure mandating heat treatment.

Hot work tool steels are chosen in HPDC applications due to their good hot strength and hardness, toughness, and hardenability which ensures these properties in thick die steel sections after heat treatment. The H13 heat treated microstructure is characterized as tempered martensite. These steels are alloyed with chromium (Cr), molybdenum (Mo), and vanadium (V) to improve hardenability and high temperature properties (1). These elements form carbides that have high temperature stability and sustain preferred properties over long life cycles. During repair procedures, the H13 heat affected zone has regions that austenitize then transform to untempered martensite upon cooling. Untempered martensite has low ductility and is more susceptible to hydrogen cracking (or delayed cracking) (1, 2, 5, 6).

Modern hot work tool steels are formulated to provide excellent service properties, but often require precise heat treatments to achieve them. These heat treatments are designed to form a stable tempered martensitic microstructure (1,5,6). Carbides nucleate and grow during tempering heat treatments, resulting in a microstructure of ferrite and carbides with high dislocation density and good strength and toughness (1,5). Tempering involves the diffusion driven nucleation and growth of stable carbides, and has been described in extensive reviews by Zhu and Speich (12, 13). As-welded repairs are detrimental to material properties of hot work tool steels due to untempered martensite formation, which elicits a need for tempering PWHT (2). Post weld heat treatment is considered necessary to recover material properties lost during repairs. Since PWHT takes considerable time and expense, there is a great incentive to develop as-welded repair technologies that mitigate the need for PWHT. One method for as welded repair is temperbead welding deposition.

Both GTAW and GMAW welding processes can be used for temperbead repairs. Temperbead is a technique that use controlled weld deposit sizes that heat treat or “temper” the heat affected zone of the prior layer deposits. Temperbead repairs have been used for years in power generation, nuclear, and other industries that have high strength steel equipment that cannot be taken out of service for a furnace heat treatment (14). As such, either a local stress relief is used, or the repairs are made using a temperbead procedure. Temperbead welding is a specific welding procedure which is designed to produce a tempered martensitic microstructure in the weld or HAZ metal in the as-welded conditions. Temperbead techniques are incorporated into weld repair procedures by precisely controlling layer thickness, process heat input, and deposition sequence. GTAW is preferred for temperbead welding since its makes smaller deposits and HAZs that can be tempered more effectively with subsequent deposits.

Temperbead procedures are accomplished through precise deposition of multiple welding passes and careful control of weld heat input, Figure C2. This figure correlates the locations of the deposits' HAZs to the iron carbon phase diagram. Each weld deposit HAZ is divided into zones: the coarse grain “supercritical” HAZ, “inter-critical” HAZ, “sub-critical” tempered HAZ, and unaffected zones.

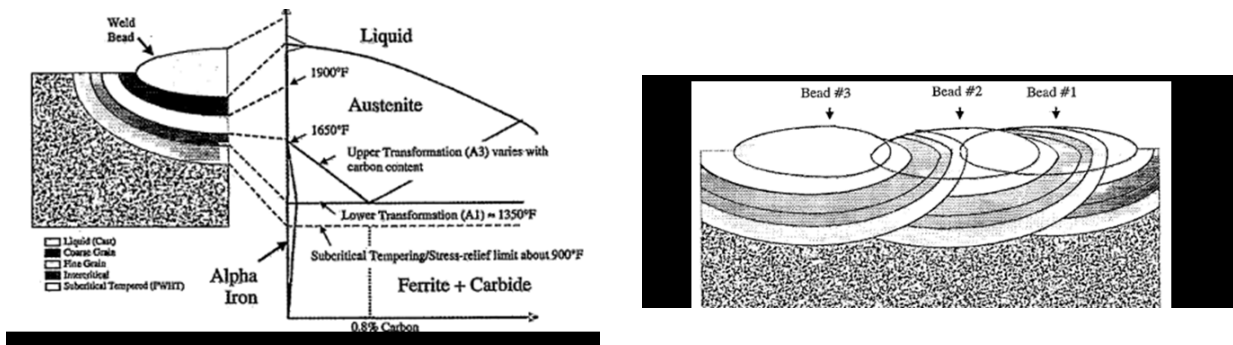


Figure C2: Temperbead Welding (6)

The supercritical HAZ region is fully austenitized during repair welding and transforms to untempered martensite. By using a subsequent layer for temperbead repair welding, a large portion of the super critical heat affected zone of previous deposit is tempered by the sub critical HAZ of subsequent passes (6). The heat of these subsequent passes, though extremely short in duration compared to normal tempering procedures, is enough to temper martensite and increase toughness (6, 8). Tempering of martensite occurs during subsequent re-heating where maximum tempering occurs near the lower transformation (A1) temperature. During temperbead welding, it is important to eliminate or minimize heating the prior pass's HAZ above the A1 temperature to avoid austenite formation as untempered martensite will form after cooling.

The majority of studies involving temperbead welding procedures involved low carbon CrMoV type steels that are used in power generation, chemical and other high strength steel

systems. The carbon content of these steels is purposely kept lower to improve weldability during fabrication and in service. Higher carbon alloy steels like H13 produce harder microstructures in the as-welded conditions and are more susceptible to hydrogen cracking (6, 8, 9). The majority of temperbead procedures use HAZ hardness as a measure of control. Typically, the procedures aim to limit the maximum HAZ hardness or achieve a hardness drop from the untempered condition to restore ductility that meets service requirements. Charpy specimens are removed from different locations in the HAZ zones are used to correlate hardness drop to HAZ toughness.

There is a need to develop temperbead techniques for hot work tool steels, especially H13 which is widely used in HPDC. Research is needed to develop temperbead procedures that maximize the tempering effect in die repairs, understand the relationship between repair procedures and HAZ microstructure and properties, and develop temperbead procedures that minimize the need for post repair heat treatment. It should be noted, that die casting dies temper or soften over time due to high cycle service where the surface is exposed to near tempering temperature for short times(10). In essence each die casting cycle provides a short temper heat treatment cycle to the surface. The acceptable as-welded hardness of the repair may be harder than the base material. A harder surface will offer better die life and will take longer to soften.

Temperbead welding procedures use the linear heat input and / or power ratio calculations to control deposit size, correlate repair procedure to properties, and develop engineering relationships that establish procedure confidence. These variables are calculated using the following equations:

$$\textit{Heat Input} = \frac{V * I}{TS} \quad \textit{Power Ratio} = \frac{V * I}{\frac{WFS}{TS} * A}$$

Heat input is measured in kJ/mm traveled during welding, with V representing welding voltage, I representing weld Current, and TS representing travel speed in mm/sec. The power ratio approach differs from the heat input approach by dividing power (V*I) by the weld deposit size. The unit of power ratio is W/mm². The welding deposit size can be calculated using the wire feed speed (WFS), travel speed and wire area (A). The power ratio calculation can be used to provide better heat input control for a given deposit size. Regardless of calculation, both can be used to develop temperbead relationships. Either heat input or power ratio should be used to ensure consistency of as-welded HAZ hardness.

This investigation used hot wire gas tungsten arc welding (HW-GTAW) to develop die repair procedures using Anviloy wire, a new tungsten-nickel-iron alloy. This alloy (W-12%Ni-5.4%Fe) is leaner in tungsten compared to other Anviloy alloys to improve formability for wire welding processes. Hot wire GTAW uses a continuously fed wire that is electrically preheated with an additional power supply, and provides independent control of wire and base material melting. The former was more important as Anviloy is harder to melt than steel. Anviloy wire has higher melting point, heat capacity and thermal conductivity as compared to steels. The preferred hot wire condition is to heat the wire to the melting point as it enters the weld pool using bridging (streaming) metal transfer mode. Preheating of filler material allows for a lower heat input for sound welds compared to cold wire GTAW. HW-GTAW is often used in power generation industries to clad corrosion resistant materials onto ferritic steels. The lower heat input of HW-GTAW procedures result in lower base metal dilution into clad layers, which can

reduce the number of layers required to meet clad composition requirements. Less clad layers result in less time repair welding and lower costs. These attributes make HW-GTAW an attractive option for overlay welding of high melting temperature refractory alloys such as Anviloy wire.

Because of untempered martensite formation after welding, welding repairs on H13 require preheat to minimize moisture absorption, promote hydrogen diffusion out of the material while repaired, and minimize susceptibility to hydrogen cracking. After cooling to room temperature, the material is post weld heat treated to temper the untempered martensite, improve properties, and reduce residual stresses for machining tolerance stability. The preheat, which is typically 300C (600F) for H13, can make weld repairs difficult. Manual welders must shield themselves from this heat while depositing repair weld beads. Preheats this high often make temperbead repairs difficult due to adverse hardness distributions in heat affected zones. For this reason, the effect of preheat temperature was evaluated for Anviloy temperbead deposition on HWTS.

Experimental Procedure

Materials

The base material used for this study was an Uddeholm Orvar Supreme HWTS, the chemical composition of which is presented in Table 1.

wt.%	Fe	Cr	Mo	V	C	Si	Mn	W	Ni
Orvar Supreme	Bal.	5.1	1.5	0.9	0.39	0.9	0.4		
Anviloy Wire	12.5							Bal.	27.5

Table C1: Chemical Compositions of Alloys (wt.%)

Orvar supreme is a general purpose, medium carbon, hot work tool steel that contains Cr, Mo, and V additions to form carbides with good thermal stability for die casting applications. The heat treat condition of the welded plates was in the soft-anneal condition, with a starting microstructure consisting of ferrite and coarse alloy carbides, with a hardness around 180HV. The material is supplied in this condition for ease of machining. A full heat treatment is used after machining to transform the microstructure to tempered martensite for service. Uddeholm recommends preheat of around 300C for Orvar Supreme for repair welds. After heat treatment, the target hardness for die casting applications is usually between 44-52HRC (11).

The welding filler material used for this study is a new Anviloy welding wire alloy developed by Astaras, with the composition shown in Table 1. This new tungsten based alloy was developed for die casting die repair applications. Anviloy 1150 inserts are widely used in die casting in die regions that experience high thermal fatigue stresses like pins and thin inserts. Anviloy 1150 welding rod has been used in manual cold wire GTAW repair dies for years, however the 1150 alloy was only supplied in rod because of its limited ductility. The Anviloy wire used here has lower tungsten content and was found to feed well for mechanized deposition processes. Anviloy alloy deposits are strengthened by the BCC tungsten phase and do not require PWHT. For temperbead procedures, Anviloy wire deposits can be designed in a way that maximize the properties of the Orvar Supreme base material HAZ.

HW-GTAW Welding of Anviloy Wire and Orvar Supreme

Anviloy hot wire GTAW parameters were developed for both single- and double-layer clad repairs. A range of tests were performed to identify preferred GTAW current, voltage and travel speed; and hot wire current and feed speed to produce a range of deposit sizes. The goal was to deposit beads that were fully fused and sound, and minimized Anviloy dilution. Another goal was to make the Anviloy deposits as thin as possible to facilitate the tempering effect in two layer builds.

All hot wire GTAW tests were performed using a Jetline 9800 mechanized system, Miller Dynasty 500 power supply, and Jetline 200 Amp hot wire power supply. All tests were made with .045" diameter Anviloy wire and pure argon was used for the shielding gas. The Anviloy hot wire electrode extension was typically fed at a 45 degree angle above the work piece with a 25-mm contact tip to work distance.

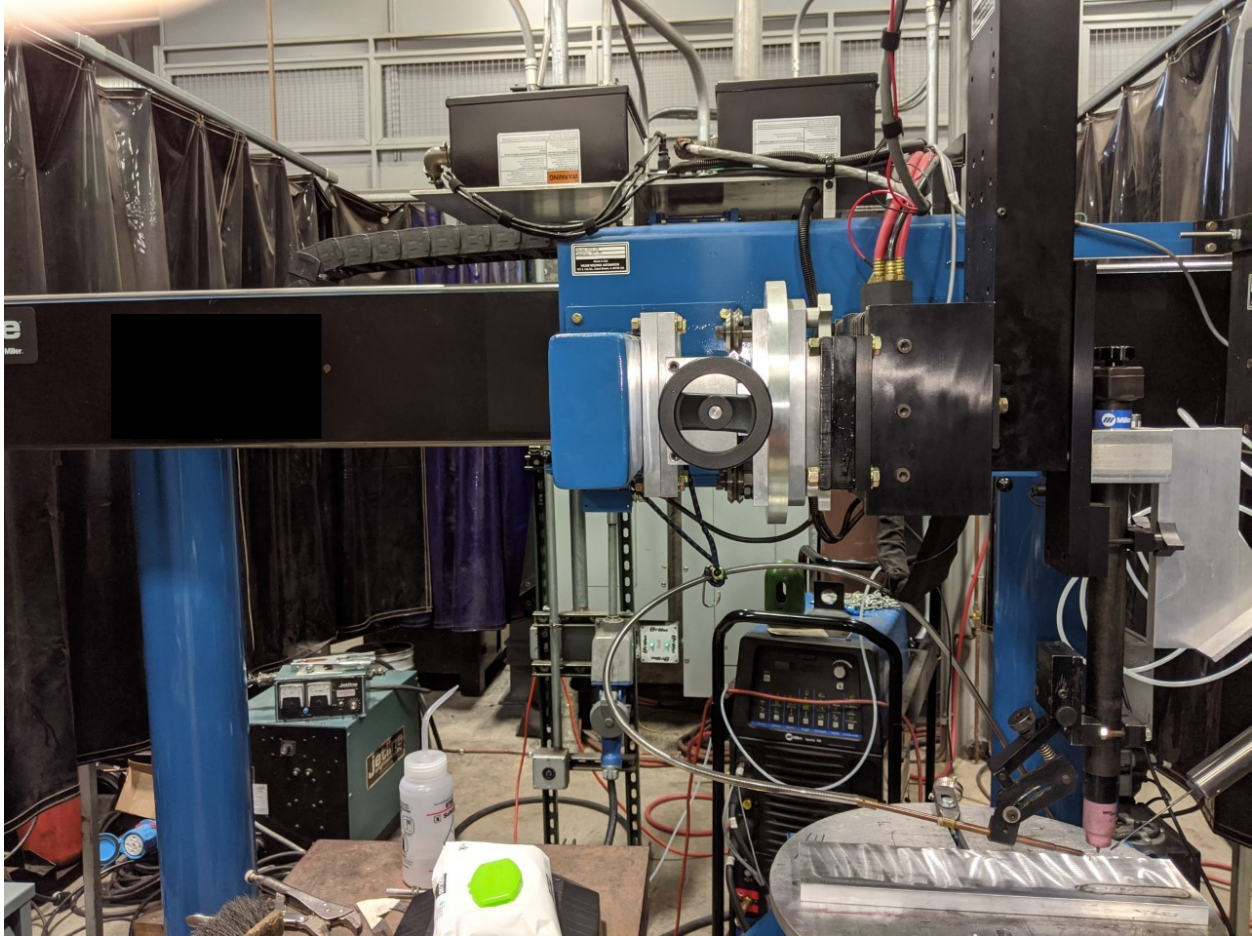


Figure C3: Jetline 9800 Mechanized Welding System

Once sound clads were achieved, multi-bead single-layer overlays were made for analysis at different heat inputs and preheat temperatures. These single-layer overlays were then sectioned and prepared metallographically to collect hardness data and to determine the HAZ size at different parameters. Heat input was varied from 12.6-46.2kJ.in using the parameters below by varying weld travel speed from 4-11 inches per minute.

I (Amps)	V (Volts)	WFS (in/min)
220	14	40

Table C2 : Heat Input Trial Parameters

Preheat tests involved making welds at 25C and 300C preheats using the parameters in Table C3.

I (Amps)	V (Volts)	WFS (in/min)	TS (in/min)
200	11	48	3

Table C3 : Preheat Trial Parameters

Variations in hardness along these traverses were used to identify total and subcritical / low temperature HAZ (LT-HAZ) lengths. Since only the LT-HAZ can be used to temper previous passes, parameters were selected to maximize LT-HAZ length vs. total HAZ length. Those parameters were selected as preferred temperbead procedure and are shown in Table C4.

	I	V	WFS (in/min)	TS (in/min)
Temperbead Layer 1	230	12.5	55	7
Temperbead Layer 2	210	12.5	40	7

Table C4 : Temperbead Trial Parameters

Hardness Mapping

All metallographic samples were prepared by polishing with 240, 400, 600, and 800 grit SiC abrasive followed by 9, 6, and 3 micron colloidal diamond abrasive. Hardness maps were performed on a Leco microvickers automatic hardness mapper using 500g load. Maps were made with a spacing of 400 microns between indents. A 500g load was chosen to maximize accuracy in low hardness regions and because a finer resolution is possible than with a 1kg load. Leco hardness mapping software was used to create heat maps in order to visualize the hardness

gradients across the weld overlays, with red corresponding to low hardness (sub 200 HV) and teal/aquamarine corresponding to high hardness (above 600 HV).

HAZ Length Measurements

To measure HAZ lengths, an etching procedure was employed using 5% nital etchant after polishing with 800 grit SiC paper. This etchant darkens regions with carbides, but does not stain untempered martensite or ferrite grains. Base material was received in the soft anneal condition with very coarse carbides dispersed in a ferritic matrix. This base material microstructure forms a contrast with darker etching LT-HAZ, which assists in identifying the weld regions. Distance from the fusion line to the end of the untempered martensite (white) region to the beginning of the etched region is considered untempered heat affected zone, noted here as the high temperature heat affected zone (HT-HAZ). The HT-HAZ distance marked by the blue arrow is then subtracted from the total HAZ length marked by the red arrow to give a LT-HAZ length. This approach was validated using hardness traverses, and is within the accuracy range of 400 microns corresponding to the resolution of hardness maps conducted.

Results and Discussion

Two multi-pass welds with identical parameters, except for 300C and 25C preheats, were made to illustrate the effect of preheat on HAZ size. Figure C5 compares the heat affected zone sizes of 300C and 25C preheat welds.

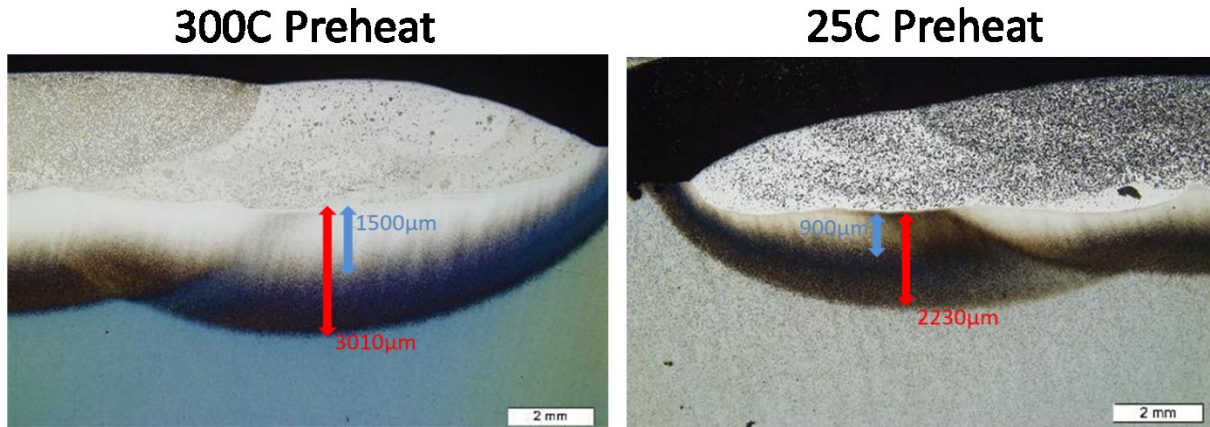


Figure C5: 300C vs. 25C Preheat HAZ Sizes

Preheat	300C	25C
Total HAZ Length (mm)	3.0	2.2
HT-HAZ Length (mm)	1.5	.9
LT-HAZ Length (mm)	1.5	1.3

Table C5 : 300C vs. 25C Preheat HAZ Size Measurements

The 300C preheat weld is representative of HAZ sizes for deposits using supplier recommended welding practices. The white color along the fusion boundary indicates a large, continuous band of untempered martensite formed after welding. This macrostructure of unbroken untempered martensite is likely adverse for repair life. Continuous bands of untempered martensite provide easy crack propagation paths once damage first initiates. This makes the 300C preheat sample's structure disadvantageous due to risk of delamination type failures of weld repairs.

The 300C sample's HT-HAZ size is also the same size as its LT-HAZ. This means bead placement would have to be exact for these welding parameters to fully temper previous passes. From a temperbead welding perspective, high preheat HAZ sizes shown here are not ideal. LT-HAZ length must be larger than HT-HAZ length to ensure maximum tempering of the prior

deposit layer HAZs. The 25C preheat weld has a smaller total HAZ length as well as a significantly smaller HT-HAZ size as compared to the 300C preheat sample. In addition to the reduced size, the HT-HAZ was discontinuous along the fusion boundary in the 25C preheat sample. Reduced contiguity of this region is likely beneficial compared to the continuous band of untempered martensite in the 300C sample.

The LT-HAZ is larger than the HT-HAZ in the 25C preheat sample, indicating this lower preheat is beneficial for a temperbead welding procedure. The LT-HAZ / HT-HAZ ratio is larger in the 25C sample than the 300C. The large LT-HAZ size in the 25C sample increases tolerance to welding process variables as compared to the 300C sample, which also is advantageous for temperbead.

To verify the metallography approach was within reasonable accuracy in determining the lengths of HAZs, a hardness map was made on the 300C preheat sample. The grid spacing of this hardness map was a consistent 400x400 microns, simplifying measurement of the tempered region. The LT-HAZ (green) of the second pass is shown by a breakdown of the first pass's HT-HAZ (teal color). The LT-HAZ is observed across 4 columns of hardness indents tracing the weld HAZ profile Figure C6.

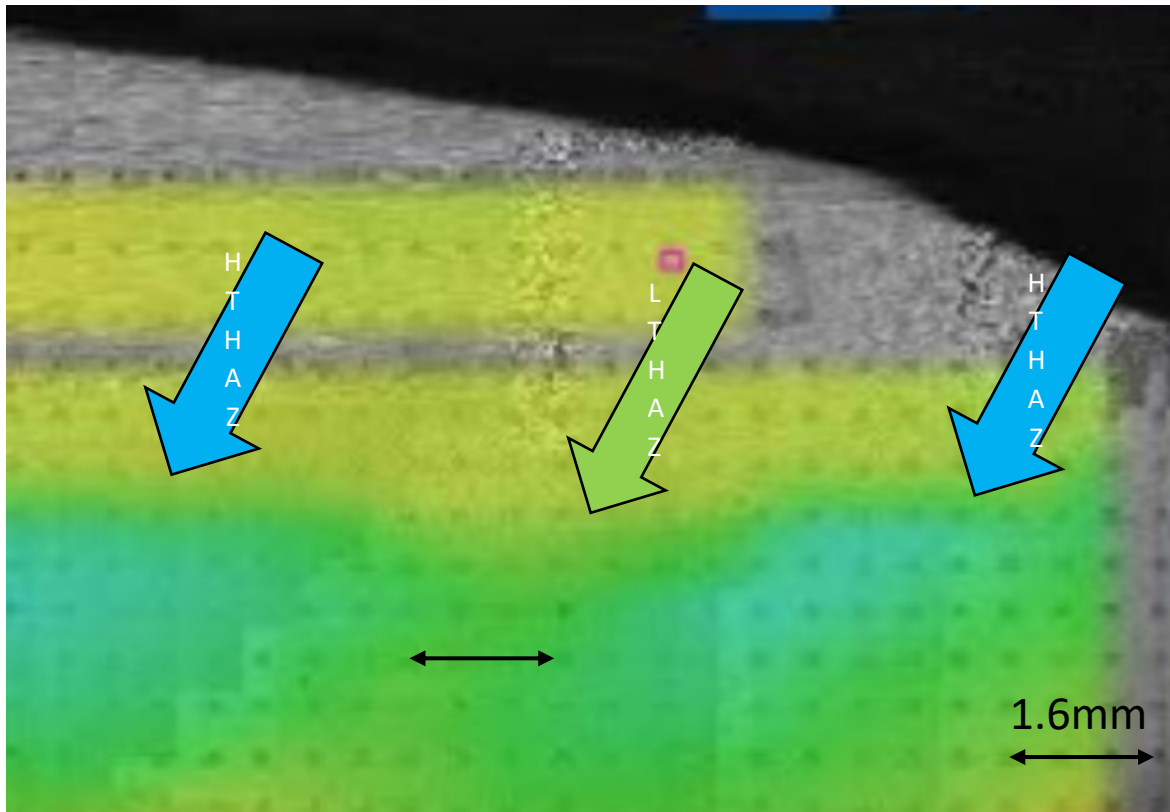


Figure C6 : Hardness Map of 300C Preheated Sample

The measured LT-HAZ length was measured where softening of a previous HT-HAZ occurred. The LT-HAZ region measured is the green/yellow zone in between the high hardness teal regions. This region measured was approximately 1.6mm, showing good agreement with the metallography method and verifying its accuracy.

With the effect of preheat on HAZ sizes understood, 10 welds were made to test heat input's effect on HAZ sizes. These tests employed identical parameters except travel speed. Travel speed was varied from 4-11 IPM at a constant 100C preheat. Resulting heat input value ranges for this trial were between 12.7 and 46.2 KJ/in. Low travel speeds resulted in higher heat

input and larger HAZ sizes while high travel speeds resulted in lower heat input and smaller HAZ sizes. The same HAZ length measurement procedure was used for heat input as the preheat trials, an example of which is shown in Figure C7. Results from all heat input trials were combined to form the graph shown in Figure C8.

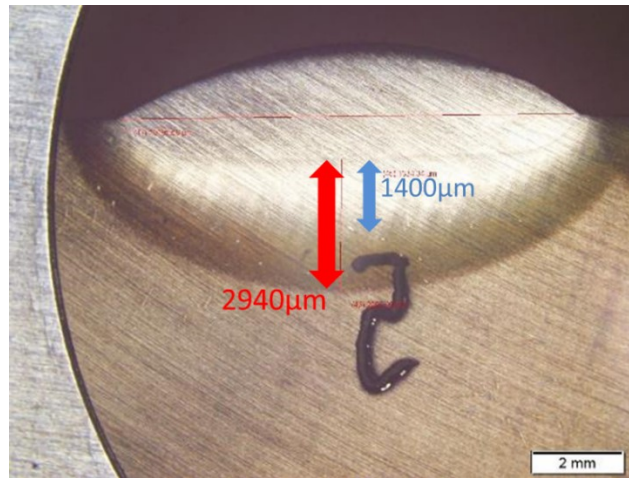


Figure C7: 5IPM Sample Travel Speed Test HAZ Measurements

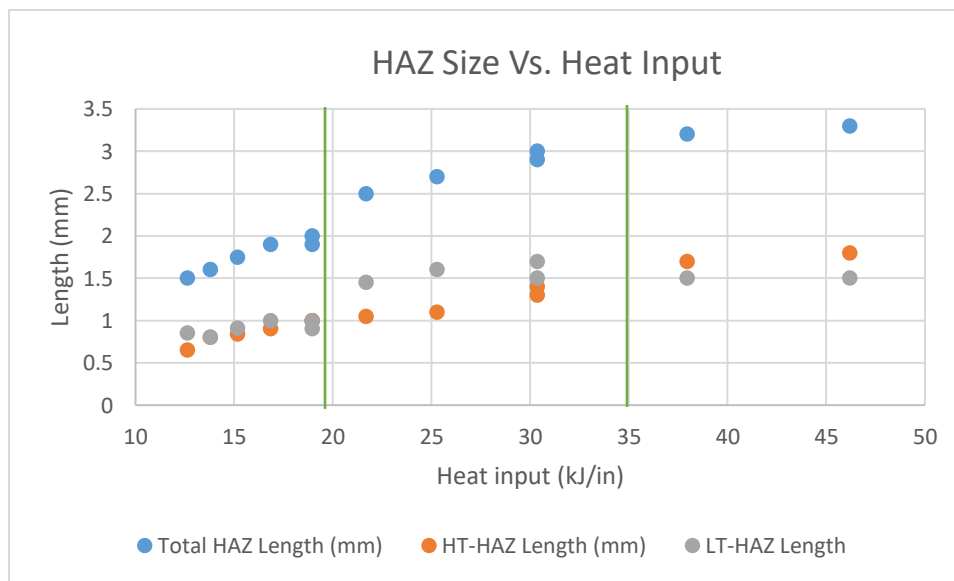


Figure C8: HAZ Sizes Vs. Heat Input

The effect of heat input on different HAZ size is shown in Figure C8. The bracketed region of 19-35kJ/in. maximizes LT-HAZ / HT-HAZ ratio, meaning this range should be used for temperbead welding to ensure process robustness. Heat inputs above this range resulted in a HT-HAZ that was larger than the LT-HAZ, promoting more untempered martensite. Excessive heat input and the resulting untempered martensite areas are detrimental to properties and must be minimized in temperbead welding.

Although one strategy to avoid property loss from welding is minimization of heat input, Figure C8 shows that may not be an effective strategy to realize temperbead welding of H13. Heat inputs below 19kJ minimize total HAZ length, but the ratio of LT-HAZ / HT-HAZ lengths lessens. This means that temperbead procedures using these heat inputs would have lower tolerance to variance than the 19-35kJ/in. range. Selection of a heat input window with good process robustness such as this is essential for temperbead welding.

To illustrate the results of these optimized temperbead welding procedures, two multi pass Anviloy Wire-H13 overlays were made. In the first overlay sample, a multi-pass weld was made using parameters developed solely for productivity and quality. This 3 pass weld illustrates a non-temperbead hardness gradient across an Orvar Supreme weld using a 100C preheat. A hardness map showing the hardness distribution across the weld fusion boundary and HAZ of that weld is shown in Figure C9.

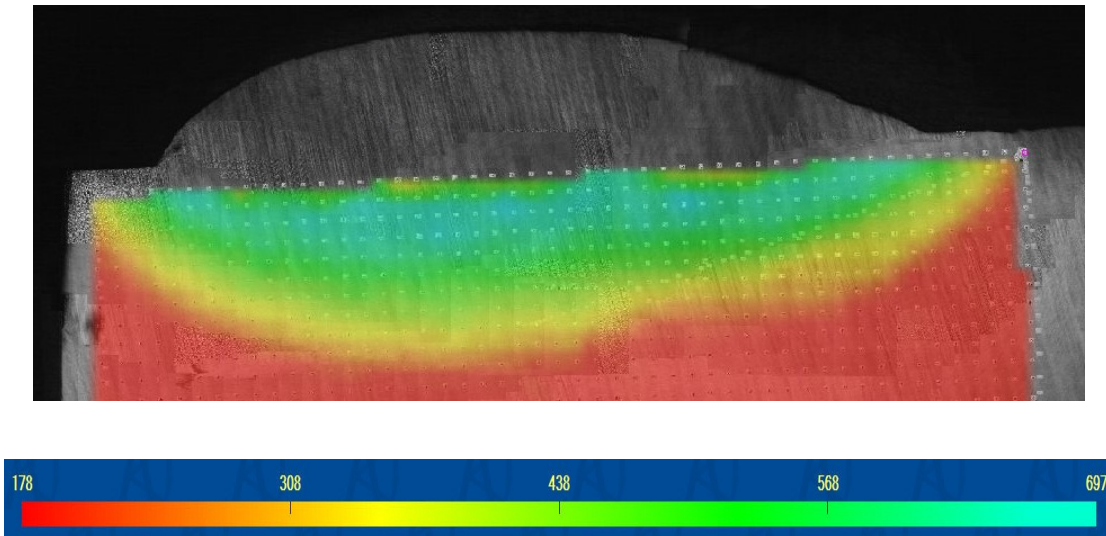


Figure C9: 3 Pass Double Layer Non-Temperbead Procedure Hardness Map

The 3 Pass Non-Temperbead overlay in Figure C9 has a continuous band along the top of the weld HAZ with hardness over 650HV. The max hardness in this sample of 697 HV is near the max hardness possible for this H13 composition. This type of hardness distribution is the norm for single layer procedures, with a large band of high hardness untempered martensite present along the weld fusion boundary. Since untempered martensite toughness is low, this simulated repair's adverse microstructure is likely to have a shorter life than a tempered HAZ. In addition, since hydrogen cracking susceptibility increases with increasing hardness in steels, this sample is at high risk for hydrogen cracking after welding when a low preheat is used vs. a more tempered sample or one using preheat/PWHT. Figure C10 shows a hardness map using the temperbead optimized procedure. This procedure employs a 100C preheat and heat input on both top and bottom passes between 22.5 and 25kJ/in.

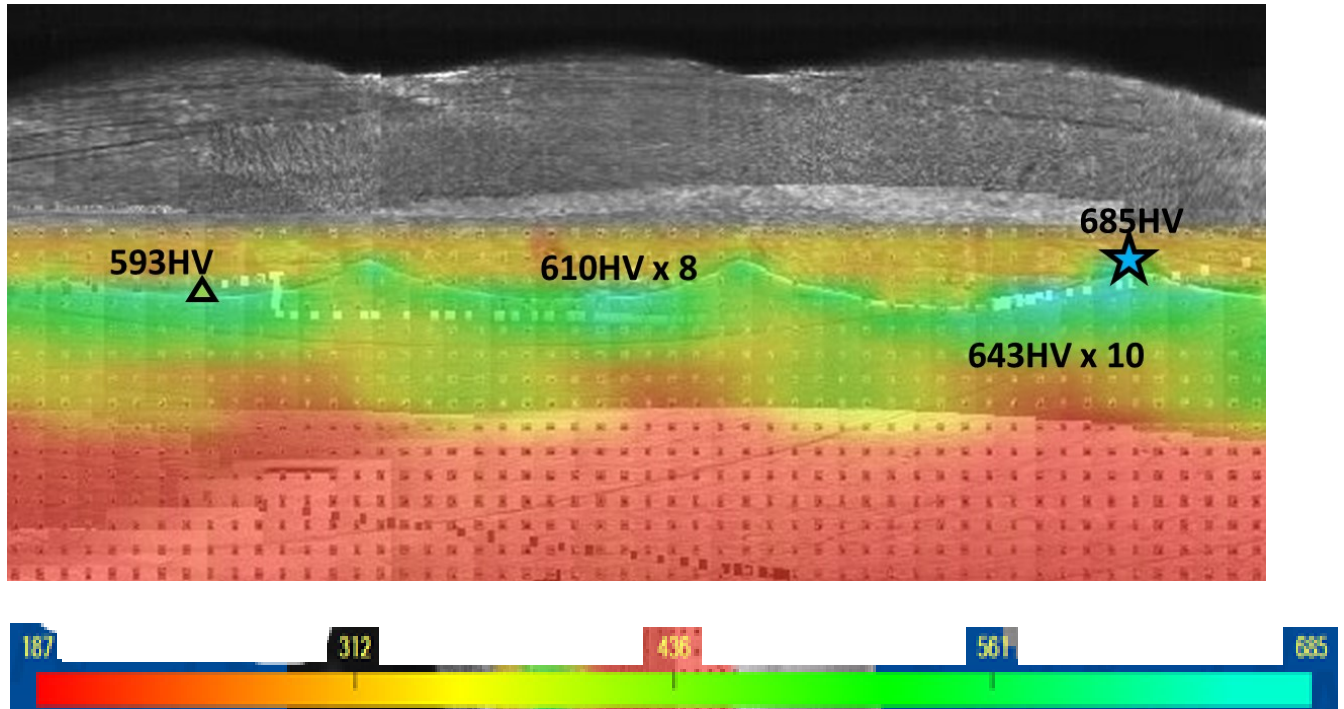


Figure C10: 5 Pass Temperbead Procedure Hardness Map

Figure C10 shows a 5 pass sequence where the HAZs of three bottom passes are tempered by the second layer. Bottom passes employed 25kJ/in. heat input. Top passes used 22.5 kJ/in to temper the previous passes. Labels indicate the number and average hardness of indent clusters above 600HV. Max hardness is labeled for the most effectively tempered (triangle) and least tempered (star) of the three HT-HAZs. Figure C10 clearly shows a more tempered microstructure than Figure C9, evidenced by the isolated regions with hardness over 600HV. No indents above 593HV (~54 HRC) were measured on the left side of the overlay. This is near the target hardness after tempering for Orvar Supreme, which is 48-52HRC depending on the intended application, which correlates to a Vickers hardness of 502 to 565 HV (11).

Though the deposits in Figure C10 have smaller regions of high hardness vs. the deposits shown in Figure C9, it still contained one indent measuring 685HV. High hardness regions can be

accepted if their size can be reduced enough to prevent failure, with critical size depending on application and industry. The deposits shown in Figure 7 has two regions with 600HV+ hardness. It should be noted that a complete overlay would deposit another pass to the right of the 10 indent grouping, which would likely further reduce its size and max hardness. Figure C11 shows proportions for 4 hardness ranges vs. total number of indents for the temperbead and non-temperbead welds shown in Figures C9 and C10.

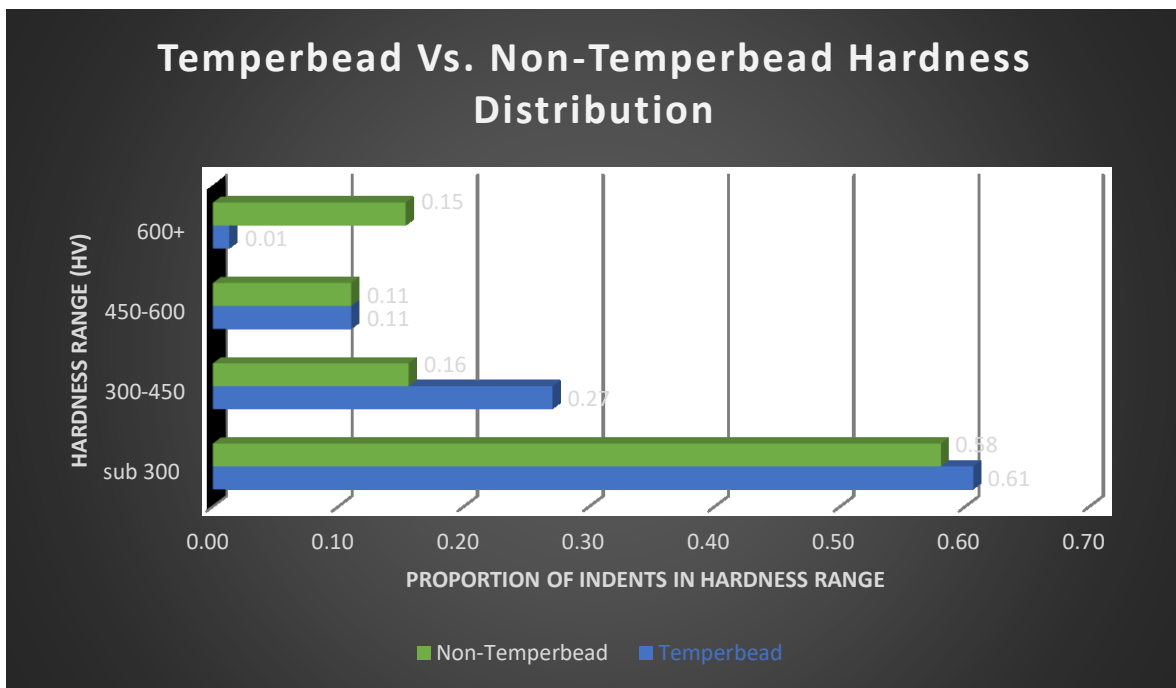


Figure C11: Temperbead Vs. Non-Temperbead Hardness Distribution

Figure C11 shows how effective optimized temperbead procedures can be at reducing the hardness of H13 weld HAZs. The non-temperbead procedure had 15% of total indents over 600HV. In contrast, the temperbead welding procedure resulted in a microstructure with just 1% of total indents over 600HV. This dramatic reduction in high hardness HAZ size is likely to have beneficial effects for die casters on repair toughness and longevity if applied. The results shown here indicate the feasibility of temperbead welding of hot work tool steels and showcase the

potential for temperbead welding technology to improve emergency repair welding procedures for die casters. In plant trials are planned to evaluate Anviloy overlay repair procedures and will compare a range of overlay and temperbead conditions.

Conclusions

- Anviloy HW-GTAW deposits can be used to temperbead weld H13 tool steel HAZz.
- Low preheat repair temperatures may be necessary to maximize temperbead effectiveness on H13 HAZ.
- The hardness range of non-temperbead overlays was 200HV-700HV where there was a continuous band above 600HV along fusion boundary.
- The hardness range of temperbead samples was 200HV-590HV with just small isolated regions of higher hardness.
- The preferred temperbead procedure resulted in only 1% of hardness map above 600HV / 53HRC.

Works Cited

1. J. Sjostrom. "Chromium martensitic hot-work tool steels – damage, performance, and microstructure." Karlstad University. 2004.
2. S. Jhavar, C.P. Paul, N.K. Jain. "Causes of Failure and Repair Options for Dies and Molds: A Review." *Engineering Failure Analysis*. 2013.
3. J. L. Lin, S. Myers, S Carrera. "Degradation Mechanisms of Die Coatings Used in Aluminum Pressure Die Casting." *Surface Engineering in Materials Science III*. 2005.
4. D. Schwam, J.F. Wallace, S. Birceanu. "Die Materials for Critical Applications and Increased Production Rates." Case Western Reserve University. 2002.
5. W. Sperko. "Exploring Temperbad Welding." *The Welding Journal*. 2005.
6. Steve Thompson. "Handbook of mold, tool and die repair welding." William Andrew Publishing. 1999.
7. C. Zhu. "Tempering of Engineering Steels." Trinity College Oxford. 2005.
8. J. Stewart. "Temper Bead Welding for Dissimilar Metal Welds and Overlays." The Ohio State University. 2019.
9. Zhang, Kaiwen. "Experimental and Computational Investigation of Temper Bead Welding and Dissimilar Metal Welding for Nuclear Structures Repair." The Ohio State University. 2016.
10. R. Markežiča, I. Nagličb, N. Molea, R. Šturma. "Experimental and Numerical Analysis of Failures on a Die Insert for High Pressure Die Casting." *Engineering Failure Analysis*. 2019.
11. Uddeholm AB. Uddeholm Orvar Supreme Product Brochure. Uddeholm, 2020
12. C. Zhu, "Tempering of Engineering Steels," Trinity College. 2005.
13. G. R. Speich and W. C. Leslie, "Tempering of steel," *Metall. Trans.*, vol. 3, no. 5, pp. 1043–1054, 1972.
14. S. L. McCracken, R. E. Smith, and D. Barborak, "Validity of Hardness Criteria to Demonstrate Acceptable Temper Bead HAZ Impact Properties for Nuclear Power Applications," *ASME 2013 Press. Vessel. Pip. Conf.*, no. 3, p. V06BT06A006-V06BT06A006, 2013.

Appendix D : Microstructure Characterization of Anviloy Cladding

Deposits on H13 Die Steel

Abstract:

Aluminum die casting is widely used in automotive industry to rapidly produce lightweight engine and drivetrain components. Die repair technology is an integral part of die casting sustainability to minimize production costs. Solid tungsten based Anviloy die inserts are well known in die casting for improved lifetime vs. tool steels, but are only available in insert and rod form (1). New Anviloy alloy (W-27.5Ni-12.5Fe) has enabled the production of wire that can be used for automated weld deposition processes. Using a mechanized hot wire gas tungsten arc welding (HW-GTAW) machine, hardfacing (cladding) procedures were developed for Anviloy wire on H13 tool steel die material. Fusion zone microstructures of these welds were characterized using optical and electron microscopy, and results were validated using Thermocalc simulations. EDS scan data from welds indicates formation of primary alpha tungsten BCC phase and (FeNi) FCC phases in the fusion zone, as well as possible formation of M_6C carbide and intermetallic Mu phase $(FeNi)_7W_6$ along the fusion boundary in as welded samples. Thermocalc simulations indicated the presence of primary alpha tungsten BCC phase, FeNi FCC phase, M_6C carbide phase, and Mu phase. EDS was unable to differentiate carbon content between phases. To help determine presence of M_6C carbides, 308L butter layer material was added between the Anviloy wire clad deposits on H13. These buttered deposits were heat treated with annealing and double tempers to test the effect of standard H13 heat treatment on microstructural evolution. An alkaline sodium picrate etch was used to resolve M_6C carbides, which were revealed in the H13-Anviloy wire welds but not the H13-308L-Anviloy Wire welds.

Findings suggest the presence of M_6C carbide, but further crystallography of the unknown phase(s) is required to confirm the presence of Mu phase or M_6C carbide phase in Anviloy Wire – H13 welds.

Objectives

- Characterize Anviloy wire arc melted button microstructures using metallography
- Characterize Anviloy Wire – H13 weld deposit microstructures with metallography, SEM, and EDS
- Compare Characterization results to Thermocalc simulations
- Compare H13-Anviloy clad deposits to buttered H13-308L-Anviloy clad deposits with and without heat treatment using metallography and etching techniques.

Introduction

High Pressure Die Casting Die Materials

Die casting die materials must resist all forms of damage while still maintaining cost effectiveness. For these reasons, hot work tool steels are the most common die material (2). Hot work tool steels offer the combination of hot yield strength, corrosion resistance, and moderate cost that contribute to their widespread use. The most common hot work tool steels today are H13 and H11 (40CrMoV), both of which are medium carbon steels containing chromium, molybdenum, and vanadium.

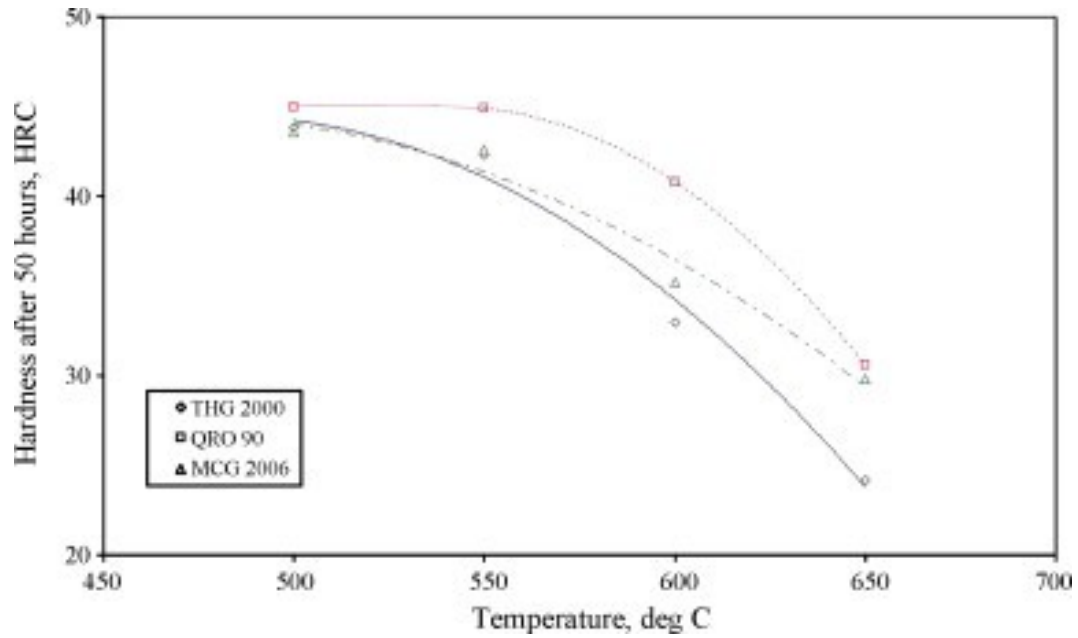


Figure D1 : Softening VS. Exposure Temp for Different Steels (3)

Alloying additions are intended to increase high temperature strength through secondary carbide precipitation. The largest contribution to elevated temperature strength comes from primary Mo M_6C carbide and primary V MC carbide since both are stable at high temperature (2).

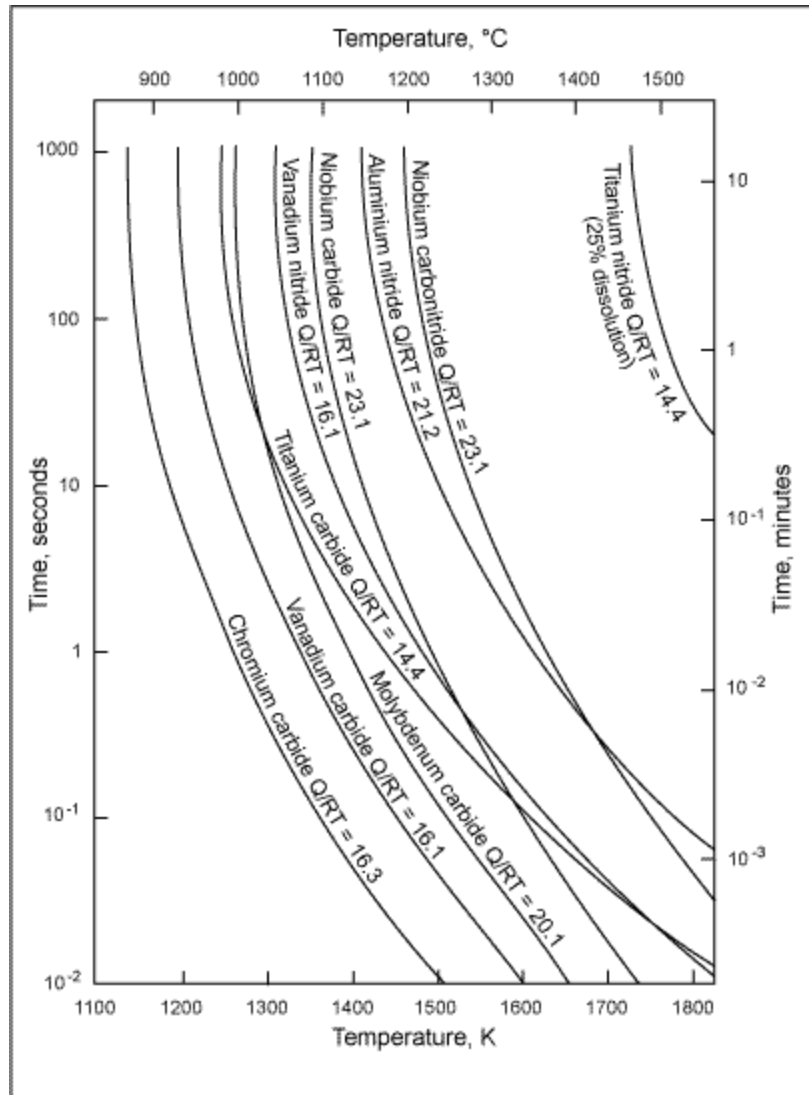


Figure D2 : Easterling Precipitate Dissolution in Steels (3)

The molybdenum and vanadium also improve resistance to overaging until temperatures around 600C. This helps limit microstructural evolution during service, retarding softening of the dies. Depending on casting conditions, hot work tool steels can begin to form heat checking cracks in as little as 500 cycles, with soldering and washout damage occurring shortly thereafter (2). Since hot work tool steels get their strength from carbides, which change morphology over time at elevated temperatures, die steels eventually degrade in service. Over time and casting cycles,

die surfaces lose strength and hardness as noted by Figure 3. In service softening lowers hot yield strength of dies, resulting in cracking and eventual need for repair.

Compared to conventional die steels, refractory alloys possess superior high temperature strength, corrosion resistance, and thermal cycling performance. Their mechanical properties also don't change during service as severely as die steels since they don't rely on carbide precipitation to achieve high temperature strength. Commonly used refractories such as molybdenum and tungsten based alloys are ideal materials to resist thermal fatigue cracking. These alloys provide high hot yield strength that resists deformation, high thermal conductivity that reduces thermal gradients in parts, and low thermal expansion that reduces thermal expansion induced deformation as noted by the Kindbom Theory (5).

Cost is the main factor limiting wide-scale use of refractory die casting dies. Since they are often an order of magnitude more expensive than die steels, wholly tungsten or molybdenum alloy dies are cost-prohibitive. This limits refractory alloy applications to bolt-on inserts for small regions of die surfaces, as evidenced by the use of tungsten based Anviloy inserts in the most challenging die regions since the 1970's (1). Claddings/overlays are often used in corrosion applications to limit expensive material usage to working surfaces only, but pure tungsten and molybdenum both form intermetallics with iron, which may degrade clad bond properties on steel dies. Tungsten and molybdenum also possess poor wire drawability, making it difficult to automate deposition processes using these pure metals. In general, tungsten is preferred over molybdenum for die casting because of its improved resistance to liquid metal corrosion, especially in aluminum (6).

A new Anviloy (W-27.5Ni-12.5Fe) alloy was developed to improve wire manufacturing for automated die repair and cladding. This new alloy provides increased ductility that enables

wire drawing, but also helps reduce intermetallic formation compared to pure tungsten when clad onto H13. The main difference versus Anviloy 1150 are higher nickel and iron alloying additions.

Ni-W-Fe System

W-Ni-Fe phase equilibria has been studied in the past and reviewed by several researchers (7, 8, 9, 10, 11). Starting with the original work of Winkler and Vogel, the phase boundary between gamma FCC and alpha BCC was investigated, reporting a somewhat controversial intermediate phase of $W\text{Ni}_6$ in addition to the alpha tungsten and gamma phases (7). Subsequent work by Posthill and Edmonds indicated that the $W\text{Ni}_6$ phase identified by Winkler and Vogel was actually a ternary $(\text{Ni,Fe,W})_{12}\text{C}$ carbide present as a result of carbon inclusion in pre-alloy powders (8). Ostlund et. al. then produced a paper confirming the presence of a $(\text{Ni,Fe})_7\text{W}_6$ intermetallic identified as Mu phase (9). Other researchers have identified M_6C and M_{12}C carbides in the system as a result of pre-alloy powder contamination (10, 11, 12, 13). However, subsequent research efforts have corroborated the existence of Mu phase in the ternary W-Ni-Fe system (14).

The generally accepted phases present in the W-Ni-Fe system are alpha BCC phase, gamma FCC phase, and TCP intermetallic Mu Phase. Much of the research involving the W-Ni-Fe system, with the exception of Winkler and Vogel, focused on the tungsten heavy side of this system (7). This is due to the commercial application of tungsten heavy alloys produced via liquid state sintering either for military kinetic energy penetrator projectiles or weights such as those used in cell-phone eccentric rotating vibration motors (14).

Ni-Fe-Cr System

The Ni-Fe-Cr system is perhaps the most widely studied ternary system due to the wide range of industrial materials that are based on it. This system is the basis for many stainless steels as well as a wide range of nickel based alloys. Alloys belonging to these families are renowned for their excellent corrosion resistance in a wide variety of applications. Austenitic stainless and nickel based alloys are also renowned for their excellent high temperature properties. These materials form the backbone of high temperature and corrosion resistant structural materials (15).

The phase stability of this system was reviewed by Raynor and Raghavan (16, 17). Isothermal sections for this system over a range of compositions were computed using the Calphad method by Miettinen et. al are shown in Figure (18).

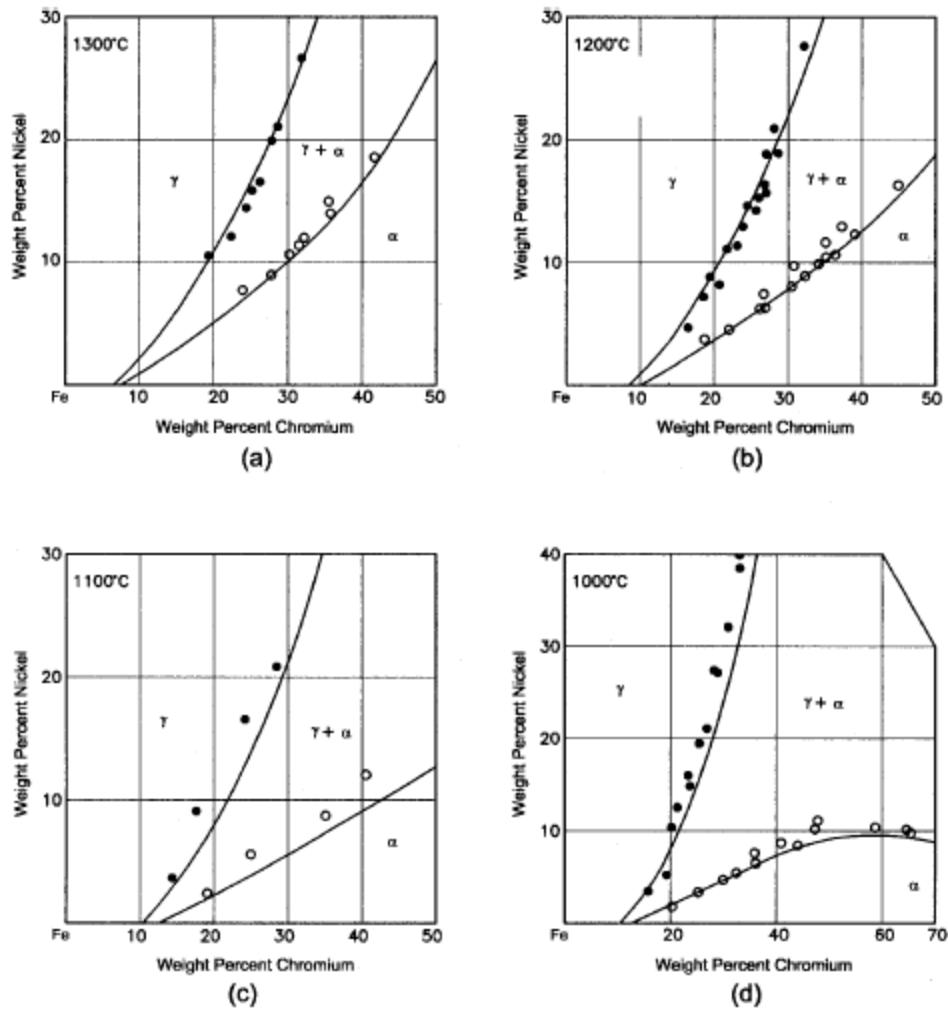


Figure D3 : Cr-Fe-Ni Isotherms at (a) 1300C (b) 1200C (c) 1100C and (d) 1000C by Miettinen

(18)

This most important feature of this ternary system is the wide range of compositions where metallic solid solutions are stable. Unlike many ternary systems, this system does not readily form intermetallics (16, 17, 18). This is beneficial for material design because properties and composition can be modified without fear of forming brittle intermetallics. The wide range of metallic solid solutions in this system have allowed for a tremendous amount of alloys to be developed based on this system.

W-Cr System

The W-Cr phase diagram belongs to the family of binary isomorphous systems, where a continuous series of solid solutions with BCC structure have stability at high temperatures (19). The Binary phase diagram for this system developed with experimental data is shown in Figure D4.

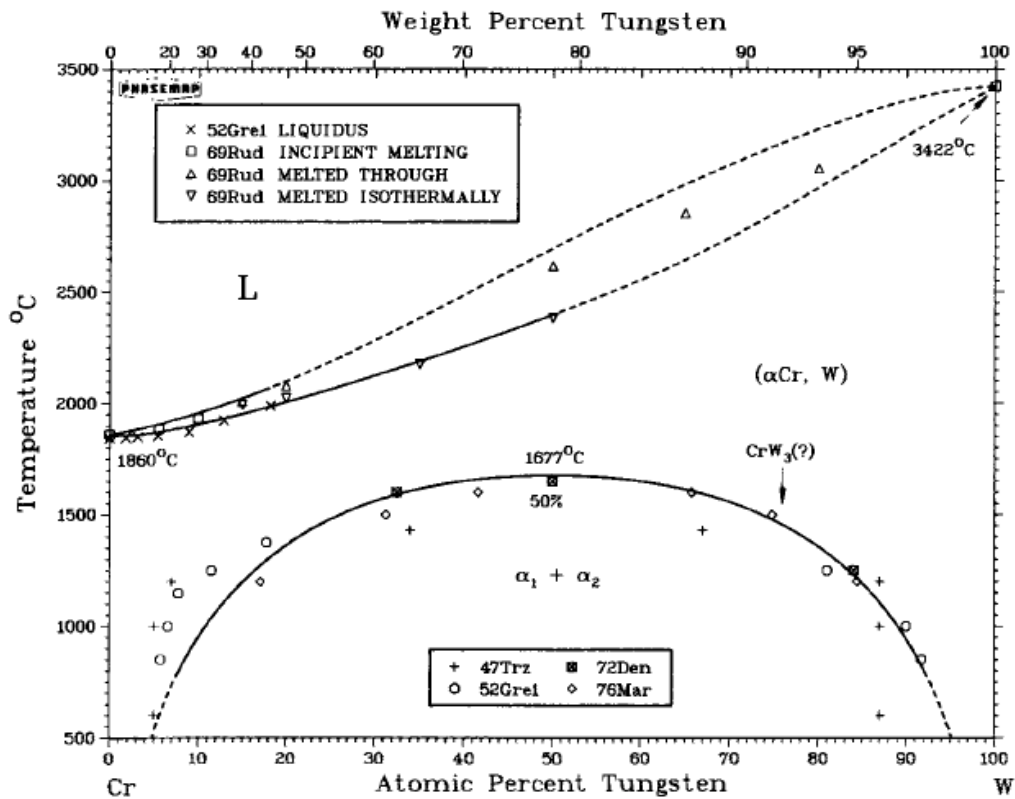


Figure D4 W-Cr Phase Diagram (19)

Although at high temperatures and at extreme ends of the compositional space a single solid solution exists, at lower temperatures this solid solution decomposes into two phases : a Cr rich BCC phase and a W rich BCC phase (19).

Experimental Methodology

Materials

Base material used in this study was Uddeholm Orvar supreme, an H13 HWTS. Its chemical composition is shown in the subsequent table along with Anviloy Wire's.

wt%	Fe	Mo	V	C	Si	Mn	Cr	W	Ni
Orvar Supreme	Bal.	1.5	0.93	0.39	0.9	0.4	5.1		
Anviloy Wire	12.5							Bal.	27.5
308L	Bal.			0.03	1	2	20		11

Table D1 : Orvar Supreme, Anviloy Wire, and 308L Compositions

Plates were welded in soft anneal condition with a hardness before welding of around 180HV, with a microstructure consisting of ferrite and coarse carbides. Orvar supreme is supplied in this condition for ease of machining. Plate thickness for each test was 3/4". Plates were cleaned prior to welding using abrasive grinding wheels and cleaned with ethanol.

Anviloy welding wire in development by Astaras was used in this study, Table D1. This W-27.5Ni-12.5Fe material is intended for die casting applications, and consists of primary alpha tungsten BCC phase in a Ni-Fe FCC matrix, described in further detail later in this Appendix.

The 308L variant used in this study was supplied by Harris welding wire group. The microstructure of this material alone consists of a fully FCC austenitic microstructure. Wire was supplied in the .045" size.

HW-GTAW of Anviloy Wire

Since the Anviloy wire is a new material, parameter windows were first established for hot wire gas tungsten arc welding (HW-GTAW) using a Jetline 9800 mechanized system. Once stable parameters were developed that achieved sound clads with acceptable surface quality based on visual analysis, bead on plate overlays were made to characterize deposit microstructure. Hot wire power supply was supplied by Jetline provide up to 200 Amp alternating current power. All clads were made with .035” diameter Anviloy wire.

HW-GTAW of 308L Butter Layer

The Jetline 9800 mechanized system shown in Figure D5 was also used to produce the butter layer clads using a 308L filler material. Stable parameters were developed to deposit the 308L material as an intermediary clad layer between the H13 base material and Anviloy wire alloy. Multi-pass bead on plate overlays were made and subjected to heat treatment and metallographic characterization to determine effect of 308L butter on clad microstructure. Hot wire power supply was supplied by Jetline provide up to 200 Amp alternating current power using .045” 308L wire.

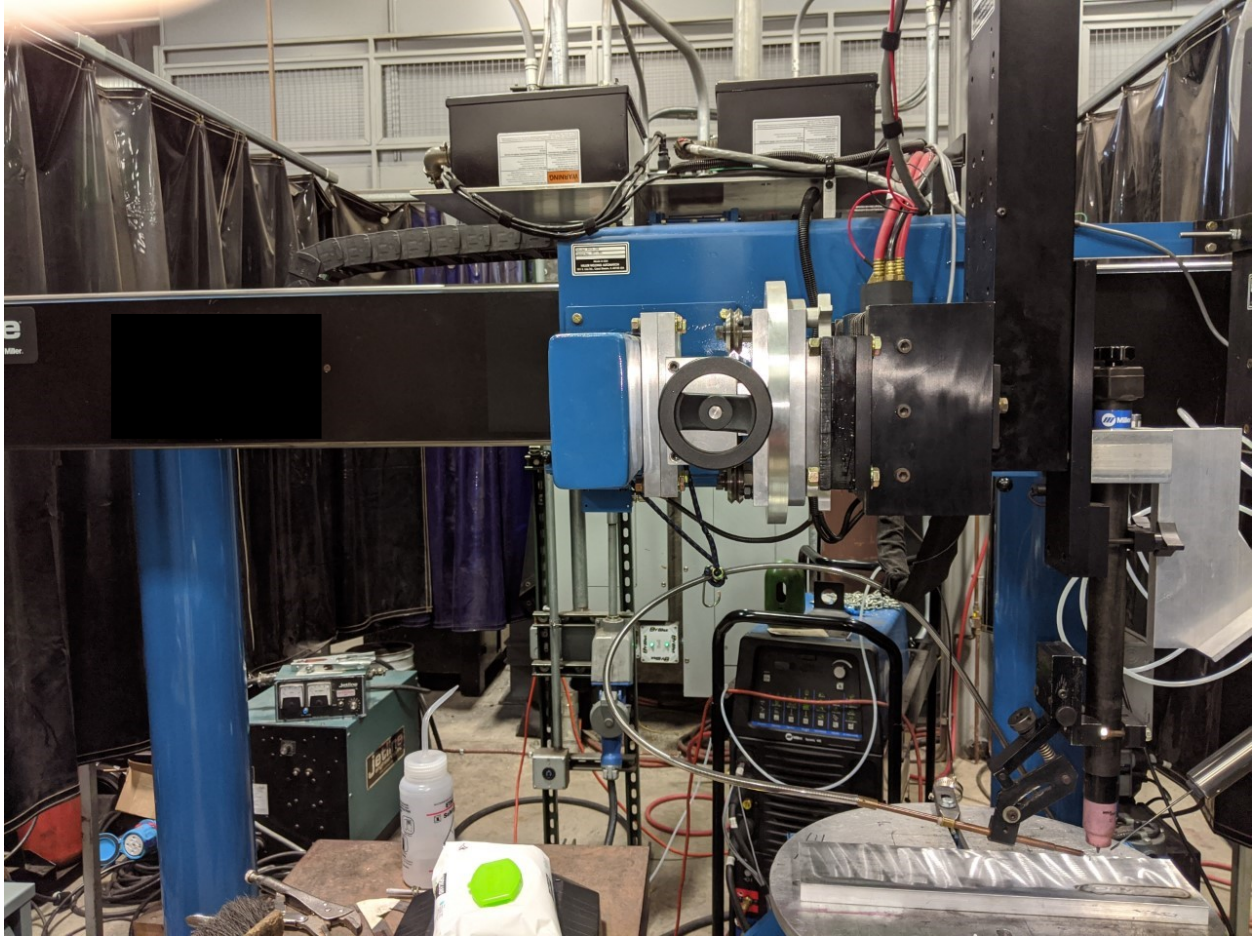


Figure D5 : Miller Jetline 9800 Mechanized Welding System

Non Heat Treated Sample Metallography

All non heat treated metallographic samples were prepared by polishing with 240, 400, 600, and 800 grit SiC abrasive followed by 9, 6, and 3 micron colloidal diamond abrasive. Samples were submersion etched using a 10% Nital (10% Aqueous Nitric Acid in Ethanol) solution for 30-45 seconds. All metallographic images were taken with an Olympus GX-51 microscope using DP2-BSW software.

Heat Treated Sample Metallography

All heat treated metallographic samples were prepared by polishing with 240, 400, 600, and 800 grit SiC abrasive followed by 9, 6, and 3 micron colloidal diamond abrasive. Samples were submersion etched using a heated alkaline sodium picrate etch for 60 seconds at a temperature of 70C. This etchant is formulated to reveal the presence of M_6C carbides with a high tungsten content by darkening them. This etchant does not darken alpha ferrite, gamma austenite, or alpha tungsten. All metallographic images were taken with an Olympus GX-51 microscope using DP2-BSW software.

SEM / EDS

A Quanta 200 equipped with a secondary electron and EDS detector was utilized for pre- and post-service characterization of Anviloy Wire-H13 overlays. The secondary electron detector was used in order to capture and analyze the fusion zone microstructure and morphology, as well as to identify regions of interest for EDS. EDS was used to approximate the elemental composition of regions of interest in an effort to identify unknown phases using TEAM EDAX software. EDS results were then compared to Thermocalc results for validation.

Thermocalc

Thermocalc's high entropy alloy package and database were employed in this study due to the high tungsten content of Anviloy deposits. The tested compositions of 10% and 40% dilution were outside of the steel/nickel database composition range. Thermocalc was used to investigate predicted phases present and to calculate the equilibrium composition of those phases. Results were used to validate EDS results and to help determine identify of unknown

phases. Because of the unique compositional space of Anviloy wire, phase diagrams are unavailable. For this reason, Thermocalc property diagrams were used instead. These diagrams use a single composition and map phases and phase fractions present, as well as each phase's composition, over a range of temperatures.

Heat Treatment

All samples were heat treated using a Lucifer Furnace model 7GT-K24 with Honeywell DC230L and DC2500 controllers using a Type K thermocouple shielded from oxidation in an Inconel 600 tube. The first heat treatment used was a standard heat treatment for Orvar Supreme involving a normalizing heat treatment at 1030C for 30 minutes and a double temper at 550C for 2 hours. Samples were air cooled to 70C after normalization and immediately tempered for the first time at 550C for 2 hours. Following the first tempering heat treatment, samples were air cooled to 70C and immediately tempered once more at 550C for 2 hours. In addition to required soak times at each heat treatment temperature, a 30 minute ramp time was used to allow samples to reach the desired temperature. Heat treated sample sizes were maintained under 4 ounces to ensure rapid and even heating and cooling.

Results and Discussion

Metallographic Characterization of Anviloy Wire

Before characterizing Anviloy wire deposits that are diluted with H13, the Anviloy wire itself was melted and examined metallographically. The melted "button" was produced via GTAW melting in a copper crucible. The Anviloy W-27.5-12.5Fe button is shown below in two micrographs of varying magnification.

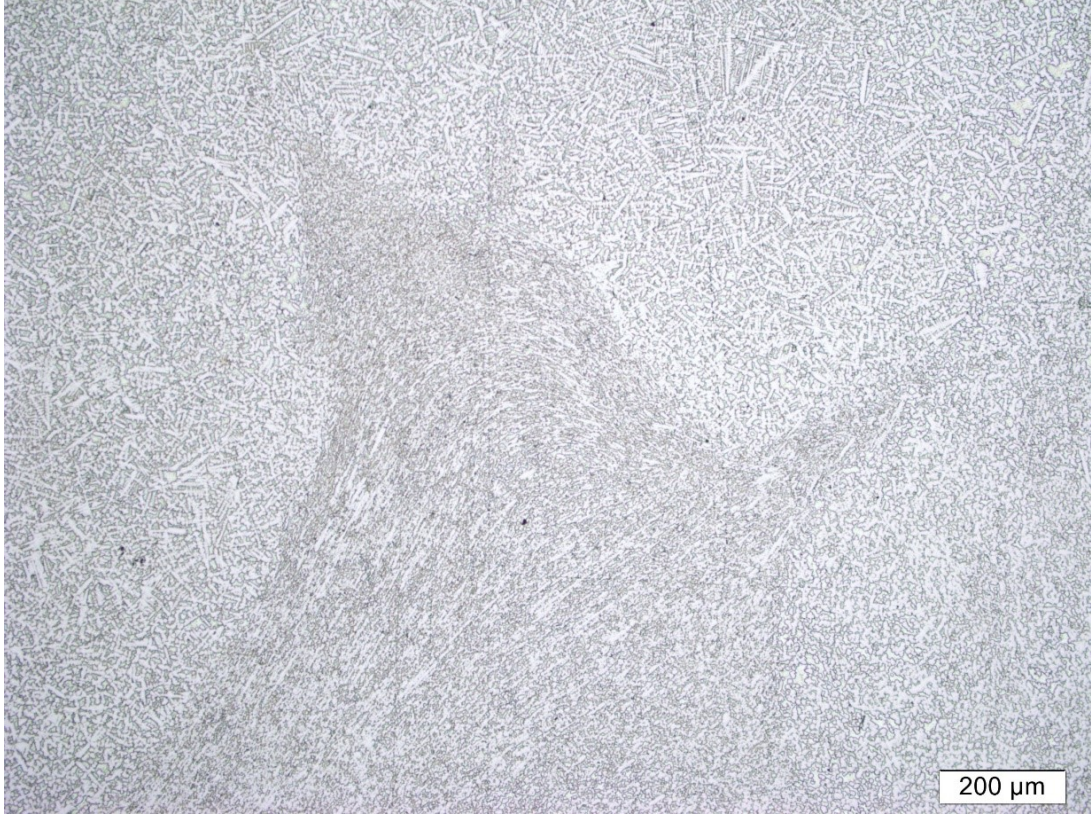


Figure D6 : Anviloy Wire Button Microstructure at Low Magnification

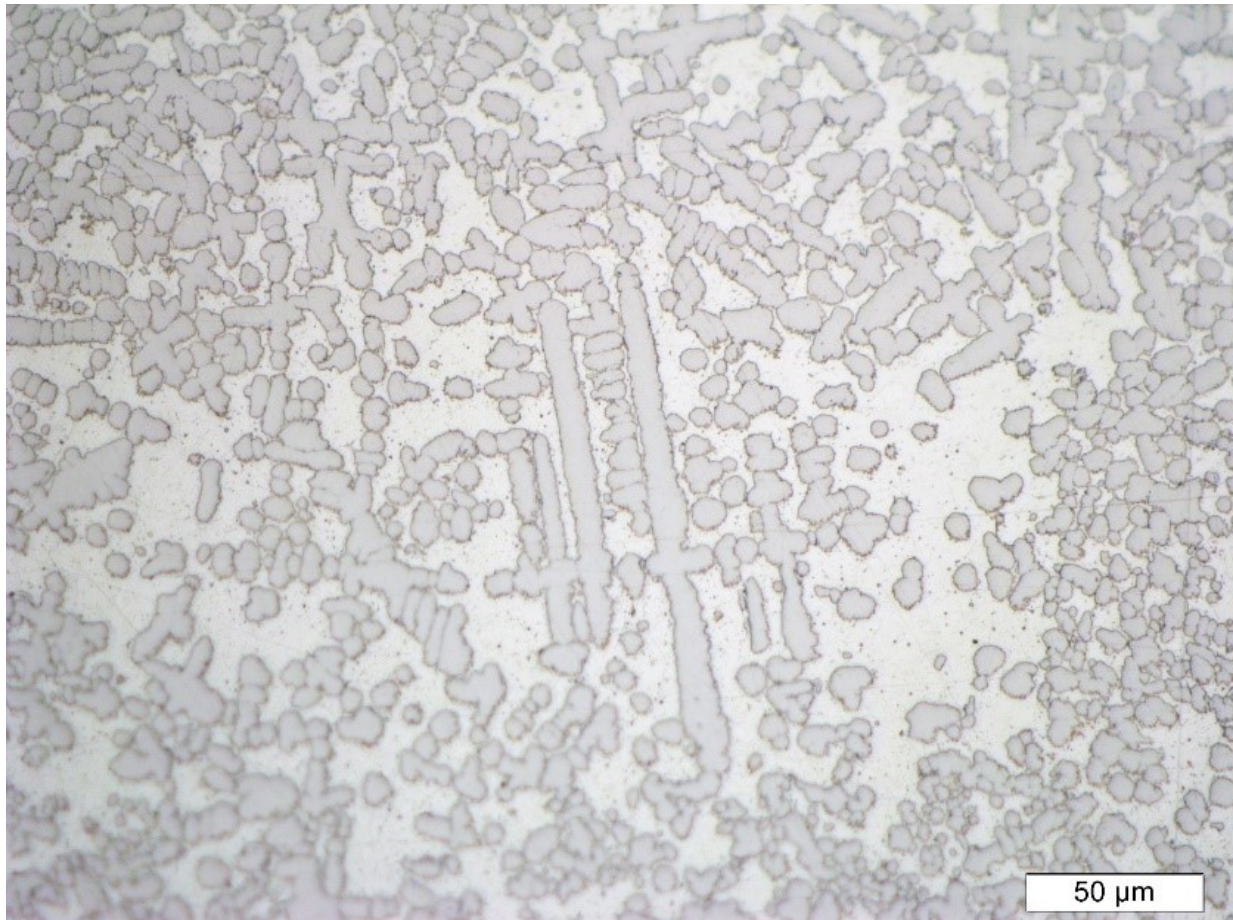


Figure D7 : Anviloy Wire Button at High Magnification

Both micrographs appear to exhibit a two phase microstructure consisting of a white matrix phase and grey dendritic phase. The morphology of the grey phase differs slightly throughout the sample, but variants of cellular and cellular dendritic shaped grains are observed. This two phase microstructure was then compared to Thermocalc results for the Anviloy wire composition to verify its integrity. A property diagram showing stable phase fractions for Anviloy Wire is shown below.

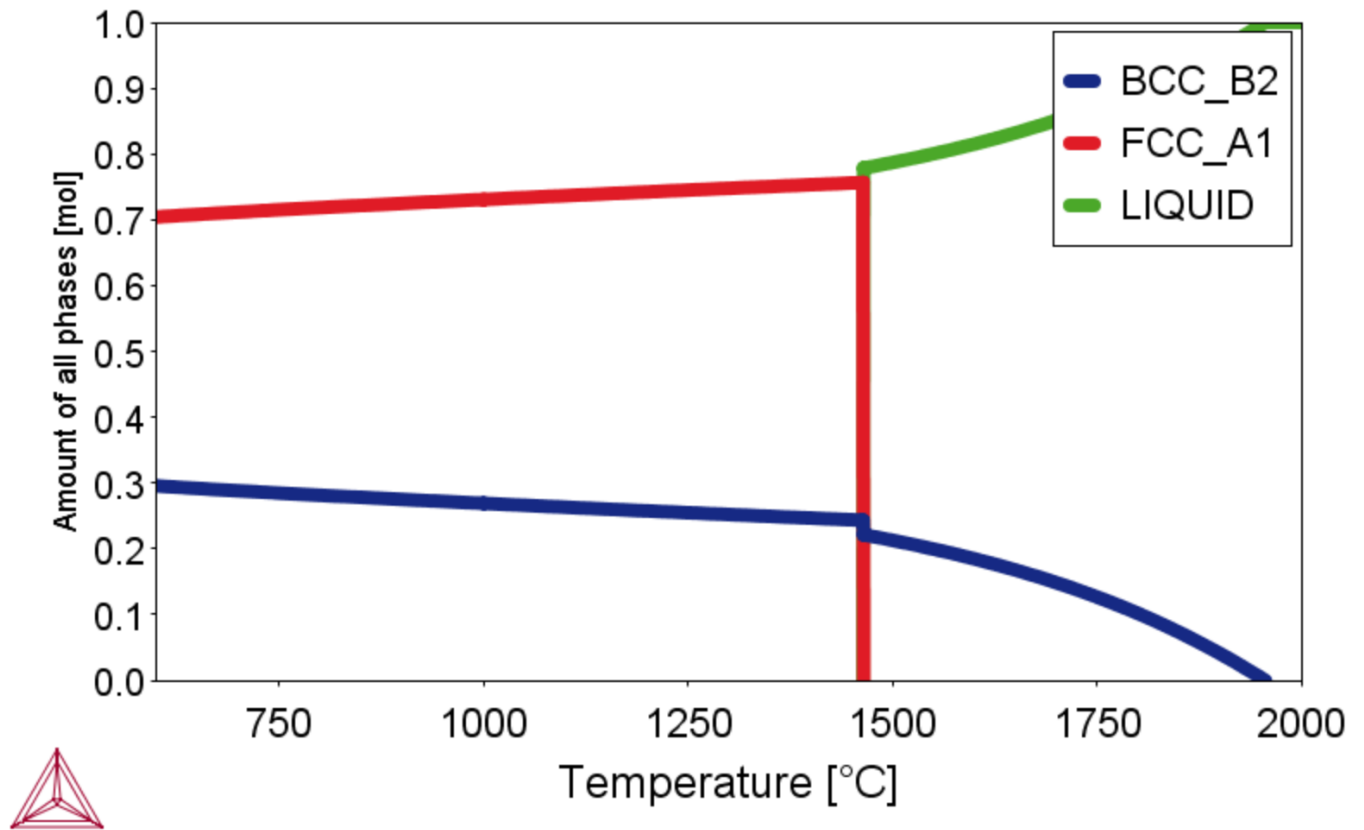


Figure D8: Anviloy Wire Property Diagram

The resultant Thermocalc property diagram for Anviloy Wire confirmed the hypothesis of a two phase microstructure. The two phases predicted by Thermocalc are primary alpha tungsten BCC phase and a Ni-Fe FCC phase with some dissolved tungsten in solution. No intermetallics or other phases are predicted. Interestingly, the property diagram shown here indicates the high liquidus temperature of the Anviloy wire consumable, which approaches 2000C. This high liquidus temperature may have implications for welding, since the liquidus temperature for H13 steel is much less at approximately 1400C.

SEM Characterization of Anviloy Wire – H13 Deposits

After parameter development resulted in sound clad deposits, a characterization effort was undertaken to understand the microstructure of both undiluted Anviloy and diluted clad deposits using SEM and EDS. To analyze the microstructure of the undiluted samples, six HW-GTAW Anviloy wire passes were made resulting in a 30mm buildup of Anviloy. It is assumed each successive pass will contain less base metal composition, and calculated dilution percentages for this sample are under 10% in the final pass. An SEM micrograph of that sample's last pass is shown in Figure D9 at 50x magnification.

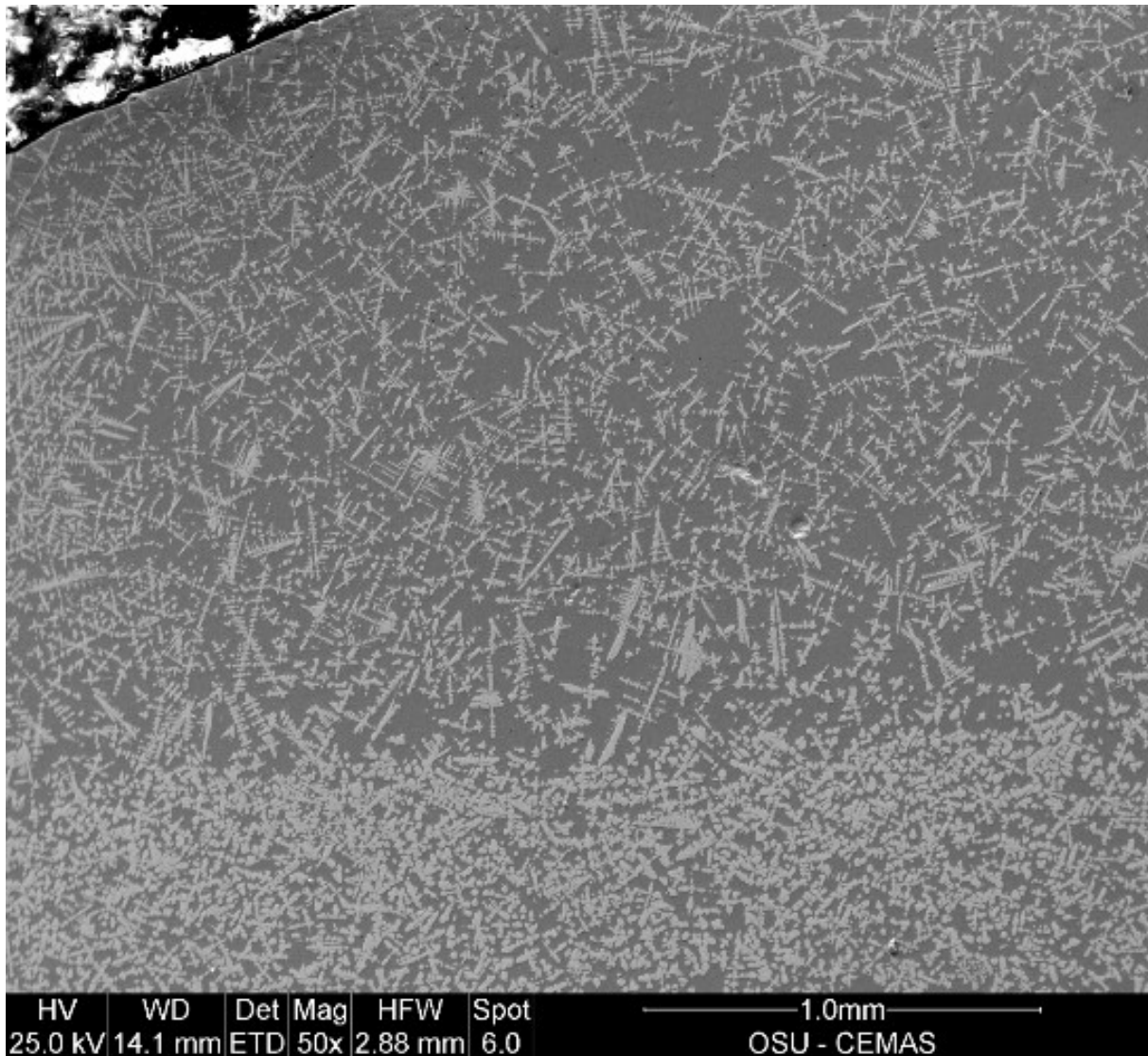


Figure D9: Secondary Electron Image of 6 Pass Anviloy Wire Build

As shown in Figure D7, two phases are apparent in the undiluted Anviloy buildup. The matrix phase appears to be dark in the secondary electron map, indicating a composition with fewer high atomic number elements relative to the secondary white phase. Since only tungsten, nickel, and iron are present in the Anviloy wire, the secondary white phase is most likely

enriched in tungsten compared to the matrix phase. Tungsten appears brighter in secondary electron images due to its higher atomic number.

Also evident in Figure D7 is a sharp change in phase fraction compared to the top and bottom sample. The secondary white phase in the bottom region of Figure D7 appears to have a cellular morphology, while the same phase has a dendritic/cellular dendritic morphology. This is likely due to the effects of reheating on the Anviloy wire microstructure. It is likely that the secondary white phase, since it appeared higher in tungsten content, has both a higher melting temperature and higher density than the matrix phase. It is likely that, upon melting of previous layers, the matrix phase melts while at least some amount of the tungsten rich secondary phase remains solid. Due to hypothesized differences in density between the phases, the tungsten rich phase sinks and causes macrosegregation in the molten pool, and results in a higher concentration of this phase towards the fusion boundary, enriching the phase fraction of the tungsten phase in that area. To corroborate these assumptions, EDS studies were conducted to determine if the secondary white phase indeed has a higher tungsten content and resultant high density and melting temperature. Figure D10 shows an EDS map made to determine the elemental composition of the phases in question.

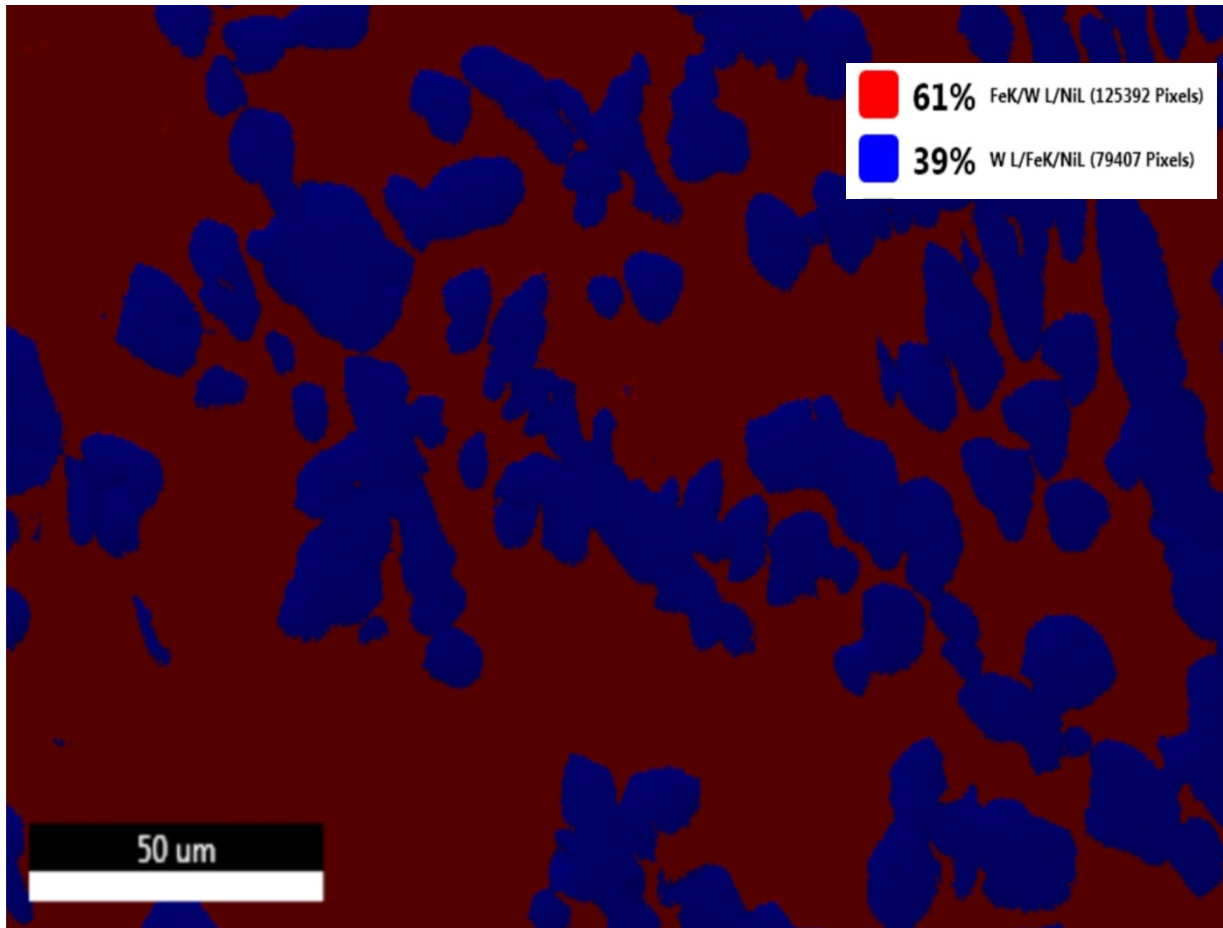


Figure D10: EDS Map of Undiluted Anviloy Wire

EDS scans were made using the Quanta 200 systems software with TEAMS phase differentiation capability. The resulting EDS maps and phase identification software validated the two phase hypothesis, as well as showing significantly higher tungsten content in the secondary phase. The matrix phase appears to be Ni-Fe FCC phase as identified by the TEAMS software.

EDS data was collected to determine the composition of the phases in this location, but it is important to note the limitations of EDS in gathering quantitative composition data on large

samples containing multiple phases. The composition of phases as gathered by the EDS detector are shown below with their corresponding counts (y-axis) vs. energy (x-axis).

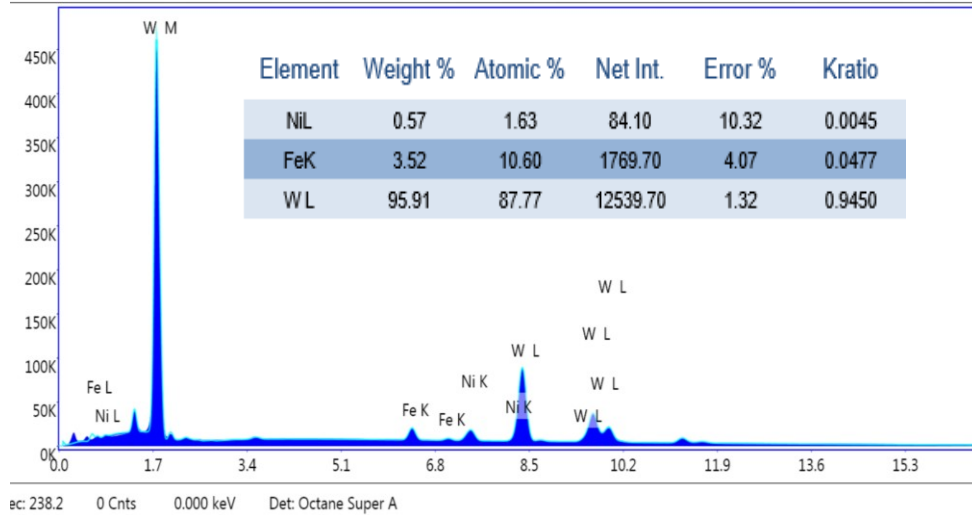


Figure D11 : Tungsten Rich Phase EDS Data

Collected EDS data indicates that the tungsten rich phase ~~indeed~~ has a high percentage of tungsten. This EDS scan also indicates a high composition of iron, which is somewhat higher than expected for the solubility of iron in the alpha tungsten phase.

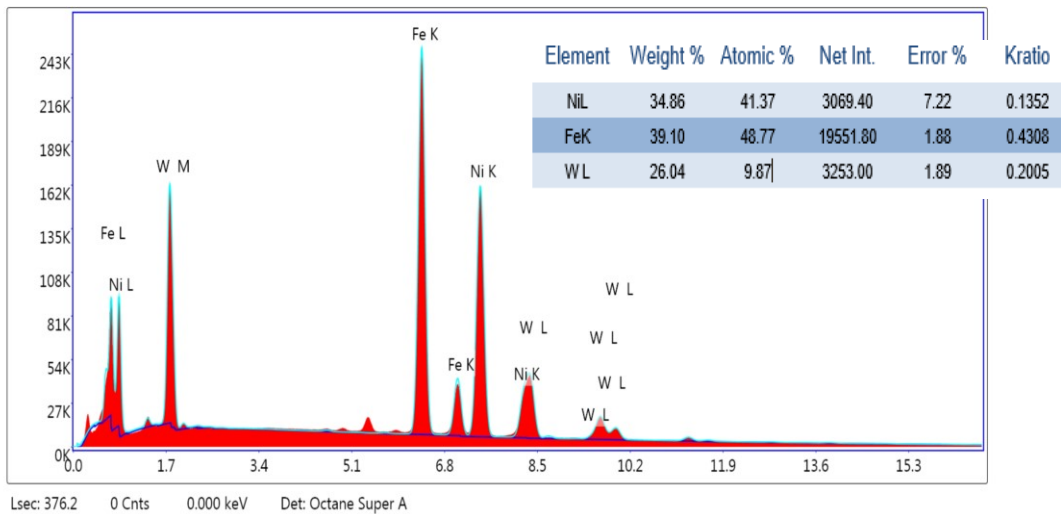


Figure D12: Matrix Phase EDS Data

The matrix phase compositions collected by the EDS detector and TEAMS software confirm the presence of Ni-Fe FCC phase. It is interesting to note that the collected data shows a tungsten content of around 9 at% in the matrix, which is approximately the max solubility limit of tungsten in FCC Ni-Fe at this Ni/Fe ratio (11).

In order to test the hypothesis of high density, tungsten rich phase macrosegregating in the deposits, Thermocalc was used to calculate the composition of each phase at the melting temperature. Phase compositions are shown for undiluted Anviloy wire as calculated at the solidus temperature, which was calculated by Thermocalc to be 1465C, in the below table.

Mole Percent W in FCC_A1	Mole Percent Ni in FCC_A1	Mole Percent Fe in FCC_A1
27.5	50.9	21.6
Mole Percent W in BCC_B2	Mole Percent Ni in BCC_B2	Mole Percent Fe in BCC_B2
99.1	.16	.74

Table D2 : Composition of Phases Predicted by Thermocalc at 1465C

The high tungsten content of the BCC phase was verified, with its composition essentially matching alpha tungsten and the solubility limits of nickel and iron in it as noted by former researchers (11). The high tungsten content predicted by Thermocalc, as well as its bright appearance in the SEM indicating a high tungsten composition, corroborate the high density of the BCC phase causing it to sink during cladding. Although this phenomena is not a major concern when deposits are limited to several layers, any future endeavors in bulk build-ups or additive manufacturing may need to consider macrosegregation of the BCC phase. This phase is

what is likely to give the Anviloy wire alloy its good elevated temperature properties for die casting, meaning its phase fraction should be maintained as high as possible to ensure good properties. Perhaps a half-bead approach, where half the last layer deposit thickness is machined away should be used so the final surface has a maximum BCC phase content.

Effect of Dilution on Anviloy Wire-H13 Fusion Zone Microstructure

With the microstructure of undiluted Anviloy wire understood, attempts were made to characterize the fusion boundary of H13-Anviloy wire clads. This region shows a different microstructure due to base metal dilution resulting in the formation of a third phase. Figure D13 below shows an overlay with a different microstructure along the H13 fusion boundary when compared to the images gathered at the top of the 6 pass build in Figure D7.

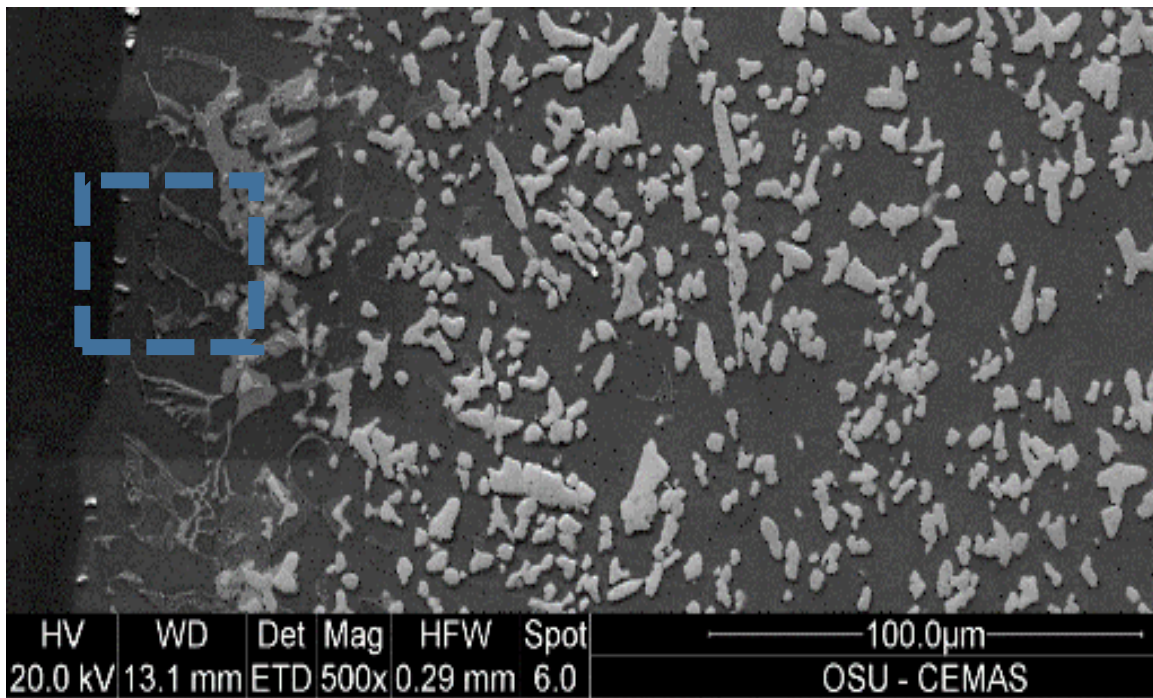


Figure D13: Anviloy Wire H13 Single Pass Overlay Diluted Structure

The far left side of Figure D13 is the H13 base material and the clad deposit fusion boundary. The microstructure along the fusion boundary appears to have different phases present than the undiluted Anviloy microstructure. This is evident when comparing the fusion boundary microstructure shown on the left side to the less diluted Anviloy wire microstructure on the micrographs right side. Note that the undiluted microstructure in this single pass clad is essentially the same as the last pass in the 6 Pass overlay build, consisting of two phases only. Figure D13 shows a higher magnification view of the fusion boundary region highlighted in Figure D13.

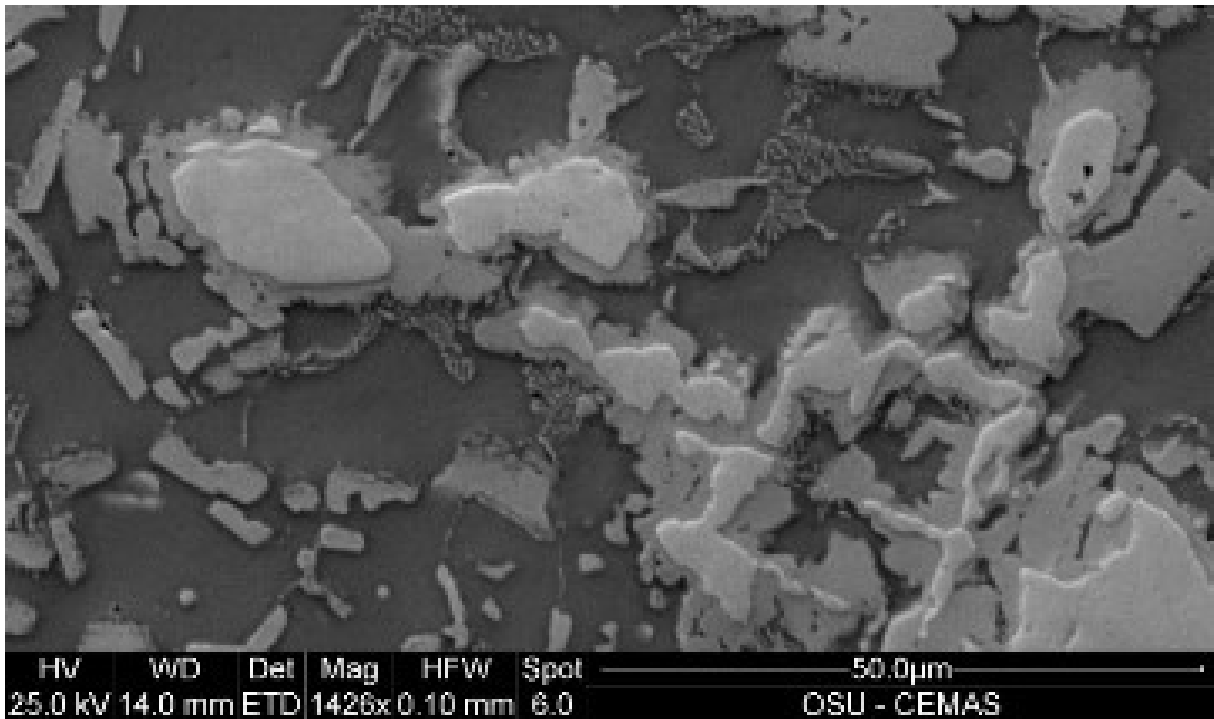


Figure D14: Fusion Boundary Microstructure in H13-Anviloy Wire Clads

The fusion boundary microstructure depicted in Figure 14 clearly differs from the undiluted Anviloy wire microstructure. It appears that, in addition to the Ni-Fe matrix phase and primary W secondary phase, new phase(s) intermediate in tungsten content form at the interface between

the primary W phase and Ni-Fe matrix phase. It also appears the new phase forms a eutectic/eutectoid with the matrix phase evidenced by the lamellar structure seen towards the middle of the figure. An EDS map of this region was performed to determine elemental composition and number of phases, and is shown below in Figure D15.

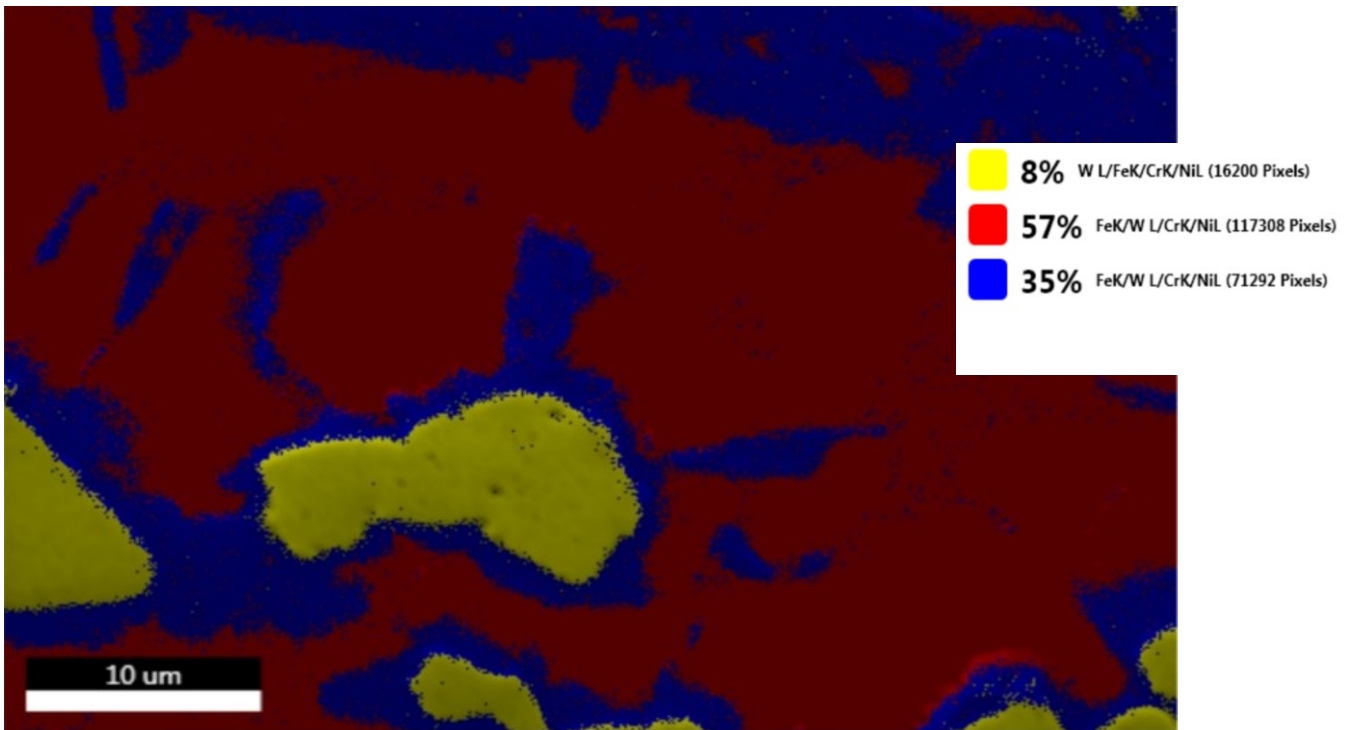


Figure D15: EDS Map of Anviloy-H13 Fusion Boundary Microstructure

Carbon measurements are unreliable for even qualitative purposes in EDS, and therefore carbon was not included in these elemental maps. It should be noted that, even if carbon is present in a sample at a significant proportion of a phase's composition, the ratio of heavier alloying elements will remain the same. This logic was used in order to identify the composition of the unknown phase. The TEAMS EDAX software confirmed the presence of at least one additional phase at the W / Ni-Fe interface, depicted in blue in Figure D14. The intermediate tungsten composition from this phase was also confirmed by EDS scans, which are shown below.

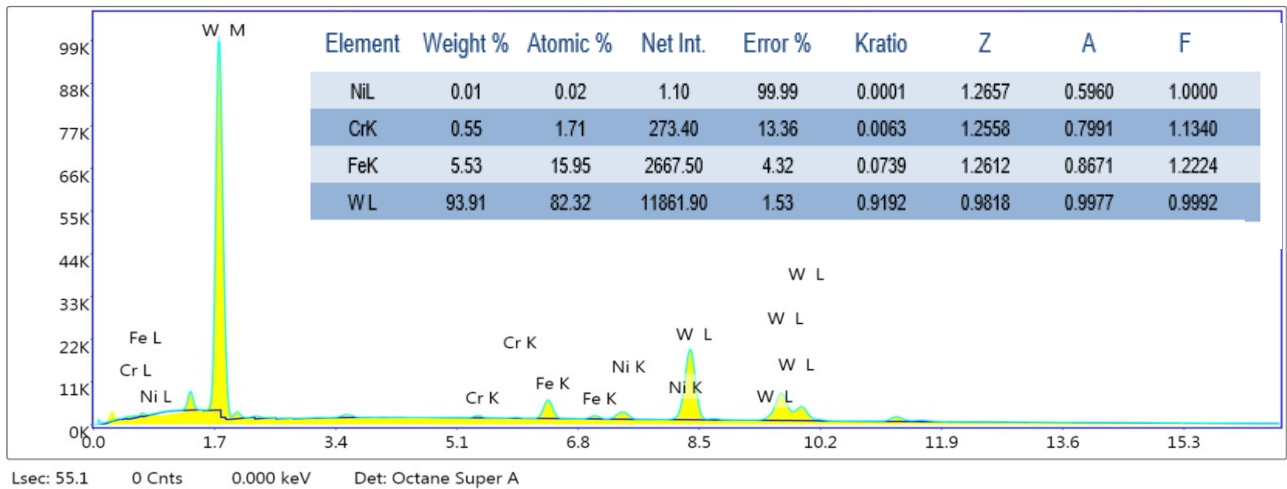


Figure D16 : EDS Data and Composition of Phase for Alpha BCC Tungsten Phase

Similar to the previous EDS scan, the tungsten rich phase showed a high percentage of tungsten vs. other elements. Interestingly, this scan also detected a non-negligible iron content in the tungsten rich BCC phase. This is in addition to a small content of chromium detected in the scans. Unlike iron, the solubility range for chromium is much higher in alpha tungsten due to the isomorphous phase diagram between chromium and tungsten (19).

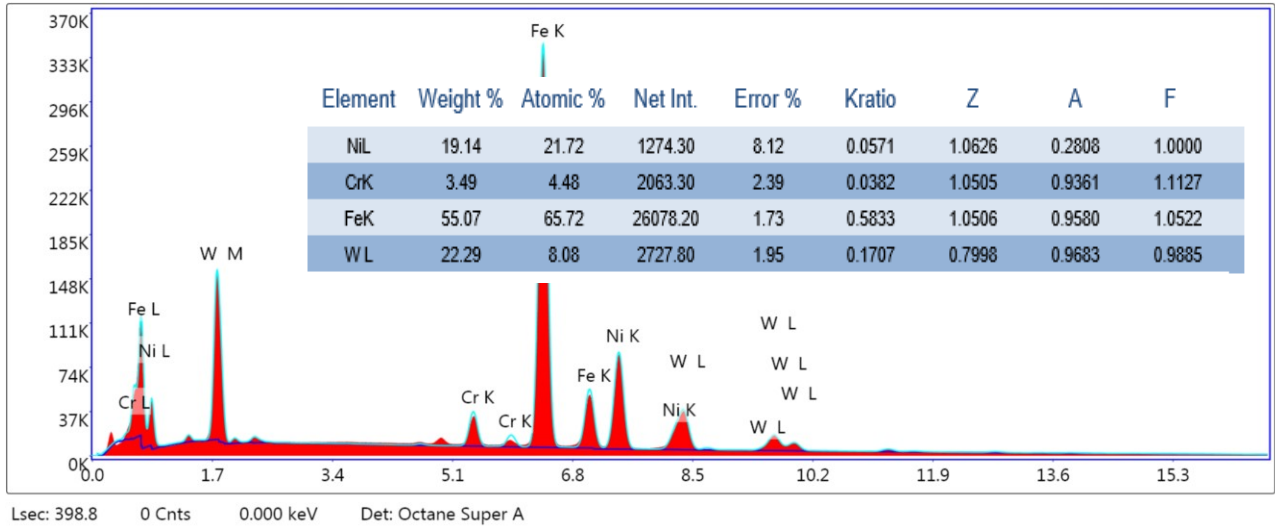


Figure D17 : EDS Data and Composition of Phase for Matrix Phase

The matrix phase in this location had a higher iron content relative to the last pass due to more dilution with the ferrous H13 base material. Tungsten content in this location was also near the predicted solubility of tungsten in this Fe/Ni ratio FCC phase.

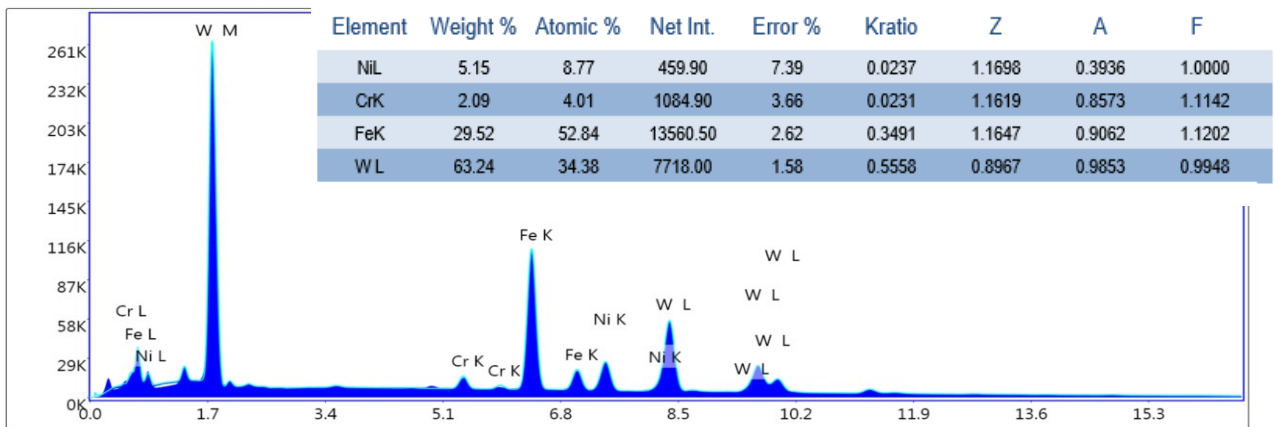


Figure D18: EDS Data and Composition of Phase for Tungsten Intermediate Phase

EDS scans showed the intermediate tungsten composition phase had iron as the most prevalent element, followed next by tungsten with chromium and nickel as minor additions under 10 mol%.

Once the presence of a third phase was confirmed and EDS identified the phase's approximate elemental composition, Thermocalc simulations were used to help identify it. Using the high entropy alloy database in Thermocalc, equilibrium phase fraction vs. Temperature plots, also known as property diagrams, were made for 10% and 40% dilution of H13 elements into Anviloy wire deposits. This dilution range corresponds to the lowest dilution achievable without defects using HW-GTAW in multi-pass clads and the dilution percentage of conventional GTAW clads using Anviloy. This gives the full range of possible compositions for this process. Dilution for the sample where EDS data was collected is likely towards the middle of this range, approximately 30%. Figure D18 below shows the property diagram for 10% dilution.

Anviloy-H13 10% Dilution

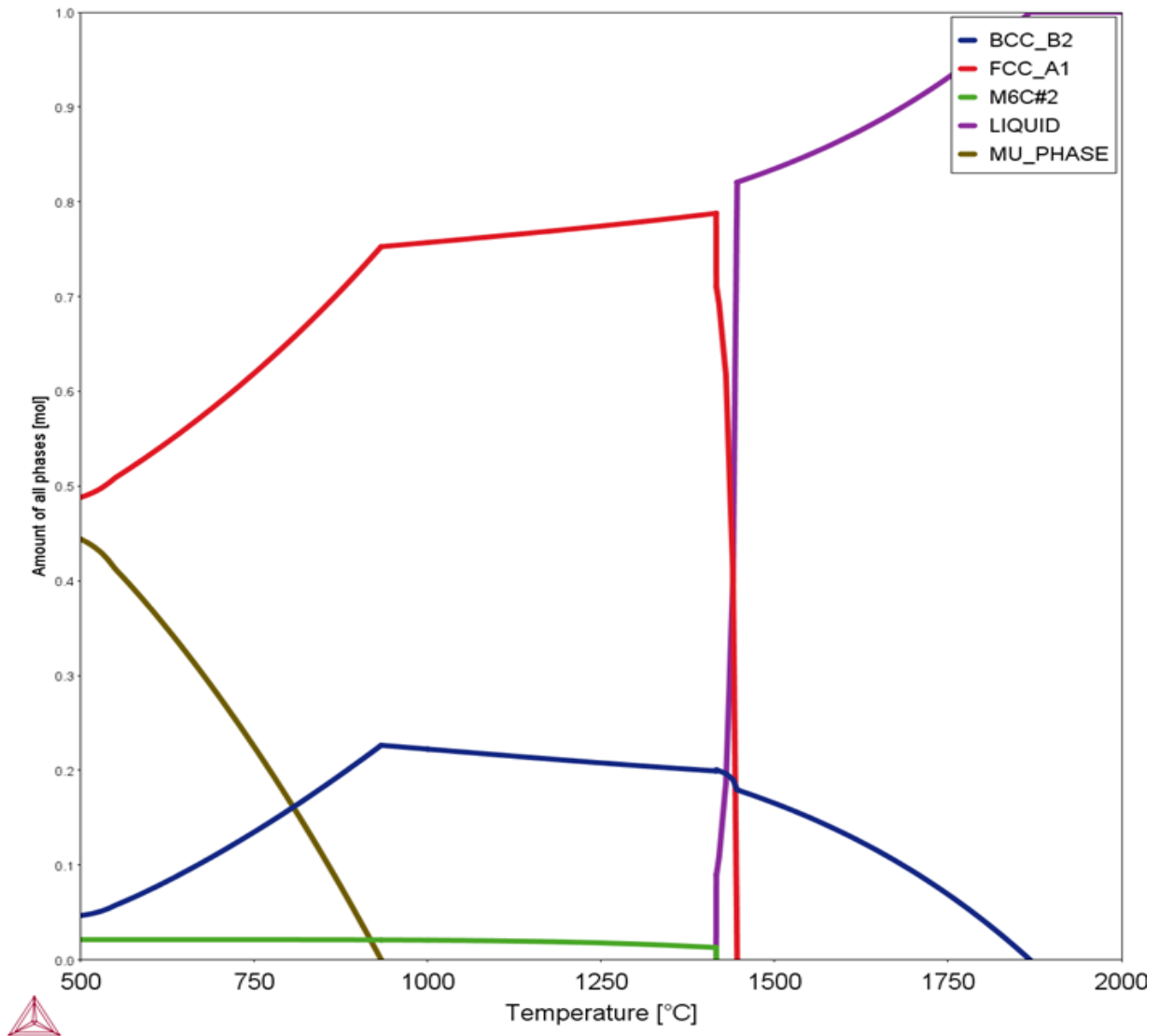


Figure D19 : Property Diagram for 10% Dilution

Figure D19 shows that, at 10% dilution, two phases form during solidification: a primary W BCC phase and a Ni-Fe FCC phase. In addition to the alpha tungsten BCC phase and Ni-Fe phase seen in the undiluted samples, two more phases are predicted by Thermocalc. It predicts a eutectic M_6C carbide to form at the end of solidification, as well as the TCP intermetallic Mu

phase at temperatures below 1000C. Predicted compositions for M₆C and Mu phases at 900C are shown below for the 10% dilution composition.

Mole Percent W in Mu	Mole Percent Ni in Mu	Mole Percent Fe in Mu
27.5	50.9	21.6
Mole Percent W in M ₆ C	Mole Percent Ni in M ₆ C	Mole Percent Fe in M ₆ C
44.6	12.2	40.2

Table D3 : Thermocalc Predicted Composition of Mu and M₆C Phases for 10% Dilution at 900C

The 40% dilution property diagram and composition of phases are shown in Figure D20.

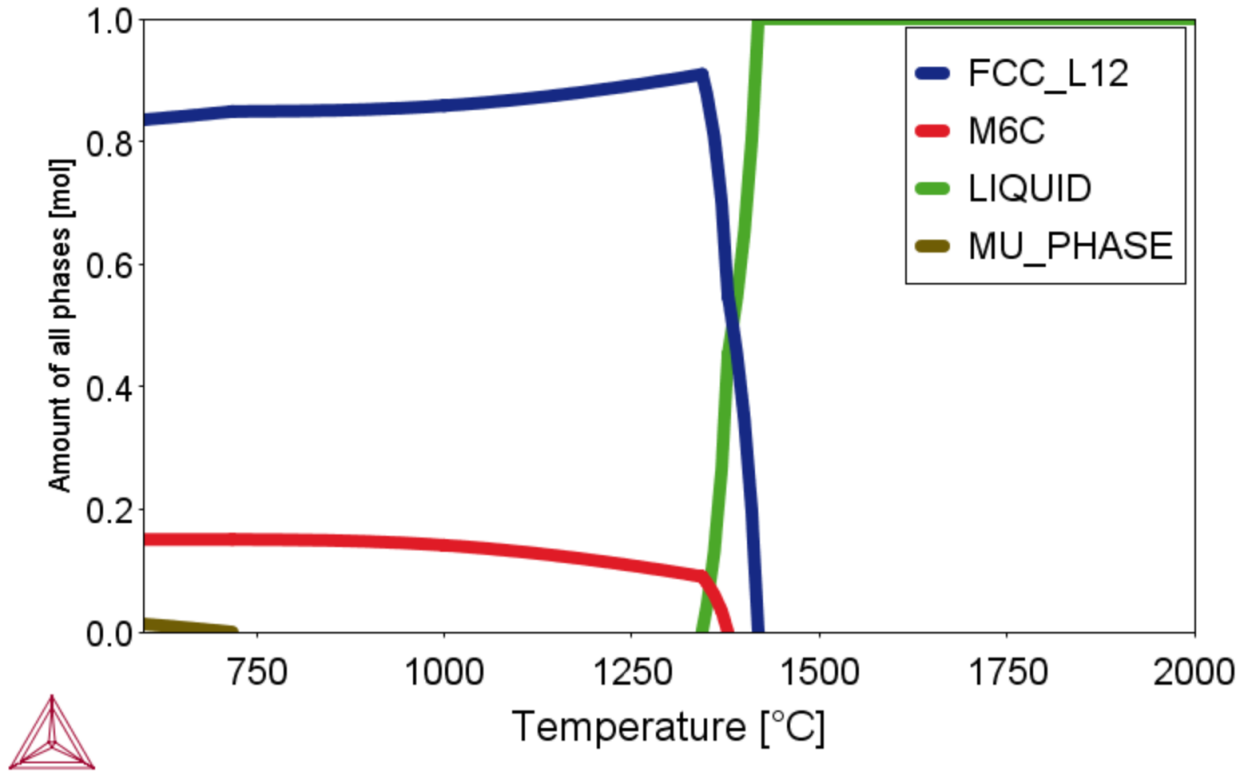


Figure D20: Property Diagram for 40% Dilution

Mole Percent W in Mu	Mole Percent Ni in Mu	Mole Percent Fe in Mu
41.2	4.4	47.7
Mole Percent W in M ₆ C	Mole Percent Ni in M ₆ C	Mole Percent Fe in M ₆ C
40.8	6.1	35.4

Table D4 : Thermocalc Predicted Composition of Mu and M₆C Phases for 40% Dilution at 700C

At this composition, dilution is too high to form primary tungsten; however, another phase with a lower tungsten content forms at lower temperatures after solidification. The Mu phase, which is a

TCP intermetallic phase, has an intermediate tungsten content between the secondary BCC phase and FCC matrix phase. The composition of this phase is very close to the unidentified third phase seen along the fusion boundary, which suggests Mu phase formation along Anviloy-H13 fusion boundary is possible. Previous work in “heavy” alloy W-Ni-Fe kinetic penetrators made with liquid phase sintering validates this hypothesis. Prior research noted that intermetallic Mu phase forms at interface boundary between primary W BCC particles and the Ni-Fe liquid sintering phase, encompassing the alpha BCC phase (14). Other researchers detected carbides, but they noted that the carbide did not fully encompass the tungsten phase (13).

It should be noted that, for the predicted Thermocalc compositions for M_6C or Mu phase at both 10% and 40% dilution, neither match precisely with the gathered EDS data; however, the Mu phase composition at 40% dilution is the closest. For this reason, the decision was made to make another EDS scan, but this time with carbon included, in an effort to develop contrast between the phases in question. Since the predicted carbon content of the M_6C carbide differs by at least an order of magnitude from the other phases, a carbide phase would likely show contrast with the others. Elemental heat maps for W, Ni, Fe, and C gathered by EDS are shown below.

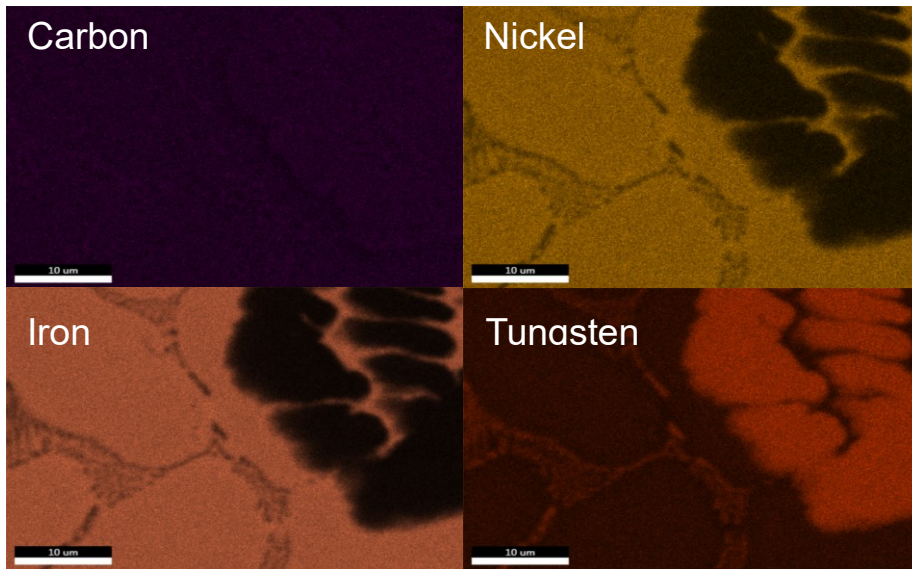
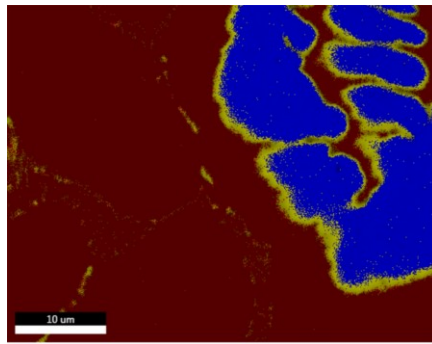


Figure D21 : EDS Phase Map and Elemental Heat Map Including Carbon

The resultant elemental heat maps produced inconclusive results. The poor contrast in the carbon elemental heat map does not rule out M_6C carbide, however, because of the poor resolution of EDS detectors for carbon. These results highlight the need for more advanced crystallography to determine the identity of unknown phase. Although the results of this study seem to suggest the possibility of Mu phase formation in Anviloy Wire-H13 clads, there is no fully conclusive evidence to validate this.

Heat Treated Anviloy Wire – H13 Clads

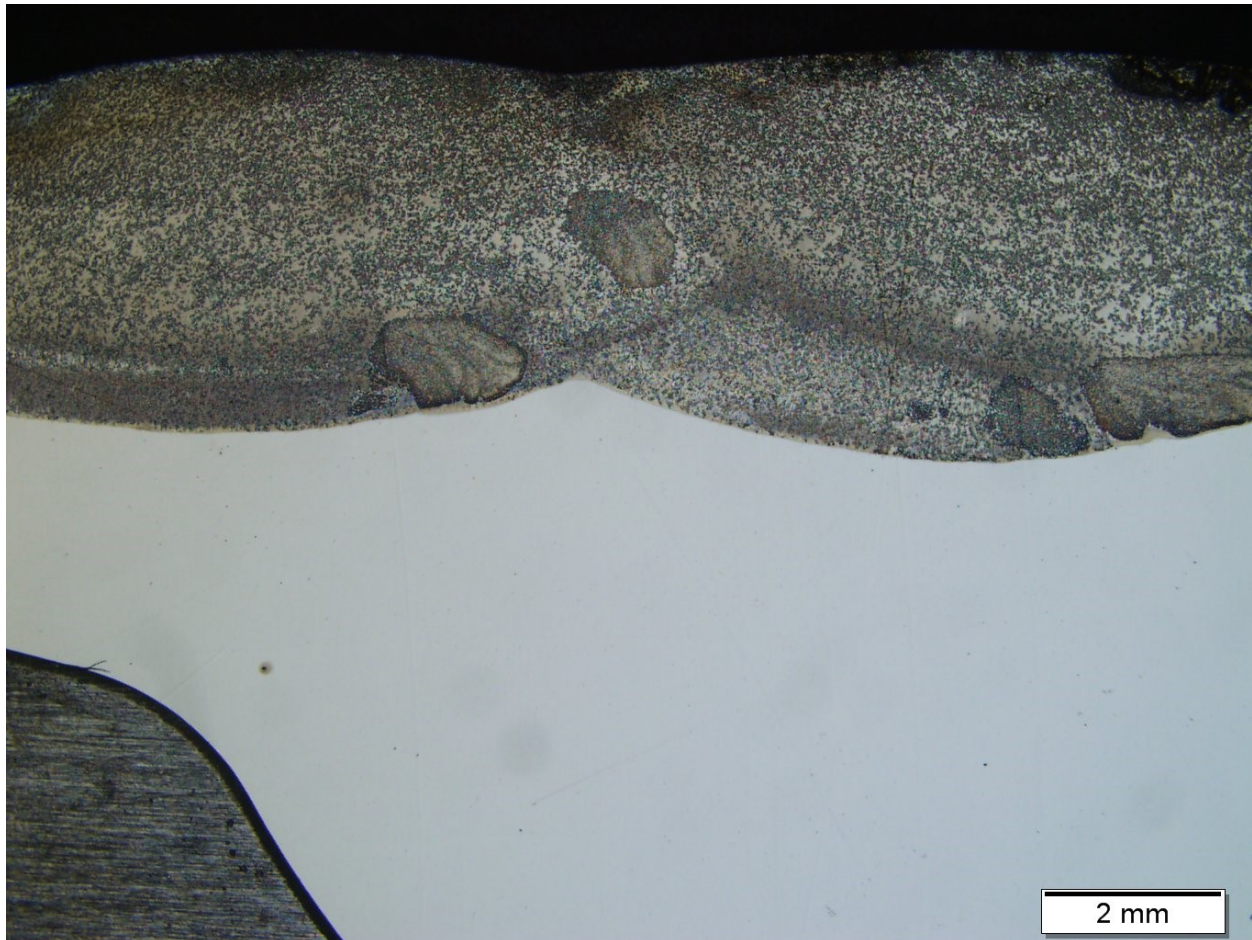


Figure D22 : Normalize & Double Tempered Anviloy Wire – H13 Clad Macro

Figure D22 shows a macrograph of the annealed and double tempered Anviloy wire-H13 clad. It is apparent from the figure that the H13 base material remained in the unetched state, evidenced by the lack of coloration beneath the Anviloy wire deposit, verifying that this etchant does not darken H13. Also evident in this micrograph is etching of the Anviloy wire deposit, which has been etched a light brown hue after being subjected to the alkaline sodium picrate etch. A closer look at the fusion boundary of this sample is shown below in Figure D23.

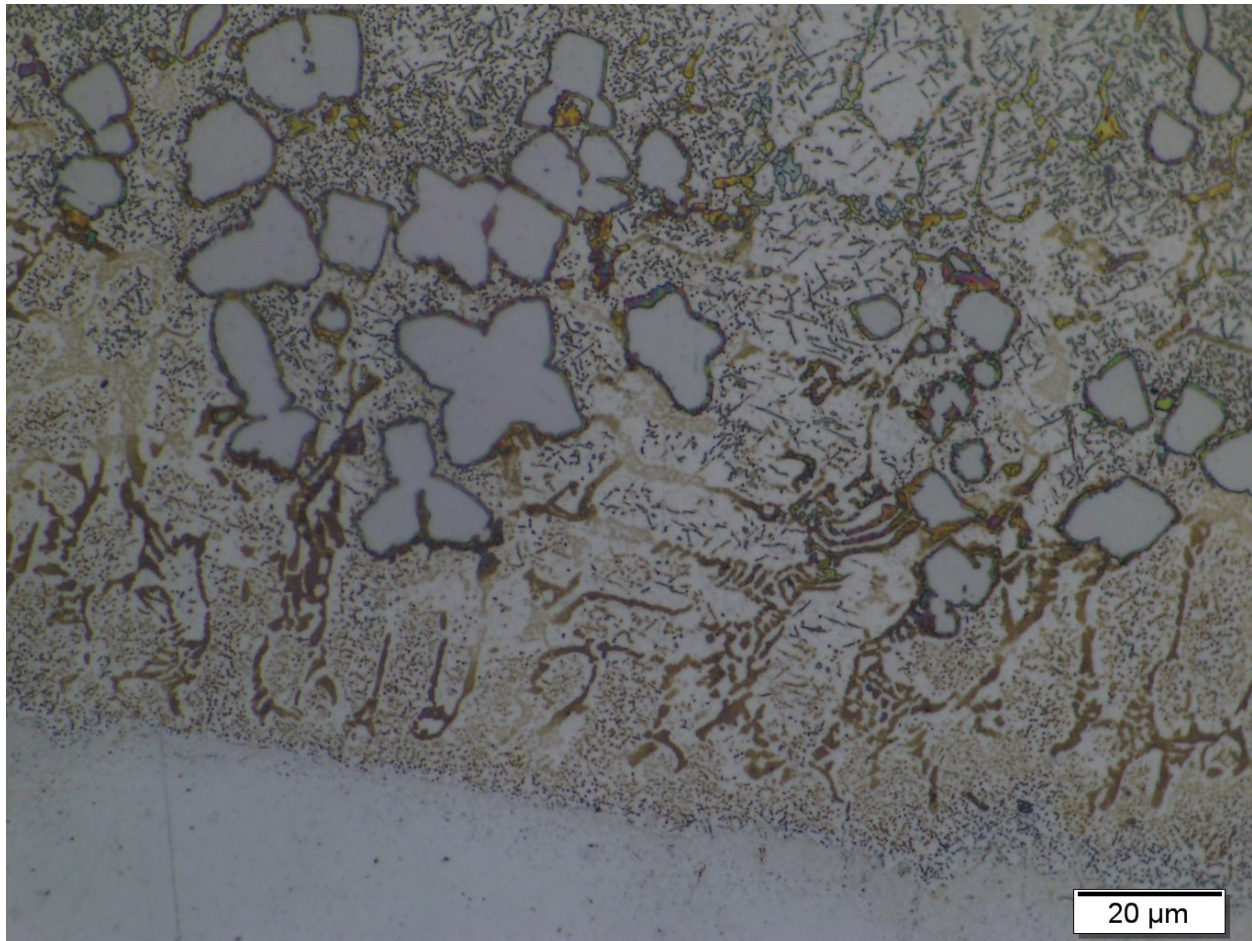


Figure D23 : Normalized & Double Tempered Anviloy Wire – H13 Clad Fusion Boundary

A lack of etching of the alpha tungsten phase is observed, although it appears the outer edges of this phase are darkened. Interestingly, the lamellar eutectic microstructure also observed in the 6 pass Anviloy build have been darkened profusely with the alkaline sodium picrate etch, indicating the presence of an M_6C carbide. To verify this same structure was observed in both the anneal and double tempered sample and the 6 pass Anviloy build fusion boundary, the 6 pass Anviloy build sample was also etched using the alkaline sodium picrate etch as shown in Figure D24.

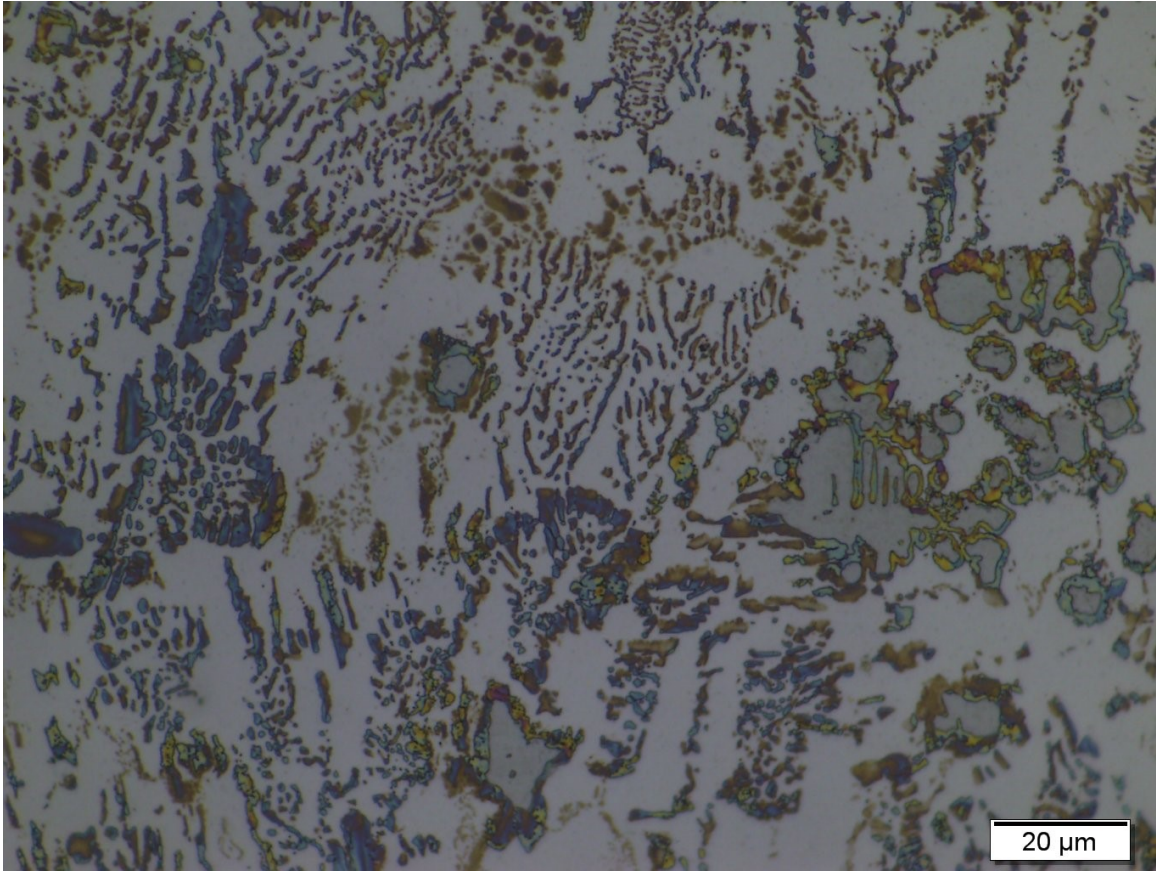


Figure D24 : Anviloy 6 Pass Build Fusion Boundary Etched with Alkaline Sodium Picrate

Figure D24 shows the same microstructure as seen in previous SEM experiments, but in this case microstructural contrast was produced with the alkaline sodium picrate etchant. The etching of the lamellar eutectic phase appears to be very similar to that seen in the normalized and double tempered sample, indicating the same phase is being identified by both the alkaline sodium picrate etch as well as in EDS scans and SEM images.

FCC matrix phase grain boundaries also appear to be preferentially etched in both samples. There is also evidence of intragranular etching in the normalized and double tempered sample. Small particles representing a high volume fraction of the matrix phase are etched in this region near the fusion boundary but where the matrix phase is unetched. The matrix phase also

appears to be unetched in the 6 pass Anviloy build sample. In order to verify the matrix phase is unetched in the heat treated H13-Anviloy wire sample, an image of the fusion zone 5mm away from the fusion boundary was collected. This micrograph is shown below in Figure D25.



Figure D25 : Normalized & Double Tempered Anviloy Wire – H13 Clad Fusion Zone

Figure D25 verifies that the matrix phase remained unetched in the heat treated H13-Anviloy wire clads. This figure also verifies the interdendritic regions of the fusion zone are preferentially etched, showing significant darkening relative to the rest of the microstructure. Etching of only the interdendritic regions away from the fusion boundary indicates diffusion along grain boundaries resulted in the formation of a phase selectively etched by alkaline sodium picrate.

The most likely phase etched is the M_6C carbide this etchant was designed to attack. Since carbon diffuses very rapidly into the Ni-Fe FCC phases from ferritic materials, a fact well studied in dissimilar clads for power generation industries, it is likely that the normalization heat treatment causes extensive carbon migration from H13 into the Anviloy Wire deposit (20). A high carbon gradient between H13 and Anviloy wire, as well as the higher solubility of carbon in the FCC matrix, facilitate carbon diffusion.

Carbon diffusion into the Anviloy wire deposit is likely to cause softening in H13. In order to verify softening of H13 due to carbon migration, hardness indents were collected 10mm away from the fusion boundary in the middle of the H13 plate, as well as at the fusion boundary. Hardness indents from these regions are shown below in Figures D26 and D27.

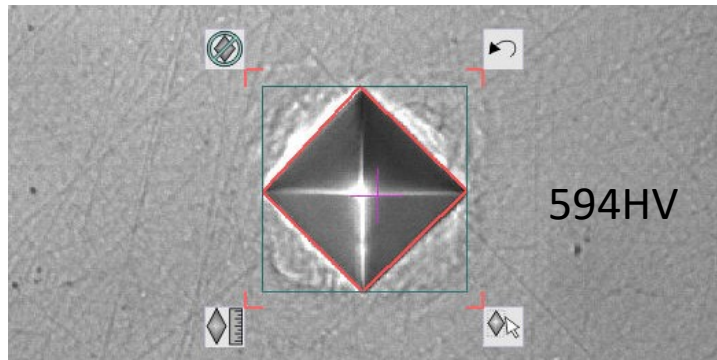


Figure D26 : H13-Anviloy Wire N+2T Hardness Indent 10mm Away From Fusion Boundary

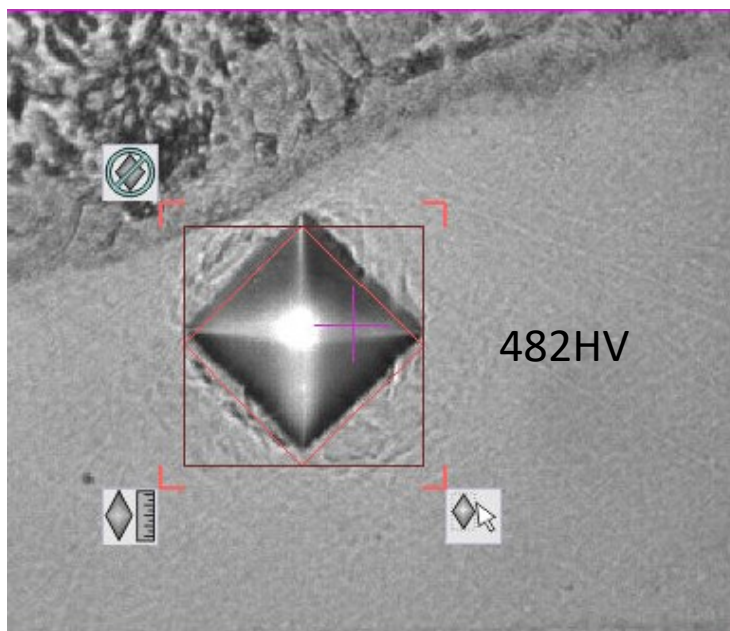


Figure D27: H13-Anviloy Wire N+2T Hardness Indent Near Fusion Boundary

Hardness away from the fusion boundary was measured to be 594HV, while hardness next to the fusion boundary was measured to be 482HV. Since these points come from the same sample and were subjected to the same heat treatment, carbon migration into the Anviloy Wire deposit from the H13 base material is the most likely cause for the softening of H13 along the fusion boundary.

One commonly used method for reducing carbon diffusion into the Anviloy wire deposit is to use a butter layer to provide a diffusion barrier between the high carbon H13 and Anviloy wire deposit. The butter layer selected for this trial was a low carbon 308L consumable. The selection of 308L was made not only because of its very low carbon content, but also because of its primarily FCC structure providing a more effective diffusion barrier. Diffusion is slower in FCC crystal structure vs. BCC crystal structures, making an austenitic filler such as 308L a good candidate to prevent carbon diffusion into the Anviloy wire. In order to test this hypothesis, H13 was clad first with a layer of 308L and then a layer of Anviloy wire and subjected to the same heat normalization and double temper heat treatment as the Anviloy wire – H13 sample. An image showing the Anviloy Wire – 308L fusion boundary as well as the 308L-H13 fusion boundary is shown below in Figure D28.

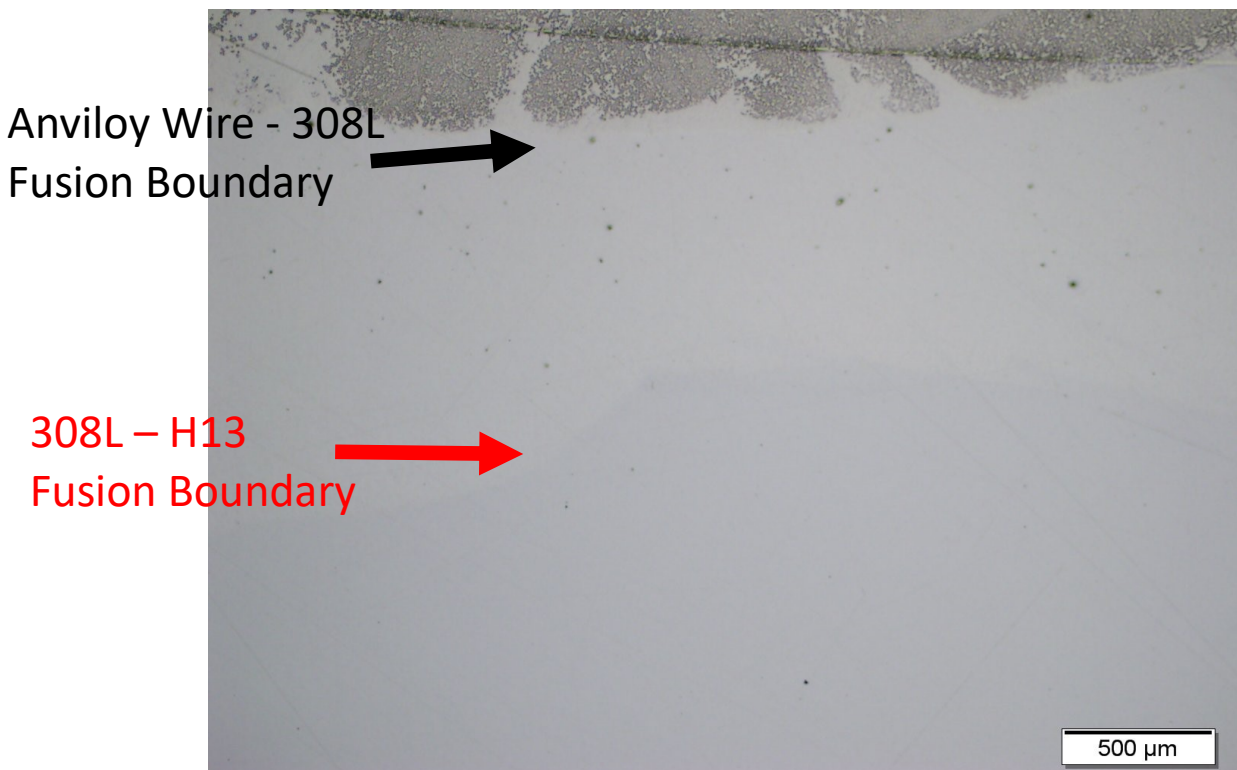


Figure D28 : H13-308L-Anviloy Wire N+2T Fusion Boundaries

No discernible etching is detected in this sample, as evidenced by the lack of brown etching phases seen in the H13-Anviloy wire clads without a 308L butter layer. Although this could indicate 308L was an effective butter layer that prevented carbon diffusion, another possibility for the lack of etching with alkaline sodium picrate exists. It is possible that, since 308L has a high amount of the carbide forming element Chromium in its composition, the carbide type formed in the deposits was no longer of the M_6C type, but rather of the $M_{23}C_6$ variety which is more thermodynamically stable for chromium. Regardless, the lack of M_6C carbide formation in the Anviloy wire deposit region indicates the 308L butter layer was effective in reducing carbon migration into the Anviloy wire deposit.

It is also possible that Mu phase was etched both the Anviloy Wire – H13 heat treated sample as well as the Anviloy wire build, but not the 308L sample. In order to determine if Mu phase formation is likely when 308L is used as a butter layer between H13 and Anviloy wire, a Thermocalc property diagram was created to show equilibrium phases over a range of temperatures for a single composition. Since dilution occurs in the 308L-H13 clad, a simulation using only 308L and Anviloy wire is not an accurate representation of what occurs in this sample. Instead, a composition of 70% Anviloy wire + 30% * (70% 308L + 30% H13) was used. This composition represents 30% dilution of previous passes into subsequent passes.

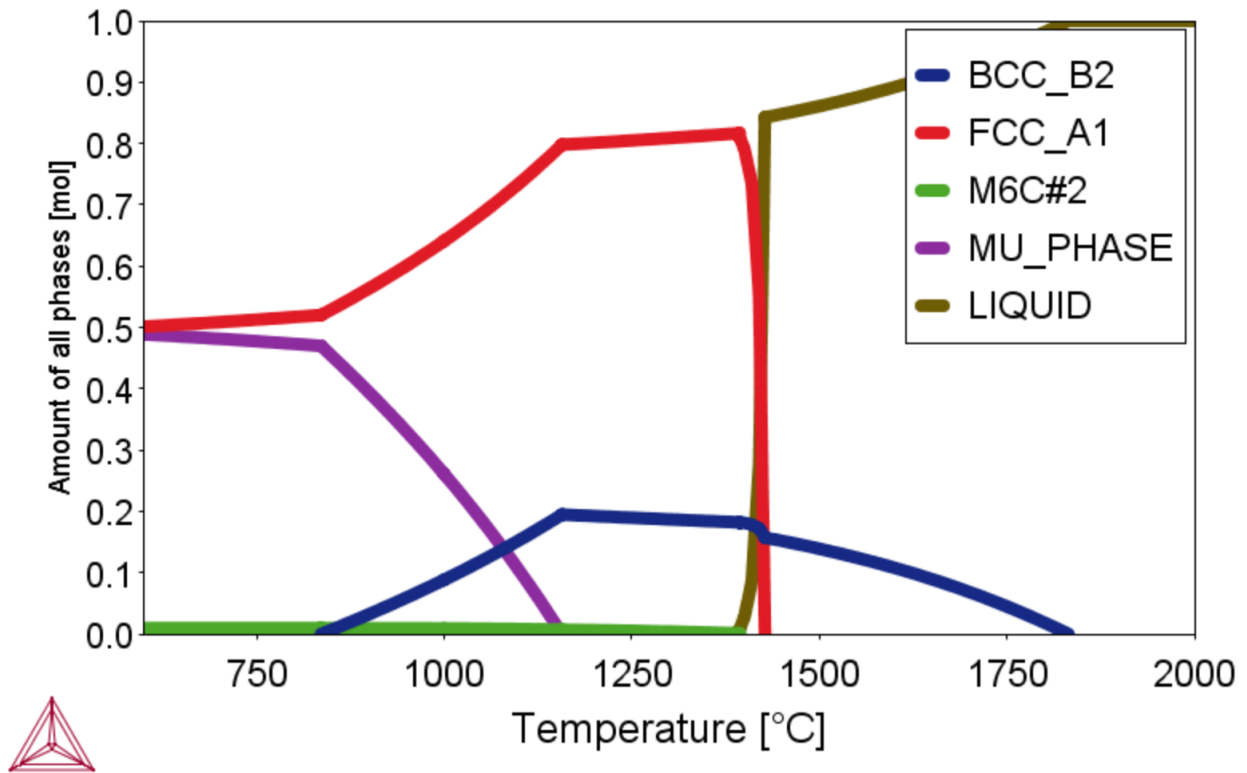


Figure D29 : Property Diagram for .7*Anviloy Wire + .3(.7*308L+.3*H13)

Figure D29 shows that Mu phase is still predicted by Thermocalc to be present in the H13-308L-Anviloy Wire sample. The lack of etching in that sample, along with Thermocalc phase prediction indicating Mu phase would still be present, suggests that Mu phase was in fact not etched via alkaline sodium picrate, but rather only M_6C carbide was etched. This strongly suggests that the unidentified phase seen in the 6 pass build, as well as the dark etching phase in the heat treated H13-Anviloy wire clads, is M_6C carbides.

Conclusions

- Undiluted Anviloy wire microstructure consists of primary tungsten alpha BCC phase and (Ni/Fe) gamma FCC phase
- Anviloy Wire – H13 deposit microstructure consists of primary tungsten alpha BCC phase, (Ni/Fe) gamma FCC phase, and potentially TCP intermetallic Mu phase or M_6C carbide phase
- Heat treated samples and hardness indents indicate carbon diffusion from H13 into Anviloy wire during heat treatment
- Alkaline sodium picrate etching strongly suggests M_6C carbide formation vs. Mu phase formation in Anviloy Wire-H13 clads, but further crystallography is required to verify identity of third phase

Works Cited

1. Endemann, A., & Hoehn, T. (2018). New materials in mould making are required to meet the new challenges in die casting. Paper presented at the *73rd World Foundry Congress "Creative Foundry", WFC 2018 - Proceedings*, 489-490.
2. Sjoström, J.
3. Medvedeva, J. Bergström, S. Gunnarsson, J. Andersson. "High-temperature properties and microstructural stability of hot-work tool steels." *Materials Science and Engineering: A*, Volume 523, Issues 1–2, 2009, Pages 39-46, ISSN 0921-5093
4. Silva, F.J.G.; Santos, J.; Gouveia, R. Dissolution of Grain Boundary Carbides by the Effect of Solution Annealing Heat Treatment and Aging Treatment on Heat-Resistant Cast Steel HK30. *Metals* 2017, 7, 251.
5. J. Buckstegge, B. Gehricke, U. Reichel. "CORRELATION BETWEEN HEAT-CHECKING RESISTANCE AND IMPACT BENDING ENERGY OF HOT-WORK TOOL STEEL DIN 1.2344." 6th International Tooling Conference. 2002.
6. Clayton A.J. "APPLICATION FOR ANVILOY 1150 IN ALUMINUM AND BRASS DIE CASTING." *Precision Metals*, Vol. 30, Issue 7, pg. 29-31. 1972
7. D. Schwam, J. Wallace, S. Birceanu. "DIE MATERIALS FOR CRITICAL APPLICATIONS AND INCREASED PRODUCTION RATES." Case Western Reserve University, U.S. Department of Energy. 2002.
8. K. Winkler, R. Vogel. "The Fe-Ni-W Phase Diagram." *Archive for Ironworks*. Volume 6, Issue 4. 1932.
9. J. Posthill, D. Edmonds. "Matrix and interfacial precipitation in the W-Ni-Fe system." *Metallurgical Transactions A*, Vol. 17, pgs. 1921-1934. 1986.
10. L. Ostlund, A. Guillermet. "Experimental and theoretical study of the phase equilibria in the fe-ni-w system." *Metallurgical and Materials Transactions A*, Vol. 17, pgs. 1809-1823. 1986
11. G. V. Raynor, V. G. Rivlin. "Critical evaluation of constitutions of certain ternary alloys containing iron, tungsten, and a third metal." *International Metals Reviews*, 26:1, 213-249. 1981.
12. J. Nooh, M. Hong, G. Kim, S. Kang, D. Yoon. "The cause of matrix penetration of W/W grain boundaries during heat treatment of W-Ni-Fe heavy alloy." *Metallurgical and Materials Transactions A*, Vol. 25, pgs. 2828-2831. 1994.
13. B. Muddle. "Interphase boundary precipitation in liquid phase sintered W-Ni-Fe and W-Ni-Cu alloys." *Metallurgical and Materials Transactions A*, Vol. 15, pgs. 1089-1098. 1984.
14. "Effect of Fe7W6 Phase (μ -phase) on Mechanical Properties of W-Ni-Fe Heavy Alloy." *KOREAN JOURNAL OF METALS AND MATERIALS*, Vol.49, No.9 [2011], p720-725
15. "Weldability of Materials - Nickel and Nickel Alloys." TWI, The Welding Institute, www.twi-global.com/technical-knowledge/job-knowledge/weldability-of-materials-nickel-and-nickel-alloys-022.
16. Raghavan, V. Cr-Fe-Ni (Chromium-Iron-Nickel). *J. Phase Equilib. Diffus.* 30, 94–95 (2009)

17. G.V. Raynor and V.G. Rivlin, Cr-Fe-Ni, Phase Equilibria in Iron Ternary Alloys, Institute of Metals, London, 1988, p 316-332
18. J. Miettinen: "Thermodynamic Reassessment of Fe-Cr-Ni System With Emphasis on the Fe-Rich Corner," Calphad, 1999, 23(2), pp. 231-48.
19. Naidu, S.V.N., Sriramamurthy, A.M. & Rao, P.R. The Cr-W (Chromium-Tungsten) system. Bulletin of Alloy Phase Diagrams 5, 289 (1984).